Durham E-Theses

Reconstruction of the East Asian monsoon variability since the mid-Holocene from the Pearl River estuary, southern China

YU, FENGLING

Reconstruction of the East Asian monsoon variability since the mid-Holocene from the Pearl River estuary, southern China

Fengling Yu

University College

Thesis Submitted for the degree of Doctor of Philosophy

Department of Geography

University of Durham

June 2009

Declaration

This thesis is the result of my own work. Data from other authors contained herein are acknowledged at the appropriate point in the text. All quotations have been distinguished by quotation marks and the sources of information acknowledged. I confirmed that no part of the material offered has previously been submitted by me for a degree in this or any other university.

The copyright of this thesis lies with the author. No quotation from it may be published without prior consent and any information derived from it should be acknowledged.

Fengling Yu

Acknowledgements

Abstract

The principal aim of this thesis is to reconstruct East Asian Monsoon (EAM) variability during the mid-Holocene, developing a relatively new proxy of bulk organic carbon isotopic signature ($\delta^{13}C$). C/N ratios and trace elements are also employed to conduct a multi-proxy case study from the Pearl River estuary, southern China. Sources of sediments within an estuary include river-derived terrestrial/freshwater input, in situ brackish-water suspended sediment and tide-derived marine input. This study assumes the three proxies can help differentiate sources of sediments relating to monsoon-driven freshwater flux and help reconstruct monsoonal precipitation history during the mid-Holocene when the sea level was relatively stable.

To achieve the aims of this thesis a range of modern samples were collected from terrestrial areas, including plants and soil samples, through to estuarine areas, including seasonal estuarine suspended organic matter (SOM) and surface sediment. Results suggest that bulk organic $\delta^{13}C$ and C/N ratios can successfully identify sources of the organic component of the estuarine sediment, and thus can be used to infer relative changes in monsoon-driven freshwater flux to the estuary. For example, more negative $\delta^{13}C$ values reflect a greater level of contribution of freshwater organic carbon, i.e. stronger monsoonal freshwater discharge. Results also show that a combination of selected metals, such as the terrigenous metals (Fe, Mn, Co and As), can be useful for indicating sediment sources and sedimentary environment.

Analysis of an estuarine core (UV1) shows that freshwater discharge from the Pearl River catchment gradually declined from 6400 to 2000 cal. years BP, suggesting a gradual weakening of summer monsoon precipitation, responding to the weakening insolation controlled by the orbital-driven precession cycle. Superimposed on this are wet/dry intervals, ranging from centennial- to millennial- scale, driven by solar activity. Changes in ENSO and high-latitude cooling events might be responsible for dry/wet events at centennial- to decadal- scale, identified during the mid-Holocene. This study also suggests that the coupling of thermal and moist conditions of the EAM might only have become stable after 4500 cal. yr BP. A sudden shift in the geochemical signature indicates agricultural activity in the Pearl River delta intensified from 2000 cal. yr BP.

Table of Contents

List of tables

List of Figures

Chapter 1

Chapter 2

Chapter 3

Chapter 6

List of Appendices

Chapter 1 Introduction

1.1 Introduction

The East Asian Monsoon (EAM) plays a significant role in the global and regional hydrological and energy cycles. The EAM forms as a result of energy distribution differences between the Asian landmass and the Pacific Ocean and Indian Ocean. The hydrological and thermal dynamic system of the EAM can be perturbed by internal and external factors at different time scales. For example, orbital forcing is the fundamental driving force for the EAM (An, 2000); however, sub-orbital forcing at a shorter timescale has become more important during the Holocene, e.g. changes in solar output and global ice volumes at the millennial timescale (An, 2000), and oscillations of El Nino Southern Oscillation (ENSO) and the Intertropical Convergence Zone (ITCZ) at a centennial to decadal timescales etc (Zhang, 1983; Xu and Zhang, 1983).

Nearly two thirds of the world's population live in the Asia. This region has one of the most diverse terrestrial ecosystems in the world, including tropical forest, deserts, coastal areas, major river systems, and upland plateaux etc. Fluctuations in the EAM greatly influence human society through significant changes to the environment. Cultural development of this area has been proved to be closely related to variability of the EAM during Holocene. For example, during a stable warm and wet phase from 7200 to 6000 cal. yr BP, the Neolithic Yangshao Culture in the Yellow River catchment and the Majiabang Culture in the lower Yangtze plain, both in China, reached their climax (Shi *et al*., 1994). However, a sudden dry and cold event around 4000 cal. yr BP recorded in the Dunde ice core, Qilian Mountain, Northwest China (Thompson *et al*., 1989; Thompson *et al*., 1993), is suggested to be responsible for the end of the Longshan and Liangzhu Cultures in East China (Shi *et al*., 1994). Thus, understanding the temporal and spatial diversity of the hydrological and thermal distribution in the East Asian region will help predict hazards and protect the society from future possible changes to the monsoon.

This thesis reconstructs variability of the East Asian Monsoon (EAM) during the mid-Holocene from the Pearl River estuary, southern China (Figure 1.1). Bulk organic carbon isotopes, carbon/nitrogen (C/N) ratios, and key metals are employed to develop a high-resolution record of the monsoon history. This research focuses on millennial- and centennial- scale changes during the period 6400-2000 cal. yr BP. Interpretation of the high-resolution record is based on a full understanding of the modern-day analogue of the proxies in the study area. Possible driving mechanisms for changes in the EAM are explored, and links are established on a range of temporal and spatial scales with existing palaeo-climatic records from the region.
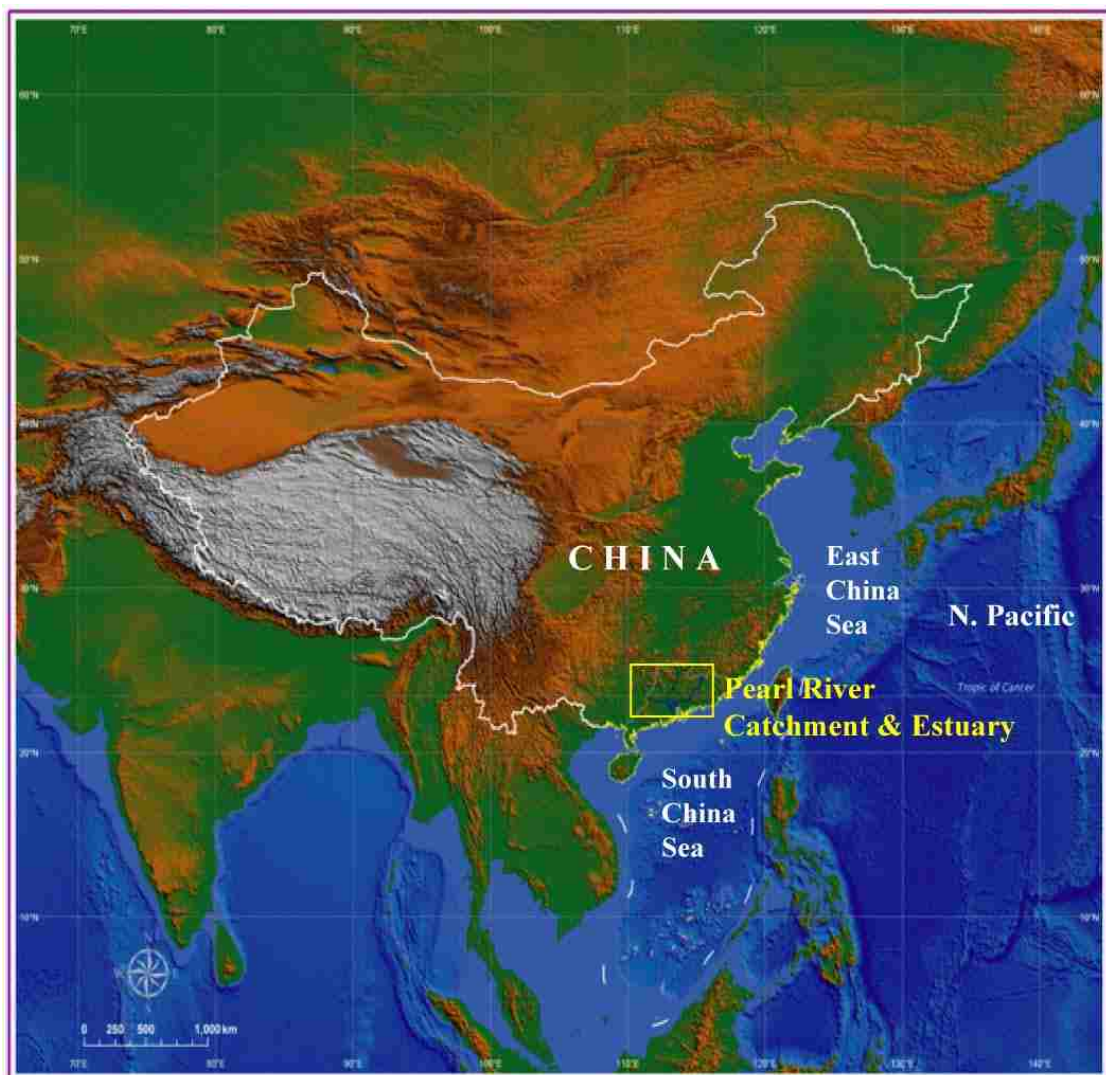
Figure 1.1 Location of the Pearl River estuary in China

This chapter outlines the formation and main characteristics of the EAM today and during the Holocene, and the key roles of the EAM in the climate system globally and

regionally. The rationale of using the Pearl River estuary as an archive for palaeo-monsoonal study is also explained. This chapter also outlines the aims and objectives of this thesis and concludes with an outline of the structure of the thesis.

1.2 Atmospheric and oceanic circulation

The atmospheric circulation is of fundamental importance for determining climate change at both regional and global scales. The unequal heating of the Earth's surface and its atmosphere by solar radiation generates potential energy, some of which is converted into kinetic energy by the rising of warm air and the sinking of cold air, such as the Hadley Cell at the equator and the Polar Cell at the pole area in the Northern Hemisphere (Roger and Chorley, 2003; Figure 1.1a). The Temperate Cell is driven by the Hadley Cell and the Polar Cell due to the different energy gradient between the two cells (Figure 1.1a). However, on a rotating Earth, this ideal three-cell-circulation system is changed due to the Coriolis Effect, which produces deflection to the left of the airflow direction in the Southern Hemisphere and to the right in the Northern Hemisphere (e.g. the Northeast Trade Wind, Roger and Chorley, 2003; Figure 1.1b).

In the East Asian area, this atmospheric circulation system is further complicated by the high-altitude Tibetan Plateau. Perturbations of the thermal and dynamic system of the EAM are produced through generating a high/low-pressure cell above over the Tibetan Plateau during the winter/summer monsoon period. For example, during the winter monsoon, the Tibetan high-pressure cell joins the Siberian High in the North, and generates stronger cold-dry winter wind from the continent. Uplift of the Tibetan Plateau sharpens the pressure gradient between the plateau and its surrounding area, and enhances variability between the summer and winter EAM. Environmental proxies examined in the loess-red clay sequences indicate that an accelerating uplift of the Tibetan Plateau during the period 3.4-2.6 Ma (Liu, 1985) enhanced the monsoon regime. This process also had an impact on global cooling (Vigdorchik, 1980) eventually leading to the development of major Northern Hemisphere glaciations (Emiliani and Geiss, 1959) and aridification of the interior of Asia (Ruddiman and Kutzbach, 1990; Rind and Overpeck, 1993; Rea, 1985; Sun *et al*., 1998). As well as a direct influence on

the climate system through atmospheric circulation, it also influences the climate system indirectly through changing the internal feedback processes, e.g. changing the scale of snow, ice-sheet cover, desert conditions and monsoon effects (O'Hare *et al.*, 2005).
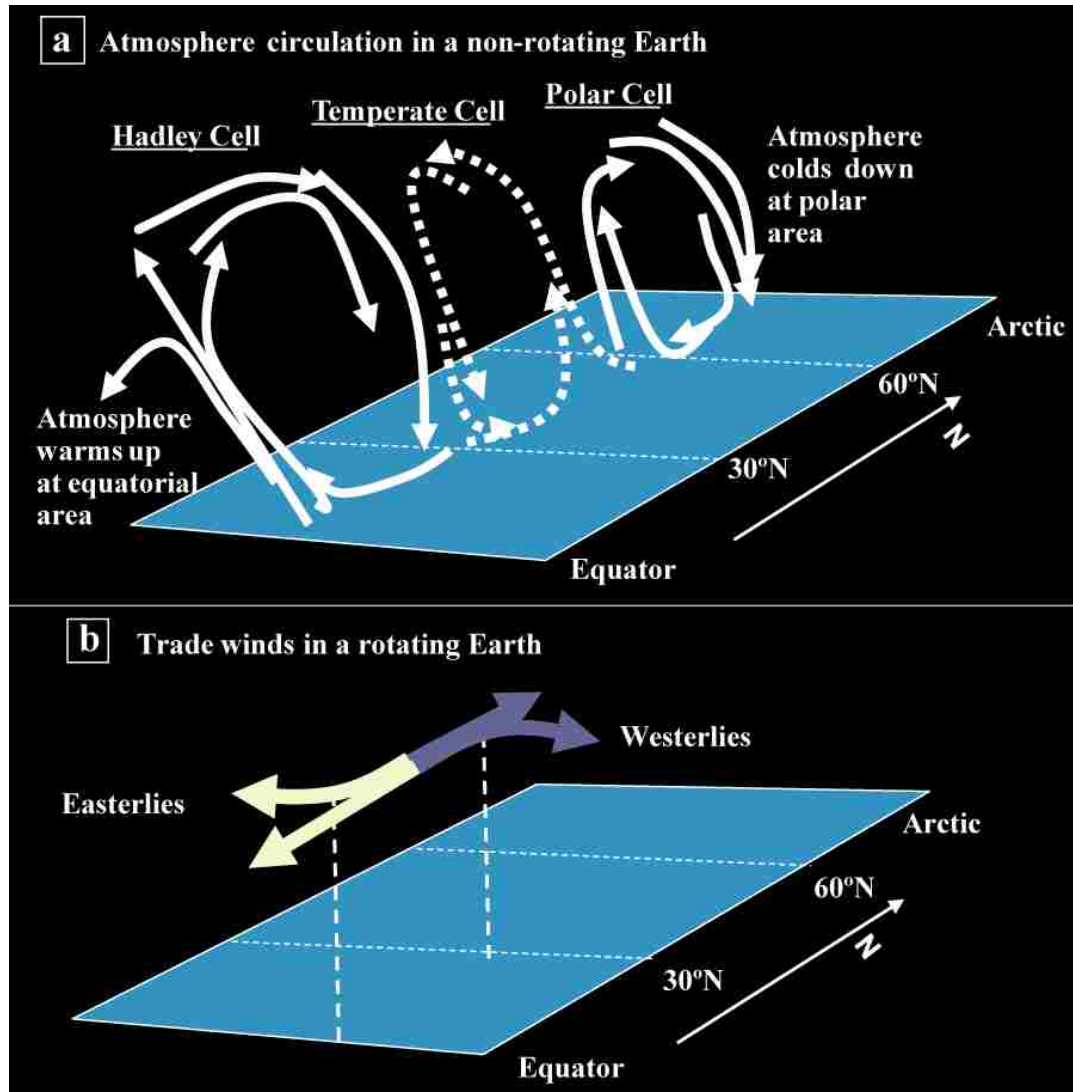
Figure 1.2 Atmosphere circulations in the Northern Hemisphere of a non-rotating Earth (A) and a rotating Earth (B) (after Roger and Chorley, 2003)

Ocean circulation is another important factor that influences climate systems. In the North Pacific area, part of the North Pacific Equatorial Current turns northward and becomes the Kuroshio Current (Figure 1.2a). On its way north, the Kuroshio Current enters the South China Sea, through the Bashi Strait. Another branch of the current enters the East China Sea, East of Taiwan (also known as the Taiwan Warm Current;

4

Figure 1.2a). The strength and changes in position of the Kuroshio Current are influenced by El Nino Southern Oscillation (ENSO) and oscillations of the Intertropical Convergence Zone (ITCZ) (Talley, 1996; Hsueh *et al.*, 1997; Wang, 2005), and are important in the generation of moisture and heat transfer to the East Asian area in summer.

1.3 Formation of the EAM and its main characteristics

The name monsoon is derived from the Arabic word (mausim) which means season, so explaining its application to large-scale seasonal reversals of the wind regime (Roger and Chorley, 2003). The loess-palaeosol record in China constitutes an excellent long-term proxy record for the EAM, and suggests that the EAM may have commenced by least 7.2 Ma ago (Sun *et al.*, 1997, 1998; An, 2000). Locations of the Asian continent and the Indian Ocean, as well as the high-altitude Tibetan Plateau, combines together to produce the monsoon climate. In the northern-hemisphere summers, the rapid warming of the Tibetan Plateau generates a low pressure cell. The northward movement of the solar radiation and the Hadley cell generate the subtropical high pressure cell north to the Western Pacific Warm Pool (WPWP, Figure 1.2a). Prevailing winds over East Asia, lying between these high- and low- pressure cells, are from the southeast, south, and southwest (Figure 1.2a). This wind brings a warm and moist air mass from the Indian Ocean and the Pacific Ocean to the East Asia landmass, and produces a warm and wet summer monsoon. In winter, the intense and rapid cooling over the Tibetan Plateau generates a cold, high pressure cell, the Tibetan High. The Tibetan High joins the Siberia High to the North, and strengthens the Westerlies (Figure 1.2b). As a consequence, prevalent winds over East Asia are from the North and the Northwest, which generates a cold and dry winter monsoon. Annually, the EAM is composed of a cold and dry winter monsoon and a warm and humid summer monsoon (Gao *et al.*, 1962). From a longer term perspective, variability of the EAM can be considered as the alteration between a cold-dry interval (strong winter monsoon) and a warm-wet interval (stronger summer monsoon) (Gong and Hameed, 1991; Zhang *et al.*, 1994; Zhang, 1995).
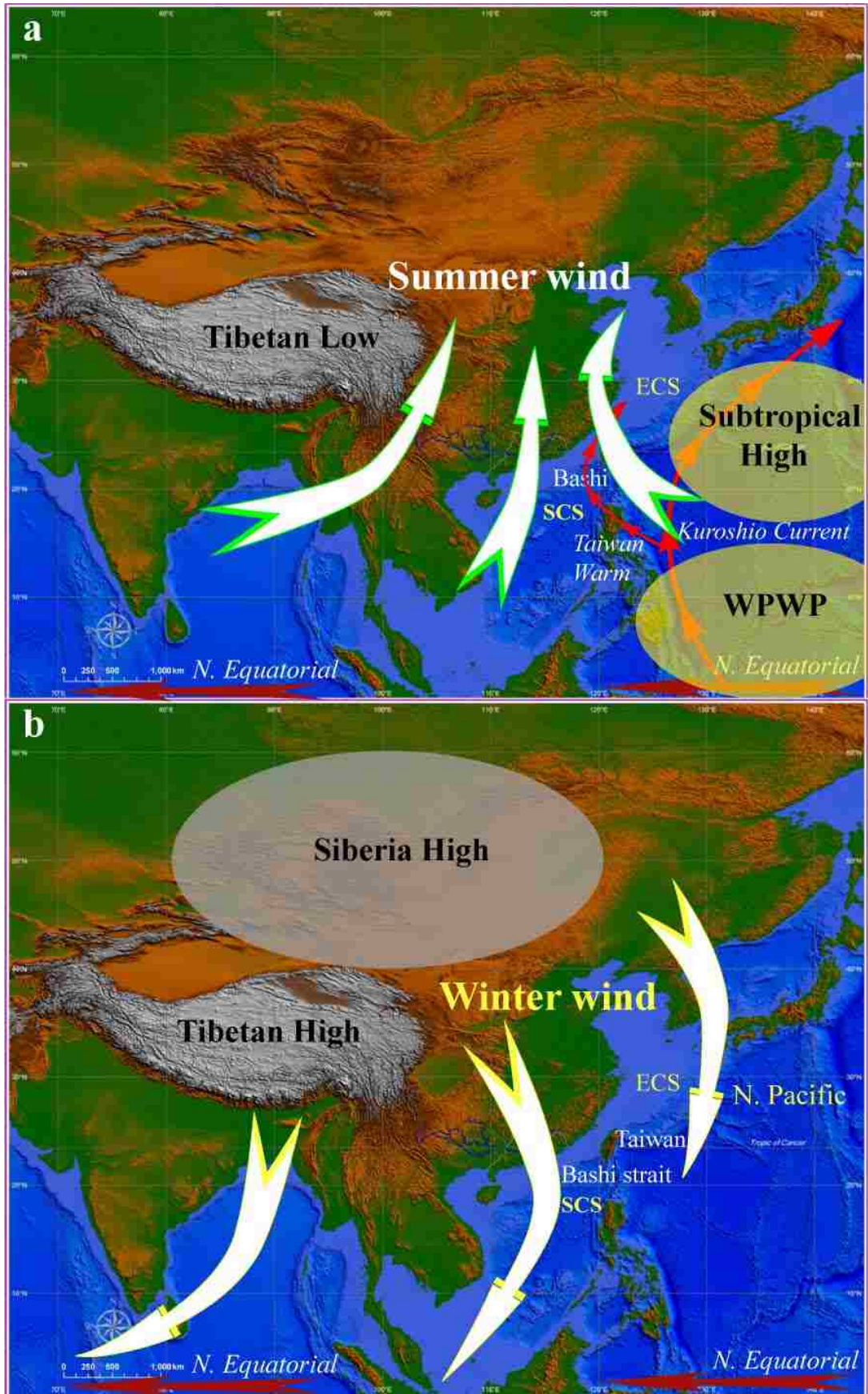
Figure 1.3 Formation of the summer (a) and winter (b) EAM. Red arrows: current flows; White arrows: wind flows.

6

1.4 History of the EAM during the Holocene

The history of the EAM during the Holocene can be regarded as an alteration between dominance of a cold-dry winter monsoon and a warm-wet summer monsoon (An, 2000). After the Younger Dryas (11 200-10 000 cal. yr BP), a cold period which might have included some dry/wet oscillations (Zhou *et al.*, 1996, 1997, 1998; Xiao *et al.*, 1998), the EAM switched to a relatively warm and wet period, the Holocene (after 10 000 cal. yr BP). Monsoonal climate during the Holocene has experienced a general weakening trend (e.g. reducing precipitation since early Holocene), with fluctuations revealed by a range of proxies such as the Loess deposit in central China (e.g. An, 2000) and the stalagmite record from Dongge Cave, southern China (Wang *et al.*, 2005). Zong *et al.* (2006) examined the bulk organic carbon isotopic record from the Pearl River estuary and suggested a strong freshwater flux during 8000-6000 cal. yr BP induced by a strong summer monsoon. From 6000 cal yr BP, the monsoonal freshwater discharge has reduced in magnitude gradually with fluctuations towards the present (Zong *et al.*, 2006).

Based on evidence from ice cores (e.g. Thompson *et al.*, 1989, 2002), lake water levels (e.g. Wang, 1991; Li *et al.*, 1990), as well as archaeological records (e.g. Zhou, 1991), Shi *et al* (1994) suggested that the Holocene Megathermal phases mainly occurred during 8500-3000 cal. yr BP, and they divided the Holocene EAM into several phases: 8500-7200 yr BP is an unstable temperature fluctuation phase with an increase in precipitation; 7200-6000 yr BP was a stable, warm and wet phase when the monsoon rainfall occurred almost throughout China; 6000-5000 yr BP was characterized by strong climatic fluctuation and adverse environment; after 5000 yr BP, the climate became warm and suitable for culture development in China; Around 4000 yr BP, the climate deteriorated and catastrophic floods occurred in East China; from 4000 to 3000 yr BP, the climate was warm and humid. Based on geological data and numerical modelling, An *et al.* (2000) suggested that the front of the EAM retreated from north to south China during the Holocene. This resulted in the Holocene Optimum, a period of maximum precipitation, occurring earlier in the north and northeast of China and later in the south and southeast. Variability of the Holocene EAM has also been reported from different archives, including historical records (e.g. Zhu, 1973; Zhang *et al.*, 1995) and

natural records, such as tree rings (e.g. Wu *et al*., 1988; Wu, 1992), ice cores (Thompson, *et al*., 1989), stalagmites (Wang *et al*. 2005), and loess deposits (e.g. Porter and An, 1995; An *et al*., 2000). Changes in the palaeo-EAM reflect interactions between the global atmosphere, ocean, land and ice systems, and are also an expression of their combined effect within the boundary conditions imposed by the East Asian continent and solar radiation (An, 2000).

1.5 Thesis aims and objectives

This research has two broad aims:

1. To investigate and further develop an estuarine proxy for monsoon reconstruction;
2. To reconstruct monsoon variability at a centennial to millennial resolution from the mid- to late-Holocene from the Pearl River estuary.

Major objectives of the research are as follows:

1. Collection of an extensive modern-day training set of material (surface sediments, suspended sediments, plants and soil) from across the Pearl River estuary from the freshwater catchment to fully marine environments for organic carbon isotope and elements analysis. This will expand preliminary investigations on the bulk organic δ^{13}C and C/N from the Pearl River estuary by Zong *et al*. (2006).
2. Investigation of the spatial signature of bulk organic δ^{13}C and C/N to investigate the sources of organic carbon. This will allow an assessment of the potential of this measure as a proxy for variations in monsoon driven freshwater flux through time.
3. Investigation of the spatial concentration of key elements to investigate the sources and sedimentation environment of the sediment. This will allow an assessment of the potential of this measure as a proxy for variations in monsoon-driven freshwater flux through time, which will help develop a multi-proxy study.

4. Collection of an undisturbed fossil core of high resolution from the Pearl River estuary. This will provide an archive to reconstruct changes of the palaeo-monsoon.

5. Analysis of the signature of organic carbon isotopes and key elements of the estuarine core to reconstruct monsoon-driven freshwater flux into the estuary through the mid- and late-Holocene. This will allow an investigation on possible driving mechanisms for the monsoonal changes at millennial- and centennial- timescales.

1.6 Thesis structure

Chapter 1 outlines the main focus of this thesis and some background knowledge of this study. It introduces basic atmospheric and oceanographic circulation systems, formation of the EAM and its main features, monsoonal history during the Holocene, and the importance of the EAM variability in a global and regional context. The aim and objectives of this research have been pointed out here.

Chapter 2 reviews previous studies on the EAM history and its possible forcing mechanisms at different time scales using different proxies. Also this chapter examines proxies used for the palaeo-EAM reconstruction, specifically application of two geochemical proxies (bulk organic carbon isotopes and C/N, and key metals) as indicators for the palaeo-environmental changes.

Chapter 3 presents situations of the Pearl River delta and estuary e.g. geological and hydrological conditions, and its suitability as for this specific research. This chapter also explains how the Pearl River estuary works as an archive for the reconstruction of the EAM history.

Chapter 4 shows methods of the data collection and data analysis for this research.

Chapter 5 demonstrates the modern-day data of the two proxies, and their indication for changes of sediment sources related to other studies.

Chapter 6 described results for the two proxies from the fossil sediment (core UV1), reconstruction of the history of the EAM during the mid Holocene, and comparisons of the results from the Pearl River estuary with those from previous studies.

Chapter 7 concludes main results and discussions of this thesis, acknowledgment of thesis limitations, as well as suggestions about possible future works for this project.

Chapter 2 Literature Review

2.1 Introduction

This chapter reviews the published literature in two broad areas of research: (1) possible driving mechanisms for EAM variations during the Holocene; and (2) proxies used for the EAM reconstruction. After a brief introduction on a range of proxies used for monsoonal change, this chapter reviews applications of bulk organic $\delta^{13}C$ and C/N and selected key elements (to a lesser extent) for EAM reconstruction, as these two proxies are employed by this study. Bulk organic $\delta^{13}C$ and C/N are the main proxies for this study, and more details of them are reviewed in this chapter, compared to selected metals. They are also discussed to a further extent than metals in Chapter 5 and 6. This chapter also points out research gaps that will be filled in this research.

2.2 Possible driving mechanisms for the EAM variability

Generally, the EAM history during the Holocene can be regarded as an alternation between dominantly cold-dry winter monsoons and warm-wet summer monsoons (An, 2000). Possible driving mechanisms behind the variability at different timescales include Milankovitch cycles, solar forcing, and regional forcing such as the El Nino Southern Oscillation (ENSO) and high-latitude cooling events.

2.2.1 Milankovitch cycles

Changes in the Earth's orbit and axis occur in respect of the eccentricity of the orbit (due to planetary gravitational influences), the obliquity of the ecliptic (due to the tilt of the Earth's axis) and the precession of the equinoxes (due to the gravitational pull exerted by the sun and the moon). Influences of these changes on the climate are known as orbital forcing. Orbital forcing affects the distribution of solar radiation at

different latitudes and at different times with a general periodicity at 100ka, 42ka and 21ka, which is also known as the Milankovitch cycles (Lowe and Walker, 1997). Comparison of palaeo-climate data with the Milankovitch cycles has led to the widespread view that orbital forcing can be considered as the primary driving mechanism in Quaternary climate changes (Imbrie *et al*., 1992, 1993; Lowe and Walker, 1997). Alternation between the dry and wet (or cold and warm) domains of the EAM history responding to orbital forcing, especially precession, has been clearly revealed by a variety of records. The magnetic susceptibility of the Chinese loess reveals cycles corresponding to the orbital periodicities, including 100ka, 41ka, 23ka and 19ka (Kukla *et al*., 1990; Ding *et al*., 1994). Those at 23ka and 19ka are suggested to be two separate interlocked cycles, instead of the 21ka cycle, for the precession of the equinoxes (Lowe and Walker, 1997). This record closely parallels the oxygen isotope record in the ocean (e.g. Kukla, 1987). Based on the comparison of the magnetic susceptibility of the Xifeng loess with the SPECMAP 84 record (Imbrie *et al*., I984), Kukla (1987) suggests a model of episodic increases and decreases of the 100 ka interval of the dry-cold and wet-warm cycles over the entire 2.5 Ma length of the loess record. Similar records are obtained from Lake Baikal, northern East Asian (Colman *et al*., 1995; Williams *et al*., 1997), where spectral analysis has also suggested a strong nonlinear 100ka rhythm.

High-resolution studies present millennial and centennial-timescale fluctuations superimposed on the orbital periodicity in the EAM, and argue that the EAM is also perturbed by other external and internal driving mechanisms (Porter and An, 1995; Wang *et al*, 2005). Forcing mechanisms for such shorter-term (from decadal to millennial time scale) climate change has, therefore, attracted much attention during recent decades (e.g. Thompson *et al*., 1989; Bond *et al*, 2001; Wang *et al*., 2005).

2.2.2 Solar forcing

Studies have suggested that solar forcing is an important driving mechanism for climate changes during the last millennium. Lamb (1965) was the first to articulate that the Medieval Warm Period (MWP) (500-1500 A.D.) centring around 1100-1200 A.D. (High Medieval, Bradley *et al*., 2003), was warm or warmer than normal mean (1931-1960). The MWP was followed by the Little Ice Age (LIA) (1400-1900 A.D.)

characterized by cooler conditions than normal mean (Crowly, 2000; Bradley *et al.*, 2003; Moberg *et al.*, 2005; Ji *et al.*, 2009). Recent studies compared the mean temperature of the Northern Hemisphere with the solar activity and suggest that solar irradiance forcing is a possible explanation for the anomalously warm conditions during the MWP (e.g. Mann *et al.*, 1999; Widmann and Tett, 2003) and the cold conditions during the LIA (e.g. Shindell *et al.*, 2001). During the MWP enhanced solar irradiance led to increased ultraviolet absorption by ozone, warming the stratosphere (Bradely *et al.*, 2003). This warming altered circulation patterns in the atmosphere below. It is possible that the MWP in Northern and Western Europe was associated with the Arctic Oscillation (AO)/North Atlantic Oscillation (NAO) (Shindell *et al.*, 2001; Bradley *et al.*, 2003) driven by the enhanced solar irradiance during the 12th century (Bard *et al.*, 2000). A minimum in solar irradiance, the Maunder Minimum, is thought to have occurred from the mid-17th to early 18th centuries (Shindell *et al.*, 2001). Accordingly, surface temperatures appear to have been at or near their lowest values of the past millennium in the Northern Hemisphere (Shindell *et al.*, 2001). Reduced solar irradiance during the Maunder Minimum has been shown to be the most important forcing for the LIA (e.g. Crowly, 2000; Shindell *et al.*, 2001). The low temperature in the Northern Hemisphere during the Maunder Minimum has been shown to be related to a change in the AO/NAO, which in return is driven by the meridional temperature gradient (Widmann and Tett, 2003).

Solar forcing is particularly important for climate change during the Quaternary. Denton and Karlén (1973) first suggested that Holocene glacier and climatic fluctuations were caused by solar variation which actually fitted within a regular millennial-scale pattern of about 2500 yrs. However this concept was not widely accepted because oxygen isotope and methane records from Greenland ice cores show no evidence of this pattern during the Holocene, except for a brief cooling about 8.2 ka ago. O'Brien *et al.* (1995) demonstrated from measurements of soluble impurities in Greenland ice that Holocene atmospheric circulation above the ice cap was punctuated by a series of millennial-scale shifts. The most prominent of these shifts appeared to correlate with the cycles identified by Denton and Karlen (1973). Bond *et al.* (1997) identified a '1500-year cycle' in the ice-rafted debris (IRD) events from the North Atlantic deep sea cores and related it to insolation changes. Cycles of similar length have been reported from many low-latitude archives. Peat cellulose $\delta^{13}C$ records (Hong

et al., 2001) from North-eastern China identified two relatively wet and cold periods (before 2200 BC and after 1200 AD respectively) and eight drought episodes over the last 6000 years. Comparing this with $\delta^{18}O$ from peat cellulose and ^{14}C from tree rings, Hong *et al.* (2001) suggest that on decadal- to centennial- timescales, the climate events are correlated to changes in solar irradiation and solar periodicities. The decadal to centennial timescale cycles are also recorded by changes in the mean grain size of sediments from the Yangtze River estuary (Xiao *et al.*, 2006), where great coherence was found in the secular variation curves of mean grain size and the number of sun spots. Spectral analysis of the mean grain size in Xiao *et al.*'s work (2006) also identifies two significant periodicities at millennial timescales of 2463 years and 1368 years. The cycle of 2463 years is statistically similar to the 2560 year cycle from the Okinawa Trough (Jian *et al.*, 2000) and a cycle of around 2500 years identified from the Camp Century ice core (Dansgaard *et al.*, 1984). The cycle of 1368 years corresponds with the North Atlantic '1500-year' cycle (Bond *et al.*, 1997), and is suggested to be driven by insolation changes. History of the EAM during the past 9000 yrs from the oxygen isotopic record from the Dongge Cave, southern China, broadly follows summer insolation, which is punctuated by eight weak monsoon events lasting ~1 to 5 centuries (Wang *et al.*, 2005). Cross correlation of the decadal- to centennial- oxygen isotopic record with the atmospheric ^{14}C record shows that some, but not all, of the monsoon variability at these frequencies results from changes in solar output (Wang *et al.*, 2005).

However, because the absolute changes in solar intensity over the timescale of decades to millennia are small (Flige and Solanki, 1999) and the influence of the solar flux on climate is not well understood, it is at present unclear how the insolation changes affect the EAM. One possible process is that the reducing insolation leads to changes in oceanic and atmospheric circulation (Xiao *et al.*, 2006). One of the results of these processes is that temperature variations between the landmass and the Indian Ocean become larger during the winter, which again generates a strong winter EAM (Xiao *et al.*, 2006). It is possible that ice volumes in high-latitude Northern Hemisphere areaa expand during periods of reduced solar intensity, which enhance the Siberian high in winter (Porter and An, 1995; An, 2000; Wang *et al.*, 2001, 2005) leading to strengthening of the winter EAM.

2.2.3 Regional forcing

Teleconnections between the EAM and high-latitude cooling events have been reported by previous studies. It is possible that ice volumes in the high-latitude areas expand, enhancing the Siberian high in winter (Porter and An, 1995; An, 2000; Wang *et al.*, 2001, 2005) and strengthening the winter EAM. Thompson *et al.* (1989) reported high dust intensity during the Last Glacial Stage in the Dunde Ice Core from Qinghai-Tibetan Plateau, Southwest China, responding to the expanded continental ice sheet in the higher latitudes. They pointed out that high-latitude cooling enhanced the wind strength causing the loess deposits to extend to the Pacific Basin (Rea *et al.*, 1995) and most likely to the North America (Thompson *et al.*, 1989). Bond *et al.* (1997) analysed two cores from the North Atlantic and suggested that the ice-rafted debris (IRD) events exhibit a distinct packing on millennial scales, with peaks at about 1400, 2800, 4200, 5900 8100, 9400, 10,300 and 11,100 years ago. Analysis of a stalagmite record from Dongge Cave (Wang *et al.*, 2005), Southern China, suggests that the Holocene EAM is punctuated by eight weakened monsoon events lasting ~1 to 5 centuries, which have been suggested to be correlated with North Atlantic ice-rafting events (Bond *et al.*, 1997).

The strength of the summer monsoon is significantly influenced by the magnitudes of both the sea surface temperature (SST) of the Western Pacific Warm Pool and the strength of the Kuroshio warm current. On a decadal time scale, the SST of the Western Pacific Warm Pool and the Kuroshio warm current could be lowered by low latitude cooling events, such as the 'volcanic winter' caused by huge volcanic eruptions in Indonesia and the Philippines (Rampino *et al.*, 1979; Rampino and Self, 1992; Kerr, 1996; Zielinski *et al.,* 1996; Bühring and Sarnthein, 2000).

Low latitude oceans may influence the precipitation distribution in East Asia, for example, the ENSO can lead to increased precipitation in East Asia by cross-equatorial flow (De Deckker *et al.*, 1991; An, 2000). In La Nina years, the Equatorial Easterlies push warm surface water towards the source area of the EAM, and in turn, this helps to increase the production of moisture. However, it is also reported that in strong La Nina years, heavy rainfall may take place over the area of the Western Pacific Warm Pool, instead of more moisture being transported to East Asia.

2.3 Proxies for the EAM reconstruction

2.3.1 A brief overview of the range of proxies used for monsoon reconstruction

To explore possible forcing for the monsoonal climate changes, a range of proxies are employed for monsoon reconstruction, including proxies derived from terrestrial and marine areas. Proxies derived from the terrestrial area include Chinese loess, ice cores, speleothems, tree rings and evidence of fluctuating lake levels. Loess records long-term monsoonal variability during the past, for example, the magnetic susceptibility analysis of loess deposits has shown clear monsoonal climate cycles driven by orbital forcing during the past 2.5 Ma (Ding *et al*., 1993; 1994). However, loess does not usually support high-resolution studies because of the low sedimentation rate. Ice cores also preserve long-term climate change, especially ice cores from high-latitude areas. For example, ice cores from the Antarctic and the Greenland provide relatively high-resolution records of long-term climate changes, e.g. the GRIP ice core from Greenland and the Vostok ice cores from Antarctica reconstruct global climate change during the past 160,000 years (Peel, 1994). However, records from ice cores from the high-altitude Tibetan Plateau for EAM study, such as the Dunde ice cap and the Guliya ice cap from the Tibetan Plateau and the Dasuopu Glacier in the Chinese Himalaya are limited to the last 25,000 years (Thompson *et al*., 2003). There are other problems for the ice core record; for example, the $\delta^{18}O$ from the ice core might be influenced by other factors such as precipitation; dust content reflecting aeolian activity is difficult to analyse, high-resolution samples are technically difficult to obtain (Lowe and Walker, 1997). Speleothems has become an important proxy for high-resolution study in the last decade (e.g. Wang *et al*., 2001; Wang *et al*., 2005; Hu *et al*., 2008). Speleothems from Dongge Cave, southern China suggest that solar forcing is responsible for monsoonal variability and teleconnections between the EAM and high-latitude cooling events at the decadal- to centennial- timescale. However, $\delta^{18}O$ of speleothems might be influenced by either monsoonal rainfall or temperature changes, or both. The certainty of correlation between stalagmite $\delta^{18}O$ and monsoonal rainfall (Wang *et al*., 2005) still needs further investigation. Tree rings and lake-level changes are also employed to indicate past temperature changes (e.g. Fan *et al*., 2009). Lake-level changes from low-latitude areas are thought to reflect major changes in precipitation regimes (e.g.

Kershaw, 1994; Van der Hammen and Absy, 1994). Lake-level changes in the western China are mainly influenced by melting snow related to temperature changes (e.g. Yu *et al.*, 2007), although they might also be influenced by sea-level changes for lakes from the eastern China (Shi *et al.*, 1994). Pollen records from Maar lakes in southern China (e.g. Lu *et al.*, 2003; Zheng *et al.*, 1999) are useful as indicators of monsoon climate and vegetation changes in this area.

Proxies derived from marine areas mainly involve microfossils such as foraminifera and diatoms from marine deposits. Foraminifera and diatom assemblages have been well established as indicators for reconstruction of coastal environmental changes (e.g. Kim and Kucera, 2000; Wang and Chappell, 2001). The $\delta^{18}O$ of planktonic foraminifera and diatoms can be used to indicate surface temperature changes (e.g. Kienast *et al.*, 2001). Recent studies also use Mg/Ca of foraminifers to reconstruct palaeo-temperature changes (e.g. Lea *et al.*, 2000). However, microfossils might be poorly preserved in some areas. Coral records from coastal areas have been helpful for high-resolution studies, indicating especially the sea surface temperature changes relating to climate changes relating, for example, to ENSO (e.g. Tudhope *et al.*, 2001; Woodroffe *et al.*, 2003).

2.3.2 Proxies used for this study – bulk organic δ^{13}C and C/N and key elements

This study employs bulk organic carbon isotopes and key elements to reconstruct EAM history from an estuarine archive. It is based on the assumption that organic matter preserved in an estuarine environment includes terrestrial organic matter delivered by freshwater runoff, marine organic matter delivered by tides and *in situ* brackish-water organic matter (Figure 3.5; section 3.9 in Chapter 3). The proportion of different sources of sediment preserved in the estuary was mainly controlled by the freshwater flux when the relative mean sea-level was stable (Zong, 2004; section 3.9 in Chapter 3). For example, the estuarine sediment is dominated by the terrigenous sediment under the strong summer monsoon conditions, when the freshwater flux was strong, and vice versa. Bulk organic δ^{13}C and C/N and concentration of selected elements of sediment vary between different sources, and thus could be used to indicate sources of the dominant organic matter relating to strength of the freshwater flux (Chapter 3). This section reviews definitions, variability of their values between different sources of sediment and application of these two proxies for environmental changes.

1) Bulk organic carbon isotope (δ^{13}C) and C/N

This study employs bulk organic δ^{13}C and C/N as the main proxies for reconstruction of the monsoonal variability during the mid-Holocene. One of the objectives of this study is to collect an extensive modern-day set of material (surface sediments, suspended sediments, plants and soil) from across the Pearl River estuary from the freshwater catchment to fully marine environments for organic carbon isotope and elements analysis. This will expand the preliminary investigations of bulk organic δ^{13}C and C/N from the Pearl River estuary by Zong *et al.* (2006). This section reviews definitions of the bulk organic δ^{13}C and C/N, their variability between different types of plants and their indication value as palaeo-climate changes. More attention is paid to bulk organic δ^{13}C and C/N than key elements in this chapter, and also discussions in Chapter 5 and 6 will focus more on bulk organic δ^{13}C and C/N than on selected elements.

Expression of isotopic composition and isotope fractionation

The use of carbon isotopes as a proxy for environmental change tends to focus on the ratio of ^{13}C to ^{12}C. Atmospheric carbon dioxide contains about 1.1% of the heavier carbon isotope ^{13}C and 98.9% of the lighter isotope ^{12}C (O'Leary, 1992). During the CO_2 fixation process of photosynthesis, plants preferentially take up ^{12}C by diffusion, resulting in organic matter depleted in ^{13}C compared to the atmosphere (Wickman, 1952; Craig, 1953; Park and Epstein, 1960). Plants discriminate against ^{13}C during photosynthesis in a number of ways which reflect plant metabolism and environment (O'Leary, 1992). The isotopic composition of plant carbon is expressed as the carbon-13 abundance ratio R:

$$R = {}^{13}C/{}^{12}C \qquad (1)$$

However, the absolute values of isotopic ratios are difficult to obtain. In plant physiology and geochemistry applications, isotopic ratios are usually expressed as a $\delta^{13}C$ values to some standard, in units of per thousand (‰):

$$\delta^{13}C \ (‰) = \left[\frac{R(sample)}{R(s\tan dard)} - 1 \right] \times 1000 \qquad (2)$$

The international carbonate standard in use is the (V)PDB (belemnite from the (Vienna) Pee Dee Formation), and the $\delta^{13}C_{VPDB}$ = 0.0112372. Organic matter is invariably depleted in ^{13}C relative to VPDB, so $\delta^{13}C$ values of organic material are negative.

The weight ratio of organic carbon to total nitrogen (C/N) is usually measured alongside $\delta^{13}C$ and can help to distinguish carbon sources:

$$C/N = total \ organic \ carbon \ / \ total \ nitrogen \qquad (3)$$

Plants use different photosynthetic pathways to fix CO_2, and show remarkably different $\delta^{13}C$ values (Figure 2.1). Values of the C/N ratio are largely controlled by the content of nitrogen in different types of plants. Organic matter dominated by a high-nitrogen content has a relatively low C/N ratio, e.g. plankton and plants high in fibre, whereas

organic matter with a low-nitrogen content has a relatively high C/N ratio, e.g. vascular plants (Figure 2.1).
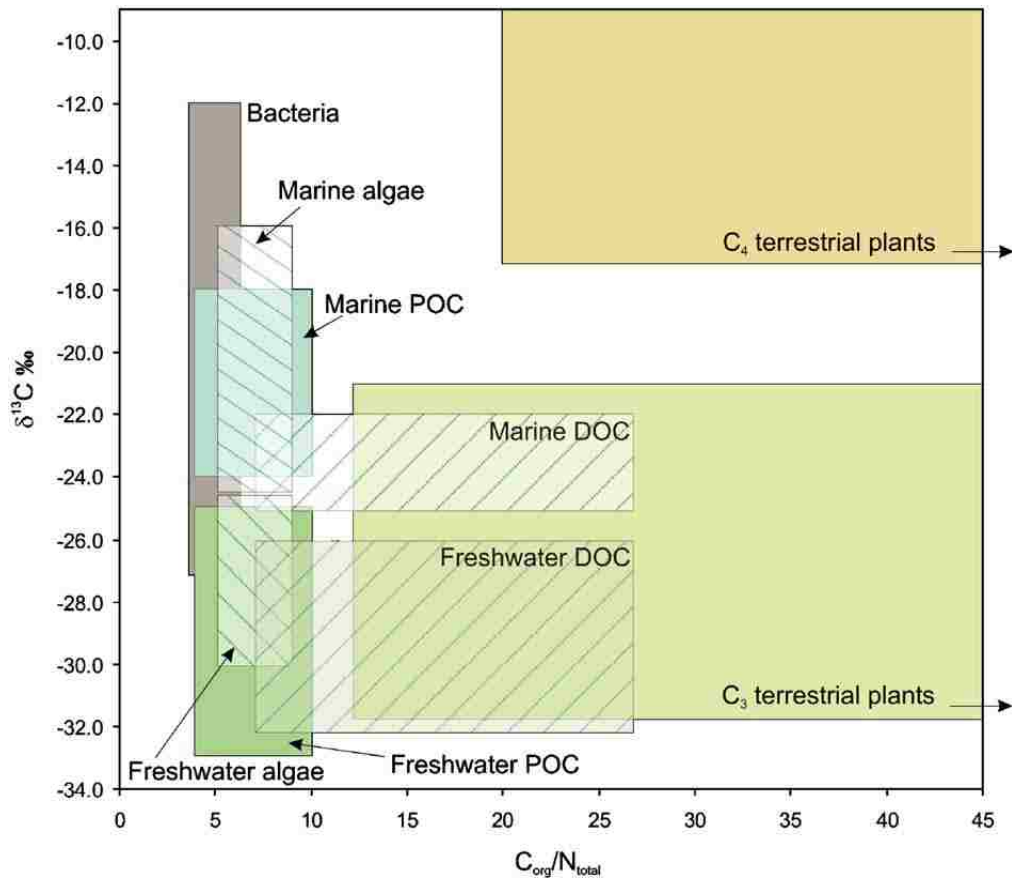
Figure 2.1 Typical $\delta^{13}C$ and C/N ranges for organic input to coastal environments (from Lamb *et al*., 2006). POC: particulate organic carbon; DOC: dissolved organic carbon.

Carbon isotopic values ($\delta^{13}C$) and C/N ratios of different sources of organic matter

This section reviews how mechanisms of photosynthesis influence $\delta^{13}C$ and C/N of different types of organic matter and how $\delta^{13}C$ and C/N vary between different sources of organic matter preserved in coastal areas. Nier and his co-workers were the first to indicate that there might be large variations in the $^{12}C/^{13}C$ of plants (Nier and Gulbransen, 1939; Murphey and Nier, 1941). This assumption was instantly confirmed by Rankama (1948), although only based on seven plant samples, and was further confirmed by Wickman (1952) with more samples. Wickman (1952) referred variations in the $\delta^{13}C$ in plants to the cycle of carbon dioxide in different environments of the plants. Craig (1953) compared the carbon isotopic signature of several hundred terrestrial plants. However, most of them were around –27‰, with only one grass sample with a value of –12‰. In a subsequent paper, Craig (1954) explained variations of carbon isotopic values in different plants controlled by CO_2 diffusion, which was later confirmed by Park and Epstein (1960).

Kortschak *et al.* (1965) and Hatch and Slack (1970) made the variation in isotopic values of different plants clearer by the identification of different photosynthetic pathways and grouped plants into C_3 and C_4 plants based on this pathway. Plants that use the C_3 photosynthetic pathway, incorporating CO_2 from the atmosphere by carboxylation of ribulose bisphosphate, typically have $\delta^{13}C$ values between -32‰ and -21‰ (Craig, 1953; Dennis, 1980) due to the light $\delta^{13}C$ of the atmospheric carbon. Many terrestrial plants use the C_3 photosynthetic pathway, constituting about 90% of all plants (Lamb *et al.*, 2006), and result in the typical light $\delta^{13}C$ values of terrestrial plants. C_4 plants incorporate CO_2 by the carboxylation of phosphoenol pyruvate (Kortschak *et al.*, 1965; Hatch and Slack, 1970), using dissolved inorganic carbon (e.g. phytoplankton). This pathway produces much less negative $\delta^{13}C$ values than the C_3 pathway, ranging from –17‰ to –9‰ (Bender, 1971; Smith and Epstein, 1970; Fontugne and Duplessy, 1978; Dennis, 1980). There is one further group, CAM plants, which uses a crassulacean acid metabolism (CAM) photosynthetic pathway during the photosynthesis. CAM plants fix atmospheric CO_2 by either the C_3 pathway or a C_4-like pathway (Osmond, 1978), resulting in a wide range of $\delta^{13}C$ values from –11‰ to –28‰ (Bender, 1971; Schleser, 1995), depending on which pathway is dominant. Plants that have adapted to tolerate very saline conditions are commonly of C_4 or CAM type (Lamb

et al., 2006). Because they are further evolved than C_3 plants and are more tolerant to difficult environments. $\delta^{13}C$ values of different types of organic matter are summarized in Table 2.1.

Based on the physiological characteristics of C_3 and C_4 grasses, there is differentiation of these two photosynthetic types in the Earth's vegetation. C_4 plants, particularly perennials, are more prevalent than C_3 plants in subtropical savannahs and grasslands with summer rains. In contrast, the main distribution area of the C_3 grasses (often annuals) is in the cold steppes. In subtropical arid climates, annual plants with C_4 metabolism are not in any way superior to C_3 plants. Rather they are inferior, whilst high precipitation C_4 perennial grasses dominate over C_3 grass. The CAM plants (e.g. the succulents) are mainly distributed in coastal deserts with cool nights (South Africa and Namibia, Chile, Baja, California, Tenerrite). The CAM plants are of rather secondary importance in comparison to C_4 plants regarding the C cycle of the earth. In the Pearl River catchment, C_3 plants are the dominant plant type at present as the regional vegetation is dominated by evergreen-broadleaf trees. Pollen records from the Huguangyan Maar Lake in the Leizhou Peninsula, southern China suggest that forests have been the dominant vegetation type since before the last glaciations, even during the coldest epoch around 27,000-24,000 cal. yr BP (Lu *et al*., 2003).

Table 2.1 A summary of $\delta^{13}C$ and C/N of different types of organic matter from literatures

Organic matter	Type	$\delta^{13}C$ (‰)	Data source	Reason	C/N	Data source	Reason
Terrestrial plants	C_3	-32 - -21	Craig, 1953; Dennis, 1980	C_3 plants use the C_3 photosynthetic pathway during photosythesis process	>12		
	C_4	-17 - -9	Bender, 1971; Smith and Epstein, 1970; Fontugne and Duplessy, 1978; Dennis, 1980	C_4 plants use the C_4 photosynthetic pathway during photosythesis process	>30	Prahl et al., 1980; Tyson, 1995	Lignin and cellulose, the predominant components of terrestrial vegetation, are nitrogen poor, especailly C_4 grasses. Plant C/N values can be highly variable in a small area mostly due to large fluctuations in the nitrogen content of plants.
	CAM	-11 - -28	Bender, 1971; Schleser, 1995	CAM plants fix atmospheric CO_2 by either the C_3 pathway or a C_4-like pathway	>12		
Aquatic plants	Freshwater	-50 - -11	Osmond et al., 1981	Concentration of HCO_3^- in marine environments is higher than in the freshwater environment	5-7	Meyers, 1994; Tyson, 1995	Aquatic plants are nitrogen rich
	Marine	-17 - -9	Deines, 1980				
POC	Terrestrial-origin	-33 - -25	Salomons and Mook, 1981; Barth et al., 1998; Middelburg and Nieuwenhuize, 1998	The terrestrial organic matter is richer in cellulose and is more difficult to degrade microbially than that of marine-origin organic matter	<8	Bordovsky, 1965	Aquatic plants are nitrogen rich
	C_3 and C_4 plants-mixed fluvial-origin	-26.5 - -23.2	Liu et al., 2003				
	Mairne-origin	-21 - -18	Peters et al., 1978; Wada et al., 1987; Middelburg and Nieuwenhuize, 1998				
Algae	Freshwater	-30 - -26	Schidlowski et al., 1983; Meyers, 1994	Influenced by types of the dominant plant in their origins	4-10	Meyers, 1994	Algae and bacteria contain a high level of labile compounds and decompose more rapidly than vascular plants
	Marine	-23 - -16	Haines, 1976; Meyers, 1994				
Bacteria	Coastal environments	-27 - -12	Coffin et al., 1989				

Depending on environment, aquatic plants can have a distinctive $\delta^{13}C$ signature. During photosynthesis, aquatic plants utilise bicarbonate (HCO_3^-) if the dissolved CO_2 is exhausted (Degens *et al.*, 1968). As dissolved CO_2 (–8‰, if in equilibrium with atmospheric CO_2) has lower $\delta^{13}C$ values than HCO_3^- (~0‰) (Keeley and Sandquist, 1992), and the concentration of HCO_3^- in marine environments is higher than in the freshwater environment, marine aquatic plants have higher $\delta^{13}C$ than freshwater aquatic plants (Lamb, *et al.*, 2006). Freshwater aquatic plants have $\delta^{13}C$ values ranging from –50‰ to –11‰ (Osmond *et al.*, 1981; Keeley and Sandquist, 1992). Marine aquatic plants have $\delta^{13}C$ values similar to the C_4 plants, ranging from –17‰ to –9‰ (Deines, 1980)

Another important component of carbon in aquatic environments is particulate organic carbon. Particulate organic carbon (POC) is suspended organic matter, including phytoplankton and zooplankton. It is the major component of the suspended organic matter (SOM) in estuaries and near continental shelf areas and it is a mixture of organic matter derived from both continental and marine sources (Fontugne and Jouanneu, 1987). The terrestrial organic matter is composed of both natural (e.g. plant fragments) and anthropogenic (e.g. sewage) origin (Lamb *et al.*, 2006). This type of organic matter is richer in cellulose and is more difficult to degrade microbially than that of marine-origin (Fontugne and Jouanneu, 1987). Terrestrial-origin $\delta^{13}C_{POC}$ values ($\delta^{13}C$ of particulate organic carbon) range from –33‰ to –25‰, reflecting the prevalence of freshwater phytoplankton and zooplankton, as well as C_3-plant debris (Salomons and Mook, 1981; Barth *et al.*, 1998; Middelburg and Nieuwenhuize, 1998). Slightly higher fluvial $\delta^{13}C_{POC}$ values occur in catchments with a mixture of C_3 and C_4 plants, from –26.5‰ to –23.2‰ (Liu *et al.*, 2003). Marine $\delta^{13}C_{POC}$ values typically range from –21‰ to –18‰ (Peters *et al.*, 1978; Wada *et al.*, 1987; Middelburg and Nieuwenhuize, 1998), reflecting a dominance of marine-origin organic matter, e.g. marine plankton algae (Yamaguchi *et al.*, 2003).

Algae and bacteria, if present in large quantities, have an effect on sedimentary organic carbon isotopic values. Generally, freshwater algae tend to have lighter $\delta^{13}C$ value (from –30‰ to –26‰; Schidlowski *et al.*, 1983; Meyers, 1994) than marine algae (from –23‰ to –16‰; Haines, 1976; Meyer, 1994). Bacteria are typically of low $\delta^{13}C$ value. Coffin *et al.*

(1989) suggested that bacterial $\delta^{13}C$ values could range from $-27‰$ to $-12‰$, depending on their origin, while Cloern *et al.* (2002) suggested that abundance in bacteria is likely to lower sediment $\delta^{13}C$ values in environments that contain some C_4 plants.

The C/N ratio of organic material is also strongly controlled by the source of organic material. Phytoplankton from both freshwater and marine environments has a relatively low C/N ratio of between 5 and 7 (Meyers, 1994; Tyson, 1995), because of their high content of nitrogen. C/N ratios of the marine particulate organic carbon (POC) is typically lower than 8 (Bordovsky, 1965). Total organic carbon to total nitrogen (C/N) ratios of organic matter have often been used to distinguish land plants and algal-origin sedimentary organic matter (e.g. Prahl *et al.*, 1980; Premuzic *et al.*, 1982; Ishiwatari and Uzaki, 1987; Jasper and Gagosian, 1990). Algae typically have C/N ratios between 4 and 10 (Meyers, 1994). Terrestrial vegetation normally has relatively high C/N ratios of >12 (Prahl *et al.*, 1980), as lignin and cellulose, the predominant components of terrestrial vegetation, are nitrogen poor. C_3 vascular plants have C/N ratios of > 12 (Tyson, 1995), whereas C_4 grasses tend to have higher C/N ratios of > 30 (Meyers, 1994). Because of the large variability of the nitrogen content of plants, the C/N ratios can experience a large range within a small area (Lamb *et al.*, 2006). Lamb *et al.* (2006) have summarized ranges of typical $\delta^{13}C$ and C/N ranges of organic input into coastal environments based on previous studies (Figure 2.1). Summarized $\delta^{13}C$ and C/N values for different types of organic matter are shown in Table 2.1 with a brief explanation of differences between them.

Application of the organic carbon isotopes as an indicator for sources of the organic matter in the estuary and coastal areas

As discussed above, organic matter from different sources has a distinctive carbon isotopic value (Hunt, 1968; Meyers, 1994; Lamb *et al.*, 2006; Tesi *et al.*, 2007a, b). Stable carbon isotopes of POC ($\delta^{13}C_{POC}$) can be used to track the distribution of terrigenous organic matter and also the seasonal changes of this distribution within the estuary and the coastal areas (e.g. Fontugne and Jouanneau, 1987; Bianchi *et al.*, 2007; Middelburg and Herman, 2007; Wu *et al.*, 2007; Harmelin-Vivien *et al.*, 2009). Fontugne and Jouanneau (1987) employed carbon isotopes of POC to examine the distribution of terrestrial sediment within the Gironde estuary, Western France, and the terrestrial POC flux into the estuary and the ocean. A good correlation between $\delta^{13}C_{POC}$ values and salinity is observed in their study, indicating a general trend of heavier $\delta^{13}C_{POC}$ values with increasing salinity seawards. Similar correlations between $\delta^{13}C_{POC}$ and water salinity are also suggested in other studies (Middleburg and Nieuwenhuize, 1998; Countway *et al.*, 2007; Middleburg and Herman, 2007; Wu *et al.*, 2007; Zhang *et al.*, 2007). Middleburg and Herman (2007) suggested that the correlation between $\delta^{13}C_{POC}$ values and salinity is more significant in river-dominated estuaries, such as the Rhine estuary and the Douro estuary, than in tidal-dominated estuaries such as the Gironde and Loire. In addition, Middleburg and Herman (2007) also pointed out that the range of the $\delta^{13}C_{POC}$ values is small in estuaries of high turbidity, between –24‰ and –26‰ (Fontugne and Jouanneau, 1987; Zhang *et al.*, 1997; Tan *et al.*, 2004), which reflects dominance of terrigenous POC input into the estuary mixed with various sources.

POC is the main component of surface sediments, especially for sediments from the marine environment (Liu *et al.*, 2007), while organic matter of surface sediments from freshwater is a combination of freshwater POC and terrestrial organic matter. The $\delta^{13}C$ of POC has been used to indicate sources of organic matter for the surface sediment in estuarine and coastal areas, and to estimate sediment flux into the sea (e.g. Hedges and Parker, 1976; Goñi *et al.*, 1997; Hu *et al.*, 2006; Kuwae *et al.*, 2007; Ramaswamy *et al.*, 2008). Birds *et al.* (2008) estimated carbon flux from the Ayeyarwady and Thanlwin into the Indian Ocean

by examining the $\delta^{13}C_{POC}$ of suspended sediments, and suggested that the Ayeyarwady-Thanlwin river system contributes a minimum of 4.6Mt/yr of POC and an additional 1.1Mt/yr of dissolved organic carbon (DOC) to the global ocean. The application of $\delta^{13}C_{POC}$ for estimating the terrigenous POC flux into the sea is constrained by the mineralization and solubility of the terrigenous POC within the estuary, as the POC can be intensively modified before it is transferred into the sea. However, this process only becomes vital in a tidal-dominated estuary with long water residence (Middleburg and Herman, 2007), where there is enough time for these processes to occur. Sackett *et al*. (1965) suggested that in high-latitude areas of the South Atlantic, temperature is an important controlling factor on the $\delta^{13}C$ of plankton. Plankton from water with a temperature of 25ºC have an average $\delta^{13}C$ value of –21.7‰, whereas for samples from water of 0ºC the average value is –27.9‰. However, in tropical/subtropical estuaries, temperature does not play an important role compared with water salinity (Fontugne and Duplessy, 1978). The influence of atmospheric CO_2 concentration on the carbon isotopic values of marine plankton accounts for less than 10% of the natural variation in the tropical and subtropical ocean, as pointed out by Fontugne and Duplessy (1978). This point is supported by Gruber *et al*. (1999), who show that CO_2 concentration in surface water of the subtropical Indian Ocean and the western Pacific Ocean does not show strong seasonal/annual changes. Comparing the $\delta^{13}C_{POC}$ from different depths of the northern South China Sea, Liu *et al*. (2007) also suggest that hydrographical and biological conditions of this area play a more important role in forming the isotopic composition of the deposited organic carbon than in the CO_2 concentration in the surface water.

There have been relatively few studies investigating the modern-day organic carbon isotopic signature of the Pearl River delta and estuary. Hu *et al*. (2006) estimated the distribution and sources of organic carbon in the Pearl River estuary and adjacent shelf by examining the sedimentary organic carbon isotopes. They found that there is proportionally higher terrestrial-derived organic carbon at the river mouth and the western coast with respect to marine-origin organic carbon. This result is supported by Zong *et al.* (2006), who found that sediments from the freshwater end of the system are more depleted in ^{13}C than sediments from the brackish and marine areas. This is largely due to different

proportions of terrestrial organic matter input into these areas. The contribution of marine algae to the sedimentary organic carbon sink is limited by the turbidity and nutrient situation of the water column (Zhang *et al*., 1997; Yin *et al*., 2000; 2004; Huang *et al*., 2003; 2004), and becomes lower at the river mouth than the inner-shelf area (Hu *et al*., 2006). A similar phenomenon has been reported from other estuaries (e.g. Fontugne and Jouanneau, 1987; Zhang *et al*., 1997; Wu *et al*., 2007). Anthropogenic input to the Pearl River delta has become an important factor that influences the organic carbon isotopic signature of the surface sediments in the estuary (Jia and Peng, 2003; Owen and Lee, 2004). Sediments deposited during recent decades tend to have elevated δ^{13}C values, which appear to coincide with rapid urbanisation, industrialisation and reclamation in this area (Owen and Lee, 2004; Hu *et al*., 2008); for example, well-nourished plants showed more positive δ^{13}C values than plants deficient in nitrogen and/or potassium (less fertilized) (O'Leary, 1981).

Application of δ^{13}C and C/N for palaeo-climate reconstructions from coastal areas

Variation of the carbon isotopic compositions in the terrestrial sedimentary archive is used to indicate the predominant type of vegetation (Fan *et al*., 2007; Cao *et al.*, 2008; Driese *et al*., 2008; Saia *et al*., 2008). Sedimentary organic matter with heavier δ^{13}C values but lower C/N ratios usually originates from C$_4$ plant dominated areas, while those of lighter δ^{13}C values but higher C/N ratios normally have a C$_3$-plant-dominated sediment supply. Changes in the dominant vegetation type between C$_3$ and C$_4$ plants since the late Pleistocene can be reconstructed according to the organic carbon isotopic signatures of terrestrial sedimentary archives in different areas of the world. During recent decades, considerable research of this type has been carried out in North America (e.g. Driese *et al.,* 2005; Saia *et al*. 2008; Swarzenski *et al*., 2008). Saia *et al*. (2008) suggest that the enrichment of ^{13}C (around −21.0‰) in soil organic matter during the late Pleistocene indicates that the plant community in the Atlantic Forest, southeastern Brazil, was a mixture of C$_3$ and C$_4$ plants. The δ^{13}C fell to lighter than −26‰ in the early Holocene, when the climate became wetter, and the C$_3$ plants became predominant. This result agrees with other work using pollen in the nearby area, which also suggests a colder and drier

climate in the late Pleistocene than the present (e.g. Behling and Lichete, 1997). Similar work has been undertaken by Driese *et al.* (2008) in an alluvial floodplain catena in southeastern Tennessee, USA. Their results show that the $\delta^{13}C$ of soil organic matter changes between –22.0‰ and –26.0‰ during the Holocene, with an obvious cyclicity of around 300yr, which indicates changes in the dominant vegetation type between C_4 and C_3 plants in response to climate changes, which have also been recorded in areas nearby (Nordt *et al.*, 1994; Yu and Ito, 1999; Poore *et al.*, 2003; Leavitt *et al.*, 2007).

In coastal areas, modern-day sedimentary organic matter is derived from allochthonous sources (e.g. fluvial derived terrestrial plants and tidal derived marine phytoplankton), and autochthonous sources (e.g. *in situ* plants growing on surface of the sediment and algae). Balance between the terrestrial input and the marine input into the coastal areas is influenced by changes such as climate changes (e.g. Shultz and Calder, 1976; Zong *et al.*, 2006; Cramer and Saltzman, 2007; Burdloff *et al.*, 2008), or sea level changes (e.g. Chivas *et al.*, 2001; Wilson, *et al.*, 2005a; Mackie *et al.*, 2007). High terrestrial supply to the Portuguese continental shelf during the Younger Dryas event was suggested by the low $\delta^{13}C$ values and high C/N ratios of sediment (Burdloff *et al.*, 2008), while up to 80% of marine input was suggested during the postglacial transgression phase. There are other factors that might influence the organic carbon signature of the sediments in coastal areas, such as the atmospheric CO_2 concentration, temperature etc. In the eastern Mediterranean, Fontugne (1992) suggests that variability of the $\delta^{13}C$ of the late-Pleistocene sapropels is more related to changes in the atmospheric CO_2 concentration than to changes in terrestrial sediment supply. Meyers and Arnaboldi (2008) examined the $\delta^{13}C$ and TOC of the Mid-Pleistocene sapropels from the Tyrrhenian and Levantine Basins, Mediterranean Sea, and suggest wetter climate during times of these sapropel deposition in the eastern Mediterranean than the west.

The application of $\delta^{13}C$ and C/N of sedimentary organic matter for reconstructing palaeo-environmental changes has been carried out in a large range of areas, including lagoons (e.g. Müller and mathesius, 1999; Müller and Voss, 1999; Yamauro, 2000), isolated basins (e.g. Chivas *et al.*, 2001; Westman and Hedenström, 2002; Mackie *et al.*, 2007), fjords (e.g. Bird

et al., 1991; St-Onge and Hillaire-Marcel, 2001; Smittenberg *et al.*, 2004), as well as estuarine areas (e.g. Fry *et al.*, 1977; Ember *et al.*, 1987; Middelburg *et al.*, 1997; Wilson, *et al.*, 2005b; Zong *et al.*, 2006). In the Pearl River area, modern-day accumulative sediment flux is linearly correlated to accumulative freshwater discharge. Palaeo- river channels and dominant vegetation types have not moved significantly since the early Holocene compared to their locations today (Zong *et al.*, 2009a). Furthermore, dominant vegetation types since the early Holocene are similar to the modern-day's (Lu *et al.*, 2003). Since the mid-Holocene, when sea level had stabilized, sediment flux into the estuary was mainly controlled by the freshwater discharge, which was induced by the monsoon precipitation. Thus it is possible to use bulk $\delta^{13}C$ and C/N of estuarine sediment to reflect freshwater flux strength and accordingly the strength of the monsoonal precipitation. Application of the bulk organic carbon isotopic signature of estuarine sediment as an indicator for monsoon-induced freshwater variability was first carried out by Zong *et al.* (2006). Zong *et al.* (2006) reconstructed the monsoonal history during the Holocene using organic carbon isotopes and C/N ratios of sediments from the Pearl River estuary. In the modern-day analogue, the $\delta^{13}C$ values vary between –21.1‰ ± 0.3‰ for samples from the fully marine environment, between –23.2‰ ± 0.8‰ and –23.7‰ ± 0.8‰ for samples from the mid to outer estuary brackish water environment, and less than –24.7‰ ±1.3‰ for samples from the inner estuary close to the freshwater sources. Similarly, the C/N ratios vary from below 7 ±0.6 in the marine end-members to over 14.8 ±3.0 in the freshwater end-members (Zong, *et al.*, 2006). Results from the fossil data (Core V37) suggest an increase in freshwater flux from c. 8500 to c. 6000 cal. yr BP, followed by a general decrease in freshwater flux during the last 6000 years (Zong, *et al.*, 2006). This result is supported by the diatom flora from the same study, and agrees with studies from nearby areas using different proxies (Thompson, *et al.*, 1989; An, 2000; Wang, *et al.*, 2005).

Combinations of $\delta^{13}C$ and C/N have also been applied to sedimentary archives of longer timescales to reconstruct climate changes (Cramer and Saltzman, 2007; Fan *et al.*, 2007; Cao *et al.,* 2008) and sea-level changes (Vecoli *et al.*, 2009). This thesis focuses on the Holocene period, so the longer time-scale studies are not discussed in detail here.

Diagenesis

The organic carbon isotopic signature is not uniform in different parts of the plant; e.g., tomato stems have an intermediate $\delta^{13}C$ value between that of their leaves (more negative) and their roots (less negative) (Park and Epstein, 1960). It also varies in different compounds of the plant: e.g., lipids are up to 8.0‰ depleted in ^{13}C relative to the whole plant (Park and Epstein, 1961). Cellulose and hemi-cellulose, which make up between 57% and 77% of herbaceous and woody plant tissues respectively (Benner *et al.*, 1987), appear to be isotopically heavier than the whole tissue (Ember *et al.*, 1987). For example, cellulose from a wide variety of C4 plants ranges in isotopic composition from −11.0‰ to −12.7‰ (Sternberg *et al.*, 1984) compared to −18.6‰ to −9.3‰ for the whole tissue (Bender 1971; Smith and Epstein, 1970). Lignin is only found in vascular plants, and accounts for 17-31% of woody plant tissues and 4-9% of herbaceous plant tissues (Bender *et al.*, 1987; Wilson *et al.*, 2005a). Lignin is more depleted in ^{13}C than the whole plant tissue by 2.0 - 6.0‰, and by 4.0 - 7.0‰ in comparison with cellulose (Bender, 1987; Ember, 1987). Spiker and Hatcher (1987) reported differences of up to 2‰ between the degrading wood and the fresh wood, due to the preferential decay of cellulose and the proportional increase in lignin.

In the inter-tidal and supra-tidal area, it is the process of selective preservation of more refractory biochemical components (e.g. lignin) of plants over the more labile ones (cellulose) that is thought to thought to account for the more negative carbon isotopic values of surface sedimentary organic matter compared to the overlying vegetation. For instance In the coastal wetlands of Louisiana, USA, Chumra *et al.* (1987) reported a shift of 0.5-3.3‰ between the carbon isotopic value of surface sediments and that of the overlying vegetation, and this is consistent with results found in other marshes around the USA coastline. Changes in C/N ratios because of the decomposition process also occurred (Valiela *et al.*, 1985). In inter-tidal and supra-tidal sediments, this may result in much lower sedimentary C/N than that of the overlying vegetation. Wang *et al.* (2003) compared the C/N ratio from freshwater marsh and saltmarsh sediment cores with that of the dominant plants in Plum Island marsh in Massachusetts, USA. They found that C/N ratios

31

of surface sediment were between 14 and 18, which were much lower than that of the dominant plants (around 50), and stayed at a similar level down core. Similar results were reported by Wilson *et al.* (2005a) from a saltmarsh fringing the Mersey Estuary, UK, where the C/N ratio of the surface sediments (10-12) is much lower than that of the overlying vegetation (29). However, in saltmarshes and other coastal areas, the contribution from other sources of organic matter, such as tidal-driven marine organic matter, would surely result in low C/N.

In sub-tidal areas (e.g. estuaries, lagoons), shifts in carbon isotopic values and C/N are due to degradation of phytoplankton, as most of the terrigenous organic matter has already been extensively degraded on land or further upstream and should be relatively resistant to further degradation (Hedges and Keil, 1995). Protein, which accounts for up to 34% of phytoplankton, is relatively rich in nitrogen (15-19%, Bordovskiy, 1965b), and it is responsible for the relatively low C/N ratio of phytoplankton in comparison with vascular plants. Nitrogen content does not increase in phytoplankton detritus during degradation of the carbon (Valiela, 1995). Alteration in the $\delta^{13}C$ value of phytoplankton (around -21 per mil) is due to the preferential degradation of protein and carbohydrates, which together account for 63-93% of the phytoplankton biomass (Bordovskiy, 1965a; Meryers, 1997), and the subsequent proportional increase in the more refractory ^{12}C-enriched lipids (Lamb *et al.*, 2006). Differences in the carbon isotopic signature between the sedimentary organic matter and the suspended organic matter have been reported by previous studies (Cifuentes, 1991; Middelburg and Nieuwenhuize, 1998; Liu *et al.*, 2007), also showing spatial variability and seasonality within the same estuary. Middelburg and Nieuwenhuize (1998) compared changes in the $\delta^{13}C$ value and C/N ratio between the surface sediment and the suspended sediment from the Schelde Estuary, located on the border of the Netherlands and Belgium. They found that, in the upper estuary, the C/N ratio and $\delta^{13}C$ of suspended sediment (8.9 and –28.9‰ respectively) was much lower than that of the surface sediment (17.0 and –26.3‰ respectively), whereas, in the lower estuary, the $\delta^{13}C$ value of the suspended sediment (-20.1) is higher than that of the surface sediment (–23.5‰), while differences in the C/N between the two facies are not so significant, at 9.1 and 10.3

respectively. Liu *et al.* (2007) also reported higher δ^{13}C values of surface sediment (–21.3 - –19.0‰) than suspended sediment (–24.0 - –22.1‰) from the South China Sea.

Shifts in the δ^{13}C and C/N ratios between sedimentary organic matter and overlying vegetation due to decomposition are only significant during the early stages of deposition, which lasts up to a year (Rice and Tenore, 1981; Valiela *et al.*, 1985; Benner *et al.*, 1991; White and Howes, 1994). After that, the C/N ratios become stabilized, as carbon and nitrogen are lost at approximately the same rate (Melillo *et al.*, 1989; White and Howes, 1994) and changes in C/N ratios over a longer time period due to diagenesis are thought to be insignificant. Wilson *et al.* (2005b) found that C/N ratios of the sub-tidal deposit of the Mersey Estuary, UK, decreased from 13.3 in the early Holocene to 11.3 in the mid-Holocene, which are slightly higher than modern-day saltmarsh sediments, at around 10.6. C/N ratios of the Holocene sediments from the Pearl River estuary, increased from 10.2 in the early Holocene to around 11.5 in the mid Holocene and 12.7 in the mid-late Holocene (Zong *et al.*, 2006). The δ^{13}C from the Holocene sediment is reported to be 2-4‰ lower than modern-day sediment from the coastal area (DeLaune, 1986; Fogel *et al.*, 1989; Wilson *et al.*, 2005b; Zong *et al.*, 2006). The δ^{13}C values from the Holocene deposit from the Pearl River estuary are around 2.0‰ more negative than that of modern sediments. However, the contribution of the degradation process to the alteration in δ^{13}C values in Holocene sediment is not sufficiently known. Measurements on a sediment core from the York River estuary (eastern USA) by Arzayus and Canuel (2004), also demonstrated that δ^{13}C and C/N remained largely unchanged below 15m, indicating little further degradation occurred after deep burial.

Diagenetic alterations in isotopic composition of the sediment organic matter occur as soon as degradation starts. In the Pearl River estuary, sedimentary organic matter is mainly derived from riverine and marine areas (Zong *et al.*, 2006). Because of influences of the degradation process on the isotopic signature, it is more reliable when comparing this proxy with others, e.g. diatoms, pollen, foram (e.g. Mackie, *et al.*, 2007). Previous studies on the diagenetic effect from the Pearl River delta and estuary were rare. Degradation influence on organic matter in the Pearl River delta and estuary will be discussed in Chapter 5.

2) Selected elements

To undertake multi-proxy research, a range of selected elements are also employed by this study as secondary proxies. Results from these elements are discussed to a less extant compared to the bulk organic $\delta^{13}C$ and C/N in this thesis.

The distribution of elements in sediment is controlled by combination of types of bedrock, climate condition and mobility of the element itself. Once leached from bedrock into soils during weathering, some elements are absorbed by clays, or are present in the form of clay minerals and remain *in situ*, while others go into solution as carbonate (e.g. manganese). Those with relatively higher mobility are dissolved in solution, in forms of ionic solutions or as colloidal dispersions and particulate substances. After entering streams, in whatever form, elements are finally delivered into the ocean. Some elements become enriched in seawater, such as potassium, and some are precipitated from seawater and become enriched in marine sediments, such as boron. This process might be influenced by biological activity, e.g. calcium is taken from seawater and becomes the main component of marine shells; other elements are found to be enriched in plants.

A brief introduction to the weathering cycle of key elements

To undertake a multi-proxy study, in addition to organic carbon isotopes, this study also explores the variability of concentrations of iron (Fe), manganese (Mn), cobalt (Co), arsenic (As), lithium (Li), barium (Ba), aluminium (Al), potassium (K), rubidium (Rb), strontium (Sr), sodium (Na), magnesium (Mg), calcium (Ca), boron (B) and beryllium (Be) between different types of sediment in terrestrial and estuarine areas. Measurements were also made from the sediment core to investigate trends in element concentration that might relate to monsoon variability. A brief introduction to the general circulation of these elements is presented below.

Manganese (Mn) and Arsenic (As)

During weathering of igneous rocks, manganese is dissolved, mainly as the bicarbonate, $Mn(HCO_3)_2$. The decomposition of the bicarbonate leads to the formation of Mn^{4+} compounds, and in the zone of weathering, they are directly converted into manganic oxides and hydroxides. The formation of hydroxides is an important step for the cycle of Mn. The general rule is that both forms of manganese go into solution at low redox potentials and are precipitated at high potentials. Under certain circumstances, precipitation of manganese as $Mn(OH)_4$ or MnO_2 takes place, often in fresh waters. Most of the remaining manganese is delivered into brackish water at the river mouth (Rankama and Sahama, 1950). The manganese precipitated is deposited in oxidate sediment, often in the form of concretions, nodules, and slabs (manganese pans). Under reducing conditions the precipitated manganese hydroxide may again pass into solution. The content of manganese in seawater is rather low (Clarke, 1924).

Arsenic mainly originates from terrestrial rock/soil weathering and volcanic explosions in the natural world, and types of bed rock and climate are two key factors for the enrichment of arsenic in soil. Arsenopyrite is the most important ore of arsenic, and it occurs most commonly with quartz, often in metamorphic schist (Clarke, 1924; Rankama and Sahama, 1950), so weathering of silicates and carbonic stones can release a certain amount of arsenic. After release from weathered rocks, some soluble arsenic salts are bound to clays in the water, but most of them remain in soil. According to Goldschmidt and Peters (1934), the average content of arsenic in argillaceous sediments is of the same degree of magnitude as the average in igneous rocks. The mean concentration of arsenic in natural soil is 0.1-42μg/g, and 0.0002-0.23ng/L in natural water (Yang *et al.*, 2004).

Iron (Fe) and Cobalt (Co)

Geochemical migrations of iron in aqueous solutions depend very much on processes of oxidation and reduction. In freely drained soils and in the oxidation zones of ore deposits, oxidation is in many cases indicated by the precipitation of yellow, brown, or red ferric

compounds, which also are recognized by their colour in may sedimentary rocks (Goldschmidt, 1954). In many cases the action of oxidative conditions on dissolved ferrous iron leads to the precipitation of ferric iron ores at the bottom of shallow bodies of oxygenated fresh or marine waters, and at soil or rock surfaces (Goldschmidt, 1954). Some general rules may be mentioned which govern the fixation and the mobilization of iron, which are valid in the processes of weathering and soil formation and also in the genesis of sedimentary rocks (Goldschmidt, 1954). Rule 1: oxidizing conditions promote the precipitation of iron, reducing conditions promote the solution. Rule 2: acid conditions (low pH) generally promote the solution of iron; alkaline conditions (high pH) promote the precipitation of iron. Owing to the high pH, about 8, of sea water, the solubility of ferric iron is extremely low, and iron is among the minimum factors involved in marine organic production. Only a small part of iron liberated during the weathering ever reaches the open ocean. The bulk is deposited in lake and bog iron ores, in oolitic iron ores, and in some iron-bearing silicates, such as glauconite and greenalite (Rankama and Sahama, 1950).

Cobalt is a member of the iron family, and is the closest relative of iron in the Periodic System (Rankama and Sahama, 1950). During the weathering, cobalt does not leach form hydrosilicates, but remains in the weathering solutions as bicarbonate or colloidal hydroxide. In sea water the content of cobalt is very low, and the small value of the transfer percentage shows that cobalt is also almost completely removed from sea water, being deposited in hydrolyzate sediments (Rankama and Sahama, 1950). Small amounts of cobalt are also present in sulphides found in marine sediments. Cobalt is removed by adsorption in the oxidate sediments.

Lithium (Li)

Lithium is certainly concentrated in the uppermost part of the lithosphere as it is a typical element of light residual rocks, such as granites and nepheline syenites and of the residual solutions. In the deep interior of the earth very little lithium can be present (Goldschmidt, 1954). In the processes of weathering and sedimentation, lithium is corporate in marine hydrolyzate sediments. Some lithium is present in evaporate sediments, e.g. in halite, in

which it replaces sodium in small quantities. Furthermore, average contents of lithium are higher in marine iron ores and in deep-sea sediments than in hydrolyzates.

Barium (Ba)

During weathering, barium is dissolved as bicarbonates, chlorides, and sulphates. They may migrate as bicarbonate and chloride but also as sulphate. Even though barium sulphate is only sparingly soluble in distilled water, its solubility increases when hydrochloric acid or chlorides of the alkali metals are present in solution (Rankama and Sahama, 1950). Barium may become separated from the weathering solutions as barium sulphate upon evaporation or neutralization (by limestone) of the waters or because of an increase in the concentration of the sulphate anion (Rankama and Sahama, 1950). Barium sulphate deposited in sandstones and in calcitic and dolomitic limestone may give rise to extensive deposits of barite.

The barium transported to the sea becomes largely separated already during the formation of hydrolyzate sediments, and only a small part thereof remains in sea water. The transfer percentage of barium is 0.03, or very much smaller than the transfer percentage of strontium and calcium. The Sr:Ba ratio in igneous rocks is 0.6 and in sea water 260, showing that barium is strongly impoverished in the sea in relation to strontium (Rankama and Sahama, 1950). Barium is adsorbed so strongly that it has largely been removed in the near-shore sediments, and only a negligible amount is carried to the open ocean, where it is finally precipitated in the deep-sea sediments (Rankama and Sahama, 1950).

Aluminium (Al)

Aluminium is the most abundant metal found in igneous rocks. Of all elements, only oxygen and silicon are more abundant than aluminium. During weathering under temperate conditions, and with good drainage, the more important aluminium-bearing minerals such as feldspars and feldspathoids, give rise to the clay minerals illite, averaging about 13.5% of Al, and kaolinite, with almost 21% of Al, and go into ionic solution (Rankama and

Sahama, 1950; Goldschmidt, 1954). Under normal conditions these minerals are completely dissolved, at least in the beginning of the weathering. Aluminium remains dissolved both in acid solution with pH less than 4 and in basic solution (pH >9); and aluminium hydroxide, $Al(OH)_2$, is precipitated only in the neighbourhood of the neutral point. Aluminium hydroxide is also precipitated when the solution becomes concentrated because of evaporation. Clays deposited in a cold climate usually show only relatively small chemical changes. In clays formed during intensive weathering the chemical changes are more pronounced and consequently their aluminium content is usually higher.

Although the content of aluminium in river water is low, this metal is constantly present therein. Aluminium does not remain permanently in the solutions produced during the weathering. Its hydroxide is weakly basic, and therefore the soluble aluminium salts, in common natural waters, are promptly hydrolyzed and subsequently removed in the solid products of weathering (Rankama and Sahama, 1950). Therefore, the resistates become impoverished in aluminium, whereas the hydrolyzates become enriched therein, and it is evident that the content of aluminium in the hydrolyzates will increase parallel to the degree of change in their chemical composition. The decomposition of aluminium in the hydrolyzates is almost quantitative, i.e. the quantity of aluminium liberated from the minerals during their weathering is quantitatively transported into the hydrolyzates, and only very little is found in precipitates, oxidates, evaporates and seawater (Rankama and Sahama, 1950).

Aluminium is widely distributed in all organisms, and it might be essential for higher plants. Plants contain considerably more aluminium than animals do, and some plants are known to accumulate this metal (Rankama and Sahama, 1950). The most remarkable case is that of a tree, *Orites excels*, in which a basic alumninium succinate is reported to occur in trunk cavities. *Lycopodium alpinum* may contain 33% Al_2O_3 in its ashes (Rankama and Sahama, 1950).

Potassium (K) and Rubidium (Rb)

Potassium is brought into solution during weathering, and is largely removed from the solution and precipitated, by adsorption, in clays (Rankama and Sahama, 1950). Both potassium and rubidium are notably impoverished in fresh waters before they enter the sea. However, of the total amount of Rb and K in circulation, only a small fraction is held in soils, the greater part accumulating in marine deposits (Goldschmidt, 1954). Both rubidium and potassium are frequently found in plants: the ash of sugar cane contains as much as 0.2% of Rb (Rankama and Sahama, 1950). The content of potassium in seawater is also affected by dilution with river water and by biological activities. For example, the content of potassium in seawater decreases when encounters fine-grained detrital minerals, colloid particles, and clay minerals.

Sodium (Na)

Sodium in combination with other elements occurs in considerable amounts. The distribution of sodium in the various parts of the hydrosphere, springs, rivers, lakes, the oceans, is well known, and the formation of sodium minerals as evaporates both from inland basins and from detached parts of the sea has been investigated (Goldschmidt, 1954). During the weathering, some silicate minerals, for example, the alkali feldspars, leucite, and actinolite, are completely dissolved. Sodium and potassium released during the weathering remain in ionic solution. They are carried into the sea by rivers and streams. They may remain in the weathering residue only in arid regions. Because sodium is extracted from rocks during the weathering, its absolute amount decreases in the hydrolyzate sediments which are formed as the result of chemical decomposition. As a result of weathering, transportation, and adsorption, the grand total of sodium now present in the sea is 62% of the total quantity transported thereto during the geological evolution of the Earth.

In the cycle of sedimentation, sodium minerals are rare in residual sandstones, but a few clastic grains of albite may occur. The normal amount of sodium in residual sediments is

considerably less than 1% of Na_2O by weight. In argillaceous sediments the amount of sodium is likewise rather low. In marine shales the average content of Na_2O is about 1.3% corresponding to about 1% of Na (Goldschmidt, 1954). In muds and clays from the sea bottom, variable Na_2O contents have been reported. Terrigenous mud from the ocean bottom has a Na content very close to the average for older marine shales.

Magnesium (Mg)

Magnesium is strongly lithophile, and in the Earth it is almost quantitively contained in the silicate shell. Unlike the alkali metals, magnesium is able to build both simple and complex inorganic compounds which are stable under the conditions met in Nature. According to Goldschmidt (1954), the magnesium content of argillaceous sediments is not very much lower than that of igneous rocks. During chemical weathering, magnesium is released mainly as the soluble chloride, $MgCl_2$, and sulphate, $MgSO_4$. Another portion of magnesium is transported, partly as chemically undecomposed, finely ground mineral particles and partly as magnesium-bearing clay minerals, which are derived particularly from basic and ultrabasic rocks during the weathering (Goldschmidt, 1954). This portion is finally deposited in the hydrolyzates. Still another part of magnesium becomes incorporated in the clay minerals as a result of base-exchange reactions.

Magnesium is nearly as abundant in river water as in the sea. Many of its salts are readily soluble, and therefore its bulk remains in sea water, occupying the next place in abundance in the ocean, right after chlorine and sodium. However, the enrichment of magnesium in sea water is not quite so pronounced as that of sodium, and its content remains relatively stable because of the additional quantities transported to the sea by rivers (Rankama and Sahama, 1950).

Magnesium is a constant micro-constituent of lower plants. Some marine organisms are very rich in magnesium. Lower contents are reported in the shells and skeletons of other marine organisms (foraminifers and echinoderms). In higher animals magnesium is constantly found in the skeletal parts, muscles, and nerve tissue.

Boron (B) and Beryllium (Be)

Boron goes into solution as boric acid and soluble borates, and is ultimately transported into the sea. Boron is notably concentrated from sea water in coastal soils, which may contain from ten to fifty times as much as inland soils (Rankama and Sahama, 1950). Degens *et al.* (1964) showed the distinct difference of boron content in freshwater and marine shale in Appalachian coal basins. Martin and Whitfield (1983) also reported the greater abundance of Boron in the sea (4440 µg/l) than in freshwater (18 µg/l). Boron is also found to be significantly enriched in some plants. A maximum of 3,100g/ton of boron from coal ash was reported by Goldschmidt and Peters (1932), who also reported a similar content of boron in ashes of seaweeds, whereas the content in marine calcareous algae is less.

Beryllium is an element of the hydrolyzates. During weathering and formation of sediments, beryllium becomes enriched in clays, bauxites, recent deep-sea deposits and other hydrolyzate sediments, along with aluminium. Beryllium is also concentrated by some plants, especially those growing in berylliferous areas. The ashes of wheat and coal have been reported to be enriched in beryllium (Rankama and Sahama, 1950; Goldschmidt and Peters, 1933).

Calcium (Ca) and Strontium (Sr)

Calcium in river water is predominantly derived from limestone and other rocks containing calcium carbonate and from the calcium-bearing salt deposits. These rocks are relatively abundant in the geological column, and they are dissolved and disintegrated more readily than igneous rocks (Rankama and Sahama, 1950). Calcium is the most abundant element in fresh water. When the river water joins the ocean, calcium and carbonic acid are the substances removed in the greatest quantities from river water by living organisms, and are the principal material of corals and shells (Clarke, 1924). The low content of calcium in the salts dissolved in seawater affords convincing proof of the removal of calcium from the sea (Rankama and Sahama, 1950).

Strontium, which enters the weathering cycle as an aqueous solution, may become precipitated within carbonate through loss of carbon dioxide from the bicarbonate-bearing solution and as sulphate, owing to the action of sulphuric acid or sulfates on the strontium-bearing solution. The bulk of strontium migrates into the sea, and consequently strontium is notably concentrated in the sea, in comparison with calcium; e.g. the Ca/Sr ratio in igneous rocks is 242, and the ratio in seawater is 30.8 (Rankama and Sahama, 1950; Goldschmidt, 1954).

Application of major/trace elements for palaeo-climate reconstruction

Most major/trace elements from fossil records do not provide a direct proxy for climatic parameters, such as temperature. However, they produce integrated records of overall climatic impact on weathering and erosion process. The application of major/trace elements as indicators of palaeo-environmental changes has been studied in a range of areas including lake sediments (e.g. Jin, *et al*., 2001), loess-palaeosol sequences (e.g. Chen, *et al*., 1999, 2001), and coastal and estuarine areas (Yang *et al*., 2008; Lim, *et al*., 2006; Zhou, *et al*., 2004; Zhang, 1995; Huang, *et al*., 1983; Danielsson, *et al*., 1982). Among all elements, the behaviour of alkali metals and alkaline earth metals under different environmental conditions are relatively better understood. Soils formed under a warm and humid environment usually are of high Rb/Sr, Cs/K, and Rb/K ratios, but of low Ca/K, Sr/K, Na/K and Mg/K ratios (Gibbs and Kump, 1994; Glodstein, 1988; Nesbitt and Young, 1982, 1984, Nesbitt, *et al*., 1980; Nesbitt, 1979). B/Be has been widely used as an indicator of palaeo-salinity change (e.g. Siegel *et al*., 1995; Dominik and Stanley, 1993; Davis *et al*., 1972). According to Landergren (1945), the content of boron from argillaceous sediments is directly proportioned to the salinity of the water in which the sediment was deposited. The higher the salinity, the greater the boron content of the accumulated sediments (Rankama and Sahama, 1950). Siegel *et al.* (1995) used the paleosalinity factor (B as related to clay minerals) to characterize different lithofacies from the eastern part of the Nile delta. Levinson and Ludwick (1966) argued that, in deltaic settings, increased boron content in sediment with an increased distance from a river mouth may be related to a parallel seaward increase in the proportion of clay, rather than to increasing salinity. In order to

minimize the grain size effect, Dominik and Stanley (1993) used B/Be to minimize the grain size effect, because contents of Be shows no dependence on facies but have a strong negative correlation with grain size.

Major/trace elements have been successfully applied in estuarine areas to interpret changes in salinity and in weathering and erosion over the drainage basins (e.g. Yang *et al*., 2008; Zhang, 1995; Danielsson *et al*., 1982; Brady and Carroll, 1994). Huang *et al*. (1983) examined the implication of the Quaternary trace elements in the Pearl River delta and showed that, marine water sediments have higher concentrations of B and Rb, while freshwater sediments are higher in Gallium (Ga) from Pearl River delta. Alkaline metals and alkaline earth metals (including Na, Ca, Mg and K) can be considerably leached from weathered material during intense chemical weathering, based on works from Hong Kong (Yang *et al*., 2008; Guan *et al*., 2001; Fyfe *et al*., 2000; Sewell, 1999), and thus were suitable for provenance discrimination in the Pearl River estuary (Yang *et al*., 2008). Based on concentration of Na, Ca, Mg, K and ratios of Ti/Nb, Th/Nb and Th/Sc, Yang *et al*. (2008) suggested that the Pearl River was the main provenance of the inner shelf sediments of Hong Kong during interglacial periods, whereas the local-derived granitoids was the main contributor during glacial periods.

2.4 Summary of the chapter

This chapter has reviewed studies on three themes: 1) possible driving mechanisms for the EAM variability during the Holocene; 2) bulk organic carbon isotopes and C/N as indicators for environmental changes; and 3) key metals as indicators for environmental changes. Possible driving mechanisms for EAM changes during the Holocene depend on the time scale of the changes, including Milankovitch cycles, solar forcing, high-latitude cooling events, low-latitude volcanic eruption and ITCZ. The second theme indicated that the bulk organic carbon isotopes and C/N ratios have been successfully applied to palaeo-studies, and thus can be used as an indicator for paleao-EAM variability. The third theme

identified studies where metals have been applied to palaeo-studies in certain specific areas, e.g. loess deposit (e.g. Chen *et al*., 1999, 2001) and deltaic areas (e.g. Siegel *et al*., 1995).

The literature review has identified the following research gaps, which will be addressed in this research:

1) Understanding of global and regional forcing for EAM variability during the Holocene is limited.

2) Previous studies have reported possible decoupling of the thermal and moisture conditions of the EAM. However, understanding of the controlling process is relatively limited.

3) The Pearl River estuary preserves a high-resolution sedimentary archive of monsoon variability that, to date, been relatively little studied.

4) Preliminary studies have used bulk organic $\delta^{13}C$ and C/N to reconstruct monsoon-driven freshwater flux; our understanding of the process controlling these proxies is still rather limited in this area.

5) Although previous studies have used key elements to indicate sources of sediments in the Pearl River estuary, our understanding of the process controlling this proxy is limited in this area.

Chapter 3 Study Area

3.1 Introduction

This chapter introduces background knowledge of the study area, the Pearl River delta and estuary, including location, geomorphology and geological background, monsoonal climate, hydrology and oceanography, vegetation types, sea-level changes, evolution history of the Pearl River delta and estuary, as well as human activities in this area. Special attention is paid to factors that might influence signals for palaeo-climate reconstruction, such as progradation of the palaeo-shoreline, sea-level changes and agricultural activity in this area. It also highlights the suitability of this area for reconstruction of monsoonal changes.

3.2 The Pearl River catchment and estuary

The Pearl River is the general name for the three rivers, the East River (Dongjiang), the North River (Beijiang) and the West River (Xijiang) that flow into the Pearl River delta and estuary before entering the South China Sea (Figure 3.1). The catchemnt is located between 21°20′-23°30′N and 112°40′-114°50′E. At present the delta plains cover an area of 9750 km^2, mean annual discharge of the whole Pearl River system is 330 x10^9 m^3 (Hu *et al*., 2006), and the mean annual sediment load is 89 x10^9 kg/yr (Zhang *et al*., 2008). The West River, 2214 km in length and 425,700 km^2 in catchment area, contributes most of both the water and sediment fluxes reaching the Pearl River Estuary (Kot and Hu, 1995; Zhang *et al*., 2008). The Pearl River catchment provides most of the sedimentary material reaching the Pearl River estuary (Boulay *et al*., 2003). Statistics show that 80% of the total sediment flux is transported into the South China Sea, while only 20% stays within the Pearl River Delta (Zhang *et al*., 2008).
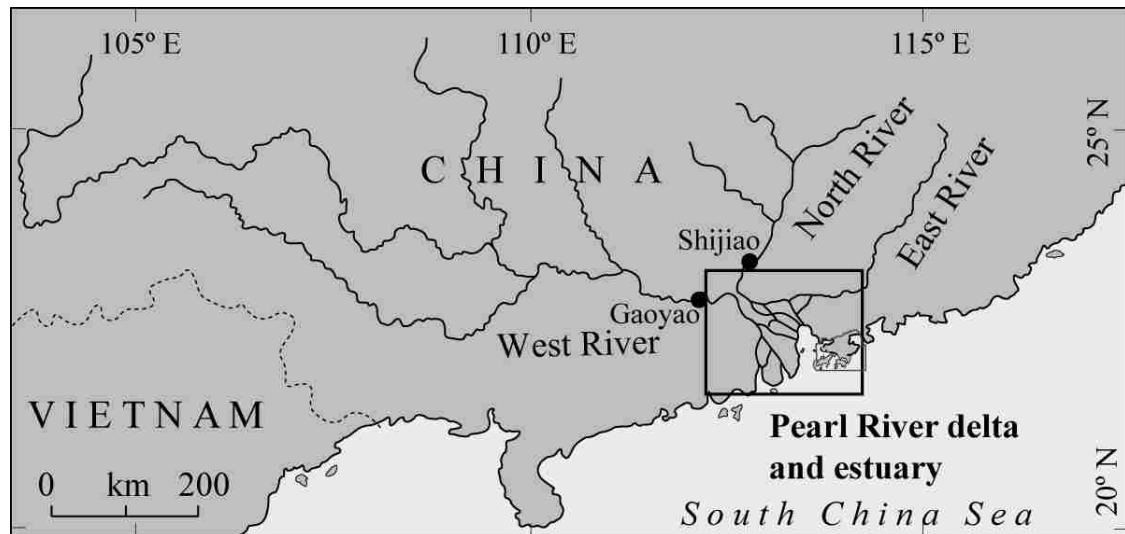
Figure 3.1 The Pearl River delta and estuary, its location in the Southeast Asian area and two hydrological gauging stations – Shijiao (North River) and Gaoyao (West Rvier).

3.3 Geology and geomorphology

The Pearl River system formed as a result of the uplift of the Tibetan Plateau during the Tertiary and Quaternary periods, lagging considerably behind the continent-continent collision of ~34 million years ago (Aitchison *et al*., 2007). Before the Late Quaternary, sediment from the river system bypassed the current deltaic basin and was deposited on the continental slope and shelf (Zong *et al*., 2009a). Only since the Late Pleistocene has the deltaic basin started to receive sediments from the river system, overlying a bedrock basement of Cretaceous-Tertiary sandstones and Mesozoic granites (Huang *et al*., 1982; Xu *et al*., 1985).

The Pearl River basin consists of various source rocks from Precambrian metamorphic rocks to Quaternary fluvial sediments (Zhang *et al*., 2007). Carbonates are widely distributed in the basin, accounting for 39% of the total basin area (PRWRC, 1991). The igneous rocks are dominated by granites with acid to intermediate composition, covering about half of the area of Guangdong Province. Small area outcrops of evaporites and pyrites are mainly scattered in the upperstream part of the Xijiang in

46

Yunnan and Guizhou provinces (Lu *et al.*, 2007). Quaternary fluvial sediments are mostly developed in the lower alluvial plain, the delta plain and the interior river valley plain of Guangdong and Guangxi provinces.

At present, the receiving basin is not completely full, leaving a sizable estuary (Figure 3.2). The upper estuary is about 2.5 km wide. The width of the lower estuary ranges between 24 km and 30 km, guarded by a cluser of rocky islands at the mouth area (Figure 3.2).

Figure 3.2 Geomorphology and geology of the Pearl River delta. Shuttle Radar Topography Mission (SRTM) image.

3.4 Monsoonal climate

The Pearl River catchment lies in the transitional area between the tropical and subtropical climate zones (Figure 3.1). The mean annual temperature of this area is 14-20°C, and the mean annual precipitation is 1200-2000mm (Guangdong Statistical Bureau, 1996). Because of seasonality of the monsoon climate (Figure 1.2), annual precipitation in this area mainly occurs during the warm-humid summer season lasting form June to October. In the longer term, precipitation flux in this area is sensitive to the strength of the summer monsoon. For example, during periods of stronger summer monsoon, the precipitation flux of this area will increase significantly, and vice versa. The history of the EAM has been considered as an alteration between dominance of cold-dry winter monsoon and warm-wet summer monsoon (An, 2000), responding to a combination of different factors (Section 1.4 in Chapter 1).

3.5 Hydrology and oceanography

As a result of the monsoonal climate, the seasonal water and sediment fluxes to the Pearl River estuary differ greatly, responding to changes in rainfall. Seasonally, over 80% of the discharge, both water and sediment, takes place in spring and summer, lasting from April to October. Huang *et al.* (2004) reported that seasonal and inter-annual water discharges vary from as low as 2000 m^3/s in an extremely dry winter to as high as 46,300 m^3/s in a 1/100year flood event. On average, the estuary discharges 302,000 million m^3 of water and 83.4 million tons of suspended sediment a year (Zhang *et al.*, 2008). As 93.1% of sediment comes from the West and North Rivers, sediment loads on the west side of the estuary are much higher than the east side. In addition, offshore currents during the strong winter monsoon are dominantly westwards and the Coriolis force also causes a westerly drift (Zong *et al.* 2009a; Figure 3.3). As a result, the east side of the estuary near Hong Kong is of low turbidity, whilst the turbidity maximum zone tends to be on the west side of the estuary, and flows southwest-wards offshore from Macau (Figure 3.2).

Tidal influence is stronger in the east than in the west as seawater water from the South China Sea enters the estuary from the southeast channel, while freshwater turns right at the river mouth and exit the estuary along the west coast (Figure 3.3a). Northwest-southeast isohalines are another result of the monsoon climate and the hydrological circulation in the Pearl River estuary (Figure 3.3). Annual salinity data were collected by the Guangzhou Institute of Geography (for the estuarine and deltaic parts) and the Environmental Protection Department of the Hong Kong government for the Hong Kong waters, who have repeatedly measured water salinity across the estuary (Table 3.1; Figure 3.3a), seasonal salinity was measure by this study in June 2006 (Figure 3.3b) and December 2006 (Figure 3.3c), and. Data show that water from the east has higher salinity than that from the west at the same latitude (Figure 3.3a), and the salinity increases from northwest to southeast. In summer (e.g. June), high precipitation generates strong freshwater flux into the estuary, resulting in a low-salinity estuarine environment. For example, water salinity at the river mouth is lower than 1‰. However, saline water intrudes much further inland in winter (e.g. December) than in summer (Figure 3.3a; b) due to significantly reduced freshwater flux in the dry winter monsoon season. The annual isohaline pattern shows decreasing freshwater influence seawards, while differences between seasonal isohaline patterns indicate seasonal variation in through freshwater flux induced by monsoonal precipitation.

Table 3.1 Sources of water salinity data

	Sampling sites	Data source	Contour map
	PE1-40	Zong *et al.*, 2006	Figure 3.3a
Annual salinity	PE41-92	Guangzhou Institute of Geography	Figure 3.3a
Summer salinity	PE41-75	This study	Figure 3.3b
Winter salinity	PE41-92	This study	Figure 3.3c
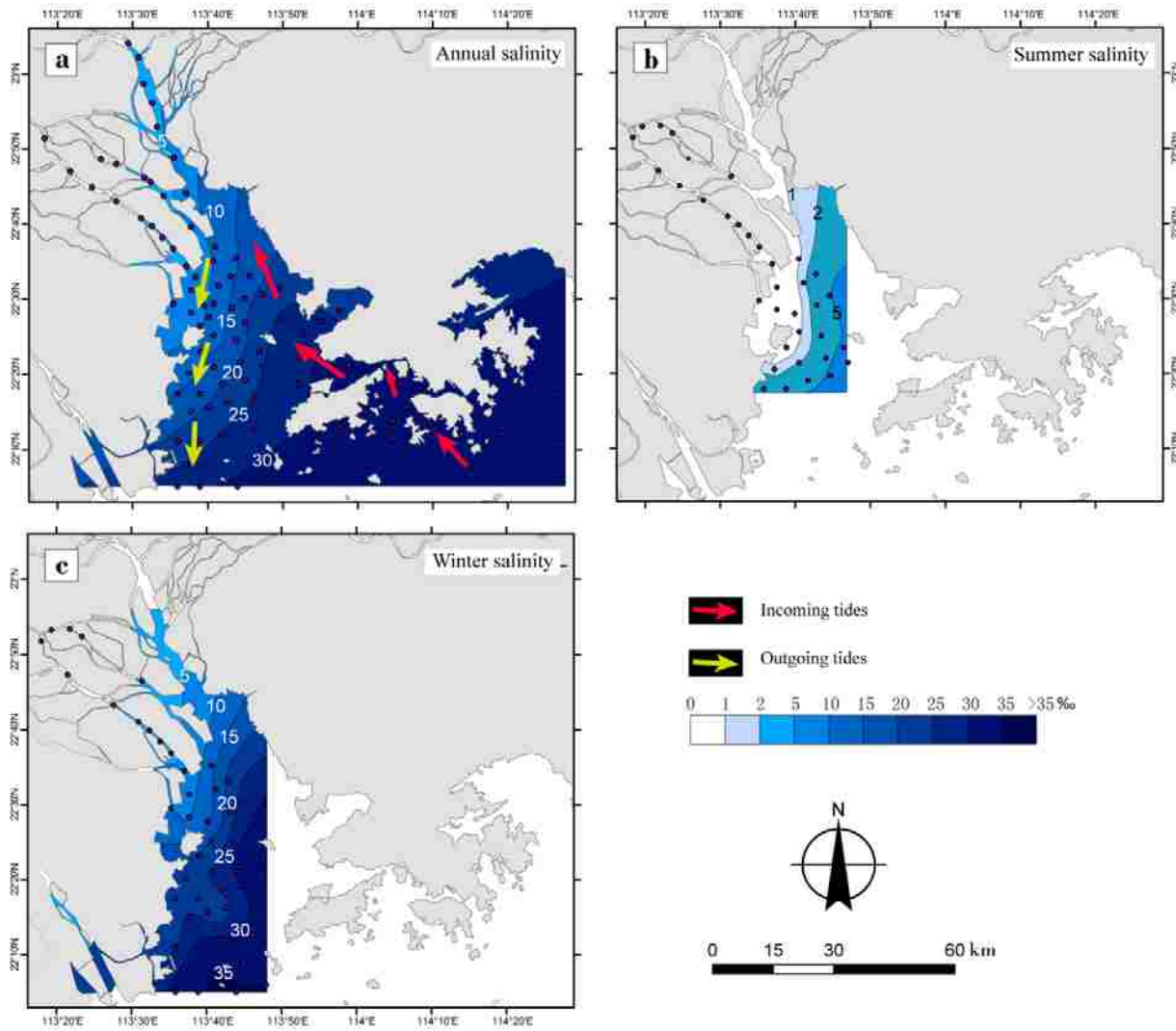
Figure 3.3 Contour map of annual mean (a), summer (b) and winter salinity (b) in the Pear River estuary

3.6 Water discharge and sediment flux

Generally, sediment load increases with increasing water discharge in the Pearl River. Records from hydrological gauging stations from the West River (Gaoyao) and the North River (Shijiao) (Figure 3.1) showed that, during the past decades, fluctuations of annual sediment load were correspondent with fluctuations of annual water discharge, e.g. years with high sediment load were correspondent to high water discharge in these years, and vice versa (Figure 3.4).
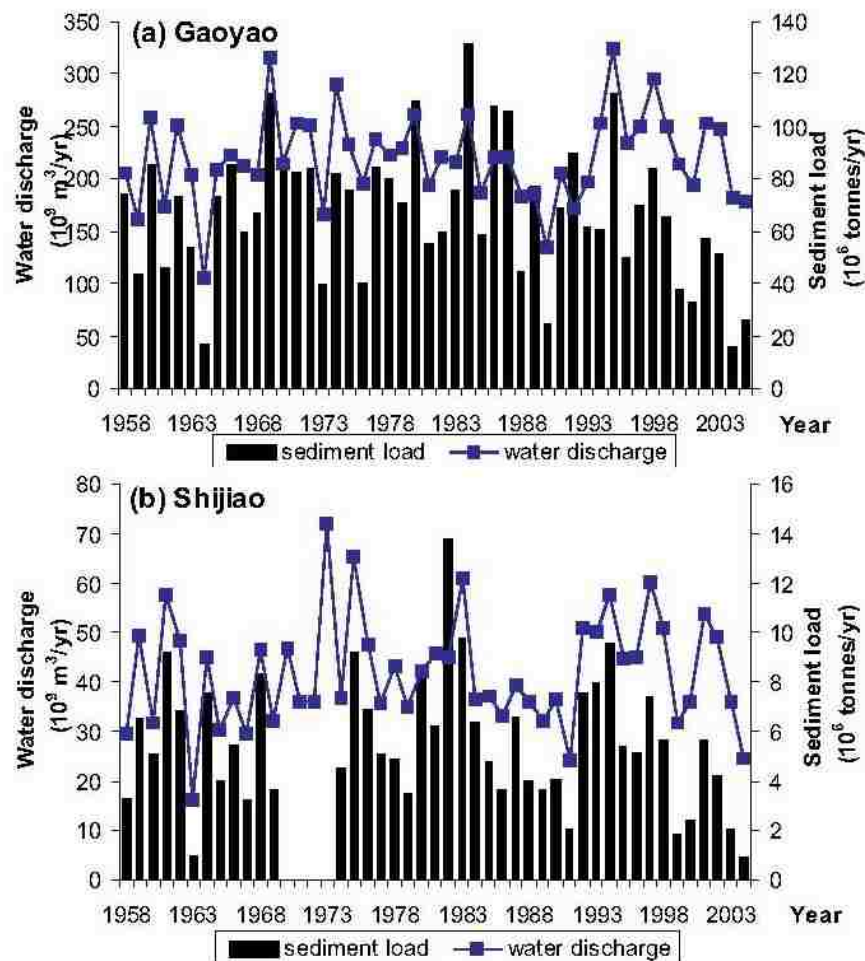
Figure 3.4 The variations of water discharge and sediment load over the past decades in the West River (Xijiang) and North River (Beijiang) at stations (a) Gaoyao (b) Shijiao (from Lu *et al.*, 2007).

51
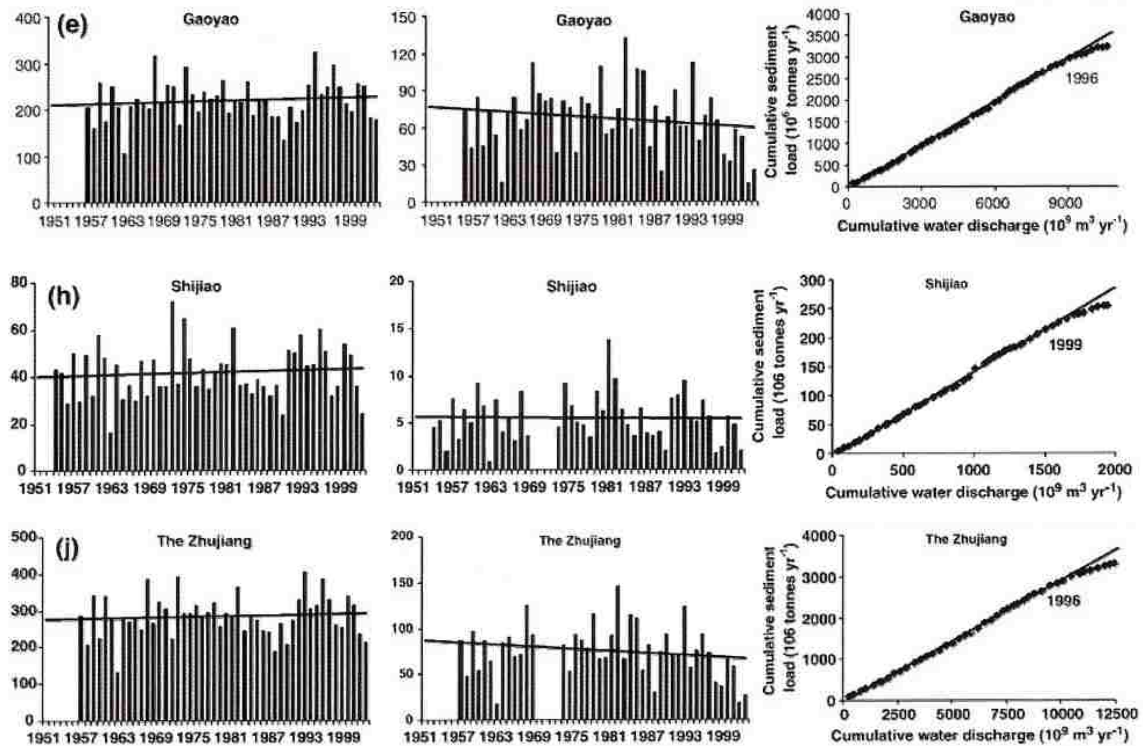
Figure 3.5 The variations of water discharge, sediment load and the associated double mass plots at Gaoyao, Shijiao hydrological gauging stations and the whole Pearl River (excluding the delta region) (from Zhang *et al*., 2007)

A positive linear correlation between cumulative water discharge and sediment load was suggested by Zhang *et al*. (2007a) by plotting cumulative sediment load versus cumulative water discharge from nine hydrological gauging stations as well as the whole Pearl River (Figure 3.5). A similar correlation between suspended sediment load and water discharge has been found in many big rivers e.g. the Yangtze River (Yu, 2006; Yang *et al*., 2007). Sediment increases with increasing water discharge, although increase in the sediment load slows down when water discharge reaches a certain value, e.g. 10 000 m3/year for the Pearl River (excluding the delta region) in 1996 (Figure 3.4; Zhang *et al*., 2007a).

During the past decades, human activities, such as sand mining, have become an important factor that influences the liner correlation between sediment load and water discharge. Zhang *et al*. (2007a) pointed out that slight increases of water discharge and significant decreases of sediment load have taken place since the early 1990s in both rivers (Figure

52

3.5). The averaged annual water discharges were 214.9 $\times 10^9$ m^3 from 1958–1990 and 231.7 $\times 10^9$ m^3 from 1991–2004 at Gaoyao, and 40.9$\times 10^9$ m^3 and 43.8 $\times 10^9$ m^3 at Shijiao for the above two periods respectively (Figure 3.5). The averaged annual sediment load was 71.4 $\times 10^6$ t and 57.9$\times 10^6$ t at Gaoyao, and 5.8 $\times 10^6$ and 4.8 $\times 10^6$ t at Shijiao for the two periods respectively (Zhang *et al*., 2007a). The slightly increased water discharge and significantly decreased sediment load since the early 1990s could contribute to sand mining (Lu *et al*., 2007).

Protected by rocky islands (Figure 3.2), wave energy within the estuary is low and insignificant. The multi-yearly average tidal range is 0.86-1.6m, while the maximum tidal range is 2.29-3.36m (Huang *et al*., 2004). Except for destruction by hurricanes and storms, sediments in the Pearl River estuary are well preserved under the weak tide regime (Owen, 2005). The estuary is under the combined influence of sea-level changes and climate changes, and more recently, human activities (Zong *et al*., 2009a).

3.7 Vegetation cover

In the modern day, subtropical and tropical forests are the dominant vegetation type in the Pearl River catchment (Figure 3.6; Winkler and Wang, 1993). Forests exist mainly on highlands surrounding the delta and upper areas of the catchment, e.g. Yunnan Province located in the upper West River catchment. The deltaic area has been reclaimed for urban development. Tidal areas along the mouth of the river have been intensively reclaimed for agricultural use during the past decades (Figure 3.6).
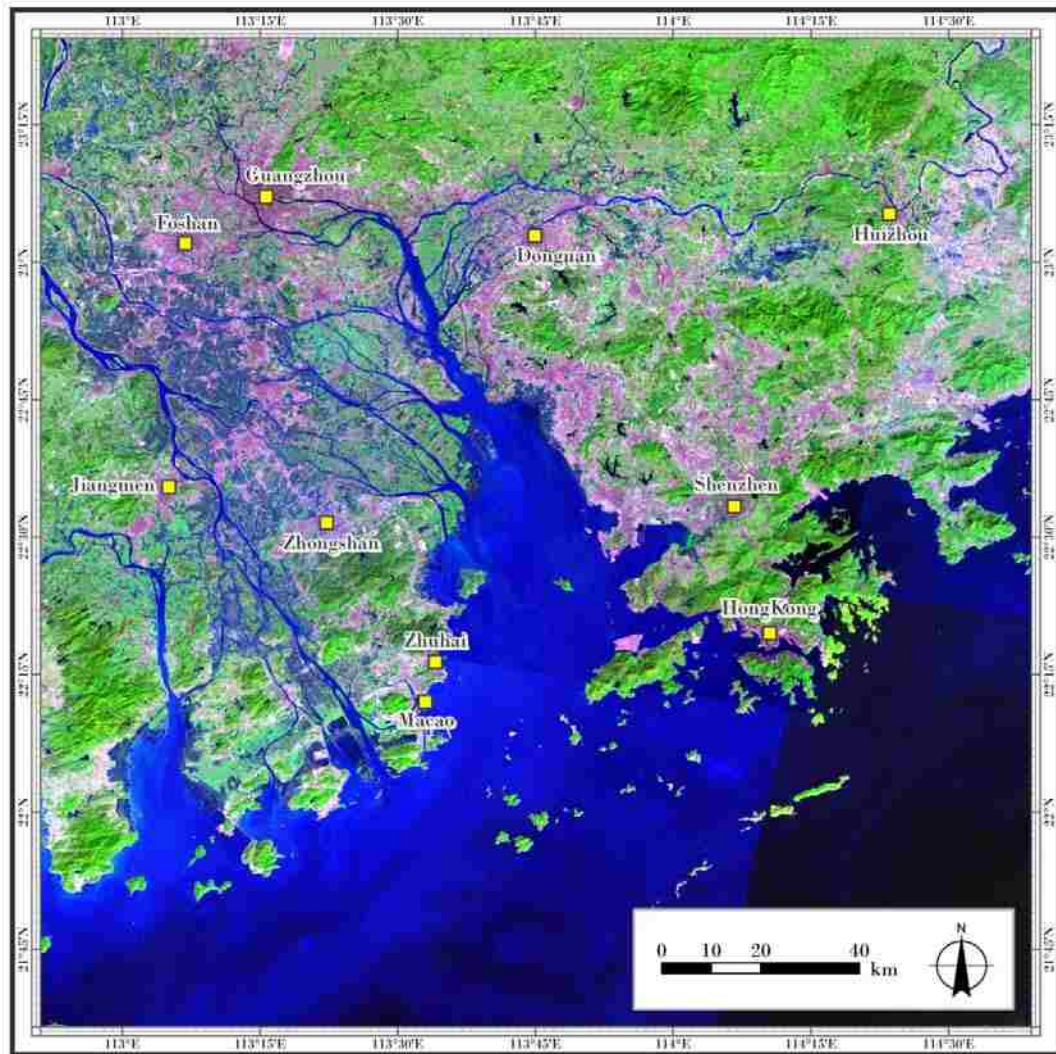
Figure 3.6 Land uses of the Pearl River catchment and delta area (LandSat image 2002-2003. Band 7, 4 and 2). Areas in red are main urban areas; green areas of higher altitude are tropical forests; green areas near the river mouth are mainly agricultural.

Although the monsoonal climate during the Holocene has experienced a weakening process with some fluctuations imposed on this trend, vegetation in south China has been dominated by tropical and subtropical forests throughout the Holocene (Winkler and Wang, 1993) according to pollen records from Taiwan (Tsukada, 1967). Tsukada (1967) analysed two cores from central Taiwan, and suggested that during the early Holocene when the climate was warmer than at present, pollen from subtropical and tropical plants dominated

54

along with pollen from warm-temperate forest trees. These types of pollen started to increase at 10,000 cal. yr BP and peaked at 8000 cal. yr BP (Tsukada, 1967). Pollen records from Huguangyan Marr Lake in Leizhou Peninsula (110°17′E, 21°9′N), southern China, reveal six main changes in the vegetation type of this area (Lu *et al.*, 2003). Those dominant vegetation types are the southern subtropical evergreen monsoon forest (65,000-56,000 cal. yr BP), middle subtropical evergreen and deciduous broad-leaved forest (56,000-50,000 cal. yr BP), southern subtropical evergreen monsoon forest (50,000-42,500 cal. yr BP), middle subtropical evergreen-deciduous broad-leaved and conifer mixed forest (42,500-14,000 cal. yr BP), tropical seasonal rain forest (14,000-5000 cal. yr BP), and the semi-evergreen seasonal rain forest (5000-0 cal. yr BP). Land use has been intensive in China for the past several thousand years. Vegetation changes associated with agriculture have been documented in pollen records from Taiwan dating back to 4000 yr ago (Tsukada, 1967).

3.8 Postglacial sea-level rise and marine transgression

Sea-level change is the major factor determining the base level and available accommodation space (Zong *et al.*, 2009a). However, the Holocene sea-level curve in the Pearl River delta may be considered largely as a result of long-term geological subsidence of the receiving basin (Zong, 2004). Sea-level curves from east Guangdong (Figure 3.7a), a region which is influenced a little by tectonic movement (Huang *et al.*, 1986), and from west Guangdong and Hainan (Figure 3.7b), a region which is geologically stable, no high sea-level highstand is shown in the mid-Holocene (Zong, 2004; Figure 3.7). In the mouth area of the basin the valleys are incised to 25-30m (Zong *et al.*, 2009a). The shallow nature of the receiving basin has resulted in it being initially inundated by the sea as late as 9000 cal. yr BP, when the relative sea level (RSL) rose to -20m (Figure 3.7; Zong, 2004). RSL rose from -20m to -12m soon after 9500-8200 cal. yr BP, followed by two sharp rises from -12m to -3m during 8200-8000 cal. yr. BP (Zong, 2004) and 7500-7000 cal. yr BP (Yim *et al.*, 2006; Bird *et al.*, 2007). RSL reached the present-day height at about 7000-6000 cal. years BP, and has changed little since (Figure 3.7; Zong, 2004). High sea level creates

conditions around a river mouth favourable to the development of deltas and estuaries as depositional centres (Zong *et al.*, 2009a).
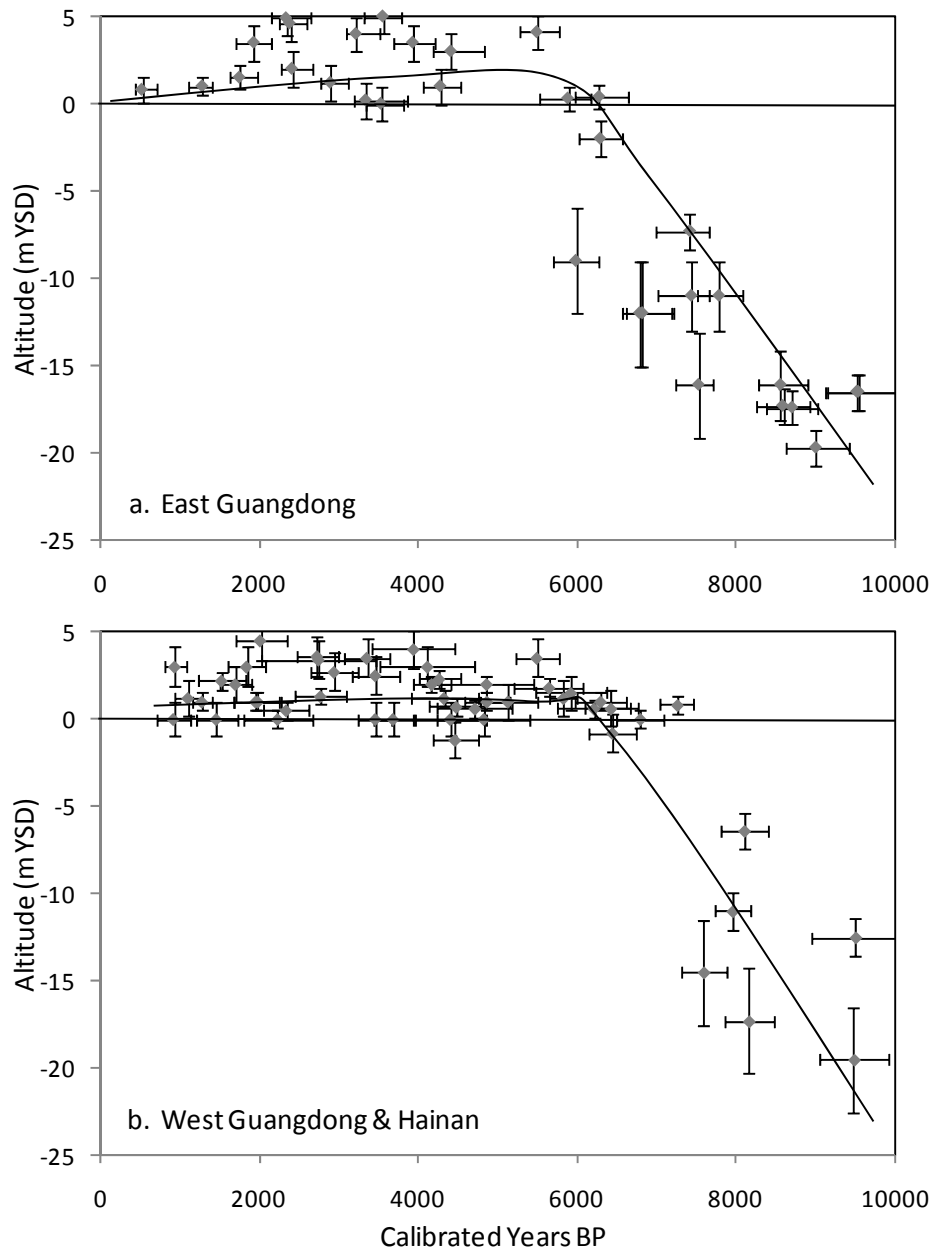
Figure 3.7 Sea-level curves from the east Guangdong (a) and the west Guangdong and Hainan regions (b) (after Zong, 2004), YSD: Yellow sea datum.

According to Zong *et al.* (2009a), the sedimentary record indicates that at the start of the Holocene deltaic sedimentation, the receiving basin was filled with an older (possibly MIS5e) estuarine unit and fluvial sands and gravels, with bedrock exposed in parts of the basin (Figure 3.8). The receiving basin was initially inundated by the sea as late as 9000 cal. yr BP, and the initial sedimentation took place along palaeoriver channels dominated by fine sands dating back to around 9500-8200 cal. yr BP. (Zong *et al.*, 2009a). As sea level kept rising (Figure 3.7), the inner part of the receiving basin was under fluvial influence, whilst the seawards part of the basin was under open estuarine conditions (Figure 3.9a).
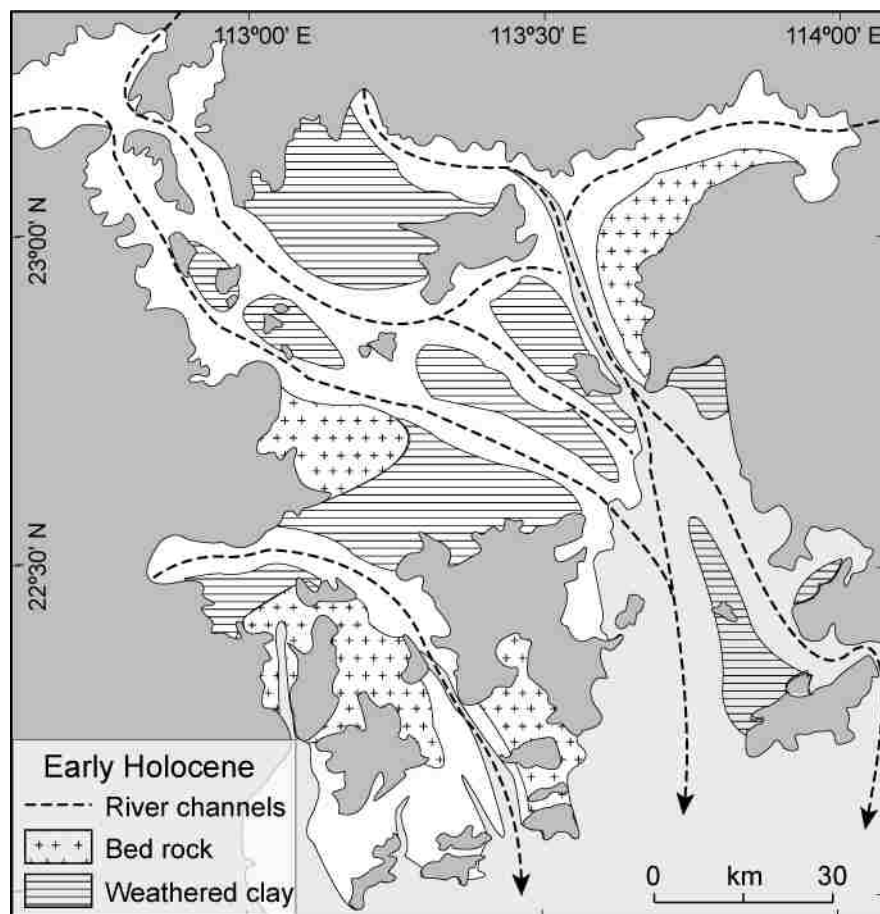
Figure 3.8 The early-Holocene palaeo-landscapes of the receiving basin, with major palaeo-valleys filled with coarse sands and gravels, areas of bedrock exposed, and areas of older marine deposits capped by weathered clay or desiccated crust (from Zong *et al.*, 2009a)

A transitional zone was located in the middle of the receiving basin (Figure 3.9a). The first deltaic shoreline was developed near the apex of the delta plains (Figure 3.9b) at about 6800 cal. yr BP when relative sea level reached its present-day height and stabilized (Zong, 2004). Consequently the transgressive process changed to a regressive process, ie, the onset of deltaic progradation (Zong *et al.*, 2009). Between 6800 and 2000 cal. yr BP, the deltaic shoreline advanced slowly seawards (Figure 3.9c) relating to climate changes during this period as the sea level stayed relatively stable (Zong, 2004; Wang *et al.*, 2005; Zong *et al.*, 2009a). By 2000 cal. yr BP about half of the deltaic plain had emerged (Figure 3.9d). Throughout the past 2000 years, people have employed various techniques to reclaim newly emerging parts of delta plain for agriculture. These activities firstly accelerated the shoreline advance, e.g. shoreline progradation rate was up to 29 m/year in the past 2000 years, which was much faster than it used to be, e.g. 10.5 m/year between 6800 and 4500 cal. yr BP and 6.4 m/year between 4500 and 2000 cal. yr BP. Secondly, these human activities slowed down the reduced sediment supply into the estuary as most sediment had been trapped behind edge of the delta plain (Zong *et al.*, 2009a; Li *et al.*, 2001).
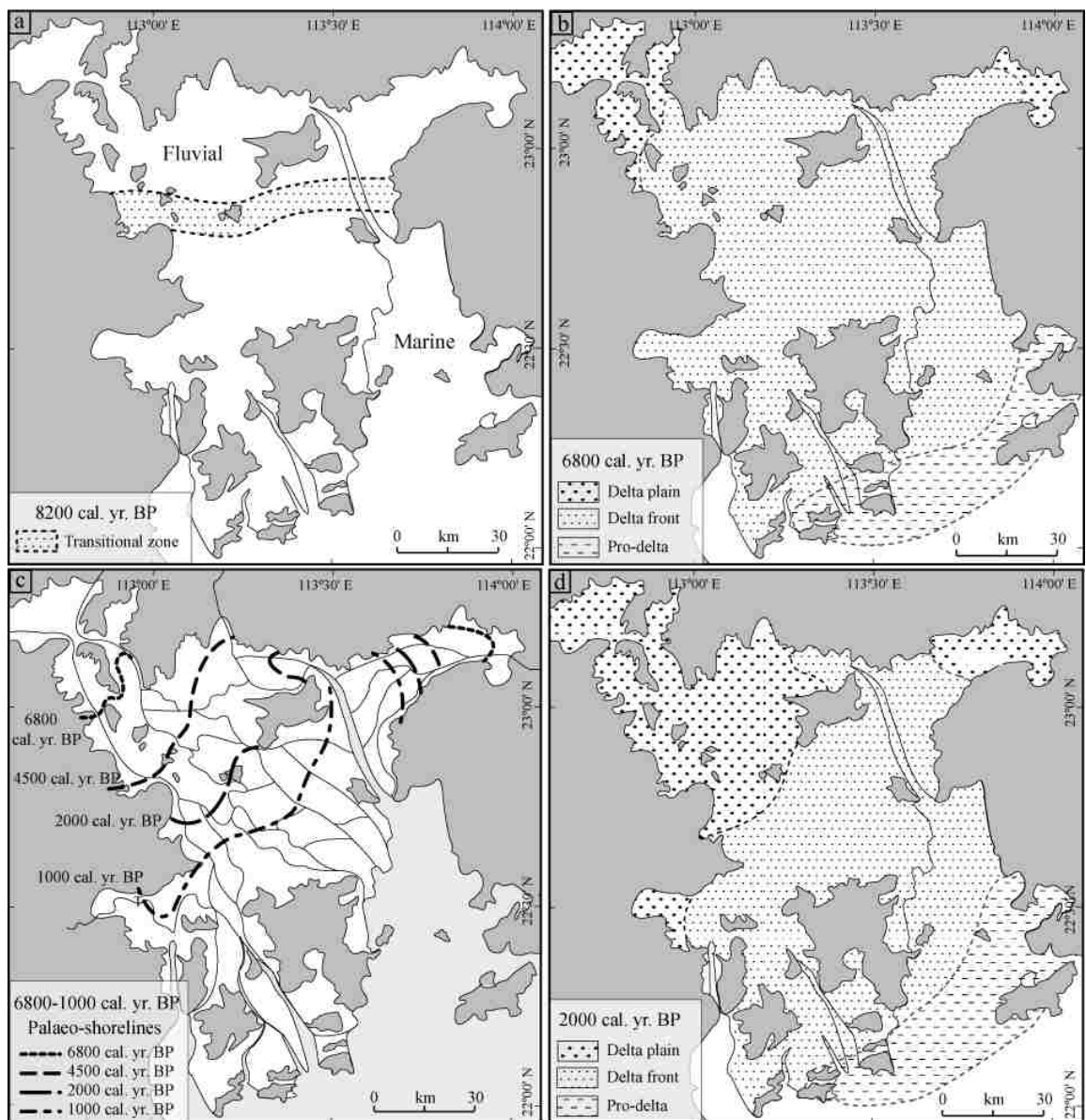
Figure 3.9 Shoreline progradation since the early Holocene. (a) The marine limit before c. 8200 cal. yr BP, based on sedimentary evidence of the initial phase of edimentation. (b) The deltaic sedimentary environments within the receiving basin when the rise in sea level stabilized and the shoreline retreated to its landward-most position around 6800 cal. yr BP. (c) Shoreline progradation during 6800-1000 cal. yr BP based on archaeological evidence and historical records. (d) The deltaic sedimentary environments within the receiving basin around 2000 cal. yr BP. (after Zong *et al*., 2009a).

3.9 Evolution of the Pearl River delta during the Holocene

The evolution of the Pearl River delta during the Holocene is the result of the interaction between climate change and sea-level change, while human activity becomes an important factor from 2000 cal. yr BP onwards (Zong *et al*., 2009a). Based on lithological evidence, microfossil (e.g. diatoms) and archaeological records, Zong *et al*. (2009a) suggested that evolution of the Pearl River delta since 9000 cal. yr BP can be divided into three stages (Figure 3.10). During the period 9000-7000 cal. yr BP, the formation of deltaic sequences was a consequence of rapid sea-level rise during this period. The rate of sea-level rise slowed down remarkably around 7000 cal. yr BP, and sedimentation progradation begins (Figure 3.10; Zong *et al*., 2009a). During the period 6800-2000 cal. yr BP, initially, both the progradation of the delta plains near the apex and aggradation of delta front sedimentation in the central and lower parts of the receiving basin were rapid (Figure 3.10), due to strong monsoon-driven runoff and, apparently, minimal sea-level variation. However, the progradation rate gradually slowed down due to the weakened monsoon-driven freshwater discharge during this period (Zong *et al*., 2009a). The rapid shoreline advance since 2000 cal. yr BP is a consequence of increased human activity trapping sediments in the encircled tidal flats along the front of delta plains (Figure 3.10; Zong *et al*., 2009a).
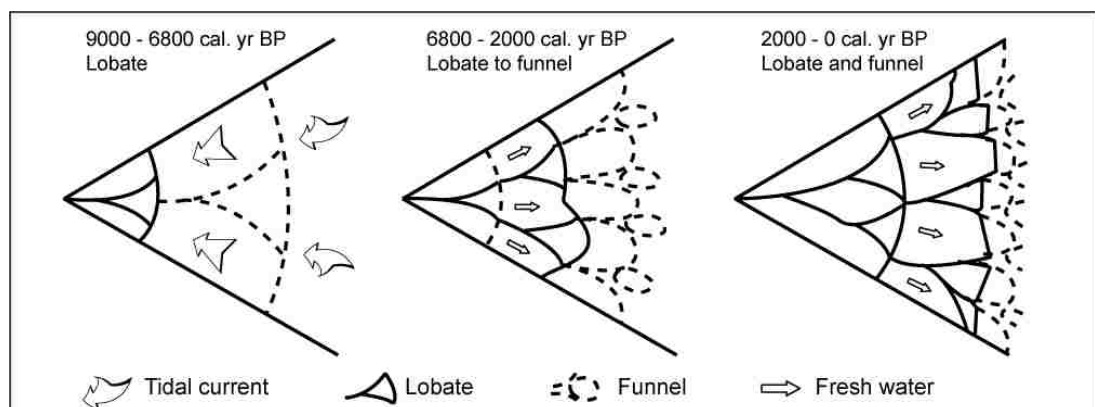
Figure 3.10 Evolution model for the Pearl River delta (from Zong *et al*., 2009a)

3.10 Suitability of the Pearl River estuary for the mid-Holocene EAM reconstruction

The Pearl River estuary receives sediments from three main sources: 1) river-derived material e.g. freshwater algae, terrestrial-plant debris and other fluvial suspended sediments, 2) tide-derived marine material from the South China Sea, e.g. marine algae, marine-plant debris and suspended sediments, and 3) in situ brackish-water material, e.g. brackish-water algae, sediment-surface plants and other suspended matter (Figure 3.11).
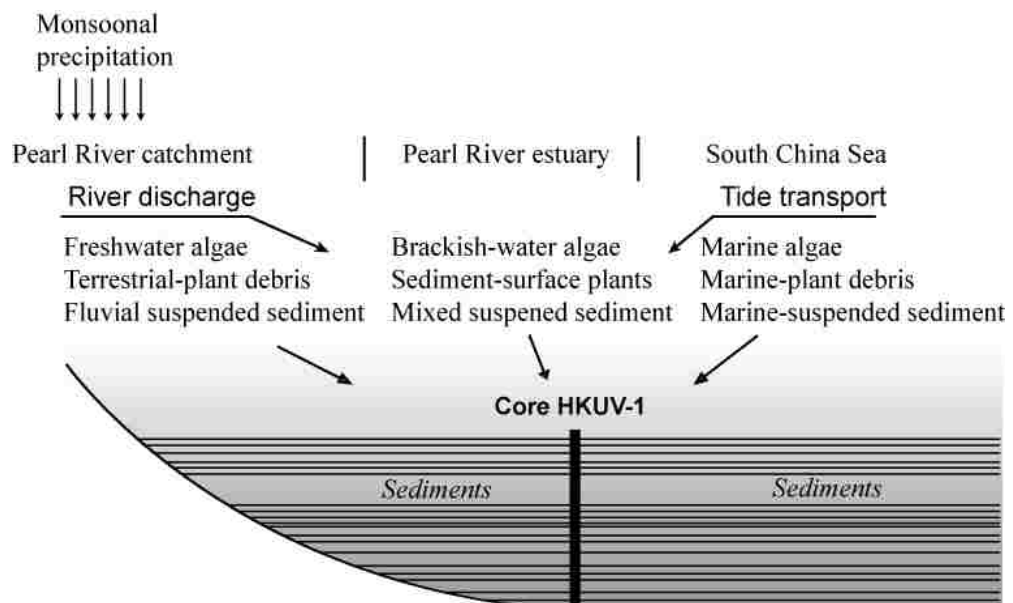
Figure 3.11 Sediment input into Pearl River estuary

At present, the proportion of the three main sources of estuarine sediment is controlled by the strength of the river discharge, which is driven by the strength of the monsoonal precipitation (Li *et al*., 1990; Zong *et al*., 2009a). Approximately 80% of the annual precipitation occurs during spring and summer (from June to October) (Xu *et al*., 1985), which produces 80% of both the river discharge and sediment load into the estuary (Li *et al*., 1990; Zhang *et al*., 2008). During the cold-dry winter monsoon season, significantly reduced precipitation generates lower freshwater discharge than during the summer season.

As a consequence, the proportion of the terrigenous sediments in the estuary decreases in comparison with brackish and marine sources.

Over a longer time scale (e.g. on a centennial or millennial time scale), sources of dominant estuarine sediment are influenced by relative shoreline movements, sea-level changes, and monsoonal climate changes. As the sea level in this area has been relatively stable during the mid Holocene (Figure 3.4; Li *et al*., 1990; Zong, 2004), the monsoonal climate becomes one of the most important controlling factors for the sediment flux into the estuary (Li *et al*., 2001; Wang *et al*., 2005; Zong *et al*., 2006). As the freshwater flux is sensitive to monsoon-induced precipitation changes, e.g. a strong summer monsoon generates large amounts of rainfall in the Pearl River catchment area, resulting in high freshwater runoff into the estuary. Furthermore, sediment flux increases with increasing freshwater flux, e.g. positive linear correlations between cumulative freshwater discharge and cumulative sediment flux (Yang *et al*., 2007; Zhang *et al*., 2007). Estuarine sediments preserved during periods when strong summer monsoon prevails over this area would have a higher proportion of terrigenous sediments compared to sediments deposited during periods of stronger winter monsoon (which would tend to have a lower proportion of terrigenous sediments relative to marine/brackish sediments). Thus, the monsoon-induced freshwater discharge can be reconstructed by examining changes in the relative dominance of sediments from the three sources identified above preserved in the Pearl River estuary.

Sediments dominated by a strong terrestrial source would be deposited under strong summer monsoon climate, when the high precipitation produced large river discharge; conversely sediments dominated by a low terrestrial source, and/or a strong marine source would be deposited under weak summer monsoon conditions, when the precipitation was low. Based on this assumption, this study employs multi-geochemical proxies (organic carbon isotopes, bulk organic carbon to bulk nitrogen ratios and major/trace elements) to undertake a case study from the Pearl River estuary, examining the East Asia monsoon variability during the mid Holocene.

Progradation of the Pearl River delta during the mid-Holocene (Zong *et al*., 2009a) results in a progressively shorter distance between the land and the site of the estuarine core, and accordingly result in higher terrigenous input. However, it is worth mentioning that the rapidly-advanced shoreline since 2000 cal. yr BP is a consequence of increased human activity trapping sediments in the encircled tidal flats along the front of delta plains (Figure 3.9d; Li *et al*., 2001; Zong *et al*., 2009a).

3.11 Summary of the chapter

The Pearl River catchment is located in the subtropical area, under the influence of the monsoon climate. Monsoonal climate results in seasonal and inter-annual differences in freshwater flux and sediment load into the estuary. Strong freshwater runoff from the West and North river results in stronger influence of freshwater in the west side of the estuary than in the east side, as well as higher turbidity in the west than in the east. The dominant vegetation type in this area during the Holocene has always been tropical and subtropical forests. The stable sea level since 6800 cal. yr BP, together with the shoreline advance during the Holocene make this are suitable for this particular study. Enhanced agriculture activities in this area since 2000 cal. yr BP have possible influences on the proxy information used in this study.

Chapter 4 Methodology

4.1 Introduction

This chapter introduces the site selection strategy and sampling methods in the field. Material collected from the field site includes plants, terrestrial soil samples, estuarine surface sediment samples, environmental parameters of the sampling sites, and a sediment core (core UV1). Samples are then analysed for the organic carbon isotopes, C/N ratios and key elements in the laboratory. Detailed sampling preparation methods and data analysis procedures using a range of computing programs are also outlined in this chapter.

4.2 Field sampling strategy

4.2.1 Site selection

To meet the aims and objectives of this thesis, this study requires modern-day samples to develop a modern-day analogue and a high-resolution fossil core to allow reconstruction of Holocene monsoonal history. Sampling criteria for modern-day and fossil samples are thus different.

The modern-day samples cover the range of different environmental conditions across the estuary from freshwater, brackish-water through to marine conditions. This sampling strategy will help investigate the spatial variability in the two proxies from freshwater through to the marine end member suitable to reconstruct temporal changes at one particular location. These samples also cover recent anthropogenic sources. An initial 40 surface sediment samples from the east side of the estuary (unfilled circles in Figure 4.1) were collected by Zong *et al* (2006), which cover the eastern part of the estuary. Due to the estuarine-hydrological circulation, the west and east part of the

estuary show significantly different geochemical features (Li *et al.*, 2001). This study collected an additional 51 surface sediment samples from the western part of the estuary (filled circles in Figure 4.1). The combination of these 2 groups of samples provides a full modern-day data set covering the full range of environments ranging from the freshwater environment (samples from the North River and East River channels) to the fully marine environment (samples from outside Lingding Island and Southeast Hong Kong), via brackish water environments (samples from the estuary).
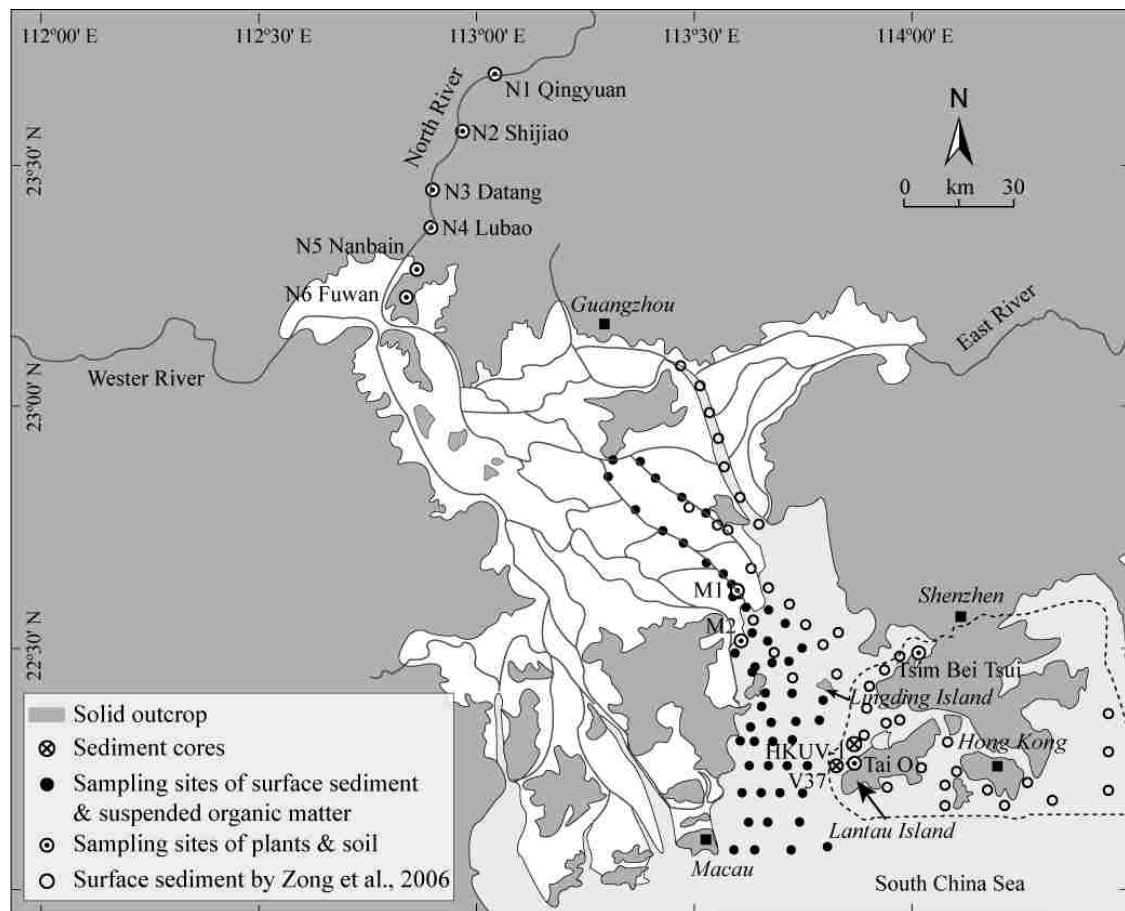
Figure 4.1 Sampling sites. Surface sediments were collected at all sites. Seasonal suspended matter was collected from sites of this study, with their environmental conditions measured.

Additional modern samples were collected to cover potential sources of the estuarine sediments, such as soil and plants from terrestrial areas. Soil samples and plants along the North River (N1-N6 and M2 in Figure 4.1) represent terrestrial material under freshwater influence. Soil and plant samples from mangrove areas (M1 and Hong Kong area, Figure 4.1) represent material under brackish water influence. Two main

agricultural products of the Pearl River delta, rice and sugarcane leaves and their soil samples, together with other agricultural plants (e.g. banana, lotus) and soil samples were collected to represent recent agricultural input into the estuary. Modern plankton samples were also collected from the same sampling sites as the surface sediments (filled circles in Figure 4.1). Plankton samples were collected in June 2006 (summer) and January 2007 (winter) to investigate possible seasonality.

Zong *et al* (2006) have suggested that carbon isotopes and C/N ratios provide a good indicator for palaeo-river discharge in the Pearl River estuary. However the core analysed in their study, Core V37 (Tai O, Lantau Island, Hong Kong, 22°15'02"N, 113°51'29"E, Figure 4.1) is only 1.5m below mean sea level and is very close to Lantau Island. Changes in fresh water discharge interpreted by the organic carbon signals from Core V37 might be disturbed by strong tide and freshwater runoff in this area. Therefore a new core, Core UV1, was collected from northwest of Lantau Island, Hong Kong, 22°17'10"N, 113°51'49"E (Figure 4.1) for this study. This area receives sediment delivered by both freshwater runoff and tide, but the depth of the Core UV1 is 9m below mean sea level. Sediment deposited in UV1 is likely to get less shelter than Core V37 due to its further distance from Lantau Island.

4.2.2 Sampling methods

Plant samples were collected with scissors. Whole grass was sampled (including leaves, stems and roots), while from trees only leaves and stems were collected (Park and Epstein, 1960). Plant samples were kept in paper bags in the field, and were dried at 50⁰C overnight in the laboratory of the Institute of Geography, Guangzhou, China, and the laboratory of the Department of Earth Sciences, University of Hong Kong, Hong Kong SAR, China before being shipped back to Durham.

Soil samples (forest soil, riverside soils, mangrove soils and agricultural soils) were collected from under the plants. The top 2-3cm of soil was cleared using a small spade to avoid fresh plant roots and disturbed soil (Liu *et al*., 2003). Samples were stored in polyethylene tubes in a fridge before being shipped back to Durham.

Surface sediment samples were obtained from a boat using a grab sampler from the 51 sampling sites (Figure 4.1). The top 10 cm of sediment was collected, which potentially represents sediment deposited during the past 6-10 years, according to the sedimentation rate of around 0.8 cm/year on shoals within the estuary (Li *et al*., 1990; Zong *et al*., 2006). Samples were sealed in polyethylene tubes and stored in a fridge at 2-3ºC before being shipped back to Durham.

Particulate organic matter (POM), mixed with suspended material, was also collected from the 51 sampling sites (Figure 4.1) by filtering water samples in the laboratory of the Institute of Geography, Guangzhou, China, in both summer and winter 2006. A volume of 5-20 litres of water from each sampling site was collected. Samples were kept in the fridge before filtering to minimize the growth of bacteria. All equipment attached to the filtering system was washed before and after filtering each sample using deionised water. Filter paper used is made of fibreglass (Fisher Brand MF200, 47mm). The amount of sample needed for organic carbon analysis depends on the organic content of samples. In order to collect enough material the filter paper was not changed until it was saturated with suspended matter. As long as there was enough water, 3-4 filter papers of suspended matter were collected for each site. However, sites of low turbidity only 2 filter papers could be collected. As the turbidity of each sampling site varies, the amount of water sample used for filtering was not fixed. From sites of high turbidity, about 5 litres of water were used, while those of low turbidity, 10-20 litres of water were filtered. Filter papers with suspended matter on them were moved to a evaporate plate, and dried at 50ºC overnight. Dried suspended matter samples on filter paper were sealed in sampling bags individually, labelled and stored in desiccators at 20ºC. An extra 10 suspended organic matter samples were collected using a 70μm net in summer. Samples were then washed from the net into a sampling tube, left in the fridge, and freeze dried in Durham.

Water salinity, pH value, dissolved oxygen and water temperature were measured using a YSI meter from the 51 sites in the estuary, in summer and winter 2006. These environmental parameters were measured with the sensor 50cm below the water surface. Data were exported from the YSI meter to a computer using the EcoWatch 3.15.00 (YSI Inc.).

Figure 4.2 Photos from Pearl River estuary during coring (photos by Dr. J.M. Lloyd)

Core UV1 was obtained through the Civil Engineering Department, Hong Kong SAR Government China. It is located at 22º17'10"N, 113º51'49"E (Figure 4.1), in the Pearl River estuary, at an altitude of -9.00m YSD (Yellow Sea Datum). The total length of the core was 35m, reaching the bedrock. Initial ^{14}C dating suggests that the top 10m of sediment was deposited during the Holocene (Zong *et al*., 2009a), and this were used for this specific study. Sediment from 0.00-0.35m and 6.00-6.25m was missed due to the length of the steel coring pipes (6 meter, Figure 4.2). The sediment core was split, and core descriptions were made. One half was kept at the Institute of Earth Science, Kong Hong University as an archive sample. The other half was sampled at 2cm intervals. Bulk samples were collected for radiocarbon dates, from depth of 0.50-0.54m, 1.32-1.34m, 1.90-1.94m, 2.60-2.62m, 4.50-4.54m, 7.50-7.54m and 9.50-9.54m.

4.2.3 Material collected

Material collected for the organic carbon isotopic analysis

Modern-day samples collected for this study represent different sources of the organic input into the estuary system. Plants and soil samples were collected to represent terrestrial organic matter (the forest, riverbank and tidal flat; Table 4.1).

Surface sediment samples and suspended matter were collected from the North River, East River and estuarine area. Environmental parameters of the suspended matter were

measured in both summer (June 2006) and winter (January 2007) and a 10m estuarine sediment core (core UV1) was obtained to reconstruct monsoonal precipitation changes during the Holocene. A brief description of the sampling sites and the type of plant and soil samples can be found in Table 4.1. Locations of all the above samples are presented in Figure 4.1.

Plants: A total of 60 plant samples were obtained for this study including: 1) 34 terrestrial plant samples: terrestrial C3 and C4 plants were obtained from the catchment (sites of N1-N6, and site M2). 2) 12 Mangrove samples were collected from Site M1, Tsim Bei Tsui and Tai O (Figure 4.1). 3) 14 plants were collected from the farmland near the mouth of the North River (near Site M1), including general grass and agricultural plants.

Terrestrial soil samples: Twenty four soil samples were collected for this study including: 1) 9 soil samples from the catchment; 2) 11 mangrove soil samples from the mangrove area; and 3) 4 samples from the farmland.

Suspended organic matter: Forty nine suspended matter samples from the winter season and 35 suspended matter samples from the summer season were collected from the North River and the west part of the estuary (filled circles in Figure 4.1).

Surface sediment samples: Ninety one surface sediment samples in total were used for the analysis of organic carbon isotopes. Fifty one surface sediment samples from the North River and the West part of the estuary were collected by this study and the other 40 samples from the mouth of the East River and the East part of the estuary were collected by Zong *et al.* (2006) (Figure 4.1).

Environmental parameters: Water salinity, water depth, pH values, total dissolved oxygen and water temperature were measured from sites of the suspended matter samples, using an YSI meter in both seasons.

Fossil data: A sediment core (UV1) was obtained from the estuary (22°17'10"N, 113°51'49"E). Total length of Core UV1 is 30m. The top 0.35m sediment was missed during the coring process. Sediment from 6.0-6.25m was also missed due to the length

of the core (Figure 4.2). Sediment from 10.29-0.35m was sampled at a 2cm sampling interval, producing a total of 501 samples.

Material collected for analysis of key elements

Terrestrial soil samples, estuarine surface sediment samples and fossil sediments were analyzed for 15 elements including: 1) alkali metals: Na, K and Rb; 2) alkaline earth metals: Be, Mg, Ca, Sr and Ba; 3) transition metals including Mn, Fe, Co, and Al; and 4) non-metals: B and As.

Table 4.1 Location and vegetation cover of sampling sites for plants and soil samples

Sites for plant and soil samples	Plants	Soil samples	Site description
N1 (Qingyuan)	B1	A1: Shrub soil	This sampling site is located on the riverbank, and has been used as a park. It is covered mainly by grass and only one kind of tree is planted. The plant sample collected here is a mixture of both the leaves and stem of this type of tree. A1 is the soil under the tree.
N2 (Shijiao)	B2-B4	A2: Shrub soil	Plants are grass or shrubs, no trees. Soil sample was under the shrubs.
N3 (Datang)	B5-B8	A3: Shrub soil	There are no trees but grass and shrubs in this site. Soil sample was under the shrubs.
N4 (Lubao)	B9-B13	A4: Shrub soil; A5: Pine soil; A6: shrub soil	Site N4 is covered mainly by grass, with some shrubs. A4 soil is the soil sample under shrubs on the riverbank. A5 is the soil sample under a pine tree inside the levee. A6 is the soil under the shrubs near the pine.
N5 (Nanbian)	B14-B17	A7: Riverbank soil (under water). A8: Shrub soil	At the riverside, plants from this site grow in water. A7 is under-water soil sample at the riverside. On the other side of the levee, plant and soil (A8) samples were also collected.
N6 (Fuwan)	B18-B29	A9: forest soil	A small woods, mixed with trees and shrubs. Plant samples are a mixture of both tree and shrubs. Soil sample A9 is under tree and shrubs from the small forest.
E1(M2)	B31-B35	PE77, G1-G4	
E2(M1)	B30	PE76	Mangroves are found near a port.
E3(Tai O)	B36-B41	A10-A17	
E4(Tsim Bei Tsui)	B42-B47	A18-A20	

Pearl River Catchment / River mouth / Tidal flat

71

4.3 Laboratory analysis and data

4.3.1 Organic carbon isotopes and C/N ratios

Procedures of the sample preparation for surface sediment samples, core sediment samples, and soil samples are the same:

1) Approximately 2g of sediment sample was placed in a 250ml beaker in a fume cupboard; approximately 100ml 5% HCL was added to the sample, it was covered with a watch glass and left for 24 hours. This step is designed to remove the carbonate from samples.

2) The digested sample was filtered with the Fisher Brand 200 filter paper, washing 3 times with deionised water, using a 500ml filter cup. This is designed to get rid of extra HCL left in sample, and protect the machine from acid.

3) Transfer sediments from the filter to evaporating plates, and dry them at 50ºC overnight.

4) Crush dried sediment samples with pestle and mortar, and weigh (25-50mg) for δ^{13}C and C/N testing. Weight of the sample used depends on the organic material concentration of the sediments.

Plant samples are placed in a –80 ºC freezer overnight followed by freeze drying over 24 hours. Samples were then crushed and homogenised in a ball mill at the speed of 500 rpm for 5-15 minutes (depending on type of plants). Samples were then weighed for δ^{13}C and C/N testing. As plants are pure organic material, only a small amount of sample is required, 1-2mg.

Plankton samples mixed with other suspended matter on the filter paper were dried at the field site, and were difficult to remove from the filter papers and weigh. Some samples were successfully scraped from the filter papers, were weighed and produced a total organic carbon and total nitrogen results. However, those samples stuck to the

filter paper had to be tested with the filter paper, and have no %C or %N results, as the exact weight of these samples could not be measured.

$\delta^{13}C$ analyses were performed by combustion in a Carlo Erba NA1500 (Series 1) on-line to a VG Triple Trap and Optima dual-inlet mass spectrometer, with $\delta^{13}C$ values calculated to the VPDB scale using a within-run laboratory standards (cellulose or broccoli) calibrated against NBS-19 and NBS-22. Replicate analysis of well-mixed samples indicated a precision of $\pm<0.1‰$ (1SD). C/N ratios were determined with by reference to an Acetanilide standard. Replicate analysis of well-mixed samples indicated a precision of $\pm<0.1\%$. All samples were prepared in Durham University, and weighed and tested in NERC Isotope Geosciences Laboratory, British Geological Survey, Nottingham, UK.

4.3.2 Key elements

Samples were prepared and analyzed in the laboratory of the Department of Geography, University of Durham, UK, following the ICP-MS Total Metals Extraction (HF-HCl-HNO_3) description. Samples were placed in a -80 ºC freezer overnight followed by freeze drying over 24 hours. Samples were then crushed and homogenised in a ball mill, at a speed of 500 rounds/minutes. After ball milling, samples were stored in a desiccator at 20 ºC. A known mass (approximately 250mg) of the sample was weighed into a HF-resistant microwave extraction vessel. The ICP-MS settings and internal standards are based on EPA method 200.8 r5.4. The reliability of the methods employed was demonstrated through the correlation coefficients for replicate and analysing samples. Repeats were taken by running double samples in different batches, as well as repeat running the same sample twice. All repeats have a relative difference of <7.5%.

4.3.3 Grain size analysis

The 91 surface sediment samples were prepared for grain size analysis. 86 fossil samples were analyzed at an interval of 12 cm. Samples were placed in a beaker filled with tap water overnight. Grain size analysis was carried out using a laser granulometer

(Coulter LS 13200) in the laboratory of the Department of Geography, University of Durham.

4.3.4 Sediment core chronology

An initial four range finder dates from depths of 1.92m, 4.52m, 7.52m and 9.52m were obtained. Following stable isotope analysis of the core further dates were obtained from 2.61m, 1.33m and 0.52m to provide a more accurate chronology of key intervals. Radiocarbon dates were derived from handpicked mixed species of benthic foraminifera, except sample at 0.52m, which used a well-preserved bivalve shell. Bulk sediment samples were left in tap water overnight to disaggregate fine-grained sediment. The sediment samples were then carefully wet-sieved through 500μm and 63μm sieves. Material finer than 63μm were discarded. No shell or other debris was found of greater that 500μm from the four samples. Material between 63μm and 500μm were collected in a beaker, and was analyzed within a couple of days. Foraminifera were wet-picked out of samples from a tray, using a fine haired pen brush, under the light microscope at a magnification between ×15 and ×50. Selected samples were attached to Chapman slides, and were transferred to pre-weighed polyethylene vials. Radiocarbon dates from 1.92m, 4.52m 7.52m and 9.52m were run at East Kilbride (NERC) radiocarbon laboratory. Radiocarbon dating from 0.54m, 1.33m and 2.61m were run at AMS laboratory in the Guangzhou Institute of Geochemistry, Chinese Academy of Sciences, Guangzhou, China, and the State Key Laboratory of Nuclear Physics and Technology Peking University, Beijing, China. The calibration program used is CALIB 5.10 and the marine04 programme (Stuiver *et al*., 1998), with a correction factor (ΔR) of -128±40 years according to Southon *et al*. (2002).

4.4 Methods of data analysis

Modern-day samples were collected to investigate the spatial signature of bulk organic $\delta^{13}C$ and C/N and concentrations of key elements relating to sources of sediment. Thus methods of data analysis applied to the modern-day analogue aim to cluster the modern-day samples into different groups, representing different dominant sources of the sediment. Hierarchical cluster analysis (SPSS for windows 15.0) was employed to cluster the estuarine sediment samples and suspended organic matter (Figure 4.3). Contour maps of key elements within the estuary were developed using the interpolation method under the Arcgis 9.2 program.

Table 4.2 Results of the interpolating of the fossil data

	Result Variable	N of Replaced Missing Values	Case Number of Non-Missing Values		N of Valid Cases	Creating Function
	First	Last	First	Last	First	Last
1	$\delta^{13}C\_3$	19	1	500	500	MEDIAN($\delta^{13}C$,100)
2	TOC	18	1	500	500	MEDIAN(C,100)
3	%N	24	1	500	500	MEDIAN(N,100)
4	C/N	24	1	500	500	MEDIAN(CN,100)

Missing data are found from 6.0-6.25m (14 samples), and from 11 samples from various depths due to low organic carbon concentration. This interpolation was specifically for the spectral analysis section, so initial presentation of the data and description do not include the interpolation. The $\delta^{13}C$ values, %C and %N were interpolated using the method of the serial median (100 points) in SPSS for windows15.0 program (Table 4.2). Missing C/N ratios were then calculated using the formula of $C/N = \dfrac{\%C}{\%N}$.

Samples from 1.01m, 1.02m and 10.09m have been rerun to check the reliability of peak values (Table 4.3), and the replicates show a precision of $\pm<0.1‰$ (1SD) for $\delta^{13}C$ values. Due to the small differences between different analyses, values from the first run are used in later chapters (Appendix 8-11).

Table 4.3 Replicates for some $\delta^{13}C$ values

Depth (m)	First run (F)	Repeats (R)	R-F
1.01	-18.46	-19.55	-0.21
1.02	-10.70	-10.74	-0.01
5.95	-25.64	-25.62	-0.02
5.99	-26.13	-26.18	-0.04
6.31	-25.23	-25.16	+0.01
6.33	-25.01	-24.92	-0.00
6.35	-25.03	-25.04	+0.00
6.37	-24.96	-24.93	+0.00
10.09	-27.28	-27.23	+0.15

Spectral analysis of the core data is undertaken using the PAST program (Hammer, *et al*., 2001). Data were detrended to remove any general trend before the spectral analysis. Exponential smoothing was applied to the results of both organic carbon and metals to produce smoothed data in SPSS for windows15.0, using the following simple model

$$S_t = \alpha X_t + (1-\alpha)S_{t-1}$$

Where X_t is the raw data, S_t is the output of the exponential smoothing algorithm, α is the smoothing factor which is $0<\alpha<1$, and t is the time series data. At the beginning of this sequence of observations $S_0 = X_0$.

4.5 Summary of the chapter

This chapter outlines the methods used in data collection, production and analysis in this thesis, including sampling strategy, and summarises the material collected. Selection of samples from the fossil core for radiocarbon dating analysis is discussed in this chapter. This chapter also presents methods used to interpolate missing data to allow spectral analysis to be performed on the fossil core data.
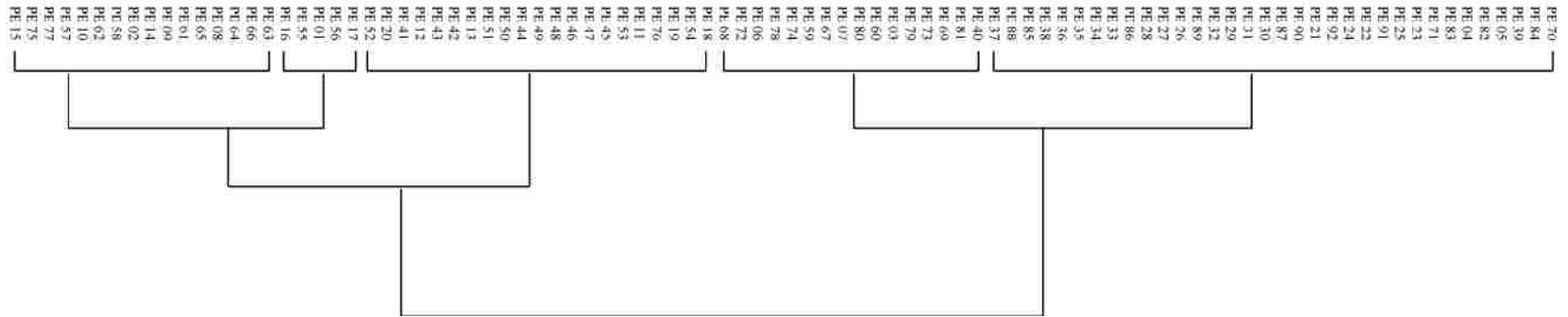
Figure 4.3 Dendrogram of the Hierarchical cluster analysis, using Average Linkage (Between Groups). Rescaled Distance Cluster Combine

Chapter 5 Modern-day geochemical features of the Pearl River delta and estuary

5.1 Introduction

This chapter discusses geochemical features of the Pearl River delta and estuary, and their implications for sediment sources. Geochemical features discussed here include two parts: 1) the organic carbon isotopic signature (δ^{13}C), C/N ratios and total organic carbon content (TOC) values of plants and sedimentary organic matter; and 2) distribution of 15 key metals in sediments within the Pearl River delta and estuary. These results carried two objectives: firstly, to construct a modern-day analogue for both proxies; and secondly, to assess the application of the two proxies as indicators for sediment sources and sedimentary environments.

Samples collected for the organic analysis include terrestrial plants and soil samples, estuarine suspended organic matter (POC) and estuarine surface sediment samples (Figure 5.1). Values of the δ^{13}C, C/N and TOC in this chapter are presented in the format of 'average value ± standard deviation (SD)'. Results and discussions of the organic matter in this chapter are based on the following set of modern-day samples:

- *Plants.* 1) 9 C_4 plants, including 6 general C_4-grass samples and 3 samples of sugarcane leaves; and 2) 39 C_3 plants, including 20 general C_3 plants, 12 mangrove samples and 7 agricultural plants e.g. banana leaves, lotus, reed and rice (Appendix 1).

- *Soil samples.* Multiple soil samples were collected from a range of locations as follows: 2 forest soil, 3 agricultural soil, 8 riverbank soil and 12 mangrove soil (Appendix 2; 6).

- *Particulate organic carbon (POC).* Samples of POC were collected during both summer and winter seasons. A total of 45 samples were collected during summer, including 35 samples on filter paper (Appendix 3) and 10 samples on a 70 μm net (Appendix 4). During the winter season, a further 49 samples were collected (Appendix 3).

- *Surface sediment samples.* A total of 91 fluvial and estuarine surface sediment samples were collected and analyzed (Appendix 5; 7).
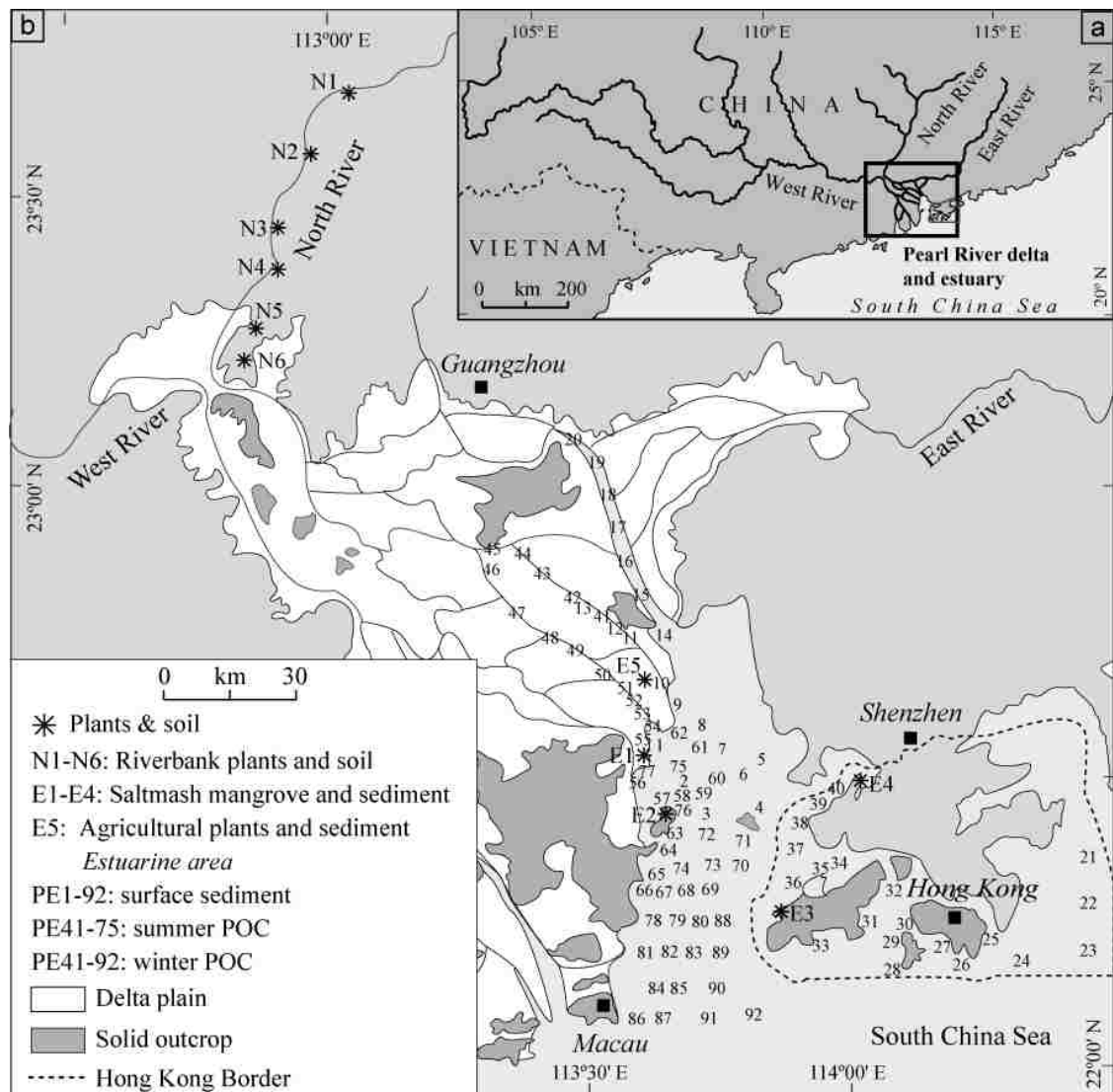
Figure 5.1 Study area, showing the Pearl River delta and estuary in the East Asian area (a) and sampling sites (b). There is no surface sediment from site PE43 and no winter POC from site PE76 and 77. 'PE' stands for the 'Pearl River estuary'.

Estuarine surface sediment samples are clustered using the Hierarchical Cluster Analysis with the method of between-groups linkage in SPSS 15.0 for Windows. Principle Component Analysis (PCA) on the key metals was also performed in SPSS 15.0 for Windows. Concentrations of metals in terrestrial soil are plotted using the 'Box-Whisker graph' under the Grapher 7.0 program (Figure 5.16-5.18). Contour maps showing the spatial diversity of the geochemical proxies within the estuary distribution

are produced using the IDW method under Arcgis 9.2 program, which interpolates the source data before generating the contour map (Figure 5.19-5.21).

5.2 Hierarchical Cluster Analysis

All 92 samples were subjected to Hierarchical Cluster Analysis (using SPSS for Windows 15.0) based on winter salinity and sand concentration. The cluster analysis defined 9 groups (G1-G9) with a clear geographical control (illustrated in Figure 5.2; Appendix 3-5). Surface sediment samples are from the 91 sampling sites (without site PE43) covering G1-G9 (Appendix 5). The POC samples are only from the western estuary, where suspended sediment concentration was high enough to allow measurements to be made, with samples ranging from G2-G6 for winter POC and G2-G5 for summer POC (Appendix 3).

The 9 groups defined by selected environment variables clearly highlight a trend from the fully-freshwater environment (G1-G3) to the fully-marine environment (G8-G9), via brackish areas (G4-G7) (Figure 5.2; Table 5.1). The freshwater groups have low annual average water salinity of 3.4±3.6 PSU, which increases to 15.8±5.3 PSU and 28.4±3.1 PSU in the brackish-water areas and reaches 32.9±0.8 PSU under the full marine environment (Table 5.1). Mean water depth is lower than 5 m in the freshwater area, getting deeper seawards, and becomes deeper than 20 m in the shallow marine area. Meanwhile, average particle size gets finer offshore with a reduction in sand component. All variables tend to be more stable in the marine area than in the freshwater area (Table 5.1).

In addition to the spatial diversity of the environmental conditions, seasonal variability is also observed. For G2-G5, mean winter salinity is 14.0±11.6 PSU, ranging between 0.1 and 33.9 PSU. This is significantly higher than that in summer of 3.1±4.8 PSU, ranging between 0.1 and 18.2 PSU. A similar situation is found in the concentration of total dissolved solids (TDS) of 15.5±12.1 g/l in winter, compared with 2.0±2.7 g/l in summer. Areas under freshwater- and fresh-brackish conditions are more sensitive to

seasonal changes than those under marine- and marine-brackish conditions, as seasonal variation of these environmental parameters are larger for G2 than G5.
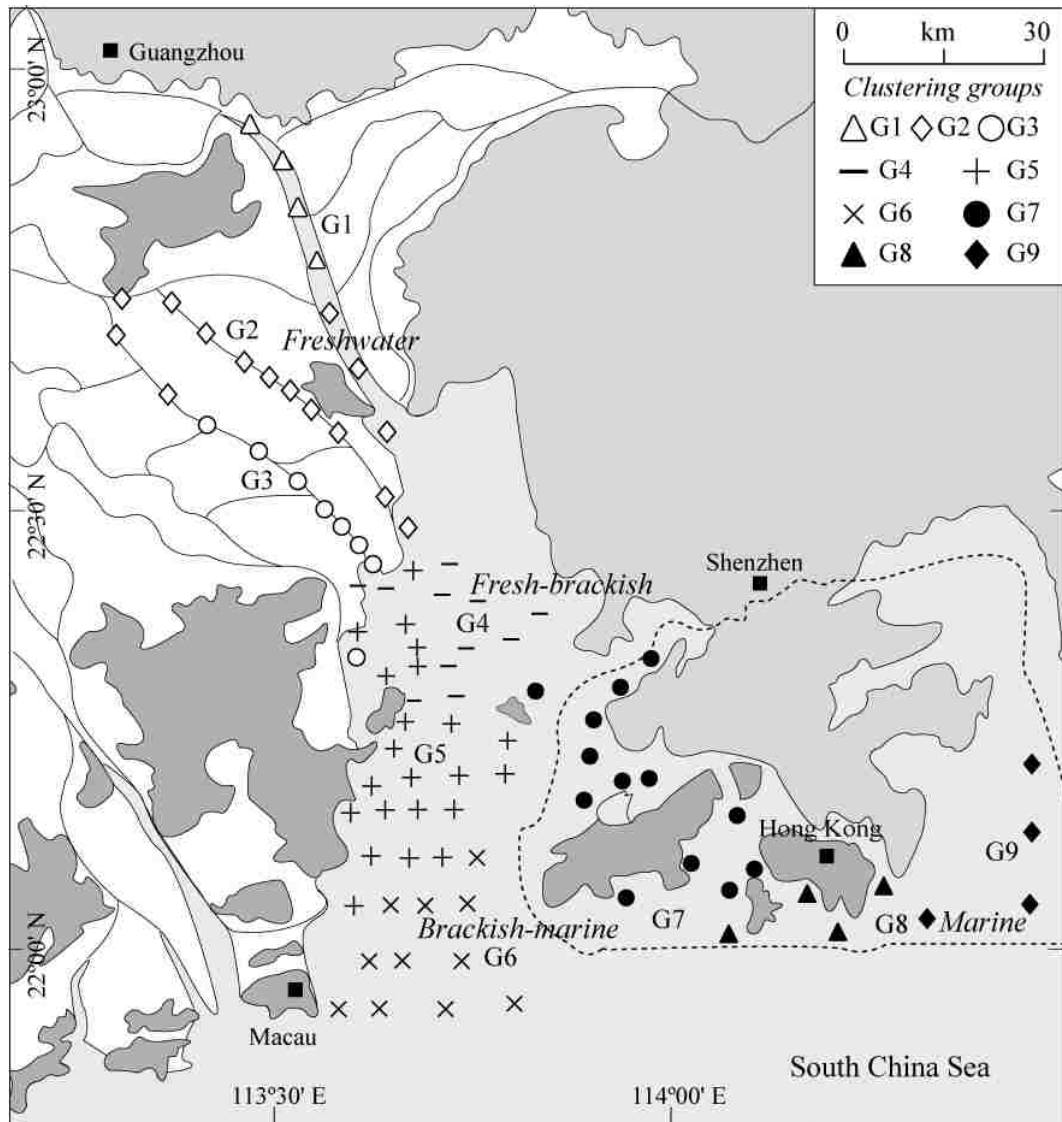
Figure 5.2 Clustering groups for the estuarine surface sediment samples and POC samples identified by winter salinity and sand concentration. Groups G1-G3 are from freshwater areas; groups G4-G7 are from brackish areas and G8-G9 are from marine areas.

Table 5.1 Spatial variation of the organic carbon signature and environmental conditions within the Pearl River estuary

Environment	$\delta^{13}C$ (‰)	C/N	TOC (%)	TN (%)	Mean Sal. (‰)	Sand (%)	Clay (%)	Silt (%)	WD (m)
Freshwater (G1-G3)	-23.8±1.5	12.7±2.3	1.2±0.7	0.1±0.0	3.4±3.6	27.8±17.7	19.8±7.0	52.4±12.7	3.7±2.0
Fresh-brackish (G4-G5)	-23.4±0.8	11.6±2.5	1.1±0.3	0.1±0.0	15.8±5.3	22.1±12.8	25.3±8.3	52.5±7.2	8.8±4.6
Marine-brackish (G6-G7)	-23.1±0.6	9.7±1.0	1.0±0.3	0.1±0.0	28.4±3.1	17.5±9.7	25.3±4.9	57.2±7.7	9.9±6.9
Marine (G8-G9)	-21.4±0.5	7.5±1.1	0.8±0.3	0.1±0.0	32.9±0.8	15.8±6.5	21.5±4.2	62.7±4.2	21.4±6.8

5.3 Organic carbon isotopic signature and C/N ratios of different types of organic matter

5.3.1 Terrestrial organic matter

Terrestrial plants in the Pearl River Delta are dominated by C_3 plants with some C_4 grass (Winker and Wang, 1993). Results show that terrestrial C_3 plants have a $\delta^{13}C$ value of –29.0 ±1.8‰, which is significantly lower than C_4 plants, around –13.1 ±0.5‰ (Appendix 1; Figure 5.3a). Among different types of C_3 plants, the general terrestrial C_3 plants show the lightest $\delta^{13}C$ value of –29.9 ±1.3‰, followed by the agricultural C_3 plants (e.g. rice, lotus and banana) and mangroves, with the $\delta^{13}C$ values of –28.2 ±1.4‰ and –27.1 ±1.7‰ respectively (Figure 5.3b). C_4 plants, including sugarcane and some general grass, have an average $\delta^{13}C$ value of –13.1 ±0.5‰ (Figure 5.1a). Specifically, the general terrestrial C_4 plants have a $\delta^{13}C$ value of –13.2 ±0.5‰, lighter than that of sugarcane around –12.7 ±0.2‰ (Figure 5.3b).
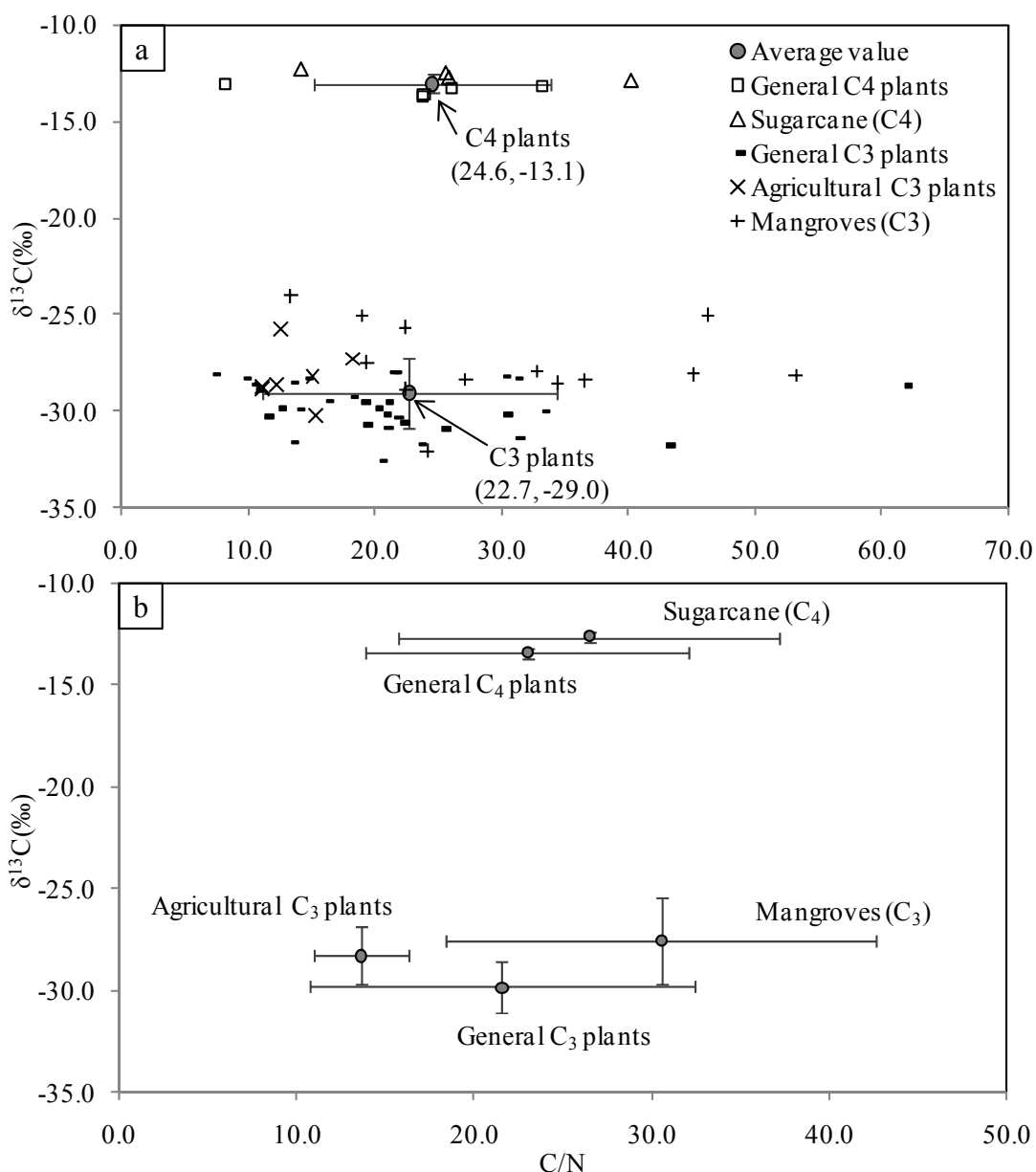
Figure 5.3 Bi-plot of the $\delta^{13}C$ and C/N of C_3 and C_4 plants. a: individual values for each plant with the average value of C_3 and C_4 plants; b: average values of different types of plants within the C_3 and C_4 groups (error bars are the standard deviation).

The C/N ratios of C_3 and C_4 plants overlap, and it is impossible to distinguish between the two plant types based on C/N ratio alone. The average C/N ratio of C_3 plants is 22.7 ±11.6, and 24.6 ±9.4 for the C_4 plants (Figure 5.3a). The range of C/N ratios of these plants is wide (the SD is 11.6 for C_3 plants and 9.4 for C_4 plants) (Figure 5.3a), with considerable overlap between C_3 and C_4 plants. Of the C_3 plants the agricultural plants have lower C/N ratios (13.7 ±2.7) than the general C_3 plants (21.7 ±10.7) and mangroves (31.0 ±12.5) (Figure 5.3b). For the C_4 plants, sugarcane has a slightly

higher C/N ratio of 30.6 ±8.4 compared to the general C_4 average of 21.5 ±8.9. It is worth mentioning that sugarcane (a C_4 agricultural plant) has much heavier $\delta^{13}C$ values and higher C/N ratios than the other C_3 agricultural plants collected from the Pearl River Delta (Figure 5.3b).

Terrestrial soil samples were collected from the same sites as the plants presented above (Figure 5.1). Terrestrial soil samples collected have $\delta^{13}C$ between –28.9‰ and –19.3‰, and C/N between 7.7 and 20.4, with a negative correlation between $\delta^{13}C$ and C/N (Figure 5.4a). As expected, soil samples from the farmland (agricultural soil) have considerably higher $\delta^{13}C$ values around –21.7 ±0.7‰ than those from the forest (forest soil) of –28.3 ±0.8‰ (Figure 5.4b). The $\delta^{13}C$ value is more variable for the forest soil than the agricultural soil (Figure 5.4a). Riverbank soil and mangrove soil have similar $\delta^{13}C$ values around –24.1 ±1.0‰, with higher variability in the mangrove soil (Figure 5.4a). The C/N ratios do seem to discriminate between the different soil groups (Figure 5.4a). The C/N ratios are higher in the forest soil samples (17.9 ±3.6) than in the agricultural soil (8.9 ±1.1) (Figure 5.4b). As with the $\delta^{13}C$ value, C/N ratios of both the riverbank soil and the mangrove soil are similar (around 12.5), though more variable for the mangrove soil (SD=3.6) than the riverbank soil (SD=2.3) (Figure 5.4b). Results of the $\delta^{13}C$ and C/N of soil samples seem to show a trend with relatively high $\delta^{13}C$ and low C/N ratio for agricultural soil through to lower $\delta^{13}C$ and higher C/N for mangrove and riverbank soil to lowest $\delta^{13}C$ and highest C/N ratio for forest soil.

Measurement of the total organic carbon (TOC) of the soil sample shows the forest soil having significantly higher TOC value (3.3 ±0.9%) than the other soil types (around 2.0%) (Figure 5.5). As with the C/N ratios, the TOC of agricultural soil is the lowest among all soil samples, but differences in the TOC between the agricultural soil and the riverbank soil and mangrove soil are not as obvious as that of the C/N (Figure 5.4, 5.5). The TOC content of each type of soil is also quite variable, especially for the forest soil, the mangrove soil and the riverbank soil (Figure 5.5).
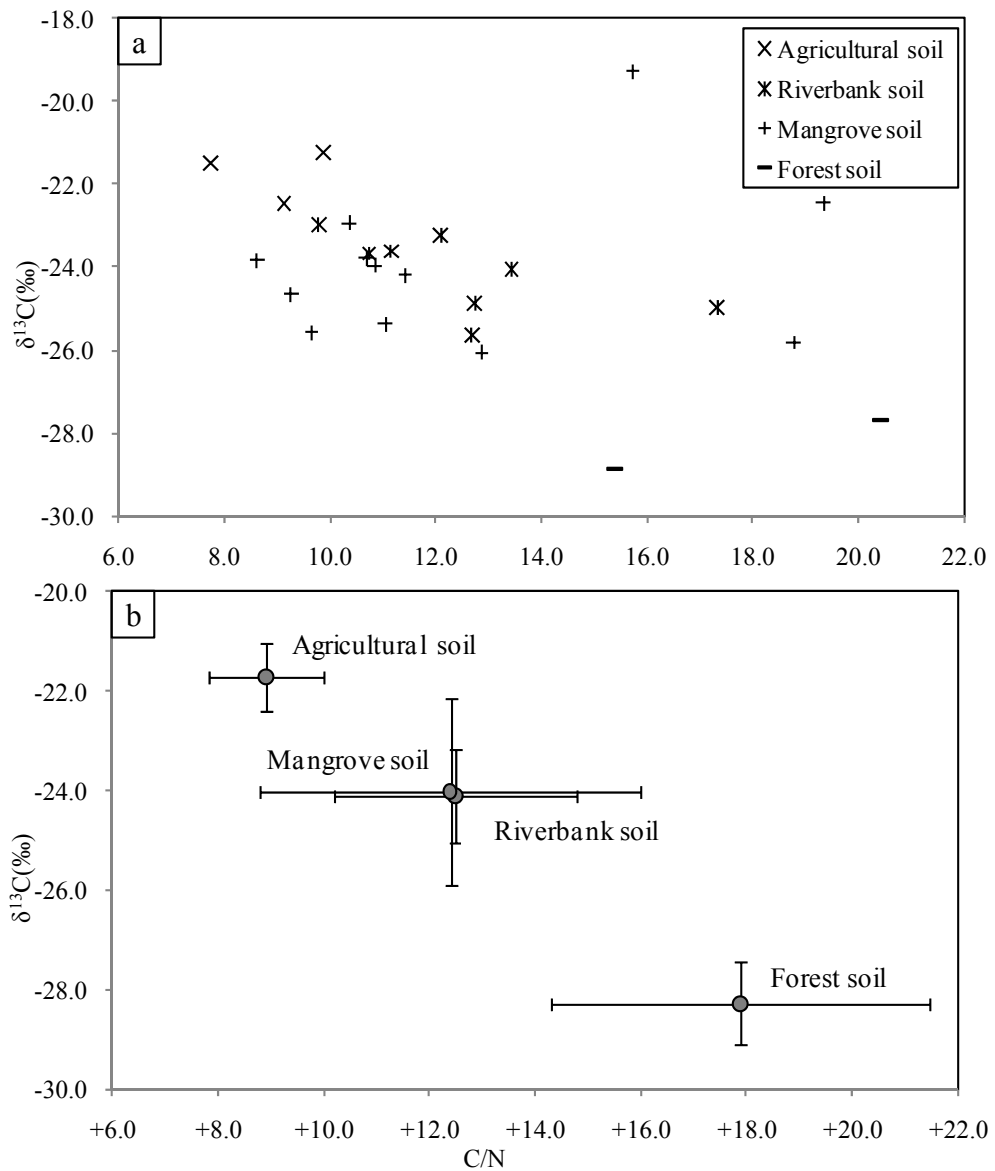
Figure 5.4 Bi-plot of the $\delta^{13}C$ and C/N of terrestrial soil samples. a: individual values for each soil sample; b: average values of different types of soil with stand deviation.
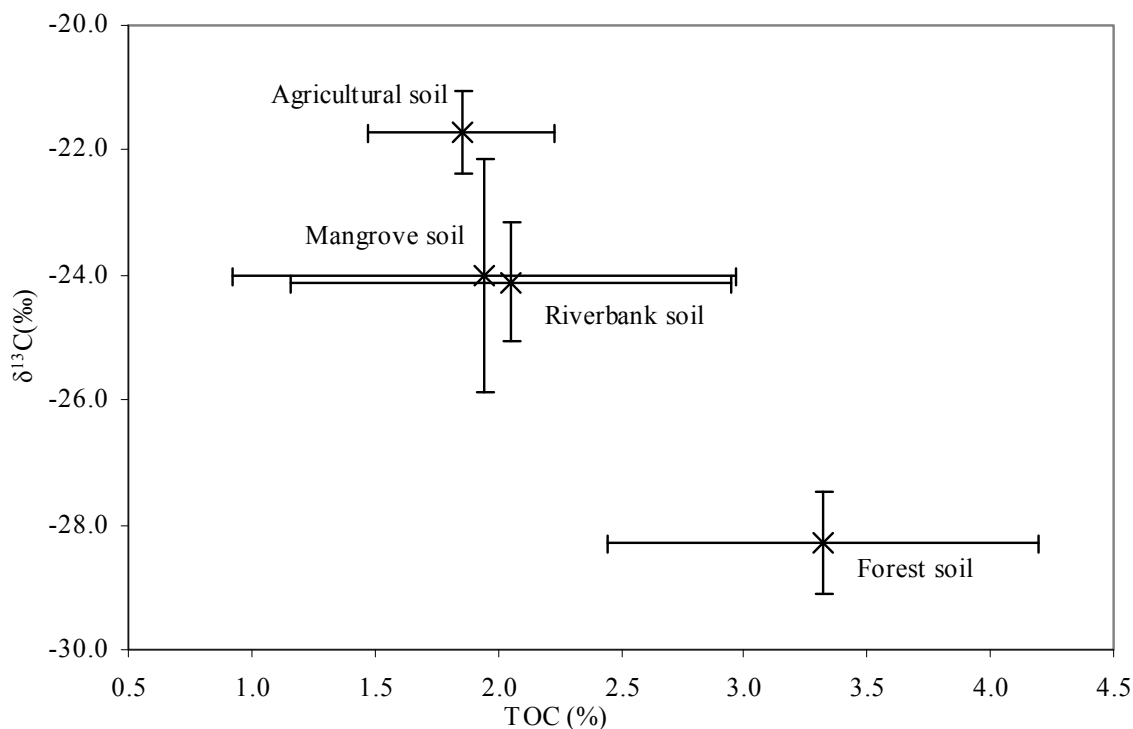
Figure 5.5 Organic $\delta^{13}C$ and TOC of the terrestrial soil

5.3.2 Particulate organic carbon (POC)

POC from both summer and winter are analysed in this study (sampling sites are shown in Figure 5.1). Both the $\delta^{13}C$ and C/N values of the POC vary greatly between seasons, and each season has its own spatial distribution patterns in the $\delta^{13}C$ value and C/N ratios of the POC. The average $\delta^{13}C$ value of the POC seems similar in summer ($-24.5‰$) and in winter ($-24.2‰$). However, it is more variable in winter (SD=1.9) than in summer (SD=1.0), showing a clearer distribution pattern (Figure 5.6). The average C/N ratio is obviously lower in winter than it is in summer, with the average value of 7.1 ±0.9 and 9.2 ±1.1 respectively (Figure 5.6). C/N ratios of the POC are typically between 6.0 and 9.0 in winter, and between 8.0 and 10.2 in summer (Figure 5.6).
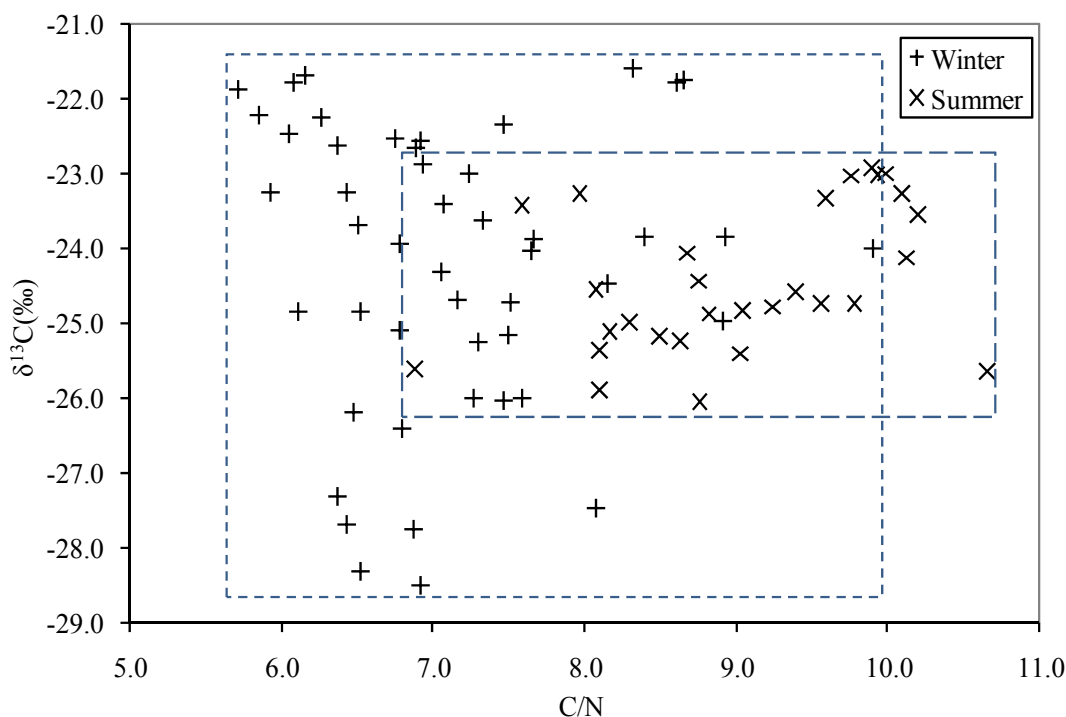
Figure 5.6 Bi-plot of seasonal $\delta^{13}C$ and C/N of the POC.

The $\delta^{13}C$ and C/N of POC vary between groups from different environments (Figure 5.2). In winter, freshwater POC has a lower $\delta^{13}C$ (–27.6±0.8‰, G2) than marine-brackish POC (–22.4±0.5‰, G6), while samples from the fresh-brackish water area have $\delta^{13}C$ between the two (–24.5±1.3‰ for G4; –23.6±1.2‰, G5) (Figure 5.7a). Variation in C/N of winter POC between groups is not as significant as $\delta^{13}C$ (Figure 5.7b). In summer, the average $\delta^{13}C_{POC}$ of each group is similar and does not show any trend between groups (Figure 5.7c). Differences in both $\delta^{13}C$ and C/N of summer POC is not significant (Figure 5.7b).

The $\delta^{13}C$ and C/N of POC show good correlation between salinity (Figure 5.7c, d), especially in the winter. In winter, $\delta^{13}C$ increases from –27.6‰ in the freshwater area further inland to around –21.6‰ in the marine-brackish area near the estuary mouth, with increasing salinity (Figure 5.7c). Correlation between C/N and environmental variables is not as significant as that of $\delta^{13}C$. The C/N raito is found to be high in the middle estuary (7.6±1.0, G5) and decreases landwards and seawards (<7.0). In summer, both $\delta^{13}C$ and C/N are more uniform than in winter and not clearly correlated to the environmental variables (Figure 5.7d).

To gain a better understanding of the spatial variability of both δ^{13}C values and C/N ratios of the POC through the estuary with salinity changes, values were plotted on map using ArcGis 9.2 (Figure 5.8; 5.9). In winter, δ^{13}C values of the POC increase from around –28.5‰ in the freshwater area further inland to around –21.5‰ in the marine-brackish area near the estuary mouth (Figure 5.8a; 5.9). Spatial variations in C/N ratios are not as significant as that of the δ^{13}C in the winter season (Figure 5a, b). C/N ratios are found to be high in the middle estuary (around 9.9) and drop landwards and seawards (<7.0) (Figure 5.8b). In summer, the δ^{13}C values are found to be the highest in the upstream freshwater area, around –23.0‰, becoming lower towards the brackish-water area (Figure 5.8c). The C/N ratio is higher in the brackish-water area than in freshwater areas (Figure 5.8d), reducing from 11.4 to 6.9. It should be noted that the range of δ^{13}C values for the summer POC is significantly smaller than that of the winter season (Figure 5.8a and 5.8c). Furthermore, a clearer trend in the δ^{13}C$_{POC}$ from the freshwater area to the marine-brackish area is present in the winter season, while the summer δ^{13}C$_{POC}$ tends to be more uniform showing a slight reversal trend (Figure 5.8a and 5.8c).
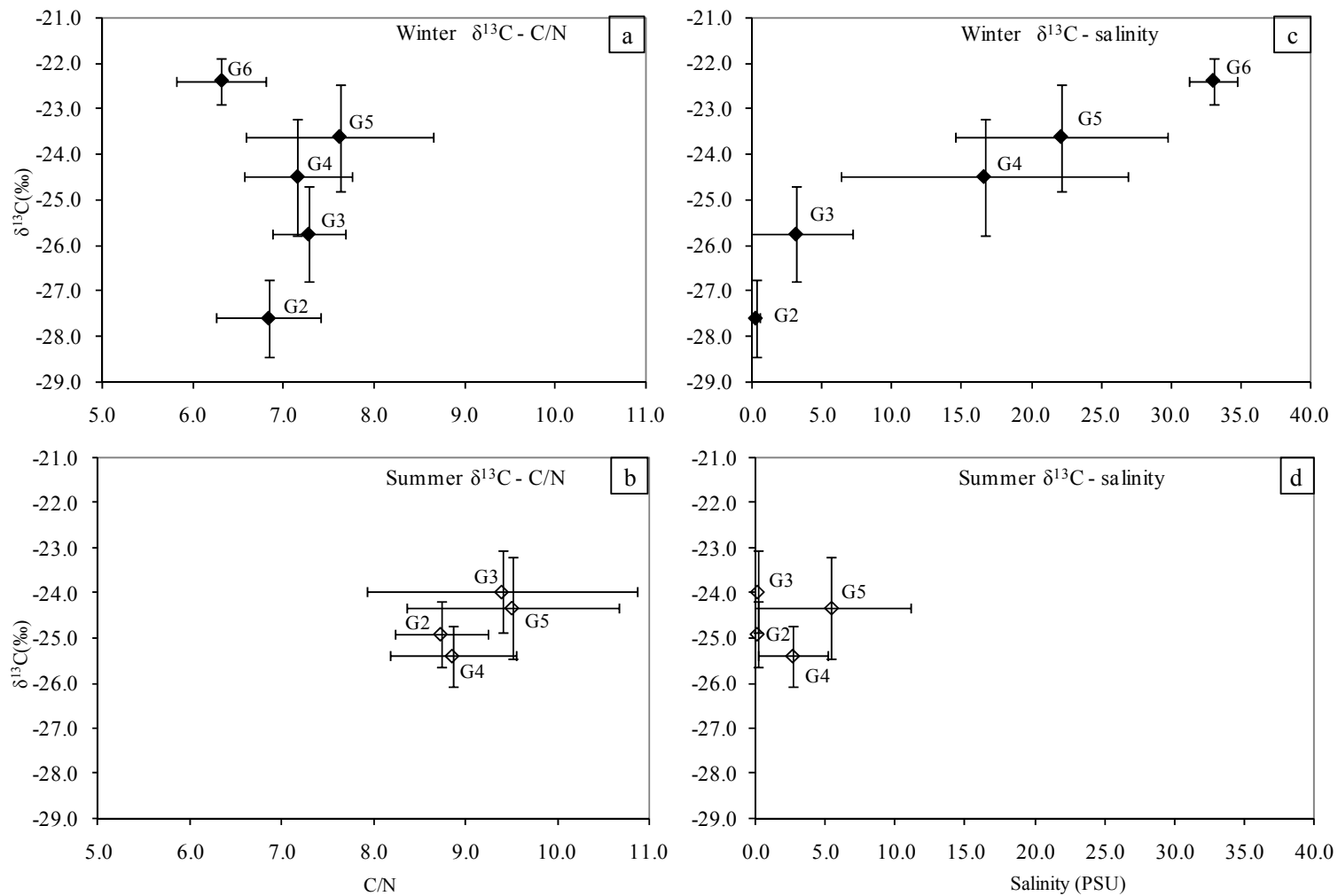
Figure 5.7 A summarized bi-plot of seasonal POC $\delta^{13}C$ against C/N (a: winter and b: summer) and a bi-plot of seasonal POC $\delta^{13}C$ against water salinity (c: winter and d: summer) of the POC for each group indentified by cluster analysis. G2 and G3-- freshwater groups; G4 and G5 – fresh/brackish groups; G6 – brackish/marine groups.
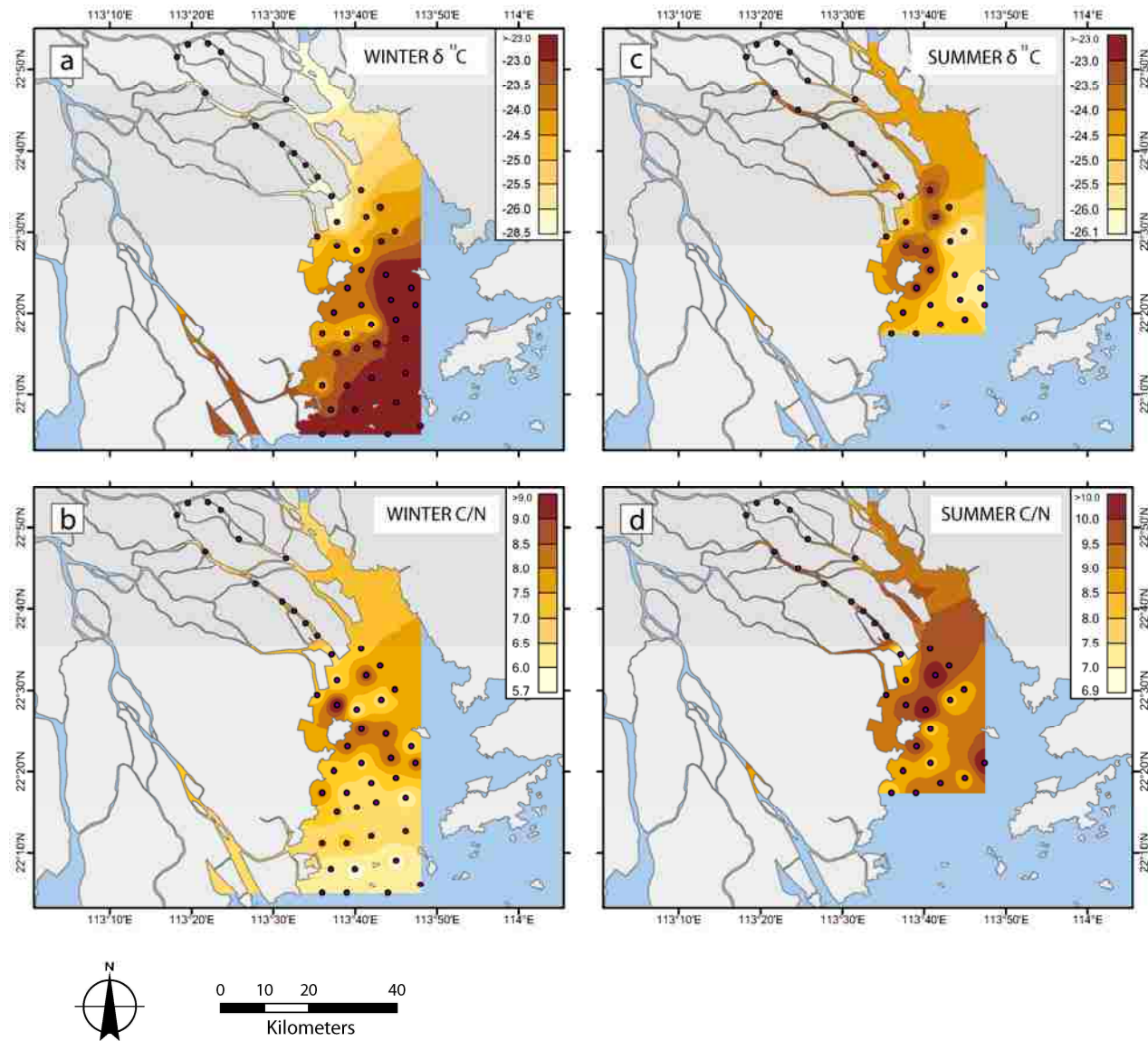
Figure 5.8 Spatial variations of δ^{13}C and C/N of POC in both summer and winter seasons.
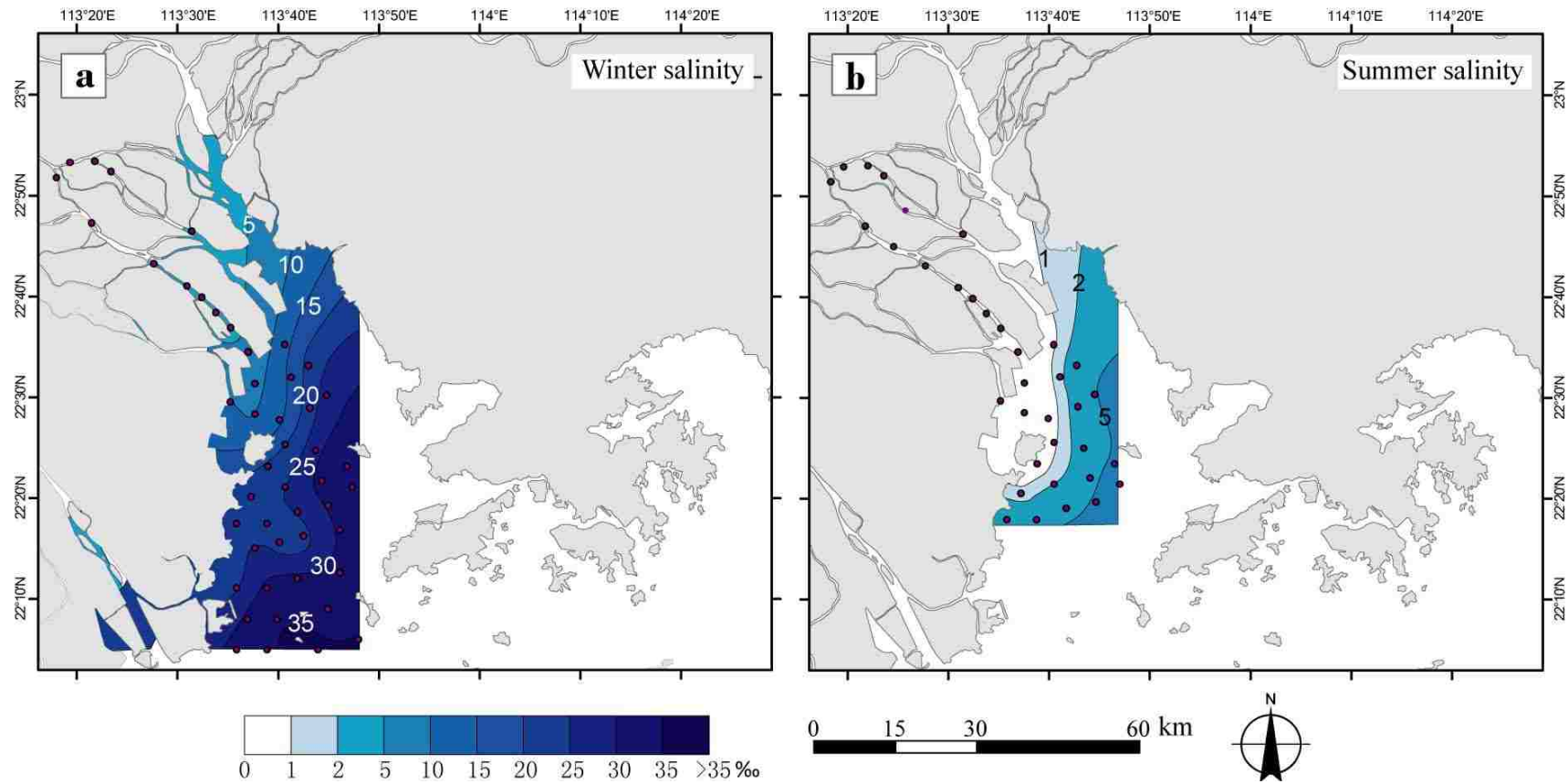
Figure 5.9 Contour maps of winter salinity (a) and summer salinity (b) of the Pearl River estuary

Results of suspended organic matter collected by a 70μm net

Estuarine particulate organic carbon is composed of organic carbon from fine-size plankton and relatively coarse TOM. As the size of plankton (e.g. diatoms) is usually smaller than 80 μm, organic matter collected on filter paper has a higher proportion of plankton/algae, while those collected in a 70 μm net presents higher proportion of TOM over plankton. Results show that the POC samples from the 70 μm net have a lower average $\delta^{13}C$ of –25.6±1.0‰, compared to the filter paper sample from the same location (i.e. –24.3±1.0‰ in summer and –24.2±1.5‰ in winter, Figure 5.10). The average C/N of the POC from the net samples is 10.7±4.5, which is higher and more variable than that of the POC collected on filter paper of 9.4±1.1 in summer and 7.8±1.0 in winter respectively (Figure 5.10). POC values from the samples collected using the net fall into two groups. POC from locations nearer to the marine area, such as PE65, PE67, PE68, and PE71 (Figure 5.1), tend to have lower $\delta^{13}C$ and C/N than POC on filter paper from both seasons, while those from the inner estuarine area have similar $\delta^{13}C$ with the POC from the filter papers but higher C/N (Figure 5.10).
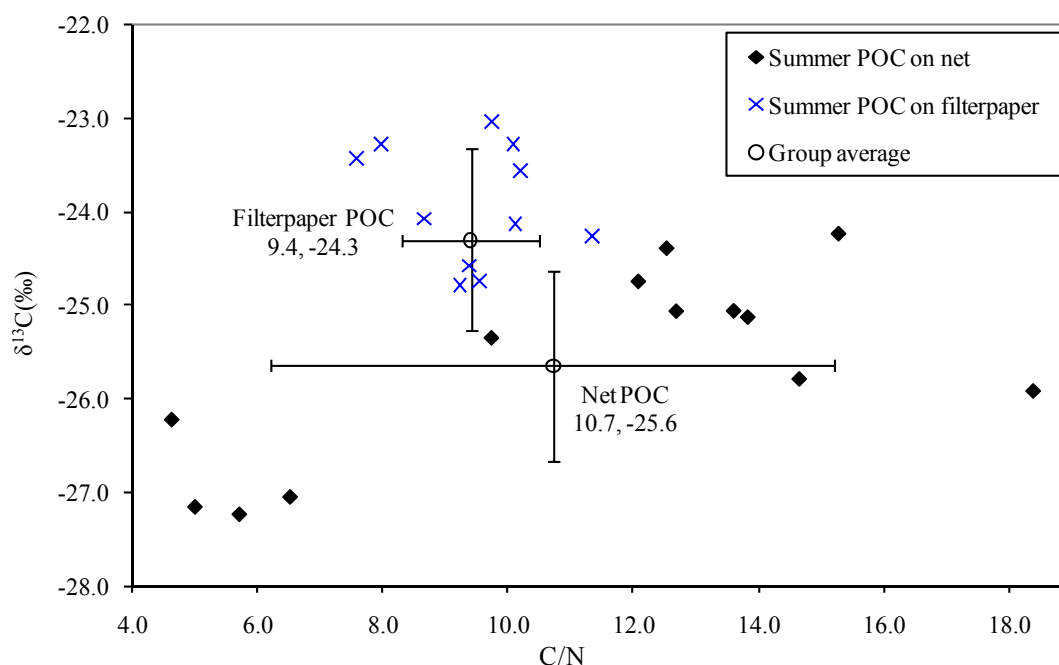
Figure 5.10 Comparison $\delta^{13}C$ and C/N values between the POC on 70 μm net and summer POC on filter paper.

5.3.3 Estuarine surface sediment

Surface sediment samples from the fully-freshwater environment to the fully-marine environment were collected for this study (Figure 5.1, 5.2). The estuarine surface sediment samples have $\delta^{13}C$ ranging from –27.0‰ to –20.8‰ and C/N ranging between 20.1 and 6.5, with $\delta^{13}C$ and C/N negatively correlated (Figure 5.11a). With the environmental change from the fully-freshwater environment to the fully-marine environment from G1 to G9, a clear trend is observed in both $\delta^{13}C$ and C/N values. $\delta^{13}C$ becomes progressively higher from G1 to G9, increasing from –25.0±1.3‰ in G1 to –21.0±0.2‰ in G9 (Figure 5.11b), with increasing water salinity and decreasing sand concentration. Meanwhile, C/N also shows a clear trend decreasing from 15.2±3.3 in G1 to 6.8±0.2 in G9. G3 does not fit in this trend with $\delta^{13}C$ of –23.0±1.6‰ and C/N of 11.1±1.3, which is lower than G_4 (Figure 5.11b). Both $\delta^{13}C$ and C/N are more stable in the marine environment compared to the freshwater.

Changes of bulk organic $\delta^{13}C$, C/N and TOC with salinity are shown in contour maps (Figure 5.12; 5.13). Contour maps of $\delta^{13}C$ demonstrate the spatial variability within the estuary (Figure 5.12). The $\delta^{13}C$ value of sediments from fluvial areas is typically lighter than –24.9‰, and increases to around -21.0‰ in the marine area (Figure 5.12a; 5.13). The C/N ratio of the surface sediment decreases from higher than 15.0 in the freshwater area to lower than 7.5 in the marine area (Figure 5.12b). Both $\delta^{13}C$ and C/N values are more stable at the marine end than the freshwater end. Generally, the TOC are higher at the freshwater end (>3.0%) than at the marine end (around 0.8%) with some depleted areas in the central estuary, with values lower than 0.6% (Figure 5.12c). Apart from samples from the central estuary, most brackish-water sediments have a TOC value between 1.0% and 1.8% (Figure 5.12c). The highest TOC is found in the East River area, but areas that are most depleted in TOC (lower than 0.4%) include the North River area and the main channel and the marine area (Figure 5.12c). From freshwater and brackish-water areas, a light-$\delta^{13}C$ centre usually comes with a high C/N ratio and a high TOC, e.g. they are –24.9‰, 18.0 and 3.4% at the East River.
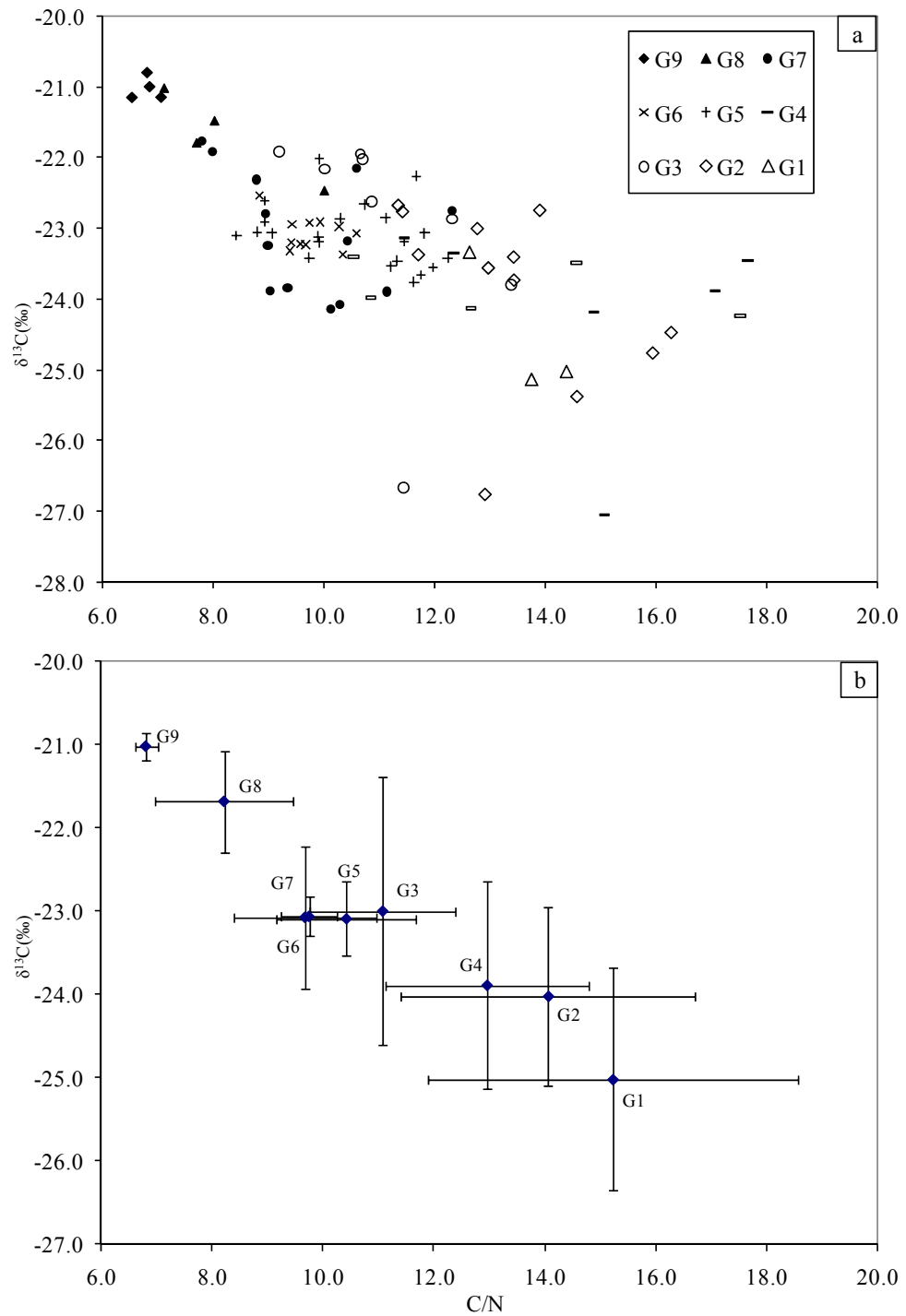
Figure 5.11 Bi-plot of the $\delta^{13}C$ and C/N of surface sediment groups. a: scattering value of the individual sample; b:average $\delta^{13}C$ and C/N values of the seven groups with standard deviation shown. G1, G2 and G3: freshwater groups; G4 and G5: fresh/brackish groups; G6 and G7: brackish/marine groups; G8 and G9: marine groups.
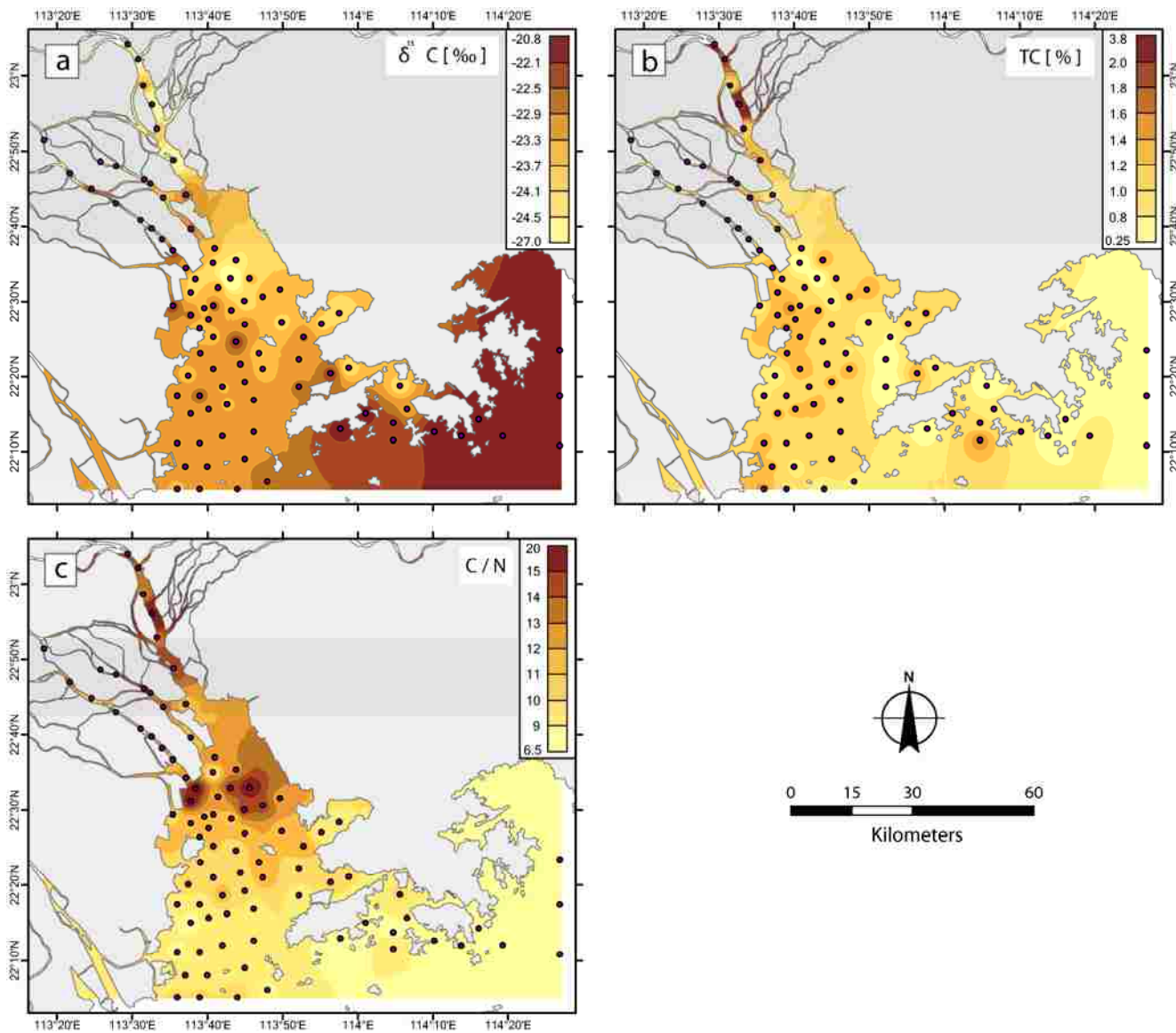
Figure 5.12 Spatial diversity of the $\delta^{13}C$ (a), TOC (b), C/N (c) and annual salinity (d) of in the Pearl River estuary.
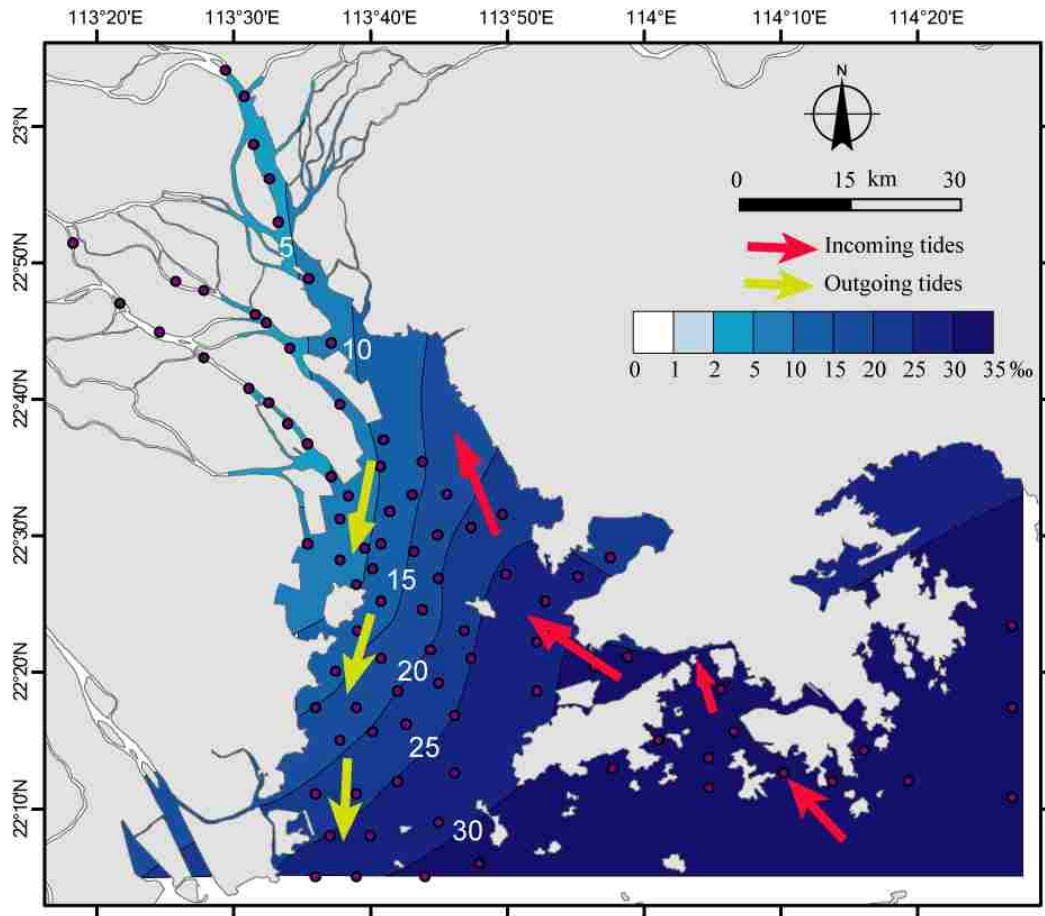
Figure 5.13 Contour map of annual salinity of the Pearl River estuary

5.4 The organic carbon signature as an indicator of sediment sources

5.4.1 Terrigenous organic matter and its sources

Plants can be placed in two main groups, C_3 and C_4 plants, based on the way they fix carbon from atmospheric CO_2 during the photosynthetic process. This produces significant difference in the $\delta^{13}C$ signature of these two groups. C_3 plants use the Calvic-Benson cycle (C_3 pathway) (Craig, 1953; Park and Epstein, 1961), through which they absorb and conserve ^{12}C from atmospheric CO_2 more effectively compared to the Hatch-Slack pathway used by C_4 plants (Hatch and Slack, 1970). This results in the greater discrimination against ^{13}C in C_3 plants than C_4 plants (Hatch and Slack, 1970). Because of this, C_3 plants are depleted in ^{13}C, producing $\delta^{13}C$ values around –28.1‰ (e.g. Graig, 1953; Fry and Sherr, 1984; O'Leary, 1988), while C_4 plants are enriched in ^{13}C and show $\delta^{13}C$ values around –13.0‰ (Bender, 1971; Teeri and Stowe, 1976; Fry and Sherr, 1984; Emerson and Hedges, 1988).

The C_3 plants analyzed here from the Pearl River delta have a $\delta^{13}C$ value around –29.6‰, approximately 1.5‰ lighter than reported by other studies mentioned above. This might be due to the high precipitation in the Pearl River delta area, with precipitation of more than over 1500 mm/yr (Li *et al*., 1990). A similar case has been reported by Austin and Vitousek (1998) where $\delta^{13}C$ of C_3 plants shifts from –29.9‰ to –25.6‰, when the sampling site changed from an area of 5000 mm/yr precipitation to an area of only 500 mm/yr. The $\delta^{13}C$ value of C_4 plants from this study is around –13.1 ‰, similar to other studies (e.g. Bender, 1971; Teeri and Stowe, 1976; Fry and Sherr, 1984; Emerson and Hedges, 1988). The fact that agricultural C_3 plants have slightly heavier $\delta^{13}C$ values than general C_3 plants (–28.2 ±1.4‰ compared to –29.9 ±1.3‰) and agricultural C_4 plants (e.g. sugarcane) have slightly heavier $\delta^{13}C$ than general C_4 grass (Figure 5.14), might be due to the fertilization process (O'Leary, 1981), and the special environment of arable land.
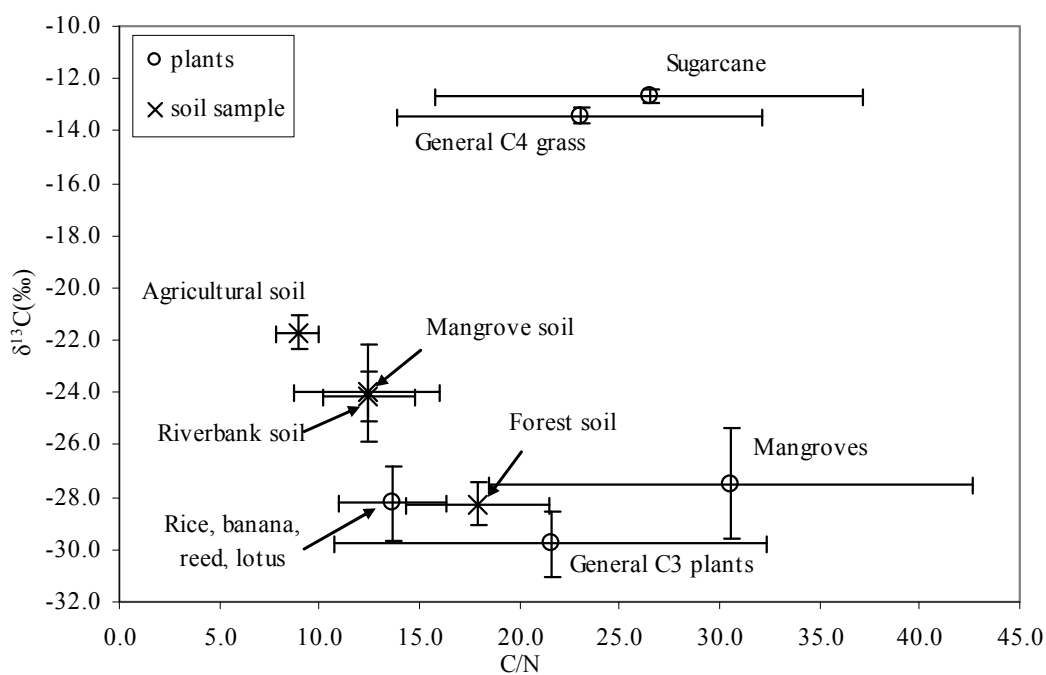
Figure 5.14 Organic carbon signature of the terrestrial organic matter

Previous studies have used the organic carbon isotopic signature of terrestrial soil to reflect different vegetation types (e.g. Wilson *et al.*, 2004; Mackie *et al.*, 2005; Fan *et al.*, 2007; Cao *et al.,* 2008; Driese *et al.*, 2008; Saia *et al.*, 2008). This is because terrestrial soil is one of the direct sinks of organic carbon from surface vegetation, and its organic carbon signature depends greatly on the dominant vegetation type. Studies by Saia *et al.* (2008) and others (e.g. Driese *et al.,* 2005; Saia *et al.*, 2008; Swarzenski *et al.*, 2008) show that $\delta^{13}C$ value of soils from a C_3-dominated area is around $-21.0‰$, and around $-26.0‰$ when the area was dominated by C_4 plants. This explains the different organic carbon isotopic signatures found in soil samples from different areas of the Pearl River delta, e.g. the forest and the riverbank and the tidal flat. Soils from the forest mainly receive organic carbon from the C_3 plants (e.g. pine), and tend to have light $\delta^{13}C$ values around $-29.6‰$, but high C/N ratios around 17.0 (Figure 5.14). Riverbank soil samples are from the flood plain along the North River, dominated by shrubs and grass (Table 4.1). The increasing proportion of C_4 grass on the flood plain produces relatively heavier $\delta^{13}C$ values of the riverbank soil compared to the forest soil. The similarity of $\delta^{13}C$ and C/N ratios found in the riverbank soil and the mangrove soil are due to the similar proportion of C_4 plants growing on the flood plain and the tidal flat (Figure 5.14). The C/N ratios of soil organic matter is usually lower than 20. However, the range is not as wide as the C/N of either C_3 or C_4 plants.

5.4.2 POC and its sources

Terrestrial organic matter enters the river system in the form of plant fragments and soil organic matter, and is mixed with freshwater algae before entering the estuarine system (Figure 5.15a). Accordingly, within an estuarine area, the suspended particulate organic carbon (POC) from the freshwater end is a mixture of terrestrial organic matter, freshwater plankton and freshwater algae. Previous research shows that terrigenous freshwater POC have a δ^{13}C value around –26.0‰ (Countway *et al.*, 2007; Middleburg and Herman, 2007; Zhang *et al.*, 2007; Bird *et al.*, 2008; Wu *et al.*, 2008). The POC from the Turbidity Maximum Zone of the Changjiang (Yangtze River) has a δ^{13}C value of –28.7‰ (Zhang *et al.*, 2007). This part of suspended organic matter is delivered into the estuarine system by fluvial runoff and dilutes the signal produced by the brackish-water and marine POC, which generally have less negative values, between –23‰ and –20‰ (Middleburg and Herman, 2007; Zhang *et al.*, 2007).

In the Pearl River estuary, the balance between freshwater POC and marine/brackish-water POC is strongly influenced by the strength of freshwater runoff, which controls the spatial and temporal variation of the carbon isotopic signature of estuarine POC. In winter, high salinity in the estuary suggests a low freshwater input induced by significant reduction in monsoonal precipitation of this season (Figure 5.9a). Low freshwater flux results in significant reduction in terrestrial organic input into the estuary, and the suspended organic matter within the estuary is dominated by phytoplankton (e.g. diatoms, dinoflagellates, green algae, euglenoides). The organic carbon signature of winter POC reflects these differences and shows a clear grading pattern from the freshwater area to the marine-brackish area. The δ^{13}C value of the freshwater plankton typically ranges from –30‰ to –25‰, and the marine particulate organic matter typically ranges from –21‰ to –18‰ (Figure 5.15a), which is also reported by other studies (Lamb *et al.*, 2006; Middelburg and Herman, 2007; Tesi *et al.*, 2007a, b). The low C/N ratio (7.1 ±0.9; Figure 5.15a) of winter POC supports the assumption that winter POC is dominated by plankton, as phytoplankton tend to have low C/N ratios of 5-7 (Lamb *et al.*, 2006) compared to terrestrial organic matter. In summer, low salinity indicates high freshwater input (Figure 5.9b), resulting in a high proportion of fragments of terrestrial plants (dominated by C_3 plants with some C_4 plants) in the suspended matter. This is supported by greatly overlaping δ^{13}C and the

relatively higher C/N ratios (9.2 ±1.1; Figure 5.15a) of the summer POC. At the same time, influence of the strong freshwater flux extends to areas further seawards of the estuary, homogenises the components of POC within the estuary, minimizing the spatial differences in the isotopic signature of the summer POC. The POC collected by a 70μm net are more dominated by plant fragment than the POC collected on the filter paper. The POC in the net is found to have lighter δ^{13}C values and wider C/N ratios than the POC on the filter paper. This result further supports the suggestion that seasonal switches in the dominant source of the POC between terrigenous organic matter and marine planktons produce the seasonal variations of the POC carbon isotopic signature and C/N ratios.

Huang *et al.* (2004) examined the spatial diversity and distribution of phytoplankton within the Pearl River estuary during wet and dry seasons. They found that the diversity of the phytoplankton is similar between seasons. There are 130 species in the wet season, with *Skeletonema costatum* accounting for 45.0% of the total amount, and 132 species in the dry season, with *Eucampia zoodiacus* accounting for 43.7% of the total. The abundance of phytoplankton in summer is much higher than that in the winter season, 6.3×10^5 cells/L and 1.4×10^5 cells/L respectively. In summer, the amount of the phytoplankton is found to be higher in the marine area than in the inner estuary, near the river mouth. An opposite distribution of the amount is found during winter, the phytoplankton is more abundant in the inner estuarine area than the marine end. Similar results were reported by Wu *et al.* (2007), showing δ^{13}C values of particulate organic matter changing from –24.4‰ in the Yangtze River to –21.0‰ on the East China Sea Shelf. Enrichment in the δ^{13}C of the suspended organic matter from the marine environment in comparison with the riverine environment is also reported from other coastal areas (Salomons and Mook, 1981; Middelburg and Nieuwenhuize, 1998; Hellings *et al.*, 1999; Boschker *et al.*, 2005), which is consistent with data from the Pearl River delta of around −28‰ from the freshwater end and around −21‰ from the marine end.
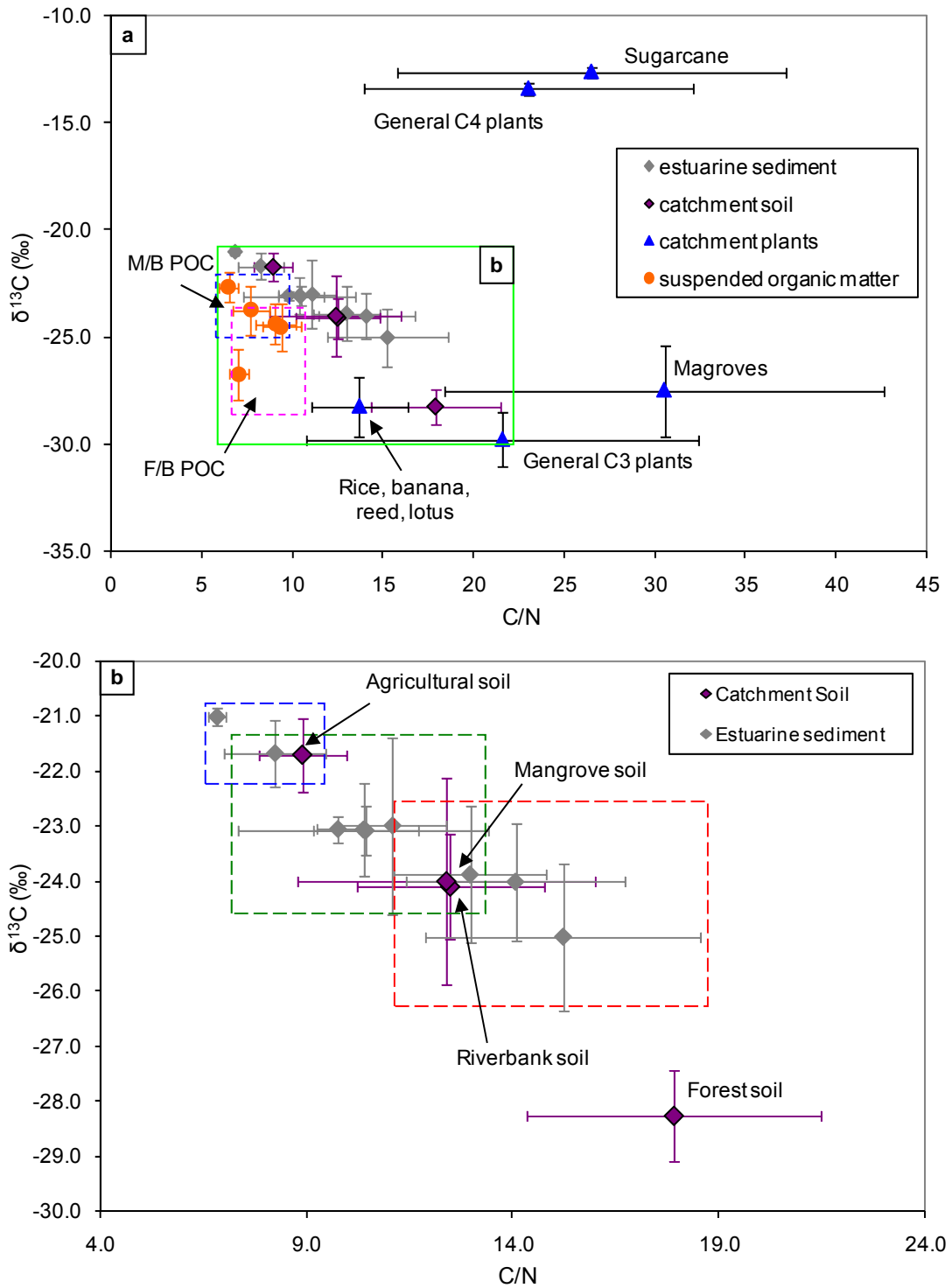
Figure 5.15 Bi-plot of $\delta^{13}C$ and C/N of all types of organic matter observed in this study.
(M/B: marine-brackish water; F/B: fresh-brackish water)

5.4.3 Estuarine surface sediment and its sources

The organic carbon isotopic signature and C/N vary for organic material from different sources, e.g. the difference between C_3 and C_4 plants, but they become more complicated when material is deposited in sediment sinks, e.g. in the estuarine sediments, due to the heterogeneous organic matter. However, there is still a clear trend through the estuary with the carbon isotopic signature of the surface sediment organic matter from the freshwater environment more terrestrial-like than that from the brackish/marine environment (Figure 5.15b). This is due to the higher contribution of terrestrial organic matter in the former sediment than the latter, e.g. the plant fragments, terrestrial soil organic matter and the freshwater POC (Figure 5.15b). As the influence of the freshwater runoff becomes weaker towards the sea, the contribution of terrestrial-origin organic matter becomes smaller and is replaced by the marine algae at the marine end (e.g. G8 and G9; Figure 5.15b), where the freshwater influence is small. This spatial contrast of $\delta^{13}C$ of the surface sediment (Figure 5.12a) agrees with $\delta^{13}C$ of winter POC (Figure 5.8a). On the other hand, as the surface sediment represents samples of a resolution of around 10 years, the freshwater sediments are comparable to the summer POC, and can be used to represent sediment receiving high terrestrial organic matter input deposited under high freshwater runoff conditions.

Surface sediment samples from the brackish/marine environment, with little freshwater influence, thus can be used to represent sediments deposited under low freshwater flux conditions and receiving mainly brackish/marine organic matter input. Different dominant organic sources between the freshwater and marine environment generate the lighter $\delta^{13}C$ values and higher C/N ratios in the freshwater sediment than the marine sediment. C/N ratios are useful for separating algae and terrestrial organic matter (e.g. Andrews *et al.*, 1998; Muller and Voss, 1999), with algae having a C/N ratio between 5 and 8, while the terrestrial organic matter has C/N ratios typically higher than 15 (Meyers, 1997). Low C/N ratios of the surface sediments at the marine end suggest a higher organic matter contribution from marine algae/plankton (Zhang *et al.*, 1999; Hu *et al.*, 2006; Wu *et al.*, 2007.) The TOC of the surface sediment generally decreases from the freshwater end to the marine end, and this is explained by progressively decreased hydraulic energy from the river mouth to the marine area (Hu *et al.*, 2006), as well as decreasing productivity seaward, which is supported by the environmental

parameters measured. Relatively low TOC values found at the North River and the main channel are due to high hydraulic circulation and the high turbidity in these areas limiting productivity (Zhang *et al.*, 1999; Hu *et al.*, 2006). This is supported by the high concentration of sand from G1. Furthermore, Hu *et al.* (2006) collected 50 surface sediment samples ranging from the inner estuarine area to the northern South China Sea, and reported a similar pattern in results of the organic carbon isotopic signatures of the surface sediments in the Pearl River estuary.

Factors that influence the organic carbon isotopic signature of POC, therefore, also become significant for the signature of the surface sediment, such as strength of the freshwater flux and hydrological conditions. The contribution of marine algae to sedimentary organic carbon is limited by the turbidity and nutrient content of the water column (Yin *et al.*, 2004; Huang *et al.*, 2003; 2004). Turbidity is higher at the river mouth (nearer the source of sediment flux); the contribution of in situ phytoplankton productivity to the sediment signal is less here than further down the estuary towards the inner-shelf area. A similar phenomenon has been reported from other estuaries, e.g. the Gironde estuary, western Europe (Fontugne and Jouanneau, 1987) and the Yangtze River estuary, China (Wu *et al.*, 2007).

5.4.4 Influences on the bulk organic δ^{13}C and C/N

Anthropogenic influence

It has been suggested that anthropogenic influence in the Pearl River delta has become an important factor that changes the organic carbon isotopic signatures of the surface sediments in the estuary (Jia and Peng, 2003; Owen and Lee, 2004). Results from this study show that agricultural C_3 plants have marginally higher δ^{13}C (–28.2±1.4‰) than general C_3 plants (–29.9±1.3‰), as well as the agricultural C_4 plants and general C_4 grass (Figure 5.14). Correspondingly, δ^{13}C decreases from agricultural soil samples to riverbank and mangrove soil, and the forest soil has the lowest δ^{13}C of all (Figure 5.14). C/N increases through these soil types, with the forest soil having the highest C/N. This increase in δ^{13}C and decrease in C/N found in agricultural soil might be due to the fertilization process (O'Leary, 1985). Sediments deposited during recent decades tend to have elevated δ^{13}C, which appear to coincide with rapid urbanisation, industrialisation

and reclamation in this area (Owen and Lee, 2004; Hu *et al*., 2008). For example, well-nourished plants show higher $\delta^{13}C$ than plants deficient in nitrogen and/or potassium (less fertilized) (O'Leary, 1985). However, compared with the natural vegetation system and carbon cycling in the Pearl River delta and estuary, the impact of anthropogenic activities on the bulk organic $\delta^{13}C$ and C/N is small, and will not influence the applicability of $\delta^{13}C$ and C/N as indicators for carbon sources.

As a relatively densely populated area, sewage could be a potentially important contributor to the sediment organic matter in the Pearl River estuary. Sediments from Victoria Bay, Hong Kong, were significantly contaminated by sewage (Hsieh, 2006). The $\delta^{13}C$ of these sediments varies from −28.59 to −22.60‰ and C/N from 10.71 to 14.73 (Hsieh, 2006), which must include the influence of sewage. Here we have undertaken biomarker analysis of the Pearl River surface samples (David Strong, pers. comm.) and show the lack of coprostanol and other 5-beta stanols indicating that sewage is an insignificant contributor to the organic carbon in these sediments. The main organic pollutants found in the estuarine area are the polycyclic aromatic hydrocarbons (PAHs) and polychlorinated biphenyles (PCBs) and organochlorinate pesticides (Kang *et al*., 2000). Concentrations of the total PAHs, PCBs and organochlorinate pesticides in surface sediments from the river to the estuarine area are 1 167 − 21 329 µg/g, 10.2-485.5 µg/g and 5.8-1 658 µg/g respectively (Kang *et al*., 2000). When compared to the TOC values from surface samples analysed here of 0.5-2% TOC (i.e. 5 000-20 000 mg/kg) the concentration of these pollutants is actually very low. Sediments with the highest concentration of these organic pollutants are from areas near Guangzhou and/or Maucau according to Kang *et al*. (2000). For example, concentration of organochlorinate pesticides in sediments from areas investigated by this study is usually between 5 and 70 µg/g (Kang *et al*., 2000). Overall we consider that the contribution of organic carbon from these pollutants is insignificant.

A possibly more important contributor that might influence $\delta^{13}C$ value of the sediment is crude oil. The light oil from the Pearl River estuary is characterized by low density (less than 0.83 g/cm^3), high contents of saturated hydrocarbons (71%-93%) and no asphaltenes (Guo and He, 2006). $\delta^{13}C$ of the crude oil from Pearl River estuary is between −27.09‰ and −26.48‰ (Guo and He, 2006), slight heavier than that of C$_3$ plants. However, according to biomarker results (David Strong, pers. comm.), the total

amount of lipids from crude oil in these samples ranges from 100 to 500 μg/g, which compared to the average TOC values of 0.5-2% (i.e. 5-20 mg/g), indicates a maximum concentration of 10% (0.5% - 10%). Furthermore, biomarker results also suggested that the apolar freactions found in the crude oil would most likely already include the PCBs.

These data indicate that sedimentary organic carbon contributors other than plants, planktons and algae, such as human waste, organic pollutants and crude oil, are less important. The maximum concentration of organic carbon from these anthropogenic sources is less than 10%. Thus, in spite of the influences of organic carbon from other sources, bulk organic $\delta^{13}C$ and C/N is still a good indicator for the source of estuarine sediment at the broadest scale from terrestrial, lowest deltaic or marine areas.

Degradation

The influence of degradation varies across the Pearl River delta area and estuary. In the Pearl River delta, results show that soil organic matter generally has higher average $\delta^{13}C$ but lower C/N than that of overlying vegetation. For example, average $\delta^{13}C$ of mangrove soil is 3.1‰ higher than that of overlying mangrove plants, and average C/N of mangrove soil is 12.4 compared to 31.0 for that of mangrove plants. Degradation effect might be an important reason for differences in $\delta^{13}C$ and C/N between SOM and overlying plants. However, SOM receives organic carbon from all overlying vegetation which is a mixture of both C_3 and C_4 types. Thus differences of $\delta^{13}C$ between the mixed type of organic matter (SOM) and individual plants should also be significant.

Sedimentary organic matter in the Pearl River estuary is mainly derived from terrestrial and marine areas. Much of the terrigenous component of riverine organic matter may have already been extensively degraded on land or further upstream and should be relatively resistant to further degradation (Hedge and Keil, 1995). Degradation of in situ POC might become significant for surface sediment $\delta^{13}C$. Results show that POC from both seasons exhibit much lower C/N ratios than surface sediments (Figure 5.15a). The contrast is particularly obvious in fluvial areas (e.g. G2, G4), and becomes more similar in marine area (e.g. G6). Similar phenomenon in C/N ratio has been reported by Cifuentes (1991) from the Delaware Estuary, southeast USA. Cifuentes (1991) has also reported differences in $\delta^{13}C$ values between the two phases. In the upper estuary, $\delta^{13}C$

of POC (−28.9‰) was lower than that of surface sediment (−26.3‰), whilst in the lower estuary, suspended sediment $\delta^{13}C$ (−20.1‰) was higher than surface sediment $\delta^{13}C$ (−23.5‰) (Cifuentes, 1991). However, changes in $\delta^{13}C$ between POC and surface sediment in the Pearl River estuary are not so significant when POC from both summer and winter are taken into consideration. This suggests that differential decomposition of organic detritus may partially explain these observations especially in C/N, seasonality may be more important in the Pearl River estuary, and possibly in the Delaware Estuary, USA (Cifuentes, 1991).

Degradation can have a potentially significant influence on both sediment $\delta^{13}C$ and C/N. Early loss of labile material in vascular vegetation can lead to significant shifts in soil $\delta^{13}C$ and C/N but is insufficient to prevent the distinction between sediments from C_3 and C_4 vegetated soil. The degradation of POC in estuarine areas suggests using either proxy in isolation might produce misleading results. It is important to combine $\delta^{13}C$ and C/N when indicating sediment sources and environmental changes from coastal areas (Wilson *et al*., 2005b; Zong *et al*., 2006).

5.5 Distribution of key metals in the Pearl River delta and estuary

5.5.1 Principle Component Analysis

A total of 34 metals were measured by in this study. In this 15 of them are selected to illustrate the inorganic geochemical feature of the Pearl River delta and estuary. Selection of these metals is based on two principles: 1) sources and distribution of the metal in the study area have been relatively well understood by previous studies; and 2) these metals have the potential to be used as environmental indicators for the modern day as well as for past times. The 15 metals seclected include manganese (Mn), cobalt (Co), iron (Fe) arsenic (As), lithium (Li), barium (Ba), aluminium (Al), potassium (K), rubidium (Rb), strontium (Sr), sodium (Na), magnesium (Mg), calcium (Ca), boron (B) and beryllium (Be). As concentration of B, a possible salinity indicator, might be influenced by grain size (Siegel *et al.*, 1995), so the B/Be ratio is used to remove the potential influence of grain size.

Principle Component Analysis was applied to results of concentrations of the 14 metals (including the B/Be ratio) in 91 estuarine surface sediment samples using the SPSS for Windows 15.0 program. The PCA analysis has extracted five principle components with the first three main components taking 60.1% of the total information. Therefore, it is reasonable to divide the 15 key metals into three main groups. The F1 metals include Mn, Co, Fe and As; the F2 metals include Li, Ba, Al, K and Rb; and the F3 metals are Sr, Na, Mg, Ca and B/Be.

5.5.2 Concentrations of key metals in terrestrial soil

Concentrations of F1, F2 and F3 metals vary between different types of terrestrial soil (Appendix 6). Box-whisker plots of key metals show the minimum, maximum, median, lower quartile and upper quartile for the metal concentrations in the terrestrial soil (Figure 5.16-5.18). F1 metals show the highest concentration in agricultural soil and similar concentrations in the other terrestrial soil (Figure 5.16). For example, the average concentration of Co is 19±1 mg/kg in agricultural soil, averaged with 3±1 mg/kg in forest soil, 9±5 mg/kg in riverbank soil and 6±4 mg/kg in mangrove soil. The distribution pattern of Co is also observed for Fe and Mn. Distribution of As in the

terrestrial soil, however, shows a different pattern relative to the other three F1 metals (Figure 5.16). Mangrove soil has the lowest concentration of As (14±5 mg/kg), slightly lower than that in agricultural soil, 24±3 mg/kg, while concentrations of As in mangrove soil and agricultural soil are much higher and more variable than in other terrestrial soil (Figure 5.16).

Differences of average concentrations (as well as mean concentrations) of F2 metals in different types of terrestrial soil are relatively small (Figure 5.17) compared to that of F1 metals, while concentrations of F2 metals are more variable (Figure 5.16, 5.17). Concentrations of F3 metals are relatively higher in mangrove soil than in other kinds of terrestrial soil (Figure 5.18), although differences between them are not as significant as the F1 metal (Figure 5.16, 5.18).
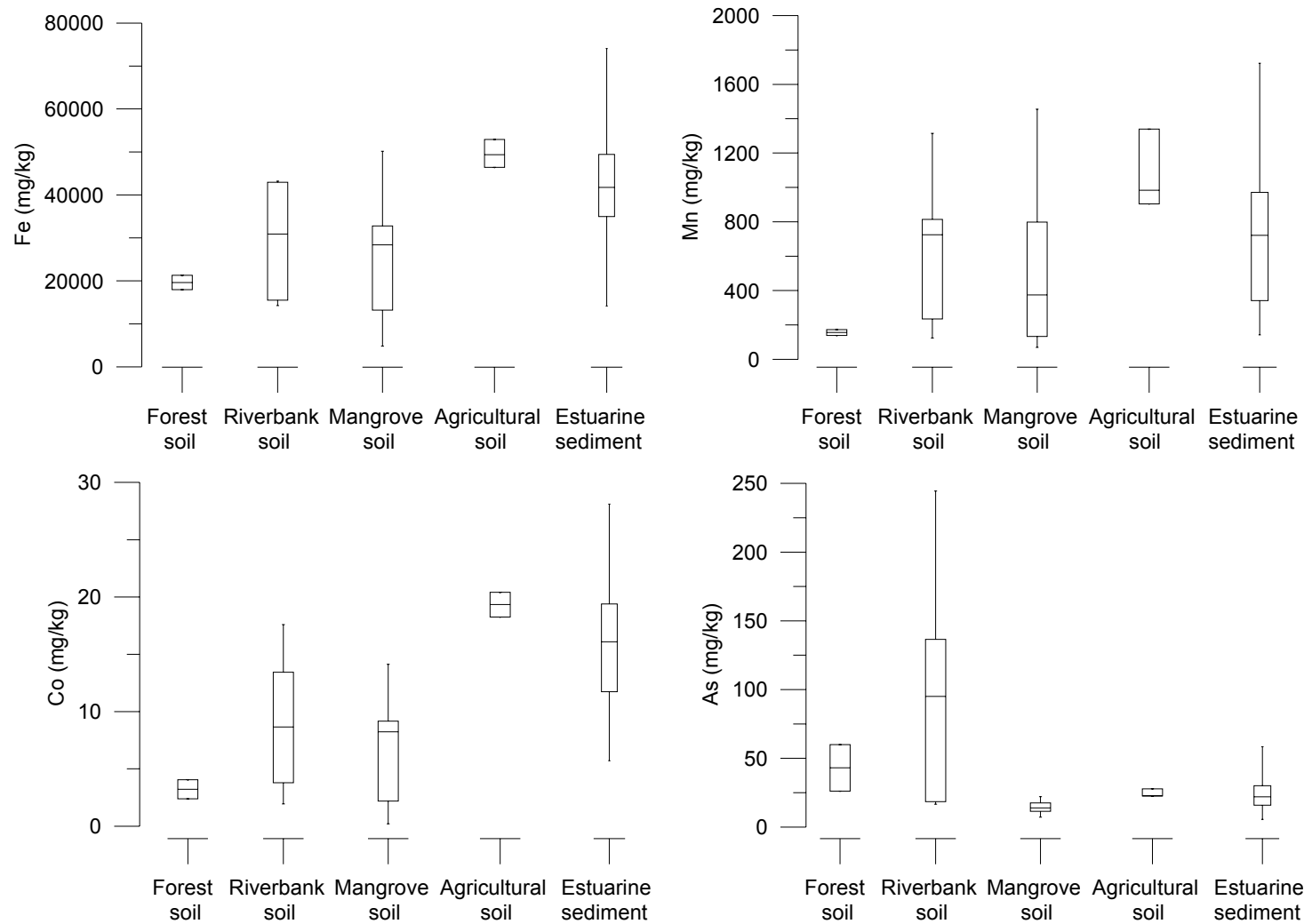
Figure 5.16 Concentrations of F1 metals in the terrestrial soil and estuarine surface sediment. The caps at the end of each box indicate the extreme values (minimum and maximum), the box is defined by the lower and upper quartiles, and the line in the centre of the box is the median.
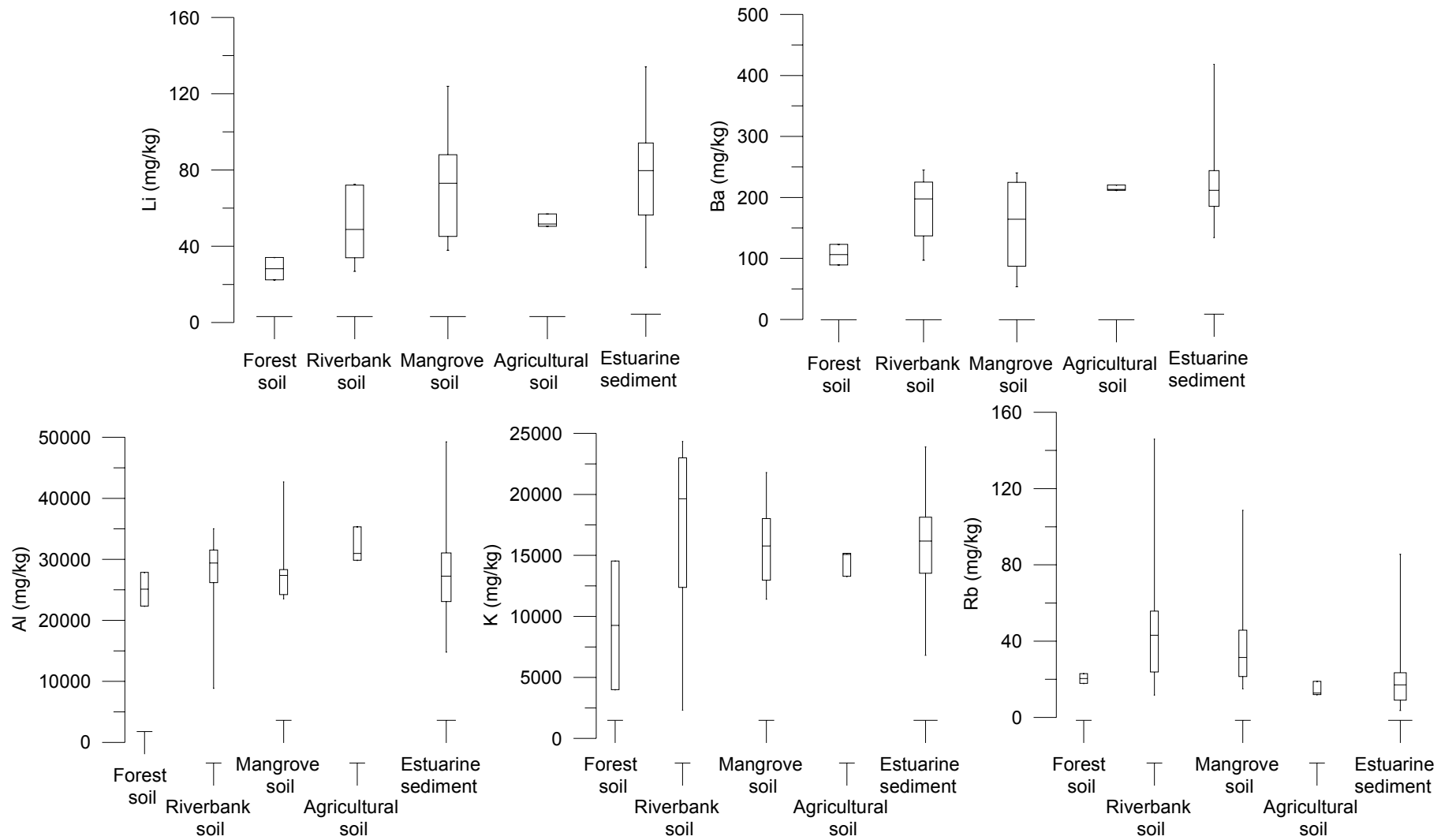
Figure 5.17 Concentrations of F2 metals in the terrestrial soil and estuarine surface sediment.
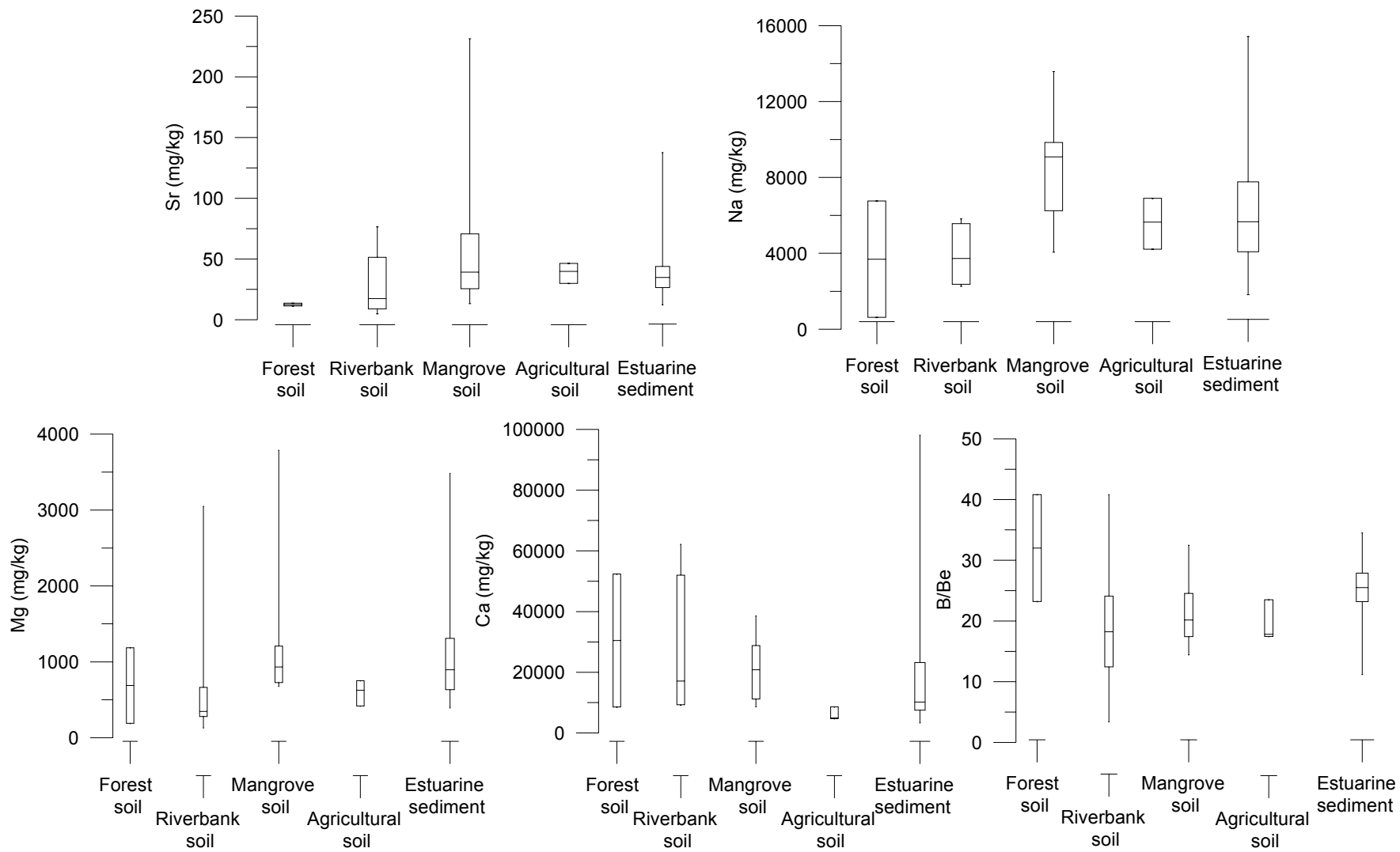
Figure 5.18 Concentrations of F3 metals in the terrestrial soil and estuarine surface sediment

5.5.3 Concentrations of key metals in estuarine surface sediment

F1 metals

Generally, with regard to natural terrestrial soil (forest soil, riverbank soil and mangrove soil), estuarine surface sediment is higher in F1 metals (except for As) and is lower in F3 metals, but has similar concentrations of F2 metals (mean values in Figure 5.16-5.18).   Specifically, average As concentration in estuarine surface sediment (23±10 mg/kg) is lower than significantly lower than in riverbank soil (95±78 mg/kg) and forest soil (43±24 mg/kg).   Co concentration ranges between 5 and 28 mg/kg in estuarine sediment, which covers all types of terrestrial soil but forest soil ranging between 2 and 4 mg/kg.

Spatial distribution of F1 metals in the Pearl River estuary is demonstrated in Figure 5.19.   Concentrations of F1 metals are higher in the western estuary than in the east, and become much lower in shallow marine areas near Hong Kong (Figure 5.19).   They are especially abundant in the river mouth area (e.g. G4), and the turbidity maximum zone (e.g. G5; Figure 5.19).   Concentrations of F1 metals in river tributaries are not as high as in brackish-water area (Figure 5.19).   For example, the average concentration of Co is 15 ±5 mg/kg in the freshwater area (G1 and G2), lower than in the brackish-water area (17 ±4 and 16 ±5 mg/kg), but it becomes the lowest in shallow marine area 9 ±1 mg/kg.

F2 metals

Compared to terrestrial soil, estuarine sediment has relatively higher mean concentrations of Li and Ba (Figure 5.15), but relatively lower mean concentration of Rb.   The difference in mean concentrations of Al and K between terrestrial soil and estuarine sediment is not significant (Figure 5.15).

In the estuary, concentrations of F2 metals show an increasing trend from the freshwater area (river tributaries) to the shallow marine area (Figure 5.20).   Sediments from the marine area (e.g. G8 and G9) have significantly high concentrations of F2 metals. Furthermore, concentrations of F2 metals in the west part of the estuary are slightly lower than in the east part, such as Ba, Li and Rb.   However, the difference is not as

significant as that between freshwater and marine areas. F2 metals are usually found to be especially low in abundance near the river mouth, especially near mouth of the West River, e.g. Li, Al (Figure 5.20).

F3 Metals

Mean concentrations of F3 metal in estuarine sediment are similar with that in mangrove soil, higher than other types of terrestrial soil (Figure 5.16). Distribution of F3 metals within the estuary does not follow a fixed pattern. Ca shows a decreases from the freshwater area to the shallow marine area, while B/Be ratios increase from the freshwater end to the marine end (Figure 5.21). Sr, Na, Mg and Ca show a much lower concentration in the area west of Hong Kong (Figure 5.21), and they are less abundant in river tributaries than in the estuarine and shallow marine areas (Figure 5.21). Furthermore, concentrations of Sr, Na and Mg are significantly low in the area west of Hong Kong (G7; Figure 5.21). For instance, Na concentration of G7 is generally lower than 5000 mg/kg, similar to that of G1 and G2 (freshwater areas) 4340 ±1654 mg/kg.
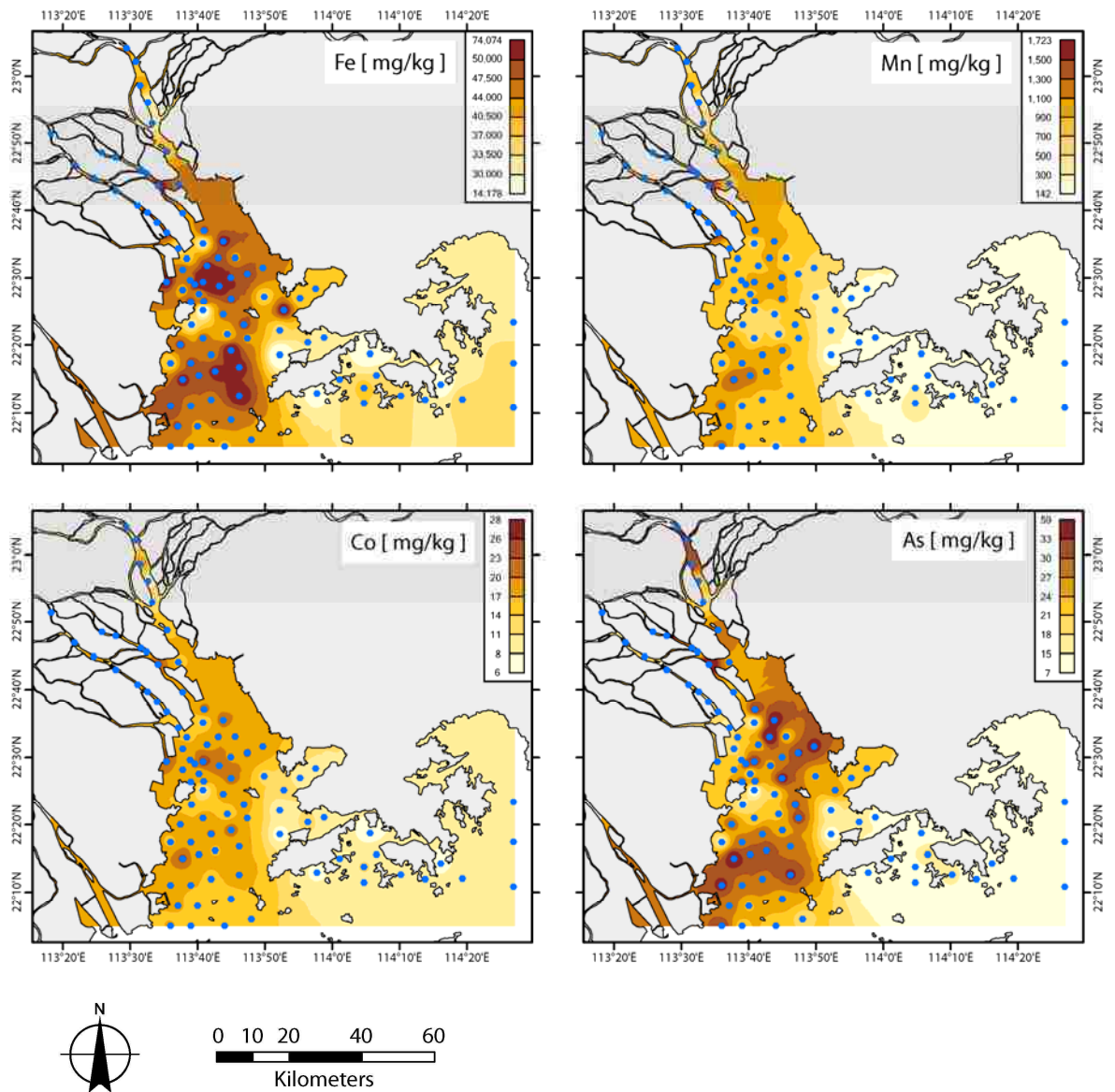
Figure 5.19 Distribution of F1 metals in the Pearl River estuary
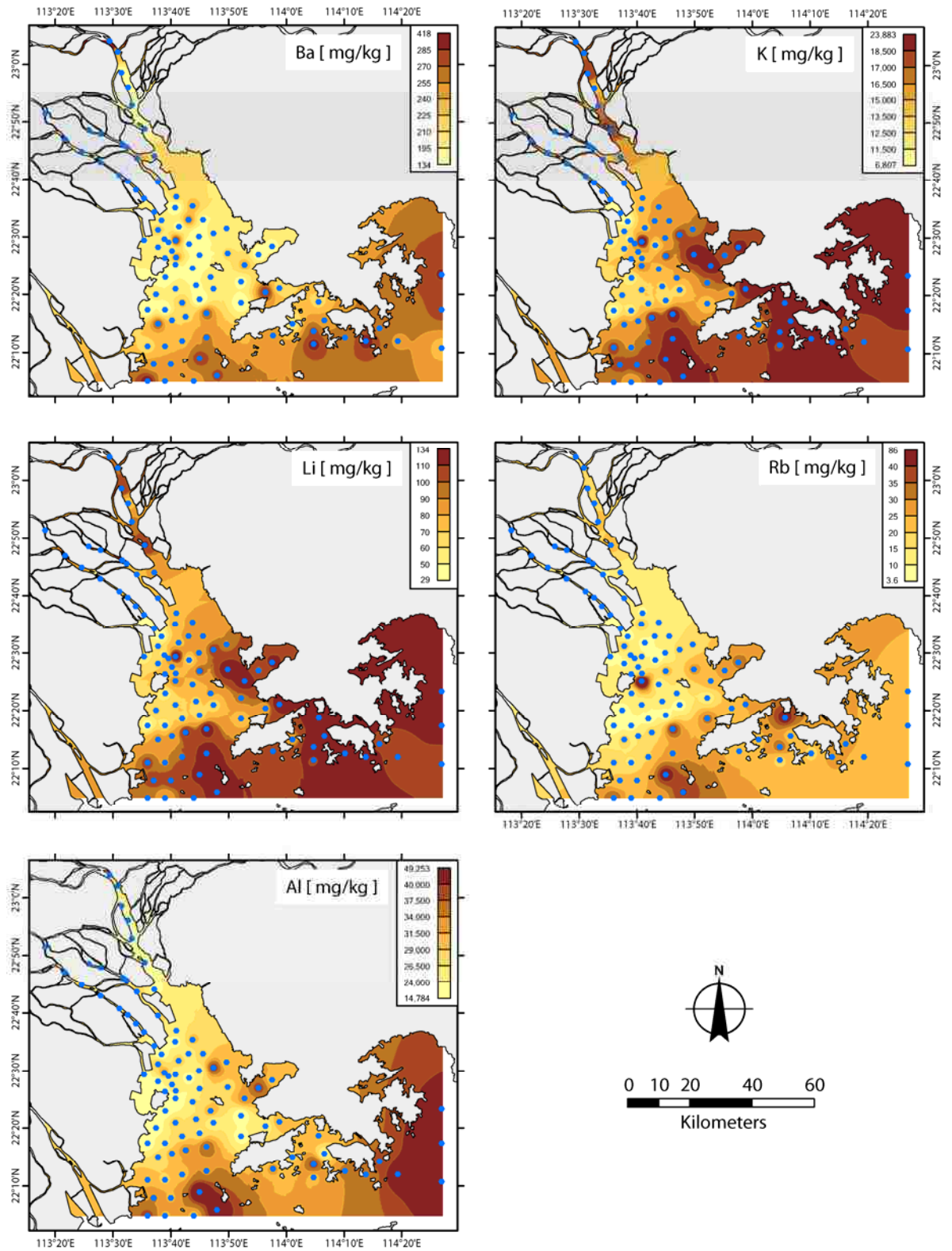
Figure 5.20 Distribution of F2 metals in the Pearl River estuary
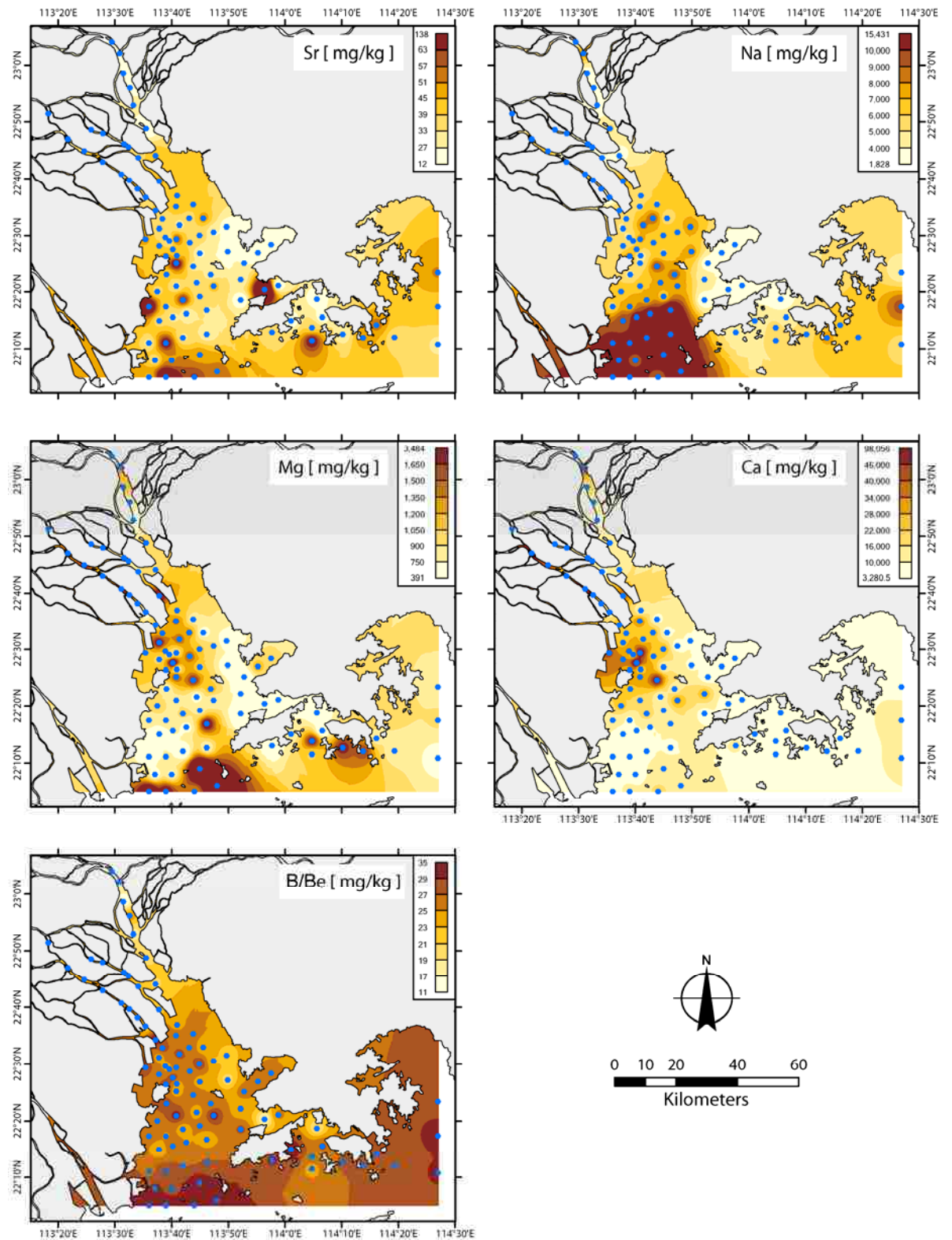
Figure 5.21 Distribution of F3 metals in the Pearl River estuary

5.6 Application of key metals as sources and environments of sediments

5.6.1 Key elements as indicators for sediment sources

F1 metals observed in this study are typical terrestrial metals as suggested by other studies (Siegel *et al.*, 1995; Yang *et al.*, 2008), which are mainly released during weathering of the bedrock. Thus, F1 metals (typically Fe and As) can usually be used to indicate terrigenous sediment, the higher the concentrations of F1 metals the larger amount of sediment originated from the terrestrial area. This explains the general decreasing trend from freshwater to marine areas within the estuary, as the freshwater area is nearer to the sediment source than is the marine area.

Those elements with relatively higher mobility are dissolved in solution, in forms of ionic solutions or as colloidal dispersions and particulate substances (Rankama and Sahama, 1950). F2 metals and F3 metals are of this kind (Goldschmidt, 1954). After entering streams, in whatever form, elements are finally delivered into the ocean. Some elements become enriched in seawater, such as potassium (K), and some are precipitated from seawater and become enriched in marine sediments, such as boron (B), and become good indicators for the amount of marine-origin sediment. This is supported by the fact that F2 metals increase with increasing salinity from the freshwater area to the marine area (Figure 5.20). However, this process might be influenced by biological activity, e.g. Ca is taken from seawater and becomes the main component of marine shells; other elements are found to be enriched in plants.

In the estuarine area, salinity is an important controlling mechanism of the geochemical feature of the Pearl River estuary. Results from the modern-day sediments show that, B/Be ratios are positively related with water salinity, the higher the salinity, the higher the B/Be ratio. In the freshwater area, sediments from the river mouth have higher B/Be ratio than those from the stream, due to higher influence from brackish water at the mouth. Thus, high concentration of the -sensitive elements, such as B, K and Rb, might indicate a marine depositional environment. Environmental conditions can be interpreted more precisely by using a combination of the three groups of metal.

Generally, in the Pearl River estuary, sediments from marine environment are characterised with high B/Be ratios (>26.0) and high concentrations of both Rb (>20 mg/kg) and K (>18 000 mg/kg), but low concentrations of As (<12 mg/kg) and Mn (<300 mg/kg). A Similar conclusion concerning the combination of elements in the marine area was also made by Huang *et al.* (2003).

5.6.2 Key elements as indicators for sedimentary environment

In the terrestrial area, the abundance of key elements in terrestrial soil is mainly controlled by types of local bedrock and the weathering process, especially for the forest soil. In the Pearl River catchment, F1 metals are usually found to be less abundant in forest soil than riverbank soil. This might indicate relatively dry-cold climate conditions in the forest, which result in low weathering activity, so that elements have not been completely leached. Further weathering occurs during the redelivery and redeposition processes.

After being removed from the source area, sediments have been reworked and redeposited, resulting in changes of the metal concentrations. In the Pearl River estuary, distribution of these elements is influenced by local environmental conditions, such as the hydrological situation, grain size structure of the sediment and water salinity. Results show that highest concentrations of F1 metals are not found to be in either terrestrial soil or in freshwater sediment, but in sediment from the river mouth and turbidity maximum zone (Figure 5.19). The re-suspending process in the turbidity maximum zone might be another reason for the high concentration of F1 metals in this area. The re-suspension and re-deposition result in finer sediment deposited in the turbidity maximum zone which tends to be rich in colloid and mineral particles and thus have higher metal concentrations (Wen and He, 1987; Li and Liang, 1995; Zhou *et al.*, 2004). Interestingly, areas enriched in F1 metals, such as the river mouth and the turbidity maximum zone, are found to be poor in F2 metals (Figure 5.19, 5.20). Chen (1994) analysed the correction between maximum concentration of some metals (e.g. Fe) and the clay content and mica. They suggested that the distribution of these metals was mainly controlled by grain size and heavy mineral distribution. High concentration of these metals found near the river mouth, might be due to the special environment under the interaction between fresh water and sea water. This process encourages absorption

of these elements in the surface sediment. Hydrological situations also include the strength of freshwater input. Fyfe *et al.* (2000) suggested that alkaline metals and alkaline earth metals including Na, Ca, Mg and K can be considerably leached from weathered material in Hong Kong during intense chemical weathering. Results of this study show that Na and Mg concentrations are found to be low in the area west of Hong Kong. This might suggest less amount of sediment has been delivered into the estuary during the past 6-10 years.

5.6.3 Further interpretation

In Pearl River estuary, higher B/Be ratios, Rb and K concentrations are found in sediments preserved in saline environments, while higher Ca/Sr ratio and Mn concentration are found in sediments from freshwater environment (Yang *et al.*, 2008; Guan *et al.*, 2001; Fyfe *et al.*, 2000; Sewell, 1999; Huang *et al.*, 1983). Dominant provenance of sediments preserved in the Pearl River estuary is highly related to the strength of river discharge, driven by monsoonal precipitation (illustrated in Chapter 4). Thus, estuarine sediments dominated by terrestrial material during periods of strong summer monsoon should have higher Ca/Sr and Mn concentrations, whereas those preserved during periods of strong winter monsoon should have higher B/Be ratios, and be enriched in Rb and K. Arsenic is not a traditional proxy for studies of environment changes; however, significant differences in its content between terrestrial and marine material found in this study suggest it is a potential indicator for palaeo-environment changes.

It is worth mentioning that the Pearl River delta is one of the most developed areas in China. Therefore, enhanced human activities have significantly changed the natural geochemical components of the sediment. For instance, Co has a relatively low concentration in terrestrial and shallow marine areas (usually <10 mg/kg; Appendix 6; 7), while in agricultural soil it reaches 19±1 mg/kg and around 17 mg/kg in sediments from other parts of the estuary. This might due to the industrial activities at the head of East River which releases large amount of Co into the river entering the estuarine system. Similarly, the enhanced agricultural activity can play a similar part.

5.7 Summary of the chapter

This chapter developed a modern-day analogue of the two geochemical proxies in the Pearl River delta and estuary and their indication of sediment sources and sedimentary environment. A summary of the main findings of this chapter is as follows:

1. In the Pearl River delta, while C_3 plants have lower $\delta^{13}C$ than C_4 plants, $-29.0\pm1.8‰$ and $-13.1\pm0.5‰$ respectively, C/N of both C_3 and C_4 are widely variable and the overlap between groups is considerable.

2. $\delta^{13}C$ and C/N for terrestrial soil organic matter are highly related to the source of organic matter. Soil samples from C_3-plant-dominant areas, e.g. the forest, tend to have lower $\delta^{13}C$ than those from C_4-grass-dominant areas, e.g. the riverside area. Their C/N, however, are widely variable and significantly overlap. Thus, while the $\delta^{13}C$ of soil can be used to indicate the predominant vegetation type, C/N cannot.

3. $\delta^{13}C$ and C/N of POC show significant variability due to seasonal variation of freshwater flux resulting in changes the balance between the TOM and in situ phytoplankton in the POC.

4. $\delta^{13}C$ of surface sediment in the estuary increases from $-25.0‰$ at the freshwater end to $-21.0‰$ at the marine end, with C/N decreasing from 15.2 to 6.8, suggesting a weakening terrestrial/freshwater input and a strengthening marine contribution seaward.

5. Anthropogenic input might elevate the $\delta^{13}C$ of sedimentary organic matter due to enhanced fertilization process and, more significantly, by an increase in the proportion of C_4 plants such as sugarcane grown in the catchment area. However, this signature is not significant enough to influence the signature produced by the natural vegetation in this area, which is dominated by the C_3 plants.

6. Based on the analysis of modern samples of organic matter from source to sink in the Pearl River catchment, delta and estuary, this study suggests that $\delta^{13}C$ and C/N of bulk organic matter can be used as an indicator for vegetation type, sediment source and environmental conditions.

7. The concentrations of key metals observed do not show significant differences in natural terrestrial soil, especially for F1 metals. Concentrations of F1 metals are significantly higher in agricultural soil than other types of terrestrial soil.

8. Terrigenous metals (e.g. Fe, Mn, Co and As) have higher concentrations in the fresh-brackish-water area than in the marine. Highest concentration of F1 metals are found near the river mouth and in the turbidity maximum zone.

9. Concentrations of F2 metals (Li, Rb, K, Ba and Al) show an increasing trend from the freshwater area to the marine areas in the Pearl River estuary. F2 metals are found to be lower in the river mouth area and in the turbidity maximum zone than other parts of the estuary.

10. Distribution of F3 metals within the estuary does not follow a fixed pattern. Ca shows a decreasing from freshwater area to the shallow marine area, while B/Be ratios increase from the freshwater end to the marine end. Sr, Na, Mg and Ca show a much lower concentration in the area west of Hong Kong.

11. A combination of these key metals is a good indicator for sediment sources and sedimentary environment. Sediment of high concentrations of F1 metals and low concentrations of F1 metals are mainly from terrestrial area or under the environment of low salinity environments. This kind of combination of metals might also indicate a sedimentary environment with strong interaction between freshwater and saline water and/or of strong re-suspension process.

12. B/Be (F3 metal) is a good indicator for salinity changes, while the indications of other F3 metals of environmental conditions and sediment sources needs further study.

13. This chapter suggests that it is possible to use the two geochemical proxies as indicators for sediment sources and environmental conditions in the Pearl River delta and estuary.

Chapter 6 History of the EAM and its possible driving mechanisms during the mid-Holocene

6.1 Introduction

This chapter presents results on the particle size, organic carbon isotopic signature (δ^{13}C), total organic carbon content (TOC), total carbon versus total nitrogen ratio (C/N), and concentrations of key metals of Core UV1 from the Pearl River estuary, southern China (Figure 6.1; Appendix 8-11). Three age models were evaluated before choosing one for this study based on seven radiocarbon dates obtained. This chapter then reconstructs EAM history during the mid-Holocene, and explores possible driving mechanisms for the changes. Also discussed in this chapter is the evidence of human activity in the Pearl River delta over the last 2000 years.

Exponential smoothing was applied to results of both organic carbon and metals analyses to produce smoothed data (see Chapter 4). In order to examine the millennial- and centennial timescale fluctuations and the potential periodicity of the EAM, the de-trending process and spectral analysis of the δ^{13}C data were undertaken using the PAST program (Hammer, *et al.*, 2001). This function removes any linear trend from the δ^{13}C data by subtraction of a linear regression line from the δ^{13}C values. The 17 key metals of the Core UV1 are divided into three groups according to their modern-day distribution (see Chapter 5). The F1 metals include manganese (Mn), cobalt (Co), iron (Fe) and arsenic (As). Concentrations of the F1 metals decrease significantly seawards and are obviously higher in the western estuary than the east. Metals of lithium (Li), barium (Ba), aluminium (Al), potassium (K) and rubidium (Rb) are the F2 metals based on the modern-day analogue, which increase seawards. Strontium (Sr), sodium (Na), magnesium (Mg), calcium (Ca) and the boron/beryllium ratio (B/Be) are the F3 metals analysed in the modern-day analogue. Concentrations of the F3 metals are slightly higher in the western estuary than the east, and they decrease slightly seawards.

6.2 Lithology of Core UV1

The Vibracore UV1 was collected from Northwest of Lantau Island, Hong Kong, China (22°17'10″N, 113°51'49″E, Figure 6.1), from a water depth of 8.6m. The total length of Core UV1 recovered is 30.0m (Table 6.1), although only the top 10.29m of the core was analysed in this study. The top 0.35m of the core was washed away during the coring process, and sediments from 6.00-6.25m were missing due to the length of the sampling tube (see Chapter 4).
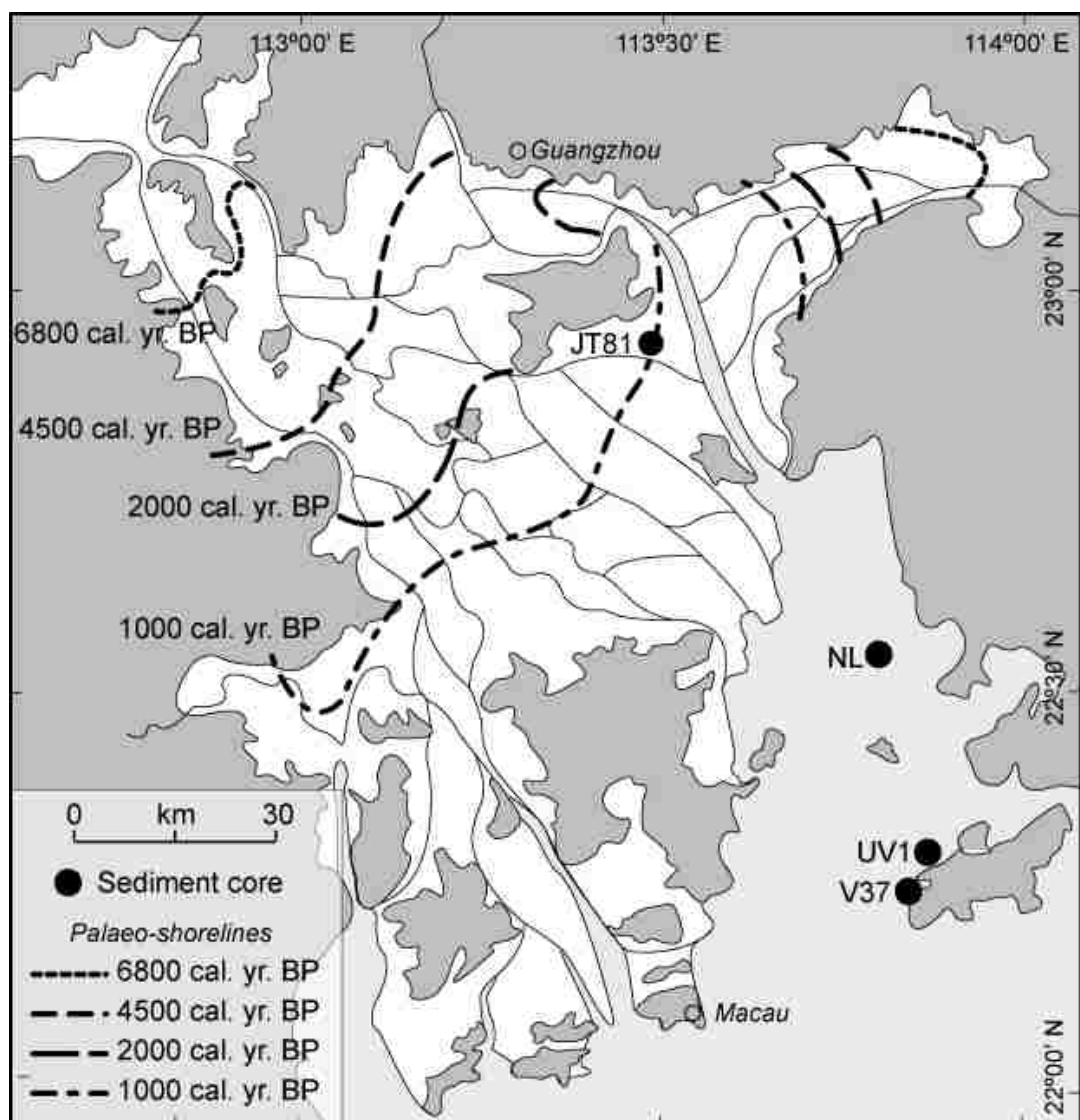
Figure 6.1 Location of key sediment cores and palaeo-shorelines (after Zong *et al.*, 2009a).

Table 6.1 sediment sequence of core UV1

Depth (m)	Lithology
0.0 – 10.2	Dark greenish grey soft silt and clay
10.2 – 10.6	Bluish grey firm silt and clay with small gravels and coarse sands
10.6 – 23.2	Bluish grey silt and clay
23.2 – 24.3	Bluish grey mottled yellow silt clay
24.3 – 30.0	Dark bluish grey silt

Sediments below 10.6m are older marine deposits (the M2 unit of the lithostratigraphic framework, devised by Yim, 1994, for this area) dating back to around MIS 5 (Table 6.1; Zong *et al*., 2009a). Sediments from 10.6-10.09m form a terrestrial deposit (T1, Zong *et al*., 2009b) composed of bluish grey firm silt and clay, with small gravel and coarse sands (Figure 6.2). Above the T1 unit is the Holocene marine deposit (M1, Table 6.1), containing soft to very soft silt and clay between 10.07-0.35m (Figure 6.2). Generally, sand concentration of the M1 unit fluctuates between 5-25% without any clear trend, while clay concentration shows a general decreasing trend from 30% to 16% from the base to the top of this section (Figure 6.2). Based on differentiation in lithology, the M1 unit is the main focus of this study and it is subdivided into two zones: Zone 1 10.07-1.31m, which is composed of dark greenish grey very soft silt and clay with the fraction of clay and silt of 88.6% (Figure 6.1, Table 6.2); and Zone 2 1.29-0.35m, which is composed of yellowish soft silt and clay with large numbers of shells (Figure 6.2). A layer of sandy sediment is found at 1.04-0.98m with a sand concentration of 49% (Figure 6.2), mixed with broken shells. The following sections will present results from the T1 unit, and Zone 1 and Zone 2 of the M1 unit respectively.

Table 6.2 Measurements of the three sections of Core UV1

Depth (m)	Age (cal. yr BP)	$\delta^{13}C$ (‰)	TOC (%)	TN (%)	C/N	Sand (%)	Clay (%)	Silt (%)
0.35-1.29	1364-1990	-23.1 ±2.0	1.0 ±0.2	0.1 ±0.0	11.3 ±1.7	17.0 ±12.1	22.2 ±4.4	60.8 ±10.8
1.31-10.07	2003-6395	-25.2 ±0.3	1.0 ±0.1	0.1 ±0.0	10.5 ±1.2	11.4 ±6.6	24.9 ±3.9	63.6 ±5.2
10.09-10.29	before LGM	-27.0 ±0.4	0.8 ±0.3	0.1 ±0.0	10.6 ±4.4			

Values are expressed using average values and standard deviations.
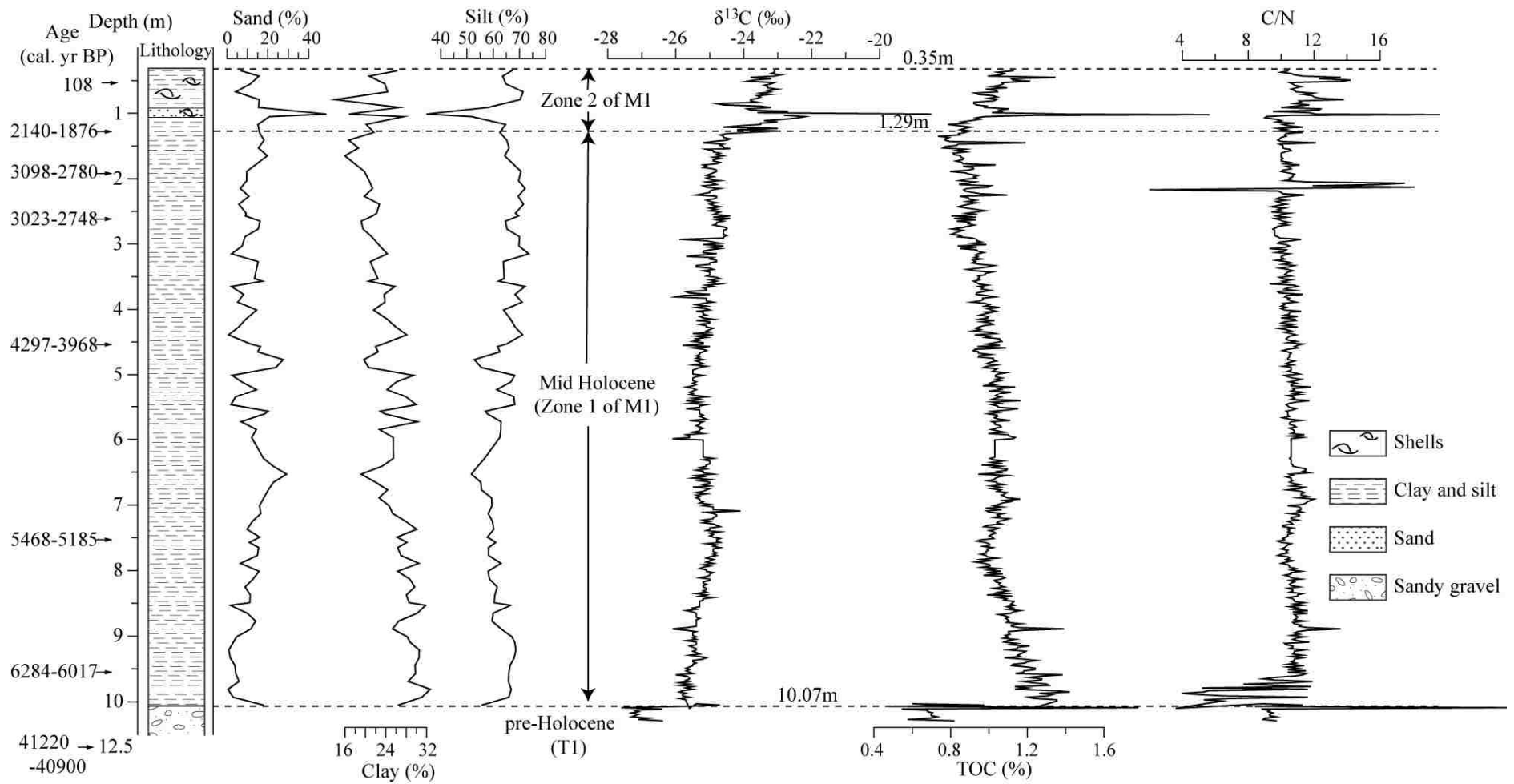
Figure 6.2 Lithology and organic carbon results of core UV1 (0.35-10.29m).

6.3 Results from 10.29-10.09m (T1)

The deposit in this unit is significantly different from the rest of the core. This section has δ^{13}C values of -27.0 ±0.3‰, significantly lower than values found throughout the rest of the core (Figure 6.2). TOC and C/N are also significantly lower than the rest of the core with values of 0.7 ±0.1% and 9.3 ±0.3 respectively (excluding the sample at 10.09m, Table 6.2). The sample at 10.09m has anomalously high values of TOC and C/N ratio of 1.8% and 23.7 respectively (Figure 6.2).

The δ^{13}C of the sediment indicates a terrestrial deposit, suggesting 10.29-10.09m is a part of Unit T1 lying on top of an older marine unit (M2, Zong *et al.*, 2009a; Table 6.2). T1 was probably deposited during the MIS3 interstadial when high freshwater discharge (Wang *et al.*, 2001; Yuan *et al.*, 2004) and low sea level (Zong, 1989; Saito *et al.*, 2001) helped to transfer the coarse sediments from the catchment to the deltaic basin (Zong *et al.*, 2009a). However, Zong *et al.* (2009a) suggested the T1 included 10.6-10.2m in this core. The results from this study (in particular the δ^{13}C signature) suggest the upper boundary of the T1 should be moved from 10.2m to 10.08m (Figure 6.2).

6.4 Results from the 10.07-1.31m (Zone 1 of the M1 unit)

6.4.1 Results of δ^{13}C, TOC and C/N

Zone 1 has higher δ^{13}C and TOC than the T1, while the C/N ratios are similar (Table 6.2), except for lower part of Zone 1 (Figure 6.2). The δ^{13}C values show a general increasing trend throughout the section. Superimposed on this increasing trend, the δ^{13}C values fluctuate between -26.4‰ and -24.1‰ (Figure 6.3). Exponential-smoothing of the δ^{13}C data suggests two complete cycles are recorded in this section (Figure 6.3). The first complete cycle extends from the base of this section to 5.5m. Within this cycle, δ^{13}C increases from -26.0‰ at 10.07m to -24.7‰ at 7.5m, it then decreases to -25.7‰ at 5.5m (Figure 6.3). The second cycle runs between 5.5m and 1.31m, with the highest δ^{13}C value of -24.4‰ at 2.7m (Figure 6.3), although the last part of the second cycle is not so clear.

126

However, the second cycle may not be complete. The δ^{13}C value is relatively stable at 7.0-6.3m and 4.6-3.8m fluctuating around the mean value of -25.2‰. The δ^{13}C values from 10.07-8.60m and 6.0-4.5m are below the mean level, while those from 8.6-7.0m and 3.8-1.3m are higher than the mean value (Figure 6.3).

The TOC data shows the opposite trend compared with the δ^{13}C, showing a general decreasing trend from 1.4% to 0.8% throughout the core with the average value of 1.01% (Figure 6.3). The exponential-smoothed TOC reveals that, below 5.0m, TOC values are constantly higher than the mean value. They decrease to the mean level around 5.0m, and keep decreasing upwards to the top of this section at 1.31m (Figure 6.3; Table 6.2). The general trend in C/N is not as clear as that found in the TOC and δ^{13}C values. From 6.0-3.6m the C/N ratio is relatively stable close to the mean level, 10.07-6.3m and 3.5-1.3m record significant fluctuations in the C/N ratios, with the extremely low (4.0-9.0) and high C/N ratios (9.9-18.1) found at 10.07-9.63m and at 2.17-2.05m respectively.
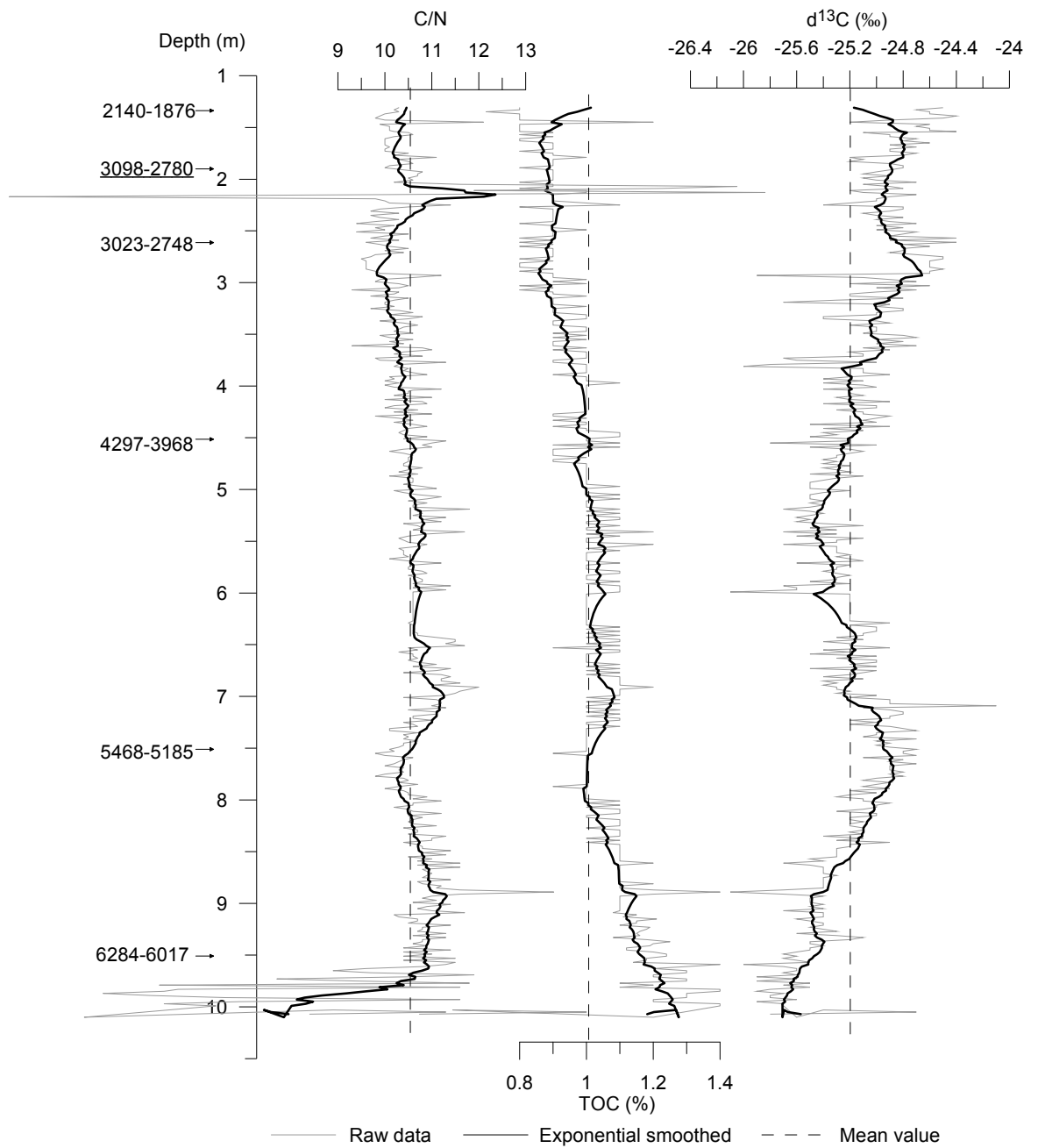
Figure 6.3 Results of the δ¹³C, TOC and C/N of the Core UV1 (1.31-10.07m)

6.4.2 Results of selected metals

The three groups of selected metals (F1, F2 and F3 metals) defined based on their distribution within the modern-day Pearl River delta and estuary (Chapter 5) show different behaviour through the core (Figure 6.4; 6.5; 6.6). Concentrations of the F1 metals (Fe, Mn, Co and As) show a general decreasing trend upwards, with some fluctuations. Concentrations of all four metals show a decreasing trend in the lower part of the core (10.07-9.0m). At 9.0-6.3m, the concentration of Mn and Co increases from 400 to 600 mg/kg and from 11 to 16 mg/kg, respectively, while concentrations of Fe and As stay relatively stable around 37000 mg/kg and 13.5 mg/kg (Figure 6.4). The concentration of all the F1 metals is lower above 6m than below, and keep declining (with minor fluctuations) to the top of the core. Specifically, concentrations of Fe and As in sediments below 5.0m are higher than their average values, and it become lower than their average values in sediments above 5.0m (Figure 6.4).

Changing trends are not clearly shown in F2 metals compared to F1 metals. Weak decreasing trends are found in concentrations of Li and Al throughout the core (Figure 6.5). Similar to some F1 metals (e.g. Fe and As), concentration of Al is lower than its average value of 32467 mg/kg in sediments below 5.0m, and becomes higher in sediments above 5.0m (Figure 6.5). Furthermore, concentrations of these F2 metals are more variable above 6m than below (Figure 6.5).

Changing trends in the concentrations of F3 metals are not obvious in core UV1 (Figure 6.6). Concentrations of F3 metal increase to a level higher than their average values at around 3.5m, except for B/Be, for which the increase occurs earlier at around 4.5m (Figure 6.6). Concentrations of F3 metals below 3.5m (4.5m for B/Be) are generally lower than their average values, and no clear trend is presented, especially for Na (Figure 6.6). A slight increase is found in concentrations of Na, Sr, Mg and B/Be at 10.07-9.5m, followed by a relatively stable stage at 9.0-3.5m.
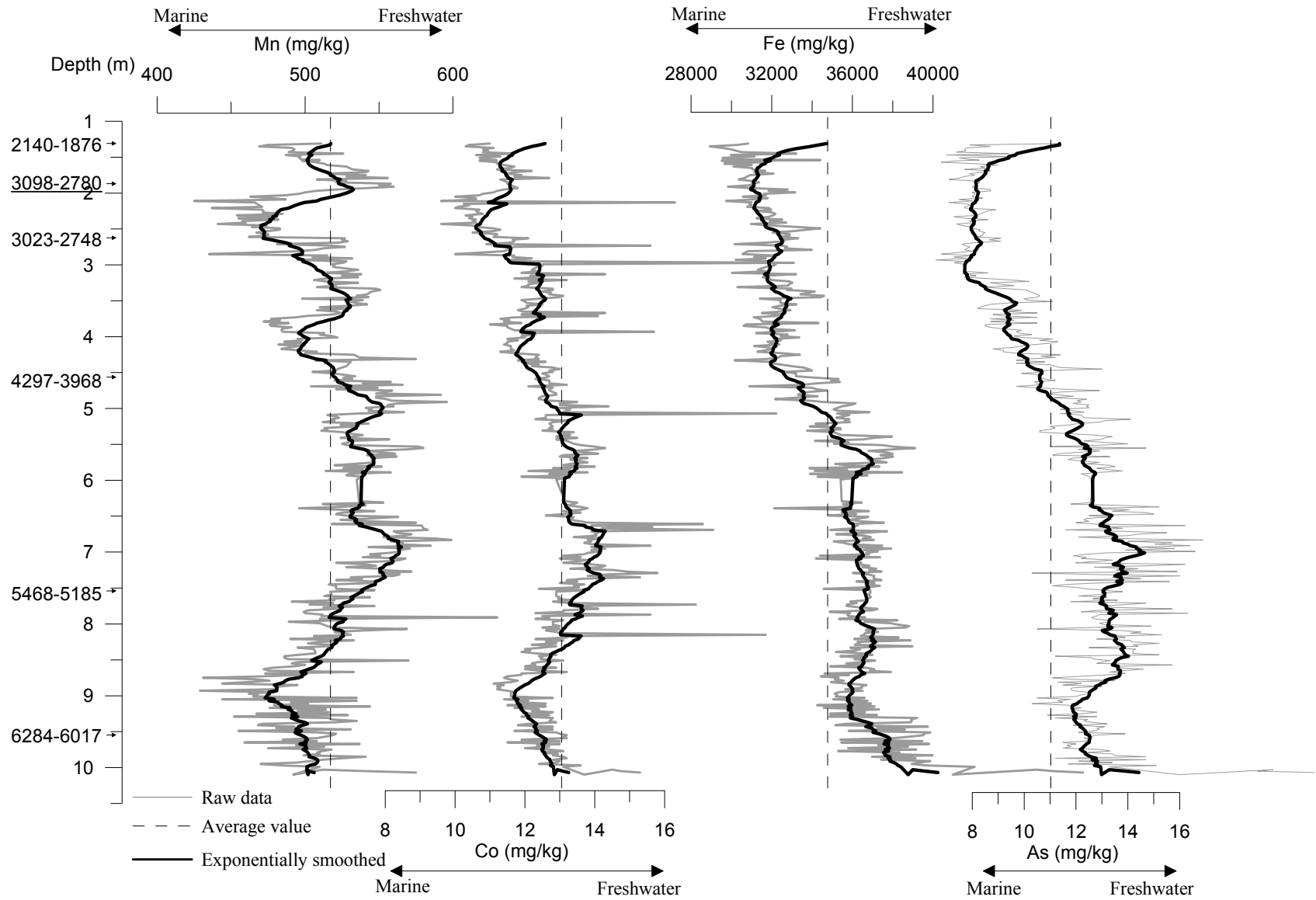
Figure 6.4 Result of F1 metals of the Core UV1 (10.07-1.31m)

130
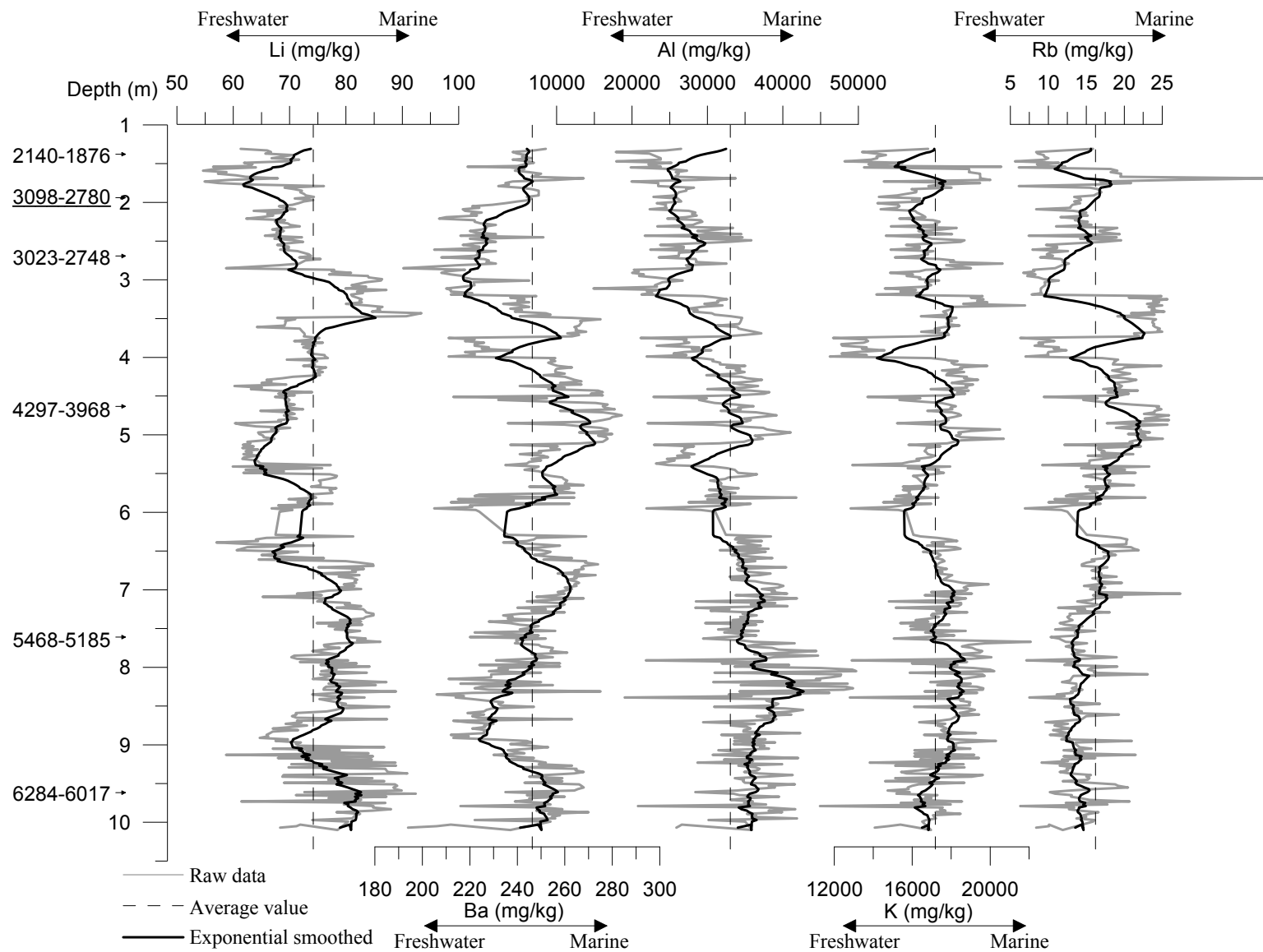
Figure 6.5 Result of F2 metals of the Core UV1 (10.07-1.31m)
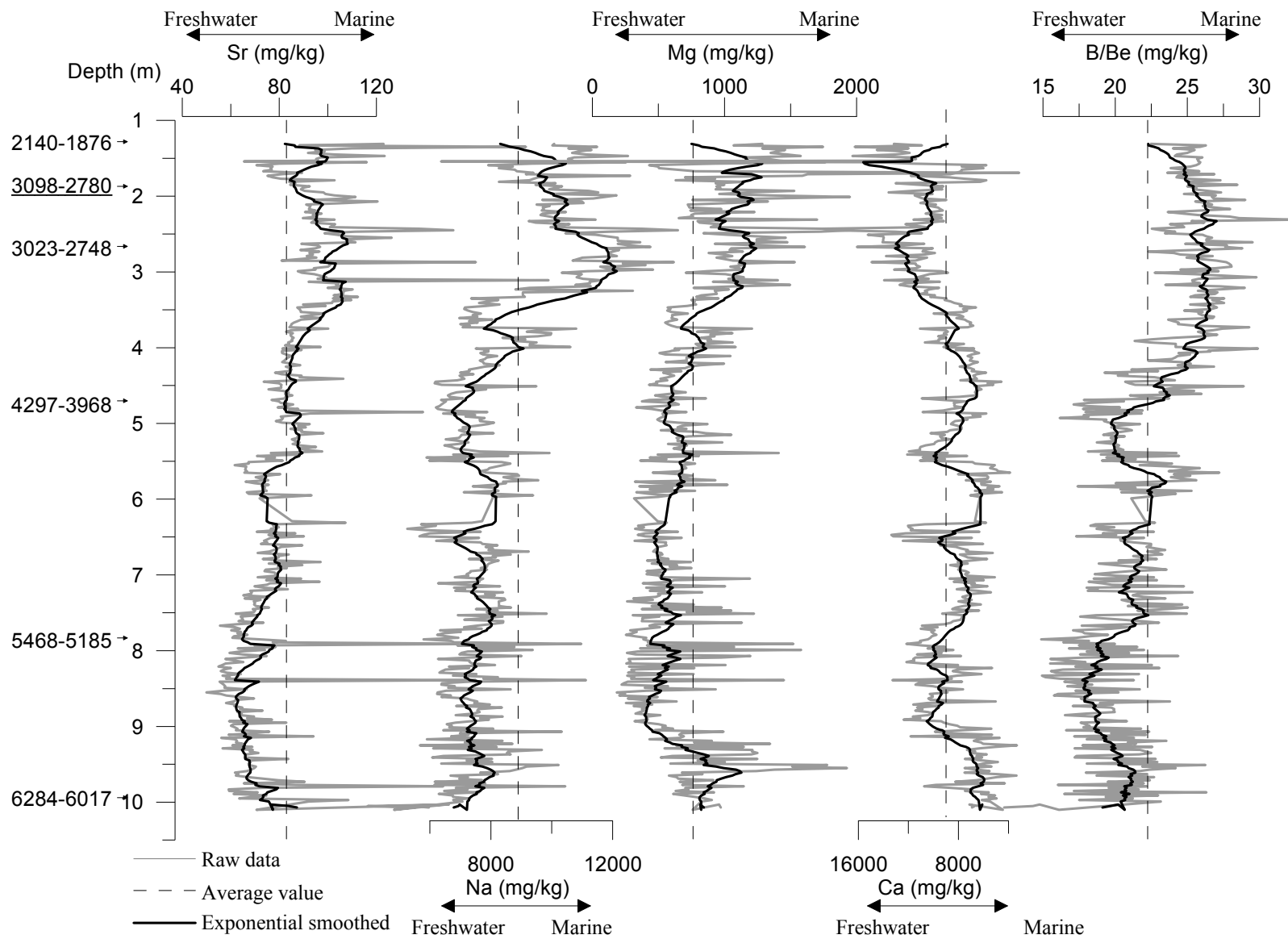
Figure 6.6 Result of F3 metals of the Core UV1 (10.07-1.31m)

132

6.5 Results of 1.29-0.35m (Zone 2 of M1 unit)

6.5.1 Results of δ^{13}C, TOC, C/N and the grain size

Sediment from 1.29-0.35m is composed of yellowish coarse sediment, mixed with numerous shells (Figure 6.2). An abrupt change was found in a layer around 0.98-1.04m. The sand concentration in this layer is 48.7% (at 1.01m). This is over double the concentration for the rest of this zone (Table 6.2). Extreme values of organic carbon signals are also recorded at 1.01m and 1.02m, e.g. the δ^{13}C values are -10.7‰ and -18.5‰, the TOC values are 1.4% and 2.2%, and the C/N ratios are 12.1 and 19.6 respectively (Table 6.2).

Excluding samples from 1.01m and 1.02m, sediment from 1.29-0.35m has a sand concentration of 17.0 ±12.1% and a silt concentration of 60.8 ±10.8% (Table 6.2). The δ^{13}C and C/N values are -23.2 ±0.5‰ and 10.8 ±1.3 respectively, significantly heavier δ^{13}C and higher C/N values and more variable than those of the zone 10.07-1.31m (-25.1 ±0.3‰ and 10.7 ±0.6 respectively, Figure 6.2; Table 6.2). The mean TOC concentration is similar to the previous section of 1.0 ±0.1%.

6.5.2 Results of selected metals

The concentration of a number of metals, including V, Cr, Ni, Zn, Ba, Mg and Ti, changes little throughout the core. According to Woods (2009), in a study from 3 short cores across the estuary, some of these metals, such as Cr, Ni and Zn, have shown significant increases since the late 1980s, reflecting the development of light industry in the delta area over the last three decades. Concentrations of metals related to more traditional metal working, such as As, Cu, Al, Fe and Pb, show a sudden increase at 1.29m (Figure 6.7). Excluding some extremely low/high values at 1.01-1.02m, concentrations of these metals from 1.29-0.35m are 20-88% higher than that of the lower section (Figure 6.7). For example, concentrations of As and Cu are 9.1 ±1.4 mg/kg and 20.8 ±5.1 mg/kg respectively at 5.0-1.3m. This increases substantially to 17.1 ±2.9 mg/kg and 32.0 ±7.5 mg/kg at 1.29-0.35m. Some of the metals also show a slight decreasing trend from 5.0-1.3m, such as As, Fe and Al (Figure 6.7).
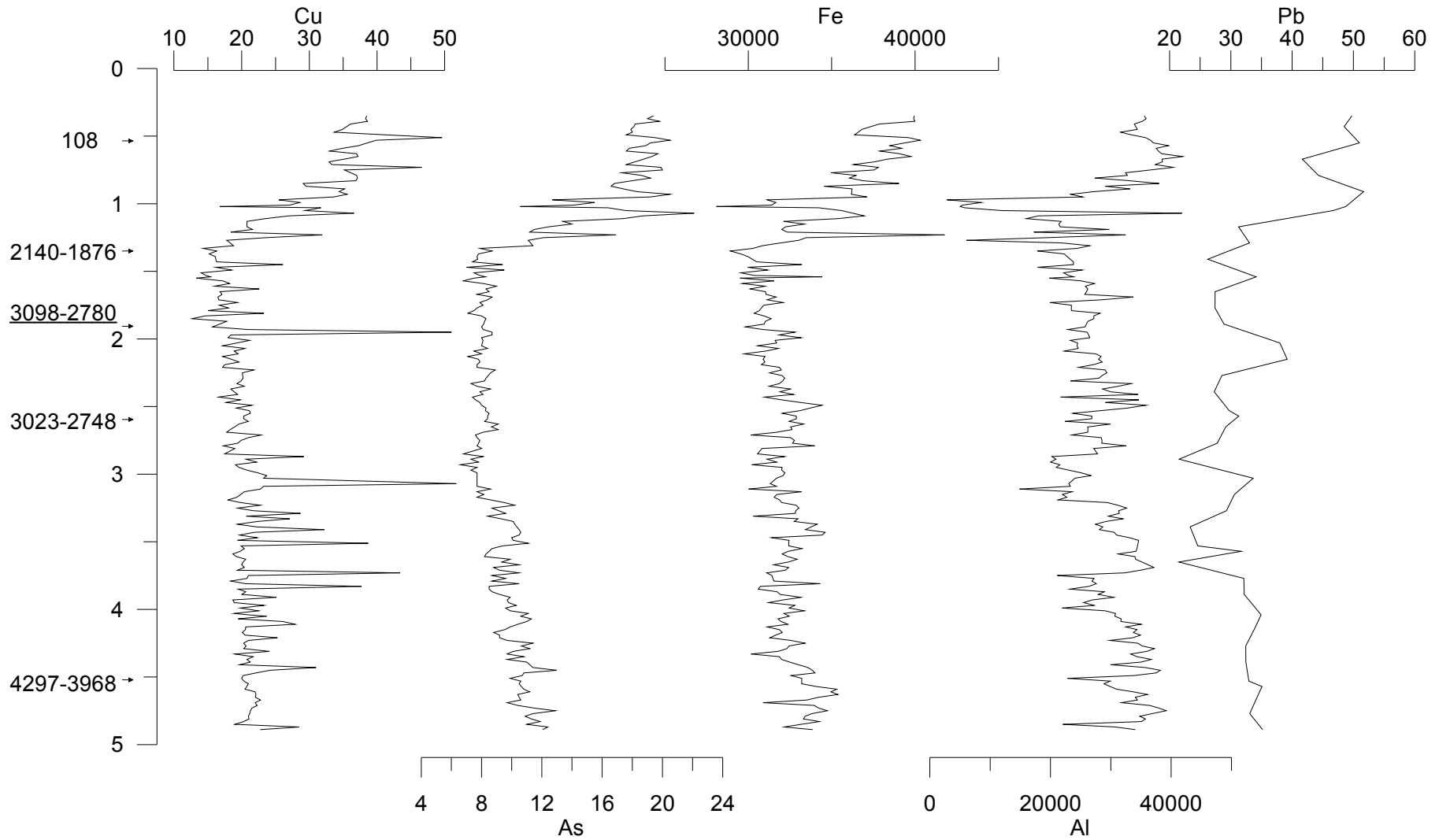
Figure 6.7 Key metals from top of the Core UV1 (4.89-0.35m)

6.6 Core chronology

6.6.1 Results of the radiocarbon dating

Seven radiocarbon dates were obtained from benthic foraminifera, and the sample at 0.52m is based on a bivalve shell. All dates have been calibrated to calendar years before present (cal. yr BP) using the CALIB 5.10 and the marine04 programme (Stuiver *et al.*, 1998), and have been corrected for the Marine Reservoir Effect with the correction factor of -128±40 years, according to Southon *et al.* (2002). Radiocarbon dating results are shown in Table 6.3. Calibrated ages are expressed at the ±2σ level, and the ages of median probability are presented. A further OSL date at 12.5m below the section studied here (within the M2 unit) has also been measured by Zong *et al.* (2009b).

Table 6.3 Results of radiocarbon dating for the Core UV1.

Depth (m)	Material	^{14}C age	Cal. year BP (±2σ)	Median probability (Cal.yr BP)	^{14}C Enrichment (% Modern± 1σ)	Carbon content (%, by weight)	δ^{13}C (‰, VPDB) ± 0.1	Publication code
0.52	Shell	Modern			pMC 108.19± 0.42			GZ2211
1.33	Forams	2254±30	2140-1876	2011				GZ2212
1.92	Forams	3019±35	3098-2780	2935	68.67 ± 0.30	9.8	-3.1	SUERC-9602
2.61	Forams	2974±33	3023-2748	2878				GZ2213
4.52	Forams	3963±35	4297-3968	4137	61.06 ± 0.27	8.8	-4	SUERC-9605
7.52	Forams	4847±35	5468-5185	5331	54.69 ± 0.24	9.7	-4.1	SUERC-9606
9.52	Forams	5633±36	6284-6017	6184	49.60 ± 0.22	9.0	-2.6	SUERC-9607
12.5*	Marine shell	37900±320	41220-40900 (±1σ)	41600				OS-51226

* OSL date from Zong *et al.*, 2009b.

The age from 9.52m of 6184 ±134 years, together with the OSL dates from 12.5m (41600±380 cal. yr BP, Table 6.3), suggests that sediments deposited during the early Holocene are absent in this core. Reliable Holocene sedimentation is recorded in UV1 from 6400 until 2000 cal. year BP at 10.07-1.31m. This is supported by the lithostratigraphy and δ^{13}C results showing that T1 unit ends at 10.09m at the base of the

M1 unit above (Figure 6.2). One of the possible reasons for the absence of early Holocene deposition is that the core site was sub-aerially exposed at this time, when the sea level was low (Zong *et al.*, 1989, 2009; Zong, 2004). The date at 1.33m is 2254±30 years, while the radiocarbon date from 0.52m suggests a modern age for sediments above this section.

6.6.2 Age model for core UV1

The six radiocarbon dates from 1.31-10.07m are used here to produce an age model for Core UV1 (Table 6.3). There is a minor age reversal between the dates at 1.92 and 2.61m (Figure 6.8). The median-probability age of the date at 1.92m is 2935 cal. yr BP, older than at 2.61m (2878 cal. yr BP). This is most likely because of reworking of older foraminifera around 1.92m. The other possibility is that the foraminifera from 2.61m are too young, e.g. bioturbation of the sediment incorporating younger foraminifera from above. Including both of these dates in the age model (Figure 6.8) will reduce the accuracy of the age model due to the reversal.
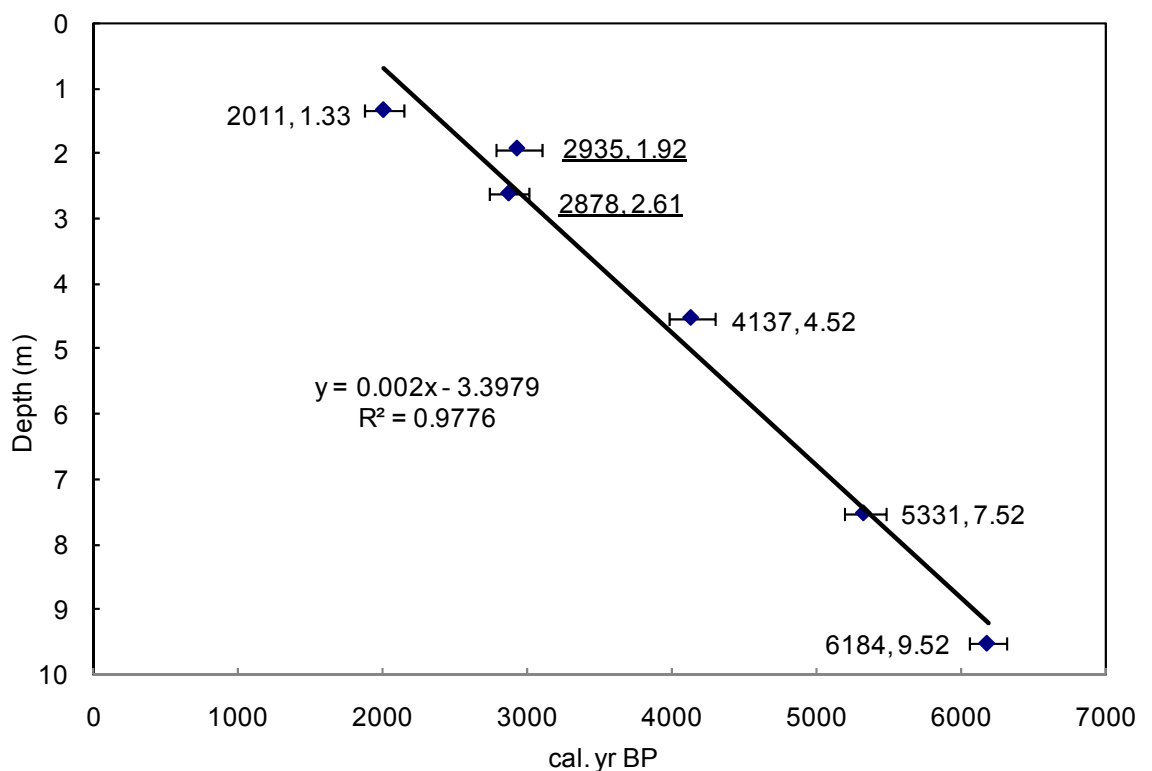
Figure 6.8 Age model based on the six dates

To choose which of these two dates to include to generate a reasonable age model, sedimentation rates of different periods were calculated (Figure 6.9; Table 6.4) and compared to nearby cores (Figure 6.10). Sedimentation rates are calculated according to calibrated ages (Table 6.3) using the following equations:

$$R_{min} = (D1-D2) / (A_{1max}-A_{2min})$$
$$R_{max} = (D_1-D_2) / (A_{1min}-A_{2max})$$
$$R_{ave} = (Rmin+Rmax)/2$$

Where R is the sedimentation rate (cm/yr); D1 is the depth of the date A1, and D2 is the depth of date A2 (D1>D2, m); and A_{min} and A_{max} are the range of 2σ calibrated ages (cal. yr BP, Table 6.3). Sedimentation rates are then expressed as '$R_{ave} \pm r$', where r = $(R_{max} - R_{min})/2$ (Table 6.4).

Table 6.4 Sedimentation rate of different cores

Age range	Sedimentation rate (cm/year)		
(Cal.yr B.P.)	UV1	V37	NL
2000-3000	**0.16 ±0.05** (*0.07 ±0.02*)		
3000-4000	**0.16 ±0.04** (*0.24 ±0.06*)	0.08 ±0.01	0.18 ±0.02
4000-5000	0.27 ±0.07		
5000-6000	0.27 ±0.09	0.14 ±0.01	
6000-7000			

Italic: sedimentation rates calculated using the Age Model IB (Figure 6.9A);

Bold: sedimentation rates calculated using the Age Model IC (Figure 6.9B).
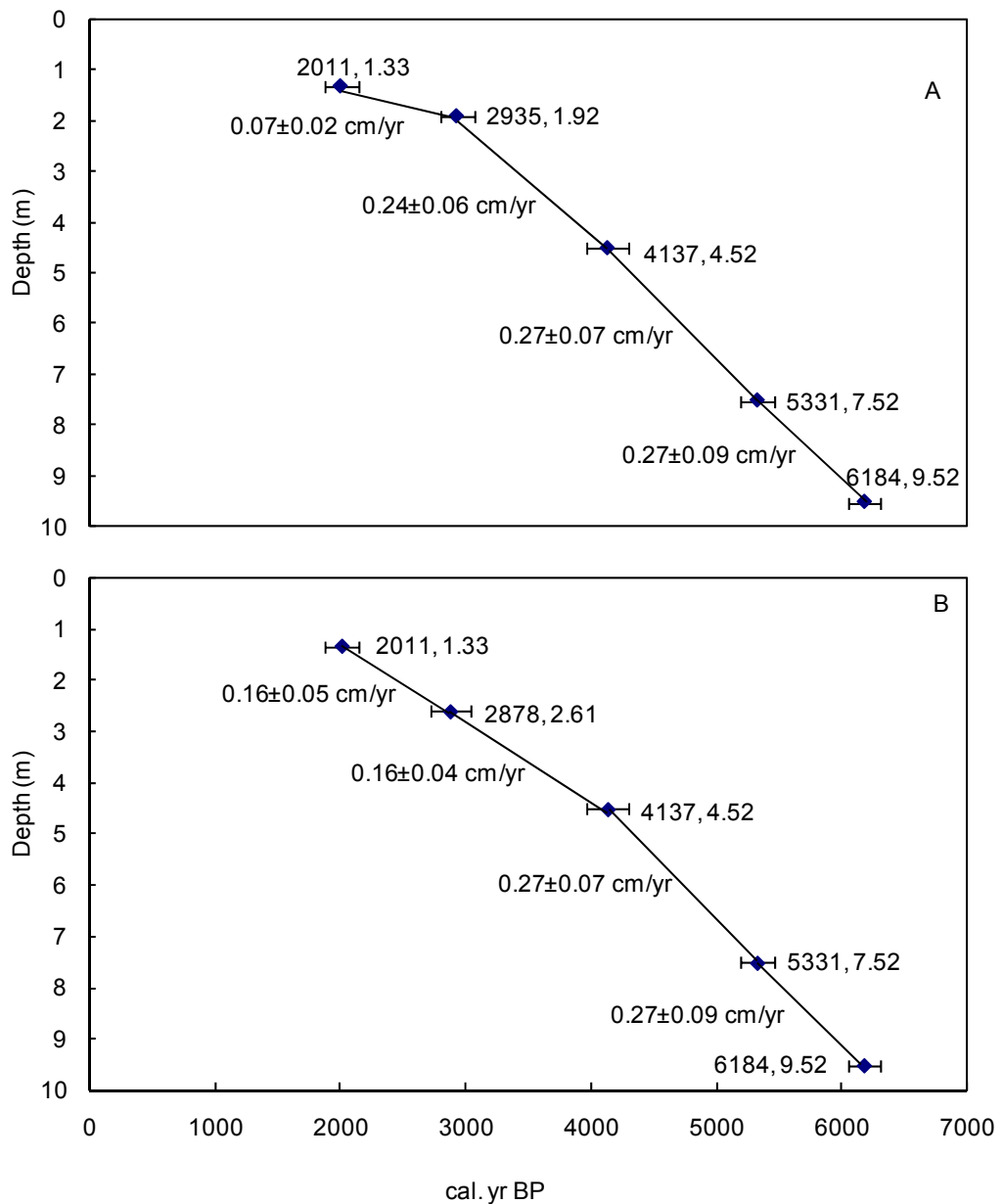
Figure 6.9 Sedimentation rates of different periods using different ages. A: five dates including the age at 1.92m; B: five dates including the age at 2.62m.

Results show that from 6000-4000 cal. yr BP, sedimentation rate stayed relatively stable around 0.27cm/year (Table 6.4, Figure 6.9). Different sedimentation rates after 4000 cal. BP were generated by different age models, e.g. using the age from 1.92m (Figure 6.9A) or using the age from 2.61m (Figure 6.9B). The five ages including 1.92m generate a sedimentation rate of 0.24 ±0.06 cm/year during 4000-3000 cal. yr BP and 0.07 ±0.02 cm/year during 3000-2000 cal. yr BP (Figure 6.9A; Table 6.4). If the

sudden reduction in the sedimentation rate after 3000 cal. yr BP was true, the reasons for this change should be related to these key controlling factors for sediment deposition in this estuary, such as changes of river-channel positions, and/or changes of tidal strength. For example, movement of the river channel away from the core site before 3000 cal. yr BP would have resulted in much lower sediment input into the core site and generate a much lower sedimentation rate, e.g. a sedimentation rate reduced from 0.24 ±0.06 cm/year to 0.07 ±0.02 cm/year. However, according to Zong *et al.* (2009a) the position of the palaeo-river channels has been relatively stable since the early Holocene, because of the surrounding rocky areas (islands) along the channel (Chapter 3). Thus influence of channel movement on the sedimentation rate would have not been significant enough to generate such a reduction around 3000 cal. yr BP. Another possible reason is that the tidal influences became extremely high at this time, which pushed the freshwater stream landwards; accordingly terrigenous sediment would have mainly stayed in landward areas of the estuary. If this is the case, then much higher sedimentation rate at this time would be expected to have occured in cores near the river mouth, such as core NL. However, records did not show any sudden change in sedimentation rate from core NL or core J81 (Figure 6.10).

This study suggests that the age at 1.92m is more likely to be older than it should be due to reworking of the older foraminifera. The sedimentation rate during 4000-2000 cal. yr BP becomes around 0.16cm/year when replacing the date from 1.92m with the one from 2.61m (Figure 6.9B; Table 6.4). This produces a more reasonable sedimentation rate when comparing to other nearby cores, e.g. core V37 and core NL (Figure 6.1). According to Zong *et al.* (2009a) sedimentation rates of core UV1 are about twice as high as those of core V37, but similar to core NL (Figure 6.10; Table 6.4). During 4000-3000 cal. yr BP, the sedimentation rate is 0.08 ±0.01cm/year at core V37 and 0.18 ±0.02 cm/year for core NL. These data indicate that a sedimentation rate around 0.16 cm/year during 4000-2000 cal. yr BP at core UV1 is more likely. Therefore, the age model for core UV1 is generated based on the five dates from 9.52, 7.52, 4.52, 2.61 and 1.33m (Figure 6.11).
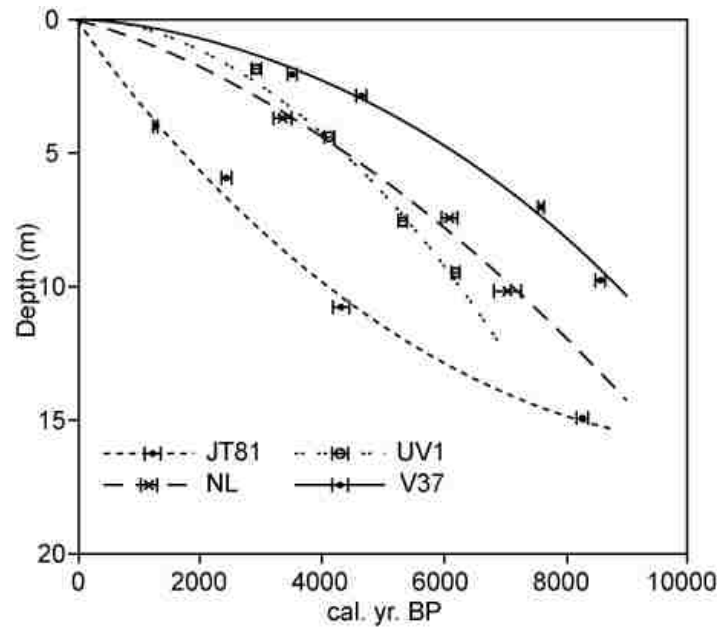
Figure 6.10 Sedimentation rate record from different cores (From Zong *et al*., 2009a)

The results reveal significant changes in sedimentation rates in different parts of the core: around 0.27cm/year below 4.52m and around 0.16cm/year above 4.52m (Figure 6.9B; Figure 6.10). The age model shown in Figure 6.11 suggests that sediments from 10.07-4.52m were deposited during 6395- 4134 cal. yr BP at the rate of 0.27 cm/year, and sediments from 4.52-1.31m were deposited during 4134-2003 cal. yr BP at the rate of 0.16 cm/year. The following discussion of results from Core UV1 is based on a chronology developed using the following age models (Figure 6.11):

$$Y=665.89X+1130.9 \tag{1}$$

$$Y=408.50X+2281.6 \tag{2}$$

Model (1) applies to 1.31-4.52m and Model (2) applies to 4.53-10.07m, where Y = Age (cal. yr BP), X = Depth (m).
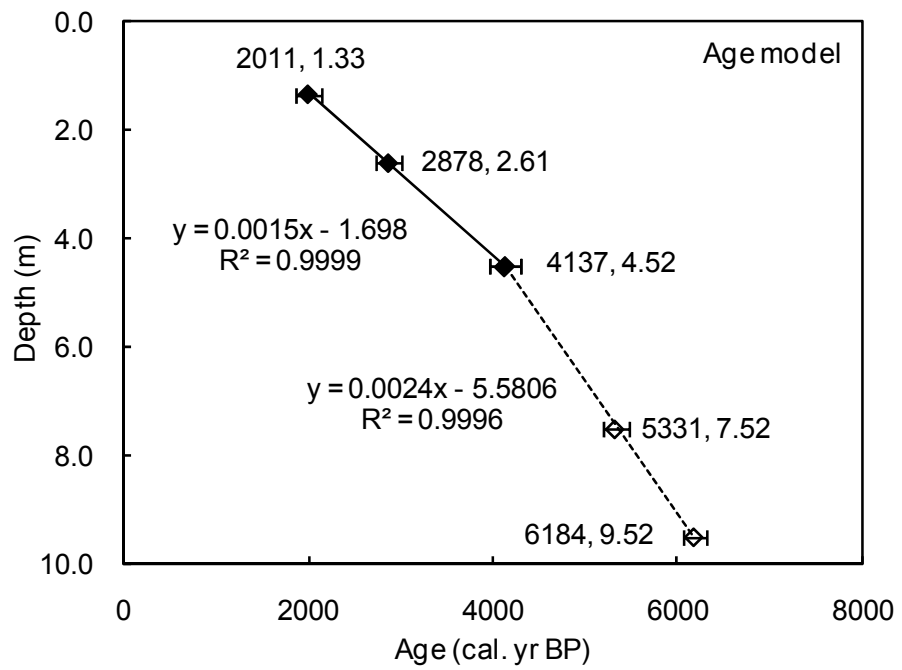
Figure 6.11 Age model of the Core UV1 for this study

6.7 East Asian monsoon history during the mid-Holocene

6.7.1 Decreasing monsoonal precipitation from 6400 to 2000 cal. yr BP

The organic $\delta^{13}C$ and C/N ratios of the fossil sediment have been widely used as an indicator for palaeoenvironmental changes from coastal archives (Lamb *et al*., 2006). Possible forcing mechanisms that influence the proportion of sediments from different sources in UV1 during the mid-Holocene are sea level change, delta progradation and freshwater flux during this period. The receiving basin (the estuary) was initially inundated by the sea as late as 9000 cal. yr BP when the relative sea level rose to -20m (Zong, 2004). Sea level rose from -20m to -12m from 9500-8200 cal. yr BP, followed by two sharp rises from -12m to -3m during 8200-8000 cal. yr. BP (Zong, 2004; Figure 3.7 in Chapter 3) and 7500-7000 cal. yr BP (Yim *et al*., 2006; Bird *et al*., 2007). Sea level reached its present-day level about 6800 cal. yr BP and has been relatively stable since then (Figure 3.7 in Chapter 3; Zong, 2004). Therefore, sea level will not influence the $\delta^{13}C$ signal preserved in UV1 during the period 6400-2000 cal. yr BP. However, as a consequence of stable sea levels, the transgressive process changed to a regressive process. Between 6800 and 2000 cal. yr BP, the deltaic shoreline advanced slowly seawards (Zong *et al*., 2009b; Figure 6.1). The delta progradation during the mid-Holocene has led to Core UV1 being more proximal to terrestrial source areas, which will result in larger amounts of terrestrial sediment being delivered to UV1. However, the long-term trend of increasing $\delta^{13}C$ in UV1 during the mid-Holocene indicates a decreasing proportion of terrestrial organic matter (Figure 6.12; 6.12), suggesting that changes in freshwater flux is the dominant control on the proportion of terrestrial organic matter in UV1.

As mentioned above, during the period 6400-2000 cal. yr BP the $\delta^{13}C$ of UV1 shows an increasing trend, while the TOC and C/N ratios of UV1 show a decreasing trend (Figure 6.12). These trends indicate a long-term trend of weakening precipitation-induced freshwater discharge linked to a weakening summer monsoon during the period 6400-2000 cal. yr BP. Surface estuarine sediment from the freshwater area usually has a $\delta^{13}C$ value of -25.0‰, compared to lower values of sediment from the marine area of -21.0‰ in the modern-day (see Chapter 5). The mean $\delta^{13}C$ value during 6400-2000 cal. yr BP

is -25.1‰ (Figure 6.13). From 6400-4100 cal. yr BP, δ^{13}C tends to be lower than the average value of the whole core (Figure 6.13), indicating a relatively high proportion of terrestrial organic matter in the estuarine sediment during this period. However, the proportion of the terrigenous organic matter has become much lower since 4100 cal. yr BP, as the summer monsoon has further weakened, resulting in less terrestrial organic matter being delivered into this area, and thus the portion of marine/brackish-water derived organic matter becomes higher. This is supported by the results of C/N and TOC values from 6400-2000 cal. yr BP. The modern-day data suggest that organic matter in the surface estuarine sediment is mainly composed of particulate organic matter (Chapter 5), which has a C/N ratio typically lower than 10. The whole core average C/N ratio is 10.5 (Figure 6.12). The C/N ratio from 6400-4100 cal. yr BP is typically higher than the whole core average value of 10.5. After 4100 cal. yr BP the C/N ratios is lower than 10.5. This is due to the decreasing portion of terrestrial/freshwater-origin organic matter (C/N>10), and/or an increase in the marine/brackish-water algae, e.g. marine algae, which have a low C/N ratio (6-8) (Lamb *et al.*, 2006). Higher TOC concentration is observed in modern-day samples from terrestrial/fluvial areas than from marine areas (see Figure 5.5 and 5.11 in Chapter 5). Thus, the decreasing TOC concentration during 6400-2000 cal. yr BP shows a clear trend of the weakening terrestrial sediment input (Figure 6.12). The increasing δ^{13}C, decreasing C/N ratios and TOC concentration from 6400-2000 cal. yr BP is a result of the decreasing portion of the terrigenous organic matter in the estuarine sediment, reflecting a weakening monsoon during this period.

A weakening freshwater flux during 6400-2000 cal. yr BP is also revealed by the composition of the major and trace metals in the sediment (Figure 6.12). The modern-day data suggest that the F1 metals (Fe, As, Co and Mn) are mainly derived from the Pearl River delta. For simplicity, this thesis will use Co to represent the terrestrial metals (the F1 metals), this being suggested to be a useful indicator for the provenance discrimination of the Pearl River sediment (Yang *et al*, 2008). Mn and Fe are among those transition elements which are easily contaminated during sediment transport and deposition, and might not be so suitable for provenance discrimination (Rollinson, 1993; Yang *et al.*, 2008). As it is suggested by other studies and the modern-day analogue (Sewell, 1999; Fyfe *et al.*, 2000; Guan *et al.*, 2001; Chapter 5) that Na, Ca and Mg can

be considerably leached from weathered materials in Hong Kong, Na is selected by this study to represent the F3 metal. Decreasing concentrations of the terrestrial metals (e.g. Co) and increasing concentrations of the marine metals (e.g. Na) suggest that, due to the weakened freshwater output, the tidal flux pushed the front further westwards, and delivered more sediment from the Hong Kong and the shallow marine area, while less terrestrial sediment could reach the site (Figure 6.12). Approximately 200-year time lags were found between bulk organic carbon records and metal variability from the Pearl River estuary. For example, organic carbon records show an increase in freshwater flux during 5600- 4500 cal. yr BP, while the increase started about 200 year earlier in metal records (Figure 6.12). This time lag is possibly due to delayed response of vegetation to climate changes compared to metals in sediments.

It is worth mentioning that some F2 and F3 metals do not support the conclusion of increasing marine influence on the core site. For example, according to modern-day analogues, concentrations of Al (F2 metal) are lower in terrigenous sediment than in marine sediment (Figure 5.17 in Chapter 5). The concentration of Al shows a decreasing trend of Al concentration since the mid-Holocene, suggesting an increasing freshwater influence through time (Figure 6.5). The same is also found for concentration of Ca (F3 metal). Concentrations of Ca are found to be higher in terrigenous sediments than in marine sediments in modern-day analogues (Figure 5.18 in Chapter 5). Increase in Ca concentration since around 3500 cal. yr BP would suggest a stronger freshwater influence in this area (Figure 6.6). According to Fyfe *et al.* (2000), Ca can be considerably leached from the Hong Kong area; one possible explanation for the increase of Ca concentration since 3500 cal. yr BP is that more sediments from Hong Kong area were delivered into the core site due to less freshwater input from the Pearl River. Sediments from the Hong Kong area became the main sources for Ca.

Concentrations of Al are closely related to Al-bearing minerals, such as feldspars and feldspathoids (Goldschmidt, 1954), and this might be the reason for higher Al concentration in terrigenous sediments than in marine sediments. For example, the clay mineral illite contains about 13.5% of Al, and kaolinite contains about 21% (Goldschmidt, 1954). However, biogeochemistry of Al is another significant factor influencing Al concentrations (Hutchinson, 1943). Certain plants are accumulators of

aluminium.   Among seed plants, *Symplocos* is the most effective aluminium accumulator, which only grows at the altitude of 400-2600m in evergreen rain forests. There is no *Symplocos* growing in dry areas.   Accumulation of Al in club mosses and also in certain tree-ferns has also been observed (Goldschmidt, 1954).   Butler (1953) suggested that Al accumulator plants may have been involved in the formation of the coal. This suggests that decreases in these Al-accumulator plants might be responsible for the decreasing Al concentration in core UV1 since the mid-Holocene.   In clays formed during intensive weathering the chemical changes are more pronounced, and consequently they contain higher Al than clays formed under cold situation (Rankama and Sahama, 1950).   Thus, another possible reason for the decreasing Al concentration since the mid-Holocene is because clays are less intensively decomposed in the late-Holocene than in the mid-Holocene due to the cooling weather since the mid-Holocene climatic optimum.   These results suggest that more factors, e.g. organic concentration, rather than just sediment sources, need to be taken into consideration when interpreting metal results.
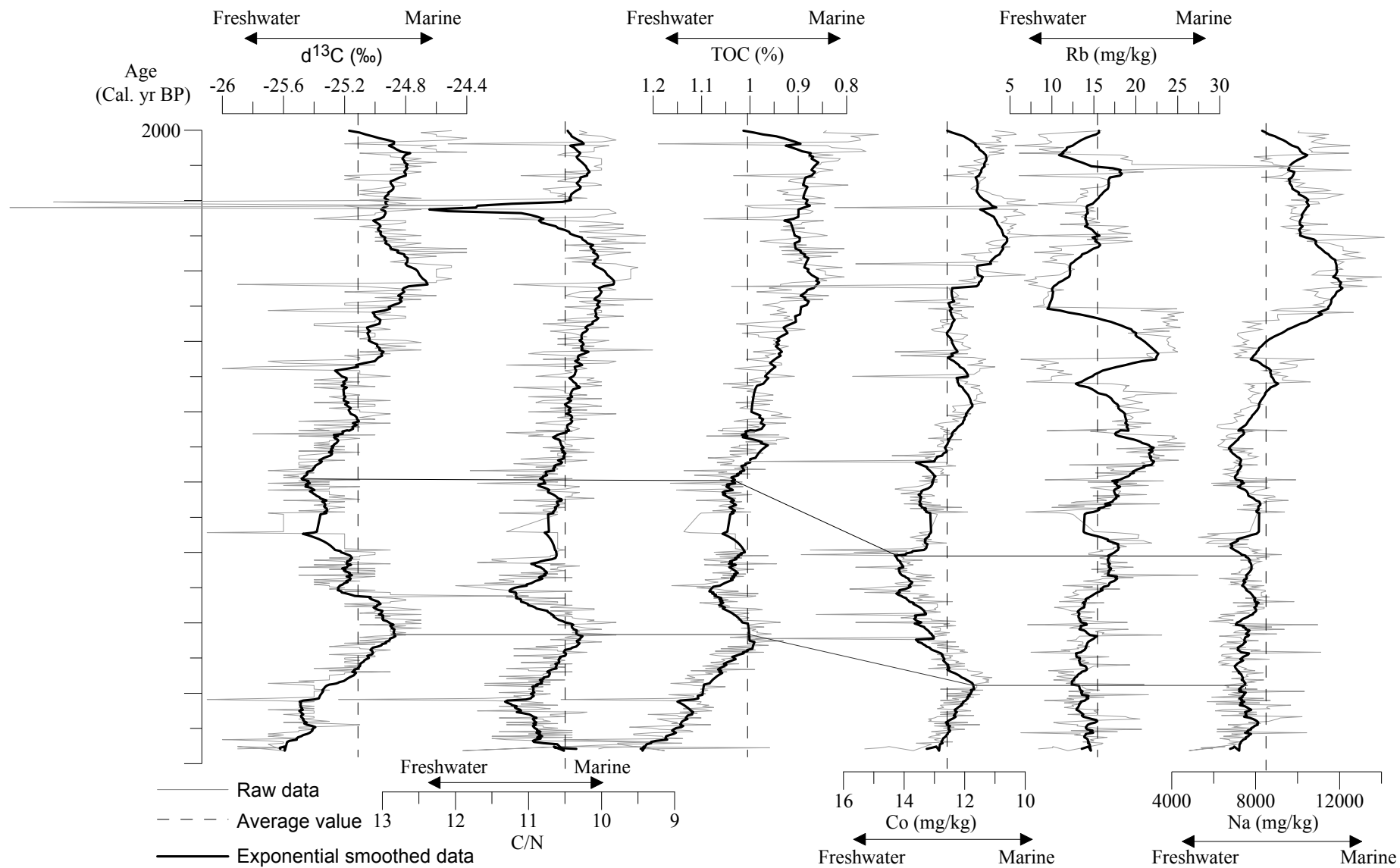
Figure 6.12 Values of the δ¹³C, TOC and C/N during the mid Holocene

146
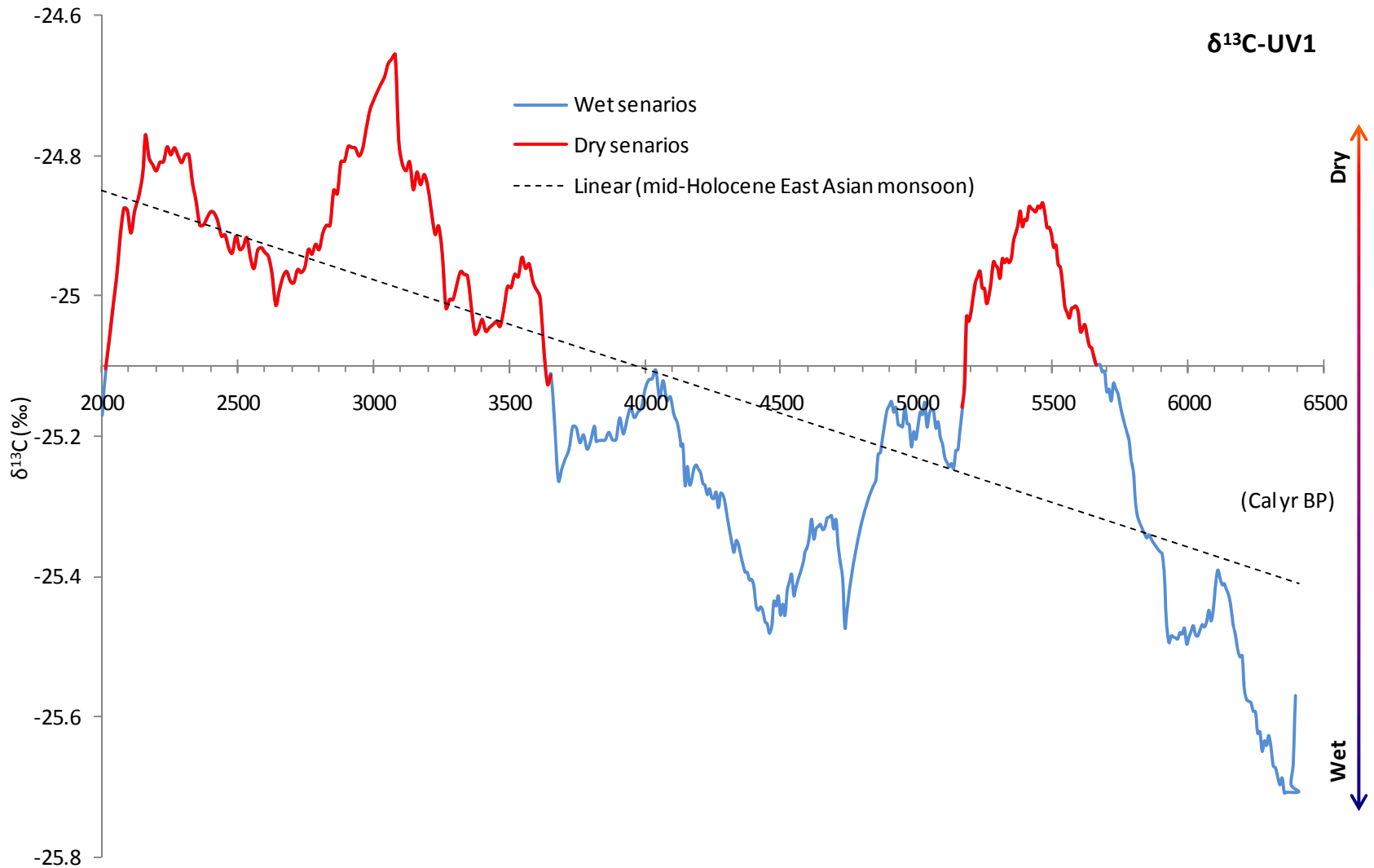
Figure 6.13 Wet/dry scenarios of the EAM during the mid-Holocene (exponential-smoothed δ^{13}C data)

147

6.7.2 Wet/dry scenarios of the East Asian monsoon during 6400-2000 cal. yr BP

Superimposed on the general weakening trend discussed above, the $\delta^{13}C$ data from UV1 suggests monsoonal precipitation has experienced wet/dry fluctuations ranging from decadal to millennial time scales during the mid Holocene (Figure 6.13). The reduced sedimentation rate, which reduces from 0.27cm/yr before 4500 cal. yr BP to 0.16cm/yr after 4500 cal. yr BP, suggests significantly reduced monsoonal freshwater flux after 4500 cal. yr BP (Figure 6.9). This reveals a considerable reduction in sediment flux from the main source, the Pearl River deltaic area, responding to the more significant reduction in monsoonal precipitation from 4500-2000 cal. yr BP than the period 6400-4500 cal. yr BP. A similar conclusion can be made based on metal results from UV1 (Figure 6.12). As sediment flux from the deltaic area has reduced, so the proportion of sediment from the Hong Kong area has increased. Metals which are enriched in the weathered material from the Hong Kong area, such as Co (Yang *et al*., 2008), become more variable in the core, responding to environmental changes (Figure 6.12). Based on palaeo-shoreline evolution during the Holocene, Zong *et al*. (2009b) suggest a deltaic progradation rate of 10.5m/yr between 6800-4500 cal. yr BP and 6.4m/yr between 4500-2000 cal. yr BP for the North and West Rivers. They also suggest that the gradual reduction in sediment supply resulting from the reduced monsoonal-driven freshwater discharge (Figure 6.13; Zong *et al*., 2006) is the key driving mechanism for the slow down in progradation rate.

The $\delta^{13}C$ signature of UV1 is influenced by the balance between terrestrial and estuarine/marine organic matter resulting from changes in the strength of freshwater flux driven by the monsoonal precipitation. Relatively lower $\delta^{13}C$ indicates a higher proportion of terrestrial/freshwater-water organic matter in UV1, delivered by stronger river discharge during a wetter period (higher monsoonal precipitation), and vice versa. The $\delta^{13}C$ signature of UV1 shows considerably lower $\delta^{13}C$ at 6400-6000 cal. yr BP than the whole-core average value of 25.1‰ (Figure 6.13), suggesting much wetter conditions during this period (increased monsoon precipitation). Monsoon precipitation decreases after this, culminating in a dry period recorded around 5600-5200 cal. yr BP as indicated by the relatively higher $\delta^{13}C$ (Figure 6.13). Increased monsoon precipitation and wet conditions are again recorded during 5200-3800 cal. yr BP, with

peak wetness around 4500 cal. yr BP. The slightly higher δ^{13}C values at this time compared to 6400-6000 cal. yr BP suggest it was not as wet as during the earlier period 6400-6000 cal. yr BP (Figure 6.13), although it was wetter than the general condition of the mid Holocene. Much drier conditions are indicated during the period 3800-2000 cal. yr BP by the high δ^{13}C with significant fluctuations (Figure 6.13).

Millennial-scale fluctuations are clearly seen in the de-trended δ^{13}C data (Figure 6.14). The de-trending process is undertaken using the PAST program (Hammer, *et al.*, 2001), which removes the linear trend of δ^{13}C (Figure 6.14A). The 20-point moving average of the de-trended δ^{13}C data shows one complete cycle between 6400 and 4500 cal. yr BP and probably another cycle from 4500 to 2500 cal. yr BP (Figure 6.14B). This suggests a main cycle for the EAM precipitation change of around 2100 years. Spectral analysis was undertaken on the de-trended δ^{13}C data to investigate this periodicity (Figure 6.15). Results suggest two millennial-scale cycles of 2349 years and 1215 years at the significant level of 99% (Figure 6.15), which further supports the 2300-year cycle of the mid-Holocene EAM (Jian *et al.*, 2000; Xiao *et al.*, 2006). However, the 2300-year scale cycle is not clearly presented in Figure 6.14. This might be due to the relatively short time series (4400 years from 6400 to 2000 cal. yr BP).

The high-resolution record from UV1 also reflects oscillations at centennial- to decadal-time scales (Figure 6.12) superimposed on each millennial-scale cycle, resulting from flooding and/or dry periods. Results of the spectral analysis indicate a period of 641 years for these cycles, although they are not as significant as the millennial-scale cycles with a significant level lower than 95% (Figure 6.15).
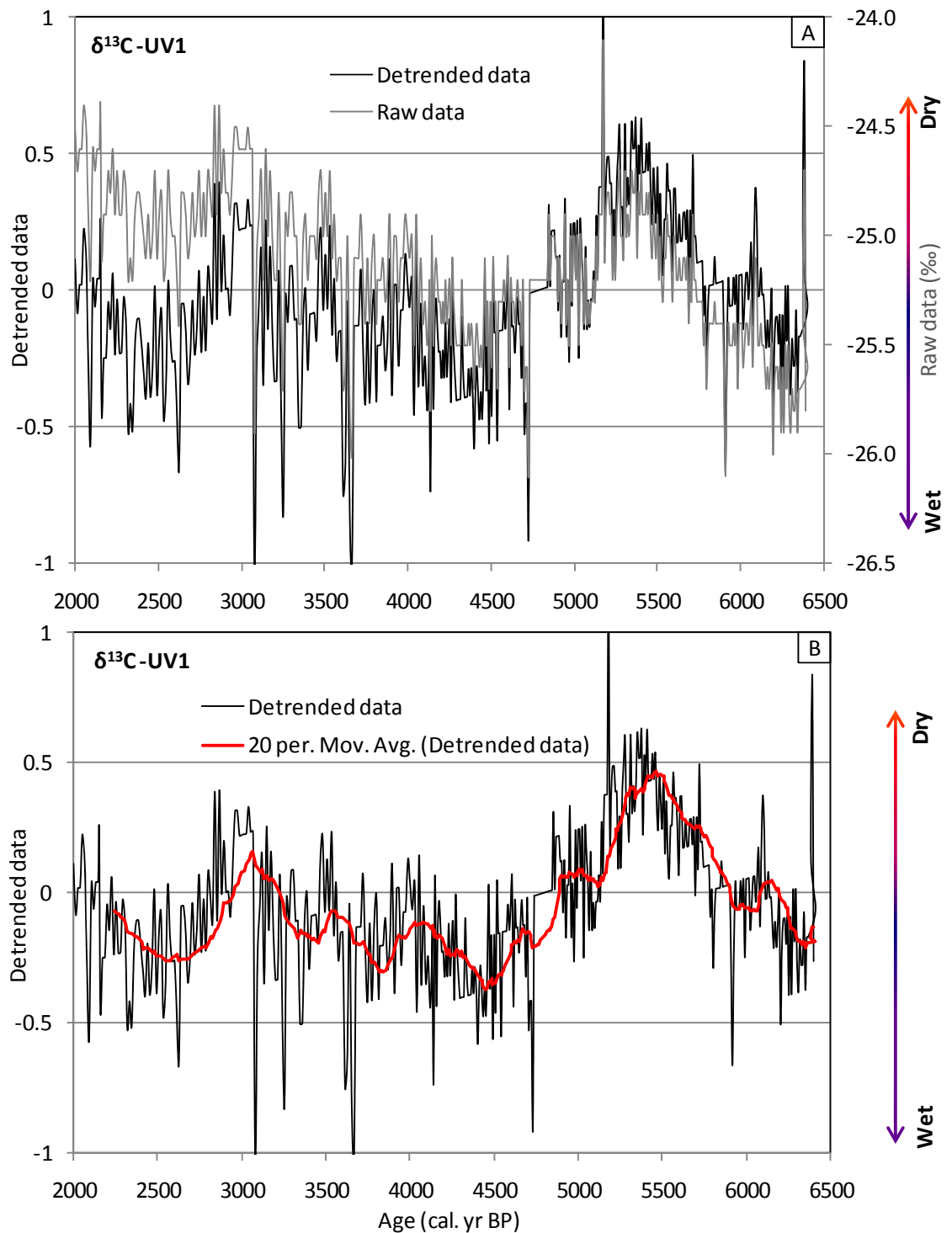
Figure 6.14 De-trended δ^{13}C data highlighting cyclicity of the EAM precipitation changes
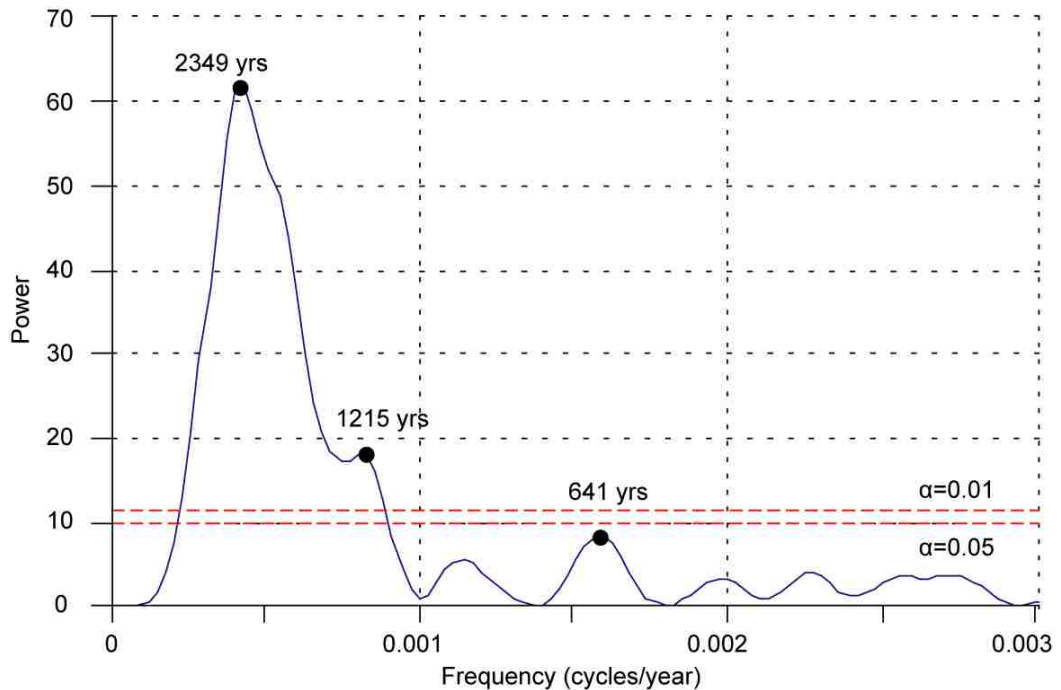
Figure 6.15 Results of the spectral analysis on the detrended $\delta^{13}C$ values

6.7.3 Possible driving mechanisms for the variability of the East Asian monsoon

The data from UV1 indicates a general weakening of EAM precipitation from 6400 to 2000 cal. yr BP indicated by the decreasing terrestrial organic matter in UV1 due to the weakening monsoonal-driven river runoff. Superimposed on this weakening trend are the wet/dry oscillations ranging from millennial- to decadal- time scales, e.g. 5600-5200 cal. yr BP and 3800-2000 cal. yr BP are relatively dry periods. Therefore, variability of the EAM can be regarded as an alternation between dominance of cold-dry winter monsoon and warm-wet summer monsoon (An, 2000), although the coupling of thermal and moist conditions might not always be stable through the whole Holocene (e.g. Liew *et al*., 2006). Possible driving mechanisms for the EAM variability indicated by this study are the Milankovitch driven precession, insolation changes, El Nino Southern Oscilation (ENSO) and possible tele-connection between the EAM and high-latitude cooling events, depending on time scales. The following section will discuss each of these in turn.
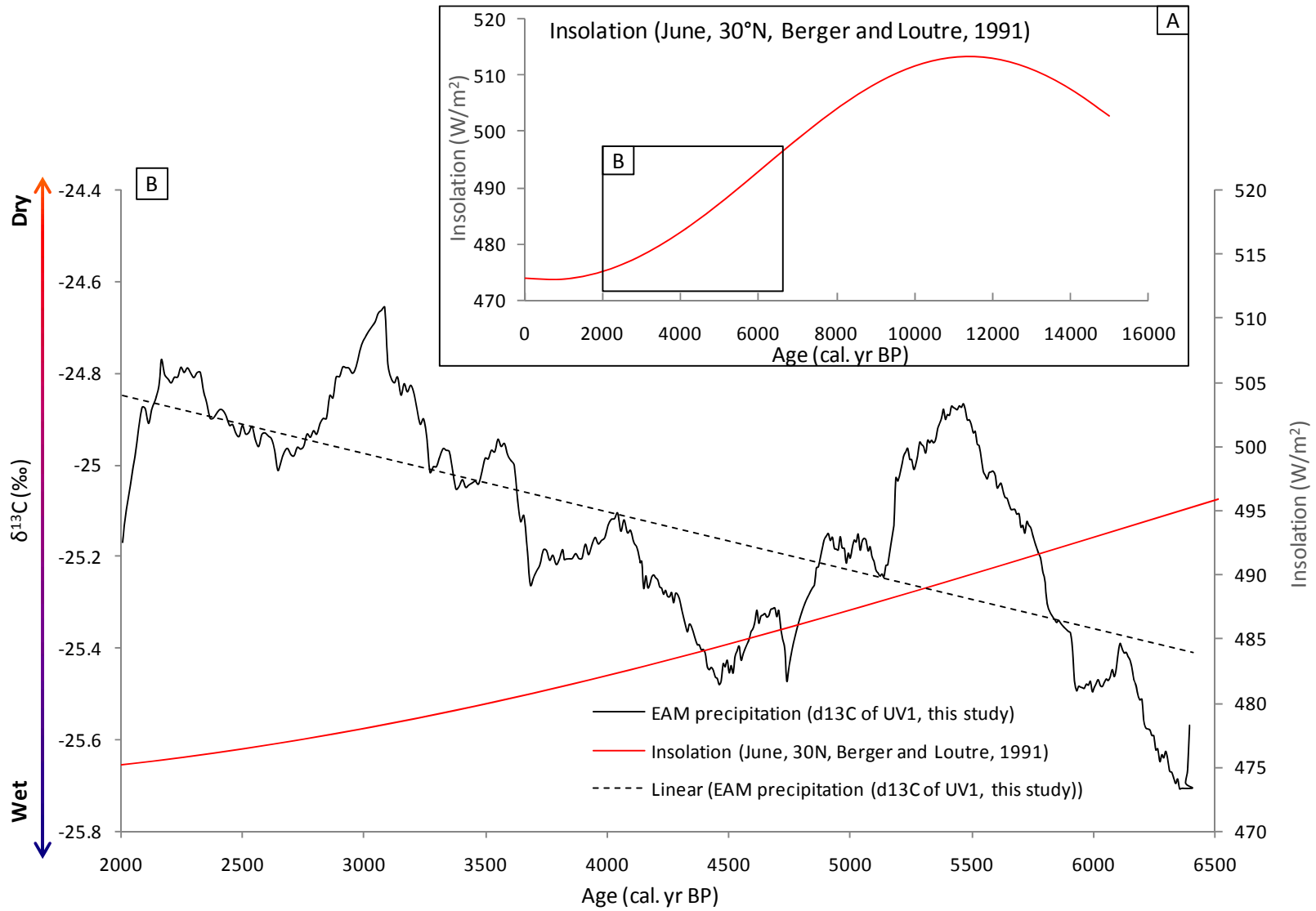
Figure 6.16 Comparison between the EAM precipitation and summer insolation changes (Berger and Loutre, 1991) during the mid Holocene

Milankovitch-driven precession

Orbital forcing, specifically precession cyclicity, is the most important driving mechanism for EAM precipitation variability during the Holocene (An and Thompson, 1998; An, 2000; Wang *et al.*, 2001; Huang *et al.*, 2008). Precession is especially important in tropical areas. Results from this study show a general weakening precipitation during the mid-Holocene following part of the precession cycle. Precession influences the monsoon through its impact on seasonal contrasts. Half a precession cycle ago (at roughly the beginning of the Holocene), perihelion occurred in the boreal summer, causing enhanced summer insolation in the northern Hemisphere, and aphelion fell in the boreal winter, casing reduced winter insolation. Such seasonal contrast was strongest at the beginning of the Holocene and has weakened towards present during the present precession cycle (Figure 6.16A; Bradley, 2003). Today, in its slightly elliptical orbit, the Earth is at perihelion around the boreal winter solstice, and at aphelion around the boreal summer solstice (Bradley, 2003). As a result, EAM precipitation should have been strongest at the beginning of the Holocene and declining towards the present. Berger and Loutre (1991) calculated the insolation values at different latitude zones in both summer and winter seasons, showing weakening summer insolation at 30°N. Results from core UV1 fit this trend well (Figure 6.16B). Thus, the weakening East Asian summer monsoon during the 6400-2000 cal. yr BP identified here is most likely to be a response to the orbital-induced weakening insolation since about 11,000 years BP (Figure 6.16; An, 2000; Wang *et al.*, 2005). There are many possible ways that insolation could influence the EAM system. One possible process is that reducing insolation leads to changes in oceanic and atmospheric circulation, resulting in changes in temperature and precipitation (An and Thompson, 1998; Xiao *et al.*, 2006; Huang *et al.*, 2008). For example, reducing insolation results in cooler tropical temperature, would be expected to weaken the Hadley circulation (Rind, 1993) and to reduce the water vapour content of the atmosphere. Thereby it would reduce the monsoonal precipitation and resultant freshwater runoff.

The general weakening EAM during the Holocene resulting from weakening insolation has also been suggested by other studies. Diatom records from the same sediment core (Core UV1) and a core nearby (Core V37) from the mouth of the Pearl River estuary

(Zong *et al*., 2009a), show generally increasing marine and brackish-water species since 6500 cal. yr BP. As the sea level reached present height and stabilized around 6900 cal. yr BP (Zong, 1994), Zong *et al*. (2006) suggest the weakening monsoon and monsoon-induced freshwater discharge is the major controlling factor for these changes. Wang *et al*. (2005) examined the $\delta^{18}O$ of a stalagmite from the Dongge Cave in southern China. They also revealed a general decreasing summer monsoon during the past 9000 years, broadly following the weakening summer insolation. Pollen records from Jiangxi province, southern China, investigated by Xiao *et al*. (1998), show a clear decrease of evergreen trees that prefer humid conditions and shrubs, replaced by herb and ferns in this area, indicating decreasing monsoonal precipitation since early Holocene.

The influence of Milankovitch-driven precession on the EAM is supported by a variety of other proxies, e.g. pollen records from the desert/loess transition of north central China (e.g. Jiang *et al*., 2006) and loess deposits from central China (An *et al*., 2000; Kukla *et al*., 1990). The other Millankovitch cycles, the eccentric cycle and the obliquity cycle, especially the eccentricity, also act as primary controlling factors on the EAM. Due to the short time series of this study, these forcings are not demonstrated in UV1. However, magnetic susceptibility records from the Chinese loess demonstrate the orbital periodicities, including 100ka, 41ka, 23ka and 19ka (Kukla *et al*., 1990; Ding *et al*., 1993), which closely parallel the oxygen isotope record in the ocean (Liu *et al*., 1985; Kukla, 1987). Similar records are obtained from Lake Baikal, northern East Asian (e.g. Colman *et al*., 1995; Williams *et al*., 1997), where spectral analysis has also suggested a strong nonlinear 100ka rhythm responding to the eccentric forcing.

Solar modulation

One of proxies used to reflect solar modulation is the beryllium 10 (^{10}Be, half-life of 1.5 $\times 10^6$ years) concentration in ice cores, which have proved to be extremely useful for deciphering the history of the cosmic ray flux in the atmosphere, and give important information about the history of solar activity and of other causes of production rate variations, such as changes in the geomagnetic field (Raisbeck *et al*., 1990; Beer *et al*., 1990, 1991, 1998; Yiou *et al*., 1997; Masarik and Beer, 1999). Studies show that high ^{10}Be concentrations can be attributed to lower solar shielding and consequently to a

lower solar activity (e.g. Finkel and Nishiizumi, 1997; Muscheler *et al*., 2004). Horiuchi *et al*. (2008) analysed an ice core at the Dome Fuji station, inland Antarctica, and found that both the concentration and the flux of ^{10}Be increased at the known solar-activity minimums during the past millennia, e.g. Oort (1010-1050 yr CE), Wolf (1280-1340). A similar result has been found from previous studies of ^{10}Be concentration in ice cores (e.g. Finkel and Nishiizumi, 1997; Muscheler *et al*., 2004, 2007).

Some studies use the cosmic ray – cloud effect to explain the link between solar activity and atmosphere process (e.g. Carslaw *et al*., 2002). For example, the intensity of cosmic rays varies globally by about 15% over a solar cycle because of changes in the strength of the solar wind, which carries a weak magnetic field into the heliosphere, partially shielding Earth from low-energy galactic charged particles (Carslaw *et al*., 2002). The stronger solar activity is associated with stronger shielding for the Earth. Accordingly cosmic ray intensity becomes low and lower cloud cover occurs, which results in higher Earth surface temperature (Carslaw *et al*., 2002). As high ^{10}Be has been proved to be related to periods of low solar activity during past millennia at centennial time scales (e.g. Finkel and Nishiizumi, 1997; Muscheler *et al*., 2004; Horiuchi *et al*., 2008), the smaller flux of ^{10}Be from the GISP2 ice core during the Holocene relative to the Pleistocene (Finkenl and Nishiizumi, 1997) suggests higher solar activity during the Holocene in comparison with the Pleistocene. The decreasing trend in ^{10}Be flux during the mid Holocene (Figure 6.17A) in response to stronger solar shielding and a weaker geomagnetic field could indicate decreasing Earth surface temperature since the mid-Holocene. This result agrees with δ^{13}C records from the Pearl River estuary, which suggest a decreasing precipitation since the mid-Holocene (Figure 6.17A), suggesting a general weakening monsoon. Oscillations in the ^{10}Be concentration of the GISP2 ice core indicate changes in cosmic ray flux and thus (activity of) solar output. Figure 6.17B uses the de-trended ^{10}Be and δ^{13}C data to show correlation between the two time series. There is a good correlation with δ^{13}C records from the Pearl River estuary with the ^{10}Be record, indicating the possible significance of solar-driven mechanisms on the EAM at millennial- and centennial- scales (Figure 6.17B).
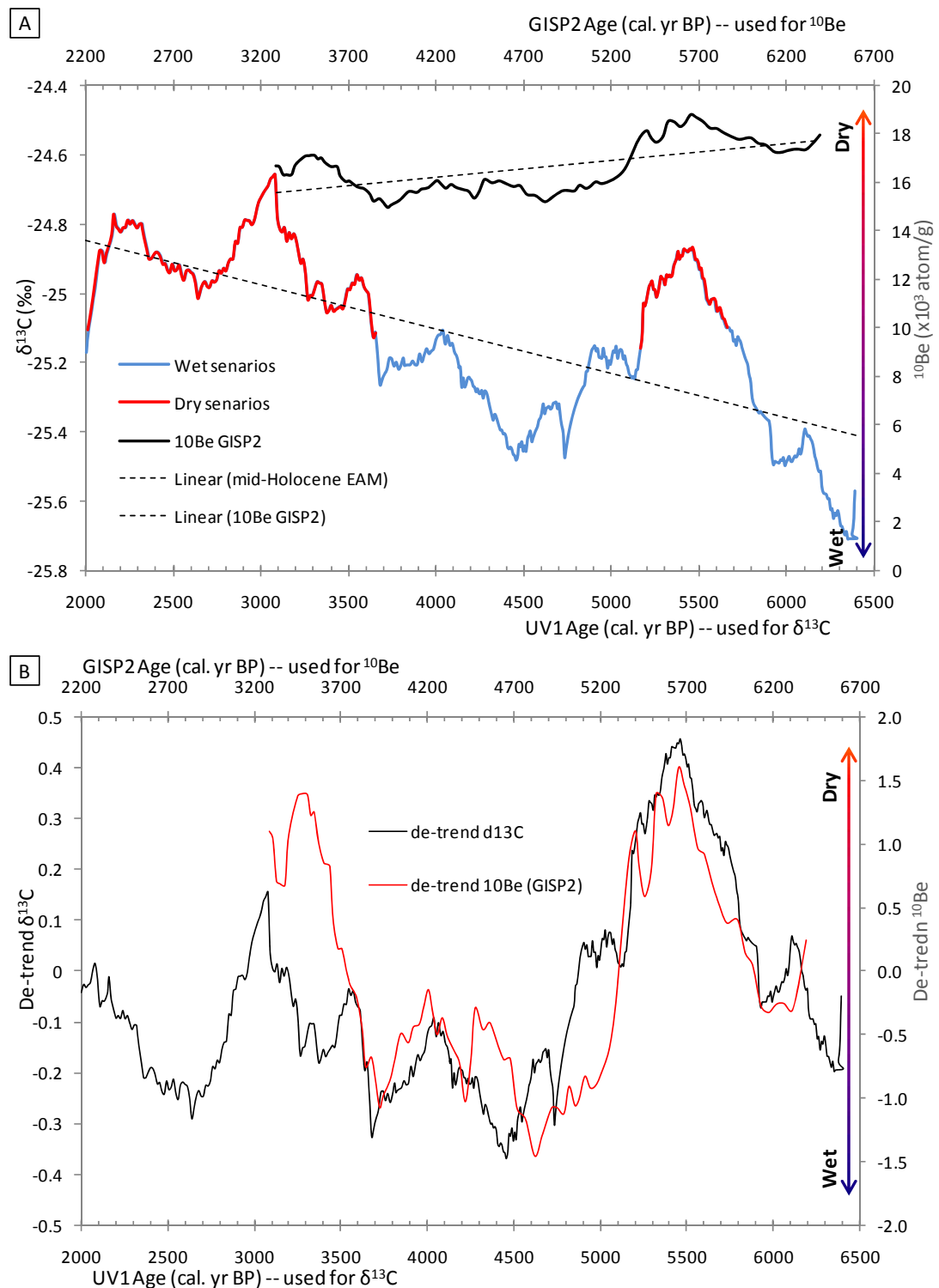
Figure 6.17 Comparison between EAM variability (δ^{13}C, this study) and insolation variability (^{10}Be, GISP2, Davis *et al.*, 1990; Alley *et al.*, 1995; Finkel and Nishizumi, 1997). 6.15A uses the exponential-smoothed δ^{13}C and ^{10}Be values; 6.15B uses the de-trended exponential-smoothed δ^{13}C and ^{10}Be. The timescales are offset by 200 years (^{10}Be at 6200 cal. yr BP on the GISP2 timescale is plotted against δ^{13}C at 6000 cal. yr BP on the UV1 core timescale, see text for explanation).

It is noteworthy that there is time-lag of around 200 years between the ^{10}Be record of solar output and EAM precipitation changes; the ^{10}Be concentration peaks uniformly precede the δ^{13}C peaks by 200 years (Figure 6.17B). This suggests that EAM precipitation changes are delayed corresponding to changes in cosmic ray flux. There are two possible reasons for this. The first is that it is within the age uncertainty of either the ice core or the UV1 core. However, the offset between the two time series constantly stays around 200 years throughout the mid Holocene. The second possible reason for the time-lag might be due to the time-lag of vegetation response to climate change (Shi *et al*., 1994), as the EAM precipitation history reconstructed in this study is based on the bulk organic δ^{13}C depending on the vegetation type of the area. The second reason is perhaps more likely, particularly as a 100 yr time-lag between the ^{10}Be record and other proxies has also been found, such as the δ^{13}C of tree rings between 8000 and 5000 cal. yr BP in Finkel and Nishiizumi's (1997) study.

There are other possible ways that solar activity influences on the EAM. One of them is through its influence on the strength of the Siberian High. The Siberian High becomes stronger during periods of low solar activity, resulting in stronger winter monsoons of low precipitation. This explains similar general patterns between solar activity and monsoonal precipitation, the synchrony of low solar activity and low monsoonal precipitation around 5700-5400 cal. yr BP and 3200-2900 cal. yr BP (Figure 6.17B), as well as centennial-scale fluctuations in precipitation responding to relatively stable solar activity around 4800-3700 cal. yr BP. Inconsistent between the EAM and the solar activities during 4700-4100 and 3500-3000 cal. yr BP might result from other regional forcing, e.g. the onset of ENSO activity after 5000 cal. yr BP (Sandweiss *et al*., 1996). The fact that changes in the EAM and other climate systems follow a pattern of millennial cycles responding to changing solar activity has been reported by a number of studies (e.g. Thompson *et al*., 1989; Bond *et al*., 1997; Wang *et al*., 2005). Another possible way for solar activity to act on the EAM is through changing the northern Atlantic atmospheric circulation. The concentration of ^{10}Be recorded in the GISP2 ice core reflects the influence of solar activity on atmospheric circulation in the northern Atlantic area, e.g. low solar activity results in cooling events in this area, such as ice-rafted debris (IRD) events (Bond *et al*., 1997). This will be further discussed in

following section about possible correlation between the EAM and high-latitude cooling events.

El Nino Southern Oscillation

Instrumental and proxy climate records about the palaeo-ENSO from western Pacific (Tudhope *et al.*, 2001) are relatively poor compared to the eastern Pacific (Duncan *et al.*, 2008; Tam *et al.*, 2008; Taylor *et al.*, 2008; Hermann *et al.*, 2009;). Coral records from Papua New Guinea, in the far western tropical Pacific region, have recently become an important archive for reconstruction of ENSO activity (e.g. Woodroffe *et al.*, 2003; Ayliffe *et al.*, 2004). Rodbell *et al.* (1999) reconstructed ENSO activity since 15,000 cal. yr BP from an alpine lake in Ecuador, 75 km east of the Pacific Ocean. They suggest that from about 15,000 to 7000 cal. yr BP, the periodicity of clastic deposition is greater than or equal to 15 years; thereafter, there is a progressive increase in frequency to periodicities of 2 to 8.5 years. This is the modern-day periodicity of the ENSO, which was established at 5000 cal. yr BP (Robell *et al.*, 1999). Analyses of pollen from sites throughout the southwest Pacific basin (Webb III *et al.*, 1993; Wright *et al.*, 1993) and of distribution of molluscs in the Sea of Japan (Lutaenko, 1993) have also suggested that ENSO-like variability began only in the late Holocene (after 5000 cal. yr BP; Sandweiss *et al.*, 1996).

ENSO variability has become more intensive since 5000 cal. yr BP (Rodbell *et al.*, 1999), and this might have caused the enhanced wet events after 5000 cal. yr BP in the Pearl River catchment (Figure 6.18). One of the possible ways that the ENSO influences the EAM is through changing the SST of the South China Sea. In this area sea surface temperature gets warmer during the mature phase of El Nino, resulting in a weaker monsoon and less marine productivity, and the situation tends to be reversed during the mature phase of La Nina (De Deckker *et al.*, 1991; Qu and Yamagata, 2009; Qu *et al.*, 2009). Kienast *et al.* (2001) reconstructed sea surface tempterature (SST) of the SCS from Core 18287-3, northwest SCS (Figure 6.18A). Their results suggest a relatively stable SST of the SCS during around 5000-3000 cal. yr BP when wet events became especially frequent. Coral $\delta^{18}O$ records from Papua New Guinea (Tudhope *et al.*, 2001) and Christmas Island, central Pacific (Woodroffe *et al.*, 2003) indicate

stronger ENSO variability in the mid- and late- Holocene than in the early Holocene (Figure 6.18C). This is concordant with the more frequent wet events after 5000 cal. yr BP (Figure 6.18B). Thus it is possible that resolution of the SST record from Kienast *et al.*'s study (2001) is too low to show detailed correlation between the SST variability and ENSO-induced precipitation changes (Figure 6.18B). Meanwhile, although coral records support high-resolution studies on reconstructing changes of SST and/or precipitation related to ENSO activities, there is no continuous record showing palaeo-ENSO variability, especially from western Pacific areas. These problems make it difficult to explain correlation between ENSO activity and EAM variability.
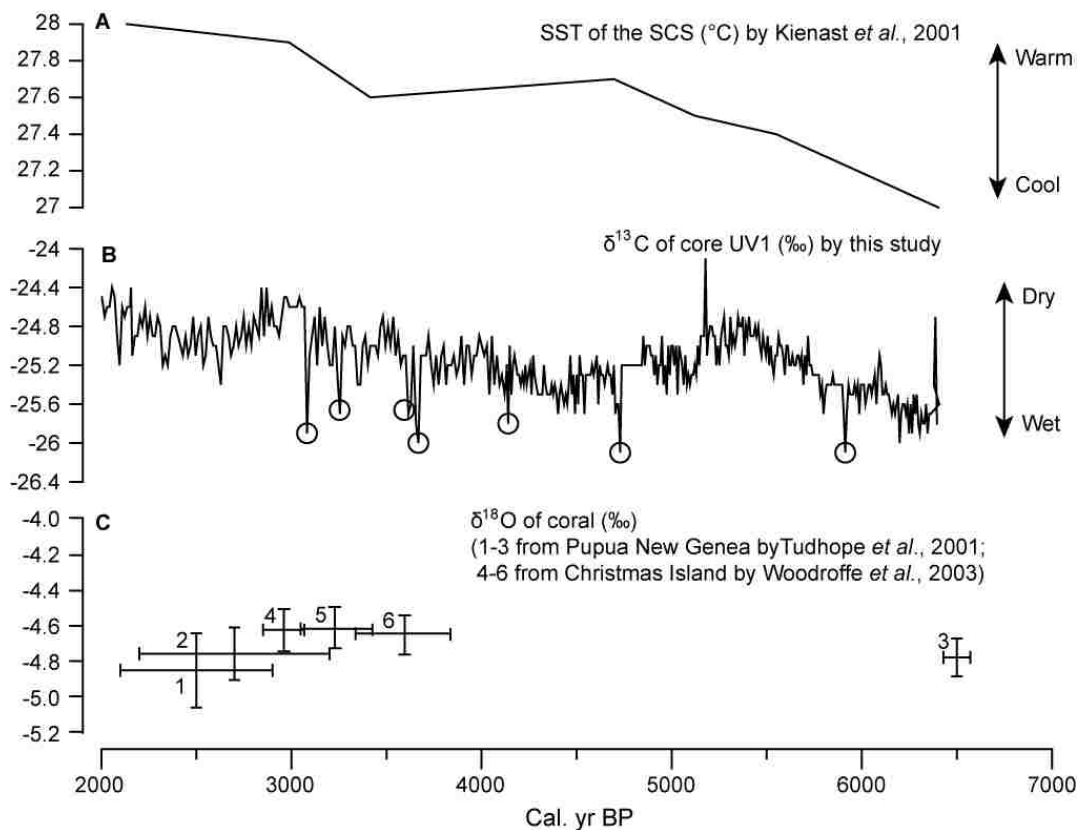
Figure 6.18 Comparison between SST of SCS (A), monsoonal precipitation (B) and ENSO variability (C). A: alkenone (UK37') SST estimates from core 18252-3 (9°14'N, 109°23'E, 1273 m water depth; Kienast *et al.*, 2001); B: δ^{13}C of core UV1 (this study), highlighting some of the wet events (open circles); C: coral δ^{18}O record: 1-core M93TBFC (2500 ±400 cal. yr BP), 2-core Laing FC2 (2700 ±500 cal. yr BP), 3-core H95-16 (6500 ±70 cal. yr BP), 4-XM1 (2800 ±80 cal. yr BP), 5-core XM6 (3200 ±170 cal. yr BP) and 6-core XM9 (3600 ±210 cal. yr BP). Vertical bars show SD and mean of coral δ^{18}O, horizontal lines indicate two-sigma range of calibrated radiocarbon ages.

It is worth mentioning that movements of the Intertropical Convergence Zone (ITCZ) could also influence ENSO variability. For example, abrupt shifts in the location of the Intertropical Convergence Zone (ITCZ) have recently been inferred from paleoclimatic data from South America (Haug *et al*., 2001). They used titanium concentration from deep-sea sediment at ODP Site 1002 to indicate river runoff to the Cariaco Basin, South America. Their results indicate abrupt century-scale variations in runoff associated with shifts in the position of the ITCZ during the period 3800-2800 cal. yr BP, contrasting with lower runoff and titanium input during the late Holocene, when the ITCZ adopted a more southerly location (Haug et a., 2001). Southward migration of the Pacific ITCZ during the Holocene produced an abrupt non-linear increase in ENSO amplitude through enhanced interaction of the locus of tropical atmospheric convection with the Southern Oscillation (Woodroffe *et al*., 2003). During the mid-Holocene, when the mean position of the ITCZ was located further north, ENSO variations in the western Pacific may have been primarily temperature driven, with an enhanced range. At this time, interaction between the Southern Oscillation and ITCZ rainfall appears to have been strong, as indicated by unexpectedly high precipitation variability observed in the Pearl River catchment (Figure 6.18B).

High-latitude cooling events

High-latitude cooling events are another possible driving mechanism for some millennial and centennial -scale events seen in the EAM. It is possible that ice volumes in the high-latitude areas expanded, enhancing the Siberian high in winter (Porter and An, 1995; An, 2000; Wang *et al*., 2001, 2005) and strengthening the winter EAM. Core UV1 reveals a periodicity of 1215 years (Figure 6.15) for EAM variability, which is similar to the 1500-year cycle suggested by Bond *et al*. (1997). Thompson *et al* (1989) reported high dust intensity during the Last Glacial Stage in the Dunde Ice Core from the Qinghai-Tibetan Plateau, Southwest China, responding to the expanded continental ice sheet in higher latitudes. They pointed out that high-latitude cooling enhanced the wind strength, causing loess deposits to extend to the Pacific Basin (Rea *et al*., 1985) and most likely to North America (Thompson *et al*., 1989).

The influence of high-latitude cooling during the Holocene has also been reported by several recent high-resolution studies. Bond *et al.* (1997) analysed two cores from the North Atlantic and suggested that the IRD events exhibit a distinct pattern on a millennial scale, with peaks at about 1400, 2800, 4200, 5900 8100, 9400, 10300 and 11100 years ago. Analysis of a stalagmite record from Dongge Cave (Wang *et al.*, 2005), Southern China, suggests that the Holocene EAM was punctuated by eight weakened monsoon events lasting ~1 to 5 centuries, which have been suggested to be correlated with North Atlantic ice-rafting events. The mid-Holocene ones were centred at 2700, 4400, 5500 and 6300 cal. yr BP (Wang *et al.*, 2005).

This study also shows that, during the mid-Holocene, the record of the EAM was punctuated by dry and wet events lasting from 10 to 300 years (Figure 6.19), and between 2200 and 2000 cal. yr BP the climate becomes intensively variable, with frequent dry and wet events (Figure 6.19). Dry events were centred at, 2900, 3500, 5200, 5300, 5700, 6000, and 6400 cal. yr BP (Figure 6.19), and wet events at 2300, 2500, 3100, 3250, 3650, 4100, 4400, 4700, 5900 and 6200 cal. yr BP (Figure 6.19). Although various studies have shown possible teleconnections between weak EAM periods and high-latitude cooling events (Bond *et al.*, 1997, 2001; Wang *et al.*, 2001; Gupta *et al.*, 2003; Hu *et al.*, 2008), results from this study do not clearly show a good correlation between the two. For example, among all the seven dry events identified in this study, only three of them (at 2900, 5300, and 6400 cal. yr BP) could correlate with IRD events identified by Bond *et al.* (1997) and/or cooling events in the EAM suggested by Wang *et al.* (2005) (Figure 6.19). Furthermore, some wet events indicated from the UV1 occurred during the cool period suggested by Wang *et al.* (2005), corresponding to the IRD events from the north Atlantic (1997), such as dry events at 4400, 5900 cal. yr BP (Figure 6.19). These dry/wet events might be influenced more by other local changes, e.g. SST of the SCS, ENSO, rather the high-latitude events. Thus, influence of high-latitude cooling events on the EAM, such as the IRD in the North Atlantic area is not clearly recorded in core UV1. This might be partly due to the short record of this study, which makes the comparison difficult.
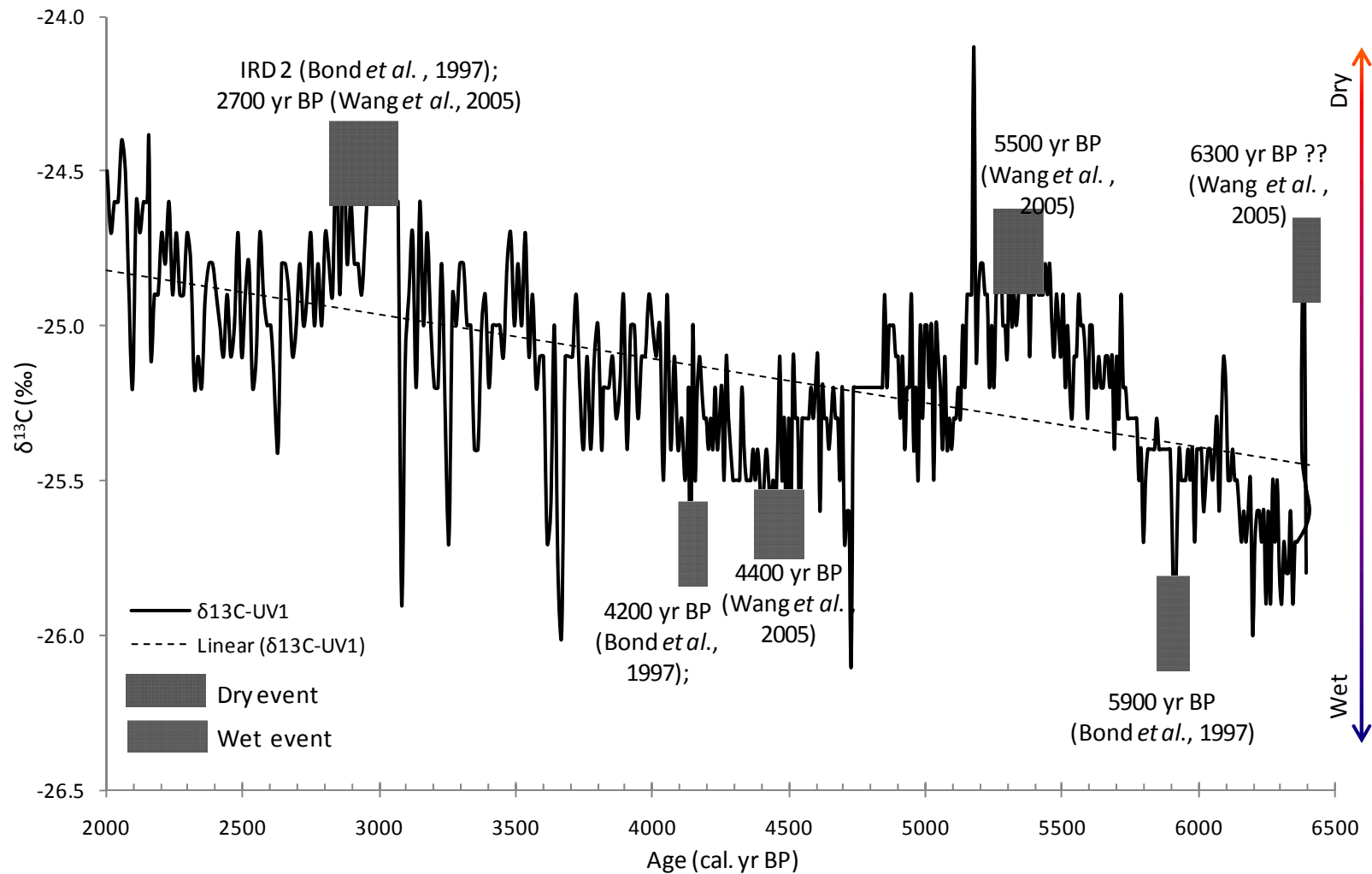
Figure 6.19 Dry/wet events identified from core UV1 with comparison to cooling events identified by Bond *et al*. (1997) and Wang *et al*. (2005). * This curve is made using raw data (Appendix 11). Some low-peak values presented are not discussed in this study. Replicates of some peak values indicate a precision of ±0.1‰ (1SD) (see Table 4.3 in Chapter 4). Data used in this graph are from the first run.

6.7.4 Possible decoupling of the thermal and moisture condition of the EAM during the early mid-Holocene

At the present day, the EAM climate is composed of a warm-humid summer season and a cold-dry winter season, which involves coupling of the thermal and moist conditions. However, the coupling of the thermal and precipitation conditions of the monsoon system might not always have been so strong in the past. The period during 6400-4000 cal. yr BP is suggested to be a relatively wetter period in general, compared to 4000-2000 cal. yr BP, according to the lower δ^{13}C (Figure 6.13). This period has also been reported to be a warm phase by many previous studies from different areas (e.g. An *et al.*, 2000; Xiao *et al.*, 2002; Wang *et al.*, 2005). For example, Liew *et al* (2006) reported a dominance of tropical forest in Taiwan, China, from 8000-4000 yr BP compared to the dominance of temperate forest during the early Holocene. Lacustrine and aeolian deposits in the Mongolian Plateau suggest a warm-humid period during 9000-4000 cal. yr BP (Feng *et al.*, 2006a, b). Xiao *et al.* (2002) reported a warm phase between 7000 and 5500 cal. yr BP in the desert/loess transition of north central China. However, Xiao *et al.* (2002) also suggest that the EAM reached its warmest condition at 5500-2700 cal. yr BP. However this study suggests the EAM was relatively dry from 4000-2000 cal. yr BP compared to 6200-4000 cal. yr BP (Figure 6.13).

This raises an important question: to what extent do temperature and precipitation correspond? The δ^{13}C signature from UV1 from this study indicates a significantly dry period during 6000-5000 cal. yr BP, similar to conditions around 2500 cal. yr BP. However, the SST during 6800-5000 cal. yr BP was reported to be 0.9-0.5 °C higher than at 2500 cal. yr BP (Yu *et al.*, 2005), based on a study of mean Sr/Ca-SST of coral from the northern South China Sea. Both the δ^{13}C record from the Pearl River estuary and the δ^{18}O record of the stalagmite from the Dongge Cave reveal general weakening monsoon strength from 6400-2000 cal. yr BP (Figure 6.20). However, the two do not agree during the period 5300-4600 cal. yr BP. The organic δ^{13}C from the Pearl River estuary indicates a significant increase in precipitation during 5300-4600 cal. yr BP, which would be expected to have been accompanied by an increase in temperature, while the δ^{18}O of stalagmite records from the Dongge Cave suggests weakening summer monsoon strength during this period (Figure 6.20; Wang *et al.*, 2005).

Figure 6.20 Comparison between the bulk organic δ^{13}C from the Pearl River estuary and the δ^{18}O from the Dongge Cave, southern China (Wang *et al*., 2005)

Furthermore, peaks in abundance of the *Salix* pollen (temperate forest) in Taiwan also suggests several cold phases during this time, at 5.2 ka, 5.0 ka and 4.9 ka BP (Liew *et al.*, 2006). From the above, it appears that some relatively dry oscillations, e.g. 6000-5000 yr BP, inferred by the $\delta^{13}C$ record from the Peal River estuary, occurred during warm periods, and some relatively wet oscillations occurred during cold periods. This indicates that the strong coupling between the thermal and moisture conditions of the EAM system only became stable after the mid Holocene, around 4500 cal. yr BP.

The possibility of decoupling of the thermal and moisture conditions of the EAM in southern China has also been suggested not only during the mid-Holocene, but also other periods. Xiao *et al.* (1998) examined the pollen record from the Nanning Mountain in Jiangxi Province, southern China. They suggest cold but moist conditions in this area during the Younger Dryas, with a precipitation of 2000 mm/yr, which is 400-500 mm/yr higher than at the present day. The Holocene optimum, for example, has also been debated not only in terms of its duration but also whether it records a maximum in precipitation and/or temperature. Liew *et al.* (2006) reconstructed the forest structure in central Taiwan and inferred a warm interval between 8000-4000 cal. yr BP, according to the dominant tropical forest. However, their records also suggest that the interval during 8000-4500 cal. yr BP was less humid than during the early Holocene (Liew *et al.*, 2006). Jiang *et al.* (2006) reconstructed the forest vegetation changes of Lake Bayanchagan, Inner Mongolia, which is the northern limit of the present EAM influence. They found that during the early Holocene increases in temperature and precipitation occurred simultaneously, but mid-Holocene cooling started at approximately 8000 cal. yr B.P., 1500 years earlier than the drying. These studies indicate that, before the mid Holocene, it is very possible that the warm period of the EAM might not necessarily have correlated with humid conditions. This agrees with the bulk organic $\delta^{13}C$ record from the Pearl River estuary.

6.7.5 The retreat of the monsoonal maximum rain belt since the early Holocene

Another possible reason for mismatches between bulk organic $\delta^{13}C$ from the Pearl River estuary and $\delta^{18}O$ from Dongge Cave, e.g. the mismatch during 6000-5000 cal. yr BP, is migration of the monsoon rain belt due to insolation-induced general circulation

changes (Gao *et al.*, 1962; Lau *et al.*, 1988; An *et al.*, 2000). An *et al.* (2000) suggested that precipitation associated with the EAM was produced by the interaction along the monsoon front of northward-moving moist summer monsoon air and a northern mass of cooler air. Since the early Holocene, the maximum rain belt has retreated from northeast China to southeast China (Figure 6.21). The maximum rain belt passed Dongge Cave and the Pearl River estuary at different time, i.e. it passed Dongge Cave around 6000-5000 cal. yr BP, and reached the Pearl River estuary after 3000 cal. yr BP (Figure 6.21).

Wang *et al.* (2005) suggested that changes in $\delta^{18}O$ from Dongge Cave indicate monsoonal precipitation changes. The maximum precipitation zone occurred in the middle and lower reaches of the Yangtze River 8000-5000 cal. yr BP (An *et al.*, 2000; Figure 6.21), when Dongge Cave was at the edge of the maximum precipitation zone (Figure 6.21). Thus, it is possible that during 6000-5000 cal. yr BP precipitation at Dongge Cave area was much higher, if not the highest, than any other area in China during 6000-5000 cal. yr BP. For example, the Pearl River estuary, under control of the stable-warm air mass (Figure 6.21), received significantly lower precipitation compared to the Dongge Cave area (Figure 6.20). Similarly, when the maximum rain zone migrated to southern China 3000 cal. yr ago (Figure 6.21), the Pearl River estuary should have experienced a period of high precipitation soon after 3000 cal. yr BP (Figure 6.20), as it was at the edge of the maximum precipitation zone (Figure 6.21), which was the case for Dongge Cave area 6000 cal. yr ago. Accordingly, areas around Dongge Cave were under the control of the stable-cold air mass and received significantly lower rainfall. Low precipitation during 6000-5400 cal. yr BP and high precipitation soon after 3000 cal. yr BP in the Pearl River area have been suggested by $\delta^{13}C$ records (Figure 6.20). Increasing rainfall in the Pearl River area observed during 5400-4600 cal. yr BP might have been caused in part by the southward moving rain zone. The $\delta^{18}O$ from Dongge Cave indicates a relatively high precipitation period during 6000-5000 cal. yr BP, and the precipitation kept decreasing since without obvious interruptions (Figure 6.20) due to the generally weakened monsoon strength.
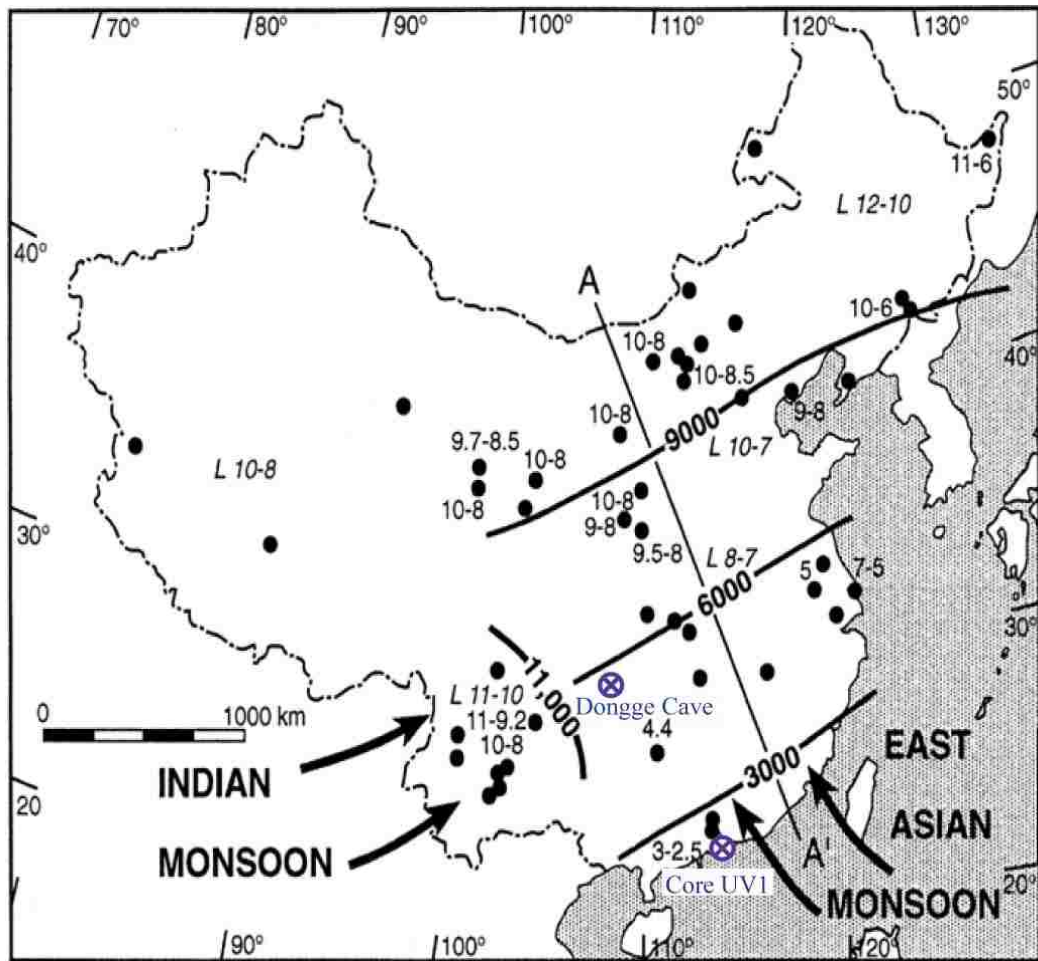
Figure 6.21 Map of China showing position of the EAM maximum through time based on paleoclimatic proxy data. Maximum precipitation/elective precipitation occurred 12,000-10,000 cal. yr ago in northeastern China, 10,000-7000 cal. yr ago in north-central and northern east-central China, 8000-5000 cal. yr ago in the middle and lower reaches of the Yangtze River, and 3000 cal. yr ago in southern China. The monsoon maximum dating to 11,000 cal. yr ago in southwestern China is related to the northeastward penetration of the Indian summer monsoon (after An *et al.*, 2000)

One of the shortcomings of this study is that the fossil record only covers the mid-late Holocene, and it is difficult to gain an overview if Holocene monsoon variability. For example, Xiao *et al.* (2002) investigated the TOC and grain size distribution at the desert/loess transition of the north central China, and suggested that during 5500-2700 cal. yr BP the EAM reached its warmest and wettest condition in the Holocene. The bulk organic δ^{13}C from the Pearl River estuary also shows considerably humid conditions during this time period in southern China. Bulk organic δ^{13}C and C/N ratios

167

from Core V37 show a strong monsoonal freshwater flux at 7500-6000 cal. yr BP (Zong *et al.*, 2006). This partly overlaps with the $\delta^{13}C$ and C/N records from the UV1 core, which suggest that the freshwater flux at 6400-6000 cal. yr BP is the strongest over the period observed (Figure 6.13). The high freshwater flux during 6400-6000 cal. yr BP might be part of the end of the Holocene Optimum. However, due to the limit of the record, it is difficult to discuss the duration of the Holocene optimum based on this study.

6.8 Possible anthropogenic influence in the Pearl River delta from 2000 cal. yr BP

As the modern plant data show in Chapter 5, the dominant organic sources for modern estuarine sediments are from the C_3 group of plants, including mangroves, tropical-subtropical trees and common agricultural crops. This group of plants has a common signature of $\delta^{13}C$, which is around -26‰ to -28‰. However, there is another group of plants, C_4 grasses and sugarcane, which are also present in the area. C_4 grasses are less common in the catchment area of the Pearl River and its delta plain, which lie in the tropical and subtropical zone under humid monsoon climate. Sugarcane is native to the region and one of the main crops in the delta plain. This group of plants has a very different value of $\delta^{13}C$, around -13‰, significantly heavier than the first group.

Modern surface sediments from the deltaic distributaries and the estuary have $\delta^{13}C$ ranging from -21‰ at the marine end to -24‰ in the distributaries, and C/N from 7.5 at the marine end to 12.7 at the river tributaries (Figure 5.11 in Chapter 5). At the head of the river, the C/N ratios from these surface samples suggest a greater amount of terrestrial input, but the $\delta^{13}C$ values are 2-4‰ more positive than the common terrestrial organic matter, which has an organic carbon isotope value ranging between -26‰ and -28‰. Such departure from the average of the $\delta^{13}C$ values for common terrestrial organic matter is possibly a result of the input of organic matter from sugarcane, which has a significantly heavier $\delta^{13}C$ value averaging -12.7‰ (as shown in Chapter 5). Agricultural soil samples measured have values between those found from sugarcane and other agricultural plants (e.g. banana, rice and lotus) of around -21.7‰. This is

because the soil is a mixture of organic matter from both C_3 (rice, banana and lotus) and C_4 (sugarcane) agricultural plants. Furthermore, because of the input of the C_4 (sugarcane) organic matter from the delta plain, the bulk organic samples from the deltaic distributaries, a freshwater environment, have a $\delta^{13}C$ value of -23.8‰, much heavier than expected (e.g. -26‰ to -28‰, Thornton and McManus, 1994; Wilson *et al.*, 2005). Therefore, in an area where sugarcane is a common agricultural crop, agricultural activity can be detected from the sediment sequences based on organic carbon isotopes.

Since 2000 cal. yr BP (Zone 2 of UV1), significant changes occurred in both the organic carbon isotopic signature and metal concentrations of UV1. The organic carbon isotope signature from Zone 2 (1.29 - 0.35m) increased significantly to around -23‰. There are two possible reasons for this shift in the $\delta^{13}C$ value. One possible reason is that this area was under significantly stronger marine influence since 2000 cal. yr BP than during the mid-Holocene. In this case, the organic matter deposited during this time should mainly derive from the marine end members, which has high $\delta^{13}C$ (around -21‰) and low C/N (usually lower than 10, Figure 5.11 in Chapter 5). According to Zong *et al.* (2009a) most of the terrestrial sediment has been trapped inside the sea wall, resulting in low sediment flux into the core site. Meanwhile, the weakening monsoon has also resulted in a lower sediment flux into the estuary (Zong *et al.*, 2006), and the core site is under higher marine influence indicated by the diatom records of core UV1 (Zong *et al.*, 2009a). Thus, it is possible that sediment preserved since 2000 cal. yr BP is of higher marine input due to significantly reduced terrestrial input.

However, this thesis suggests that an enhanced anthropogenic influence is a more important cause for the sudden increase in the $\delta^{13}C$ value since 2000 cal. yr BP than the increasing marine influence (or reducing terrestrial input). Although the $\delta^{13}C$ value of sediment since 2000 cal. yr BP is similar to the $\delta^{13}C$ value of marine organic matter, the C/N ratio during this period is much higher than that marine organic matter (Figure 6.2). This indicates that terrestrial C_4 plants, especially sugarcane, which has a high $\delta^{13}C$ value and largely variable C/N ratio (Figure 5.3 in Chapter 5), might be a more significant contributor than marine organic matter. Furthermore, Figure 6.22 shows greater similarity to the surface sediment samples from freshwater-brackish areas in

both the δ^{13}C value (Figure 6.22A) and total organic content (Figure 6.22B) compared to samples from the mid Holocene period. C$_4$ grasses are less common in the catchment area of the Pearl River and its delta plain which lie in the tropical and subtropical zone under humid monsoon climate. However, sugarcane is native to the region and one of the main crops in the delta plain and it is a C$_4$ plant. The organic carbon isotope data from top of the sediment core, therefore, provides a clear evidence for a major expansion of agricultural crop production, including sugarcane, in the Pearl River deltaic area at approximately 2000 BP. This provides a date for the development and expansion of this form of intensive agriculture in the Pearl River delta of 2000 BP.
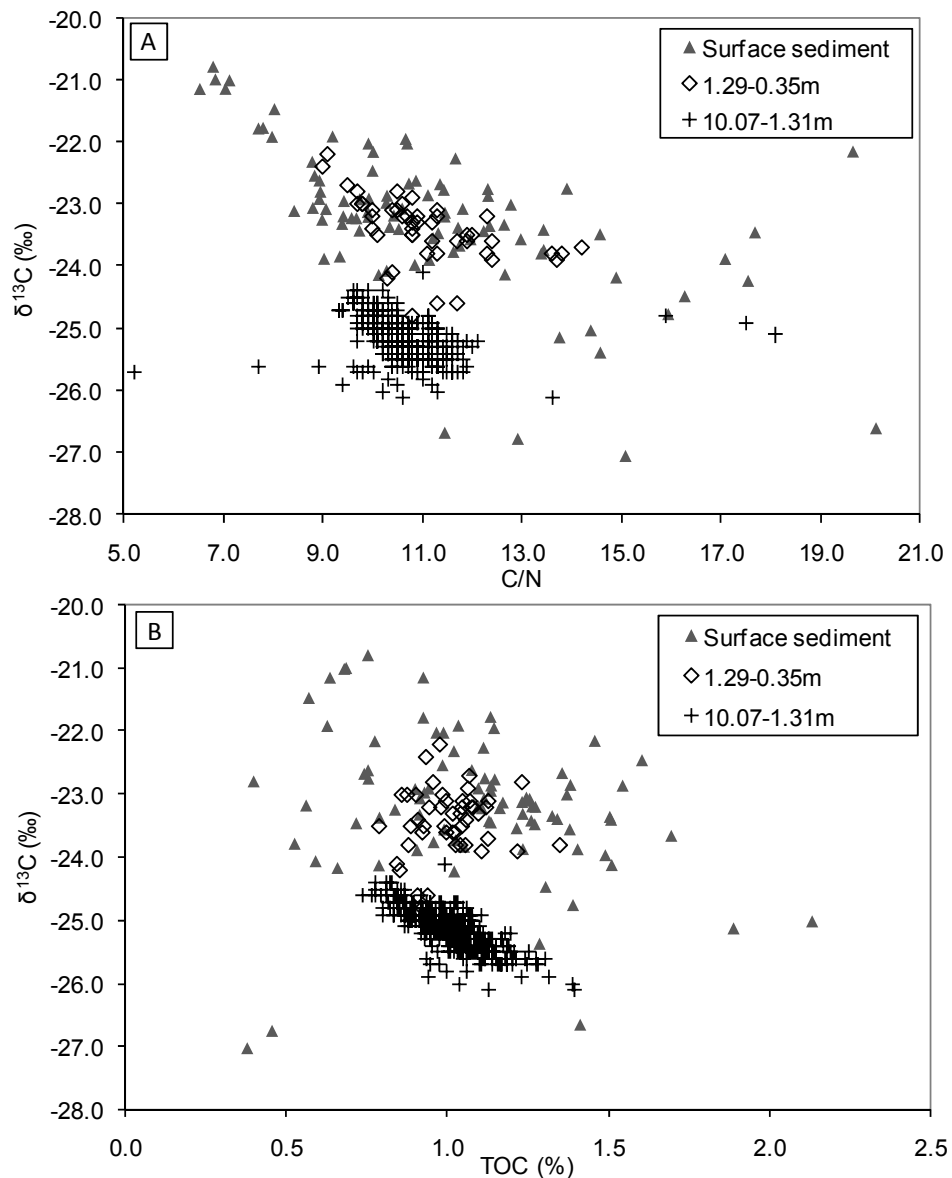
Figure 6.22 Bi-plot of the δ^{13}C value and C/N ratio of Core UV1 and surface sediment

Furthermore, concentrations of metals such as Cu, As, Fe, Al and Pb are significantly higher within Zone 2 than during the mid Holocene (Figure 6.7). For example, the concentration of copper (Cu), iron (Fe) and lead (Pb) in the sediment core was relatively constant prior to 2000 BP at a background level of 20 mg/kg, 33,000 mg/kg and 30 mg/kg respectively. These concentrations all increased in Zone 2 from about 2000 BP towards present to levels of about 40 mg/kg, 40,000 mg/kg and 50 mg/kg respectively (Figure 6.7). Such increases in concentration could be produced by increased human activity in the area exploiting the natural resources, possibly linked to population expansion and/or advances in technology. The shift seen from Zone 1 to Zone 2 at 2000 BP is, therefore, more likely to be linked to human activity (in particular enhanced agricultural activity) than linked to changes in freshwater flux or climate conditions.

6.9 Summary of the chapter

The results of the bulk organic $\delta^{13}C$, TOC concentration, C/N ratios as well as concentrations of a range of metals from core UV1 suggest a decreasing freshwater discharge during 6400-2000 cal. yr BP, responding to reducing monsoonal precipitation. On top of the general trend, wet/dry intervals of the EAM from centennial- to decadal- time scales are observed. Driving mechanisms for the EAM changes include the Millankovitch-driven precession (the primary driving mechanism for the EAM at a millennial time scale) and orbitally-induced solar modulation at centennial- to millennial- time scales, ENSO and high-latitude cooling events. However, evidence for the later two forcing mechanisms is not clearly represented in UV1. This study also suggests that the coupling of thermal and moist conditions of the EAM might only become stable after 4500 cal. yr BP, which might cause mismatches between records from the Dongge Cave and from the Pearl River estuary. Another possible reason for mismatches between the two records might be the retreat of the maximum rain belt of the EAM since the early Holocene. A sudden shift in the organic isotopic signature and metal concentrations in UV1 during the past 2000 years indicates that human activity, in particular intensive agricultural activity, in the Pearl River delta started from 2000 years ago.

Chapter 7 Conclusion

7.1 Introduction

This chapter discusses the results in relation to the original proposal aims, and assesses the limitations of this work. Future directions of research arising from the original finding in this thesis are then discussed.

7.2 Thesis aims and results

The East Asian Monsoon (EAM) is a globally significant climate system with links to different parts of the global climate system. Climatologically, the monsoon regions are the most convectively active areas on Earth and account for the majority of global atmospheric heat and moisture transport (Webser, 1998). Their activity exerts major influence on the economic and social well-being of societies living in monsoon-affected regions. The principle aim of this thesis was to reconstruct EAM variability during the mid-Holocene, developing the relatively new proxy of bulk organic carbon isotopic signature ($\delta^{13}C$), and also using C/N ratios and key elements. The key findings of this thesis and how they relate to the initial aims and objectives are presented in the following section.

7.2.1 Bulk organic $\delta^{13}C$ and C/N as an indicator for sediment sources and environmental changes

The analysis of modern plants, soil, suspended sediment and surface sediment samples presented in Chapter 5 of this thesis suggest that bulk organic $\delta^{13}C$ and C/N ratios can be used as an indicator for the source of the organic component of the sediment. In the Pearl River delta, C_3 plants have lower $\delta^{13}C$ than C_4 plants, $-29.0\pm1.8‰$ and $-13.1\pm0.5‰$ respectively, whilst C/N of both C_3 and C_4 are widely variable and the overlap between groups is considerable. In the terrestrial area, $\delta^{13}C$ and C/N of soil samples are highly related to the source of organic matter. Soil samples from C_3-plant-

dominant areas, e.g. the forest, tend to have lower $\delta^{13}C$ than those from C_4-grass-dominant areas, e.g. the riverside area. Their C/N values, however, are widely variable and overlap significantly. Thus, while the $\delta^{13}C$ of soil can be used to indicate the predominant vegetation type, C/N cannot. In the estuarine area, $\delta^{13}C$ and C/N of POC show significant variability due to seasonal variation of freshwater flux, resulting in changes in the balance between the TOM and in situ phytoplankton in the POC. The $\delta^{13}C$ of surface sediment in the estuary increases from $-25.0‰$ at the freshwater end to $-21.0‰$ at the marine end, with C/N decreasing from 15.2 to 6.8, suggesting a weakening terrestrial/freshwater input and a strengthening marine contribution seaward. Based on the analysis of modern samples of organic matter from source to sink in the Pearl River catchment, delta and estuary, this study concludes that $\delta^{13}C$ and C/N of bulk organic matter can be used as an indicator for vegetation type and sediment source and, hence has the potential to be used to reconstruct environmental conditions.

Detailed analysis of agricultural plants and soils suggests that anthropogenic input might have elevated the $\delta^{13}C$ of sedimentary organic matter due to enhanced fertilization processes and, more significantly, by an increase in the proportion of C_4 plants such as sugarcane grown in the catchment area. However, this signature is insufficiently significant to have influenced the signature produced by the natural vegetation in this area, which is dominated by C_3 plants.

7.2.2 Key elements as an indicator for environmental changes

Results suggest that combinations of certain trace metals investigated in this study, although not all of them, can be used as indicators of sediment sources and environmental changes. Terrigenous metals (F1 metals, e.g. Fe, Mn, Co and As) have higher concentrations in the fresh-brackish-water area than in the marine, whilst F2 metals (Li, Rb, K, Ba and Al) increase from the freshwater area to the marine areas in the Pearl River estuary. The distribution of F3 metals (Sr, Na, Mg, Ca and B/Be) within the estuary does not follow a fixed pattern. Ca shows a decreasing concentration from the freshwater area to the shallow marine area, while B/Be ratios increase from the freshwater end to the marine end. Sr, Na, Mg and Ca show a much lower concentration in the area west of Hong Kong. These results indicate that the combination of these key metals is a good indicator for sediment sources and sedimentary environment. For

example, sediment with high concentrations of F1 metals and low concentrations of F2 metals is mainly from terrestrial areas or environments with low salinity. Such combinations of metals might also indicate a sedimentary environment of strong interaction between freshwater and saline water and/or of strong re-suspension process.

7.2.3 History of the EAM during the mid Holocene

Results of the bulk organic $\delta^{13}C$, TOC concentration, and C/N ratios, as well as concentrations of a range of key elements from core UV1, suggest a decreasing freshwater discharge during 6400-2000 cal. yr BP, indicating a reduction in monsoonal precipitation. Superimposed on the general trend, wet/dry intervals of the EAM from millennial- to centennial- scale are observed. Possible driving mechanisms at different timescales for the EAM have also been explored by this study. The orbital-driven insolation change acts as the primary driving mechanism for EAM variability; the generally weakening insolation since early Holocene has resulted in the generally weakening EAM. Changes in solar activity at centennial- to millennial- time scale have produced wet-dry oscillations of EAM. Changes in ENSO activity and high-latitude cooling events (e.g. the IRD events) might be responsible for dry/wet events at centennial- to decadal- timescale during the mid-Holocene. However, evidence for the later two driving mechanisms is not clearly seen in UV1. This study also suggests that the coupling of thermal and moist conditions of the EAM might only have become stable after 4500 cal. yr BP. Mismatches between $\delta^{13}C$ records from the Pearl River estuary and $\delta^{18}O$ records from Dongge Cave might due to movement of the maximum rain zone since the early Holocene.

7.2.4 Possible anthropogenic influence since 2000 cal. yr BP

A sudden shift in the organic isotopic signature and metal concentrations in UV1 since 2000 cal. yr BP indicates that agricultural activity (specifically enhanced production of sugarcane) in the Pearl River delta intensified from 2000 cal. yr BP. The elevated $\delta^{13}C$ also indicates strengthened marine influence at the core site since 2000 cal. yr BP, although it is not as significant as the contribution from human activities.

7.3 Limitations of this research

The overall results of the modern-day analogue and high-resolution record produced by the geochemical proxies presented in this thesis have been successful. The geochemical proxies investigated through the modern-day analogue covers the full range of environments within the modern Pearl River delta and estuary. This helps interpret the fossil data and understand use of possible driving mechanisms for EAM variability during the mid-Holocene. However, there are still some questions unanswered.

7.3.1 Limitation of the short time series of core UV1

One of the limitations of this study is that the fossil record only covers the mid-late Holocene, so it is difficult to gain an overview of monsoon variability over the full Holocene. For example, Xiao et al (2002) investigated the TOC and grain size distribution at the desert/loess transition of north central China, and suggested that during 5500-2700 cal. yr BP the East Asian monsoon reached its warmest and wettest condition in the Holocene. The bulk organic $\delta^{13}C$ from the Pearl River estuary also shows considerably humid condition during this time period in southern China. Bulk organic $\delta^{13}C$ and C/N ratios from the Core V37 show a strong monsoonal freshwater flux at 7500-6000 cal. yr BP (Zong et al., 2006). This partly overlaps with the $\delta^{13}C$ and C/N records from the UV1 core, which suggests that the freshwater flux at 6400-6000 cal. yr BP is the strongest during the period observed. The high freshwater flux during 6400-6000 cal. yr BP might be part of the Holocene Optimum, e.g. end of the Holocene Optimum. However, due to the relatively short time series of the record, it is difficult to discuss the duration of the Holocene optimum based on this study.

7.3.2 Limitation of the proxy

A possible limitation about the proxy measured is essentially an indirect measure of monsoon variability – associated with changes in freshwater flux from the river system that could be influenced by other factors – changes within the drainage basin, changes in the location of monsoon precipitation rather than changes in the amount of precipitation.

7.4 Future study

7.4.1 Longer time scale study

Sediment cores covering the whole Holocene or even older sequences covering the full climate cycle would be helpful for understanding the EAM variability in relation to global and regional driving mechanisms. Questions can address longer term variability of EAM precipitation. There are few long, high resolution records of precipitation changes on a millennial time scale. One of the few that has been published is the study by Wang et al. (2005) using $\delta^{18}O$ of a stalagmite from Dongge Cave, southern China. However, whether the $\delta^{18}O$ of stalagmite carbonate is influenced by changes of precipitation or temperature is still open to debate. So more studies on the longer term precipitation variability are needed from this area.

7.4.2 Multi-core study

The location of the core from this study (UV1) from the eastern side of the estuary means it is more strongly influenced by marine water entering the estuary and perhaps less sensitive to variations in freshwater flux that would tend to flow on the western side of the estuary. Combining the results from UV1 with a sediment core from the west side of the estuary, e.g. near Maucau, would perhaps provide stronger support for the conclusions than relying on just one core.

7.4.3 Multi-proxy study

Although the bulk organic $\delta^{13}C$ and C/N measurements employed in this study have highlighted their potential as palaeo-environmental indicators, trace metals in the modern-day analogue are not as successful (perhaps influenced by the circulation process of industrial and natural metals within the estuary). Microfossils such as diatoms and foraminifera, on the other hand, have been well developed for palaeo-climatic changes. Although their analysis is time-consuming, it would still be worthwhile to employ these proxies together with the bulk organic $\delta^{13}C$ and C/N to produce a multi-proxy study of EAM variability.

7.5 Thesis conclusions

This thesis is an original contribution to the growing body of knowledge about EAM variability during the mid-Holocene. This study has further advanced the technique of using the bulk organic $\delta^{13}C$ and C/N to investigate variations in freshwater flux linked to monsoon intensity initially explored by Zong et al (2006). Modern-day plants, soil, suspended sediment and surface sediment samples from the Pearl River catchment and estuarine areas ranging from freshwater to marine end members were collected during this study. Results of modern-day samples suggest that bulk organic carbon isotopes and C/N are good indicators for sources of the sedimentary organic matter. Some trace metals (e.g. Fe, Mn, Co and As) are also useful for investigating sources of estuarine sediment, although indications of sediment sources by these metals is not as clear as bulk organic $\delta^{13}C$ and C/N.

Core UV1 from the Pearl River estuary provides a high-resolution record for reconstruction of EAM variability during the mid-Holocene. The EAM has weakened since 6400 cal. yr BP responding to orbitally-driven insolation changes (precession cycle). Superimposed on this general trend are centennial- to millennial- scale dry/wet oscillations driven by changes in the solar activity. Regional forcing such as ENSO could have played an important part for dry/wet events at decadal time scale by changing the ocean and atmosphere circulations. One of the possible ways that ENSO acts on the EAM is through changing the SST of the SCS. Meanwhile, the ENSO would also be influenced by the EAM system. For example, during the mid-Holocene, when the mean position of the ITCZ was located further north, ENSO variations in the western Pacific may have been primarily temperature driven, with an enhanced range. The results of this study show a possible teleconnection between the high-latitude cooling events and the EAM variability, especially at the millennial scale. However, correlation between the abrupt cooling events such as the IRD events and the EAM is not clearly shown in this study. This study also indicates enhanced human activity since 2000 cal. yr BP in this area, which has greatly changed the geochemical signals preserved in the core.

References

Aitchison J. C., Ali J. R. and Davies A. M. (2007). When and where did India and Asia collide? *Journal of Geophysical Research, Solid Earth*, **112**: B05423, doi: 10.1029/2006JB004706.

Alley R., Finkel R. C., Nishiizumi K., Anandakrishman S., Shuman C. A., Mershon G. R., Zielinski G. A. and Mayewski P. A. (1995). Changes in continental and sea-salt atmospheric loadings in central Greenland during the most recent deglaciation: Model-based estimates. *Journal of Glaciology*, **41**: 503-514.

An Z. (2000). The history and variability of the East Asian paleomonsoon climate. *Quaternary Science Reviews*, **19**: 171-187.

An Z., Porter S. C., Kutzbach J. E., Wu X., Wang S, Liu X., Li X., Zhou W. (2000). Asynchronous Holocene optimum of the East Asian monsoon. *Quaternary Science Reviews*, **19**: 743-762.

An Z. and Thompson L. G. (1998). Plaeoclimatic change of monsoonal China linked to global change. *In: Asian Change in the Context of Global Climate Change. James Galloway and Jerry Melillo (Eds.)*, **Cambridge University Press**: 18-41.

Andrews J. E., Greenaway A. M. and Dennis P. F. (1998). Combined Carbon Isotope and C/N Ratios as Indicators of Source and Fate of Organic Matter in a Poorly Flushed, Tropical Estuary: Hunts Bay, Kingston Harbour, Jamaica. *Estuarine, Coastal and Shelf Science*, **46**: 743-756.

Arzayus K. M. and Canuel E. A. (2004). Organic matter degradation in sediments of the York River Estuary: effects of biological vs. physical mixing. *Geochimica et Cosmochimica Acta* **69**: 455– 463.

Austin A. T. and Vitousek P. M. (1998). Nutrient dynamics on a precipitation gradient in Hawaii. *Oecologia*, **113**: 519–529.

Ayliffe L. K., Bird M. I., Gagan M. K., Isdale P. J., Scott-Gagan H., Parker B.,

Griffin D., Nongkas M. and McCulloch M. T. (2004). Geochemistry of coral from Papua NewGuinea as a proxy for ENSO ocean–atmosphere interactions in the Pacific Warm Pool. *Continental Shelf Research*, **24**: 2343-2356.

Bard E., Raisbeck G., Yiou F. and Jouzel J. (2000). Solar irradiance during the last 1200 years based on cosmogenic nuclides. *Tellus*, **52B**: 985-992.

Barry R. and Chorley R. (2003). *Atmosphere, Weather and Climate*. Routledge, London, 421.

Barth J. A. C., Veizer J. and Mayer B. (1998). Origin of particulate organic carbon in the upper St. Lawrence: isotopic constraints. *Earth and Planetary Science Letters*, **162**: 111-121.

Beer J., Blinov A., Bonani G., Finkel R. C., Hofmann H. J., Lehmann B., Oeschger H., Sigg A., Schwander J., Staffelbach T., Stauffer B., Suter M. and Wölfli W. (1990). Use of 10Be in polar ice to trace the 11-year cycle of solar activity. *Nature*, **347**: 164-166.

Beer J., Raisbeck G. M. and Yiou F. (1991). Time variations of ^{10}Be and solar activity, In 'Time Variations of 10Be and Solar Activity', by Sonett C. P., Giampapa M. S. and Matthews M. S. (Eds.). University of Arizona press, Tucson: 343–359.

Beer J., Tobias S. M. and Weiss N. O. (1998). An active sun throughout the maunder minimum. *Solar Physics*, **181**: 237-249.

Behling H. and Lichte M. (1997). Evidence of dry and cold climatic conditions at glacial times in tropical Southeastern Brazil. *Quaternary Research*, **48**(3): 348–358.

Bender M. M. (1971). Variations in the ^{13}C/^{12}C ratios of plants relation to the pathway of photosynthetic carbon dioxide fixation. *Phytochemistry*, **10**: 1239-1244.

Benner R., Fogel M. L. and Sprague E. K. (1991). Diagenesis of below ground biomass of Spartina alterniflora in salt-marsh sediments. *Limnology and Oceanography*, **36**: 1358– 1374.

Benner R., Fogel M. L., Sprague K. E. and Hodson R. E. (1987). Depletion of ^{13}C in

179

lignin and its implications for stable carbon isotope studies. *Nature*, **329**: 708-710.

Berger A. and Loutre M. (1991). Insolation values for the climate of the last 10 million years. *Quaternary Science Review*, **10**(4): 297-317.

Bianchi T. S., Wysocki L. A., Stewart M., Filley T. R. and McKee B. A. (2007). Temporal variability in terrestrially-derived sources of particulate organic carbon in the lower Mississippi River and its upper tributaries. *Geochimica et Cosmochimica Acta*, **71**(18): 4425-4437.

Bird M. I., Chivas A. R., Radnell C. J. and Burton H. R. (1991). Sedimentological and stable-isotope evolution of lakes in the Vestfold Hills, Antarctica. *Palaeogeography, Palaeoclimatology, Palaeoecology*, **84**: 109-130.

Bird M. I., Fifield L. K., Teh T. S., Chang C. H., Shirlaw N. and Lambeck K. (2007). An inflection in the rate of early mid-Holocene eustatic sea-level rise: a new sea-level curve from Singapore.Estuarine. *Coastal and Shelf Science*, **71**: 523-536.

Bird M. I., Robinson R. A. J., Win Oo N., Maung Aye M., Lu X. X., Higgitt D. L., Swe A., Tun T., Lhaing Win S., Sandar Aye K., Mi Mi Win K. and Hoey T. B. (2008). A preliminary estimate of organic carbon transport by the Ayeyarwady (Irrawaddy) and Thanlwin (Salween) Rivers of Myanmar. *Quaternary International*, **186**(1): 113-122.

Bond G., Kromer B., Beer J., Muscheler R., Evans M. N., Showers W., Hoffmann S., Lotti-Bond R., Hajdas I. and Bonani G. (2001). Persistent Solar Inßuence on North Atlantic Climate During the Holocene. *Science*, **294**: 2130-2136.

Bond G., Showers W., Cheseby M., Lotti R., Almasi P., deMenocal P., Priore P., Cullen H., Hajdas I. and Bonani G. (1997). A Pervasive Millennial-Scale Cycle in North Atlantic Holocene and Glacial Climates. *Science*, **278**: 1257-1266.

Bordovskiy O. K. (1965b). Accumulation of organic matter in bottom sediments. *Marine Geology*, **3**: 33-82.

Bordovskiy O. K. (1965a). Sources of organic matter in marine basins. *Marine Geology*, **3**: 5-31.

Boschker H. T. S., Kromkamp J. and Middelburg J. J. (2005). Biomarker and carbon isotopic constraints on bacterial and algal community structure and functioning in the highly polluted Scheldt estuary. *Limnology and Oceanography*, **50**: 70-80.

Boulay S., Colin C., Trentesaux A., Frank N. and Blamart D. (2003). South China Sea sediment response to the Plestocene monsoon variations. *Geophysical Research Abstracts*, **5**.

Bradley R. S. (2003). Climate forcing during the Holocene. *Pages News*, **11**(283): 18-19.

Bradley R. S., Hughes M. K. and Diaz H. F. (2003). Climate in Medieval Time. *Science*, **302**: 404-405.

Brady P. and Carroll S. (1994). Direct effects of CO2 and temperature on silicate weathering: possible implications for climate control. *Geochimica Cosmochimica Acta*, **58**: 1853–1856.

Bühring C. and Sarnthein M. (2000). Toba ash layers in the South China Sea: Evidence of contrast wind directions during the eruption, ca. 74ka. *Geology*, **28**(3): 275-278.

Burdloff D., Araújo M. F., Jouanneau J. M., Mendes I., Monge Soares A. M. and Dias J. M. A. (2008). Sources of organic carbon in the Portuguese continental shelf sediments during the Holocene period. *Applied Geochemistry*, **23**: 2857-2870.

Cao C., Wang W., Liu L., Shen S. and Summons R. E. (2008). Two episodes of ^{13}C-depletion in organic carbon in the latest Permian: Evidence from the terrestrial sequences in northern Xinjiang, China. *Earth and Planetary Science Letters*, **270**: 251-257.

Carslaw K. S., Harrison R. G. and Kirkby J. (2002). Cosmic rays, clouds, and climate. *Science*, **298**: 1732-1737.

Chen H. T. (1994). Character of the heavy minerals in the surface sediment of Lingdingyang and their reflection to the invasion of shelf water. *Acta Scientiarum Naturalium Universitatis Sunyatseni*, **33**(4): 104-109 (in Chinese).

Chen J., An Z. and Head J. (1999). Variation of Rb/Sr ratios in the loess-paleosol sequences of Central China during the last 130, 000 years and their implications for monsoon paleoclimatology. *Quaternary Research*, **51**: 215-219.

Chen J., An Z., Liu L., Ji J., Yang J. and Chen Y. (2001). Variations in chemical compositions of the eolian dust in Chinese Loess Plateau over the past 2.5 Ma and chemical weathering in the Asian inland. *Science in China (Series D)*, **44**(5): 403-414.

Chivas A. R., Garclia A., van der Kaars S., Couapel M. J. J., Holt S., Reeves J. M., Wheeler D. J., Switzer A. D., Murray-Wallace C. V., Banerjee D., Price D. M., Wang S. X., Pearson G., Edgar N. T., Beaufort L., de Deckker P., Lawson E. and Cecil C. B. (2001). Sea-level and environmental changes since the last interglacial in the Gulf of Carpentaria, Australia: an overview. *Quaternary International*, **83-85**: 19-46.

Chmura G. L., Aharon P., Socki R. A. and Abernethy R. (1987). An inventory of ^{13}C abundances in coastal wetlands of Louisiana, USA: vegetation and sediments. *Oecologia*, **74**: 264-271.

Cifuentes L. A. (1991). Spatial and temporal variations in terrestriallyderived organic matter from sediments of the Delaware Estuary. *Estuaries*, **14**: 414-429.

Clarke F. W. (1924). *The data of geochemistry*. Government Printing Office, Washington, 841.

Cloern J. E., Canuel E. A. and Harris D. (2002). Stable carbon and nitrogen isotope composition of aquatic and terrestrial plants of the San Francisco Bay estuarine system. *Limnology and Oceanography*, **47**: 713–729.

Coffin R. B., Fry B., Peterson B. J. and Wright R. T. (1989). Carbon isotopic compositions of estuarine bacteria. *Limnology and Oceanography*, **34**: 1305–1310.

Colman S. M., Peck J., Karabanov E. B., Carter S. J., Bradbury J. P., King J. W. and Williams D. F. (1995). Continental climate response to orbital forcing from biogenic silica records in Lake Baikal. *Nature*, **378**: 769-771.

Countway R. E., Canuel E. A. and Dickhut R. M. (2007). Sources of particulate

organic matter in surface waters of the York River, VA estuary. *Organic Geochemistry*, **38**(3): 365-379.

Craig H. (1953). The geochemistry of the stable carbon isotopes. *Geochimica et Cosmochimica Acta*, **3**: 53-92.

Craig H. (1954). Carbon-13 in plants and the relationships between carbon-13 and carbon-14 variations in nature. *Journal of Geology*, **62**: 115-149.

Cramer B. D. and Saltzman M. R. (2007). Early Silurian paired $\delta^{13}C_{carb}$ and $\delta^{13}C_{org}$ analyses from the Midcontinent of North America: Implications for paleoceanography and paleoclimate. *Palaeogeography, Palaeoclimatology, Palaeoecology*, **256**(3-4): 195-203.

Crowley T. J. (2000). Causes of Climate Change Over the Past 1000 Years. *Science*, **289**: 270-277.

Danielsson L.-D., Magnusson B., Westerlund S. and Zhang K. R. (1982). Trace metal determinations in estuarine waters by electrothermal atomic absorption spectrometry after extraction of dithiocarbamate complexes into freon. *Analytica Chimica Acta*, **144**: 183-188.

Dansgaard W., Johnsen S. J., Clausen H. B., Dahl-Jensen D., Gundestrup N. and Oeschger H. (1984). North Atlantic ocillations revealed by deep Greenland ice cores. *Geophysical Monographys*, **29**: 288-298.

Davis F. J., Levinson A. A. and Bayliss P. (1972). Hydrogeochemistry of the surface waters of the Mackenzie River drainage basin, Canada, IV. Boron-salinity-clay mineralogy relationship in modern deltas. *Geochimica et Cosmochimica Acta*, **36**: 1359-1375.

Davis J. C., Proctor I. D., Southon J. R., Caffee M. W., Heikkinen D. W., Roberts M. L., Moore T. L., Turteltaub K. W., Nelson D. E., Loyd D. H. and Vogel J. S. (1990). LLNL/UC AMS facility and research program. *Nuclear Instruments and Methods in Physics Research*, **B52**: 269-272.

De Deckker P., Corrège T. and Head J. (1991). Late Pleistocene record of cyclic

eolian activity from tropical Australia suggesting the Younger Dryas is not an unusual climatic event. *Geology*, **19**: 602-605.

Degens E. T., Gullard R. R., Sackett W. M. and Hellebust J. A. (1968). Metabolic fractionation of carbon isotopes in marine plankton: 1. Temperature and respiration experiments. *Deep-Sea Research*, **15**: 1-9.

Degens E. T., Reuter J. H. and Shaw K. N. F. (1964). Biochemical compounds in offshore California sediments and sea waters. *Geochimica et Cosmochimica Acta*, **28**: 45-66.

Deines P. (1980). The isotopic composition of reduced organic carbon, In 'Handbook of Environmental Isotope Geochemistry. The Terrestrial Environment', by Fritz P. and Fontes J. C. (Eds.). Elsevier, Amsterdam: 329–406.

DeLaune R. D., 1986. The use of d13C signature of C3 and C4 plants (1986). The use of d13C signature of C3 and C4 plants in determining past depositional environments in rapidly accreting marshes of the Mississippi River deltaic plain, Louisiana, U.S.A. *Chemical Geology*, **59**: 315-320.

Denton G. H. and Karlén W. (1973). Holocene Climatic Variations-Their Pattern and Possible Cause. *Quaternary Research*, **3**: 155-205.

Ding Z., Yu Z., Rutter N. W. and Liu T. (1994). Towards an orbital time scale for the Chinese loess deposits. *Quaternary Science Reviews*, **13**: 39-70.

Ding Z. L., Rutter N. W. and Liu T. S. (1993). Pedostratigrapby of Chinese loess deposits and climatic cycles in the last 2.5 Ma. *Catena*, **20**(73-91).

Dominik J. and Stanley D. J. (1993). Boron, beryllium and sulfur in Holocene sediments and peats of the Nile delta, Egypt: Their use as indicators of salinity and climate. *Chemical Geology*, **104**: 203-216.

Driese S. G., Li Z.-H. and Horn S. P. (2005). Late Pleistocene and Holocene climate and geomorphic histories as interpreted from a 23,000 14C yr B.P. paleosol and floodplain soils, southeastern West Virginia, USA. *Quaternary Research*, **63**(2): 136-149.

Driese S. G., Li Z.-H. and McKay L. D. (2008). Evidence for multiple, episodic, mid-Holocene Hypsithermal recorded in two soil profiles along an alluvial floodplain catena, southeastern Tennessee, USA. *Quaternary Research*, **69**(2): 276-291.

Du N., Kong Z. and Shan F. (1989). A preliminary investigation on the vegetational and climatic changes since 11 000 years in Qinghai Lake – an analysis based on palynology in core QH85-14C. *Acta Botanica Sinica 31: 803-814.*

Ember L. M., Williams D. F. and Morris J. T. (1987). Processes that influence carbon isotope variations in salt marsh sediments. *Marine Ecology Progress Series*, **36**: 33-42.

Emerson S. and Hedges J. I. (1988). Processes controlling the organic carbon content of open ocean sediments. *Paleoceanography*, **3**: 621-634.

Emiliani C. and Geiss J. (1959). On Glaciations and Their Causes. *Geologische Rundschau*, **46**: 576-601.

Fan M., Dettman D. L., Song C., Fang X. and Garzione C. N. (2007). Climatic variation in the Linxia basin, NE Tibetan Plateau, from 13.1 to 4.3 Ma: The stable isotope record. *Palaeogeography, Palaeoclimatology, Palaeoecology*, **247**(3-4): 313-328.

Fan Z.-X., Bräuning A., Yang B. and Cao K.-F. (2009). Tree ring density-based summer temperature reconstruction for the central Hengduan Mountains in southern China. *Global and Planetary Change*, **65**: 1-11.

Feng Z.-D., An C. B. and Wang H. B. (2006a). Holocene climatic and environmental changes in the arid and semi-arid areas of China: a review. *The Holocene*, **16**(1): 119-130.

Feng Z.-D., Tang L. Y., Wang H. B., Ma Y. Z. and Liu K.-b. (2006b). Holocene vegetation variations and the associated environmental changes in the western part of the Chinese Loess Plateau. *Palaeogeography, Palaeoclimatology, Palaeoecology*, **241**: 440-456.

Finkel R. C. and Nishiizumi K. (1997). Beryllium 10 concentrations in the Greenland

Ice Sheet Project 2 ice core from 3–40 ka. *Journal of Geophysical Research, Ocean,* **102(C12), 26**: 699-706.

Flige M. and Solanki S. K. (1999). The solar spectral irradiance since 1700. *Geophysical Research Letters*, **26**: 2465–2468.

Fogel M. L., Sprague K. E., Gize A. P. and Frey R. W. (1989). Diagenesis of organic matter in Georgia salt marshes, Estuarine. *Coastal and Shelf Science*, **28**: 211-230.

Fontugne M. and Duplessy J. C. (1978). Carbon isotope ratio of marine plankton related to surface water masses. *Earth and Planetary Science Letters*, **41**: 365-371.

Fontugne M. R. and Calvert S. E. (1992). Late Pleistocene variability of the carbon isotopic composition of organic matter in the eastern Mediterranean: monitor of changes in carbon sources and atmospheric CO_2 concentrations. *Paleoceanography*, **7**(1): 1-20.

Fontugne M. R. and Jouanneau J.-M. (1987). Modulation of the particulate organic carbon flux to the ocean by a macrotidal estuary: Evidence from measurements of carbon isotopes in organic matter from the Gironde system. *Estuarine, Coastal and Shelf Science*, **24**(3): 377-387.

Fry B. and E.B. S. (1984). $\delta^{13}C$ measurements as indicators of carbon flow in marine and freshwater ecosystems. *Contributions in Marine science*, **27**: 13-47.

Fry B., Scalan R. S. and Parker P. L. (1977). Stable carbon isotope evidence for two sources of organic matter in coastal sediments: seagrass and plankton. *Geochimica et Cosmochimica Acta*, **41**: 1875– 1877.

Fyfe J. A., Shaw R., Campbell S. D. G., Lai K. W. and Kirk P. A. (2000). *The Quaternary Geology of Hong Kong*, **Hong Kong Geological Survey, Hong Kong SAR**: 209 pp.

Gagan M. K., Ayliffe L. K., Hopley D., Cali J. A., Mortimer G. E., Chappell J., McCulloch M. T. and Head M. J. (1998). Temperature and surface-ocean water balance of the Mid-Holocene tropical western Pacific. *Science*, **279**: 1014-1018.

Gao Y. X. and Xu S. Y. (1962). *Some problems of East Asian Monsoon*. Science Press,

Beijing, 1-49 (in Chinese).

Gao Y. (1962). *Some Problems on East-Asia* Monsoon. Science Press, Beijing, pp. 49-63 (in Chinese).

Goldschmidt V. M. (1954). *Geochemistry*. Clarendon Press, Oxford, 730.

Goldschmidt V. M. and Peters C. (1932). Zur Geochemie des Bors, I, II. *Nachrichten von der Gesellschaft der Wissenschaften zu Gottingen. Mathenmatisch-Physikalische Klasse*, **III: 402-4-7; IV: 528-545 (in German)**.

Goldschmidt V. M. and Peters C. (1933). Uber die anreicherung seltener Elemente in Steinkohlen. *Nachrichten von der Gesellschaft der Wissenschaften zu Gottingen. Mathenmatisch-Physikalische Klasse*, **4**: 371-386 (in German).

Goldschmidt V. M. and Peters C. (1934). Zur Geochemie des Arsen. *Nachrichten von der Gesellschaft der Wissenschaften zu Gottingen. Mathenmatisch-Physikalische Klasse*, **4**: 11-12 (in German).

Gong G. F. and Hameed S. (1991). The variation on moisture conditions in China during the last 2000 years. *International Journal of Climatology*, **11**: 271-283.

Goni M. A., Ruttenberg K. C. and Eglinton T. I. (1997). Sources and contribution of terrigenous organic carbon in the Gulf of Mexico. *Nature*, **389**: 275–278.

Gruber N., Keeling C. D., Bacastow R. B., Guenther P. R., Lueker T. J., Wahlen M., Meijer H. A. J., Mook W. G. and Stocker T. F. (1999). Spatiotemporal patterns of carbon-13 in the global surface oceans and the oceanic Suess effect. *Global Biogeochemical Cycles*, **13**(2): 307-335.

Guan P., Ng C. W. W., Sun M. and Tang W., 2001. (2001). Weathering indices for rhyolitic tuff and granite in Hong Kong. *Engineering Geology*, **59**: 147-159.

Guangdong Statistical Bureau (1996). *Statistical Year Book of Guangdong for 1995*. Statistical Press, Beijing, 236 (in Chinese).

Guo X. and He S. (2006). Geochemical Characteristics and Origin of the Light Crude

Oils in Panyu Lower Uplift, Pearl River Mouth Basin. *Geological Science and Technology Information*, **25(5)**: 63-68 (in Chinese, with English abstract).

Gupta A. K., Anderson D. M. and Overpeck J. T. (2003). Abrupt changes in the Asian southwest monsoon during the Holocene and their links to the North Atlantic Ocean. *Nature*, **421**: 354-357.

Haines E. B. (1976). Stable carbon isotope ratios in biota, soils and tidal water of a Georgia salt marsh. *Estuarine and Coastal Marine Science*, **4**: 609– 616.

Hammer Ø., Harper D. A. T. and Ryan P. D. (2001). PAST: Paleontological Statistics Software Package for Education and Data Analysis. *Palaeontologia Electronica*, **4**(1): 9pp.

Harmelin-Vivien M., Loizeau V., Mellon C., Beker B., Arlhac D., Bodiguel X., Ferraton F., Hermand R., Philippon X. and Salen-Picard C. (2009). Comparison of C and N stable isotope ratios between surface particulate organic matter and microphytoplankton in the Gulf of Lions (NW Mediterranean). *Continental Shelf Research*, **28**(15): 1911-1919.

Hatch M. D. and Slack C. R. (1970). Photosynthetic CO_2-fixation patyways. *Annual Review of Plant Physiology*, **21**: 141-162.

Haug G. H., Hughen K. A., Sigman D. M., Peterson L. C. and Röhl U. (2001). Southward migration of the Intertropical Convergence Zone through the Holocene. *Science*, **293**: 1304– 1308.

Hedges J. I. and Keil R. G. (1995). Sedimentary organic matter preservation: an assessment and speculative synthesis. *Marine Chemistry*, **49**: 81-115.

Hedges J. I. and Parker P. L. (1976). Land-derived organic matter in surface sediments from the Gulf of Mexico. *Geochimica et Cosmochimica Acta*, **40**: 1019– 1029.

Hellings L., Dehairs F., Tackx M., Keppens E. and Baeyens W. (1999). Origin and fate of organic carbon in the freshwater part of Scheldt Estuary as traced by stable carbon isotope composition. *Biogeochemistry*, **47**: 167-186.

188

Hermann A. J., Curchitser E. N., Haidvogel D. B. and Dobbins E. L. (2009). A comparison of remote versus local influence of El Niño on the coastal circulation of the Northeast Pacific. *Deep Sea Research Part II: Topical Studies in Oceanography*, **doi:10.1016/j.dsr2.2009.02.005**.

Hong Y. T., Z.G. Wang, Jiang H. B., Lin Q. H., B. Hong, Zhu Y. X., Wang Y., Xu L. S., Leng X. T. and Li H. D. (2001). A 6000-year record of changes in drought and precipitation in northeastern China based on a δ^{13}C time series from peat cellulose. *Earth and Planetary Science Letters*, **185**: 111– 119.

Horiuchi K., Uchida T., Sakamoto Y., Ohta A., Matsuzaki H., Shibata Y. and Motoyama H. (2008). Ice core record of 10Be over the past millennium from Dome Fuji, Antarctica: A new proxy record of past solar activity and a powerful tool for stratigraphic dating. *Quaternary Geochronology*, **3**: 253-261.

Hsueh Y., Schultz J. R. and Holland W. R. (1997). The Kuroshio flow-through in the East China Sea: a numerical model. *Progress in Oceanography*, **39**: 79-108.

Hsieh M. (2006). Geochemical characterization of organic matter in Victoria Harbour sediments, Hong Kong. *PhD thesis*, University of Oklahoma, Japan.

Hu C., Henderson G. M., Huang J., Xie S., Sun Y. and Johnson K. R. (2008). Quantification of Holocene Asian monsoon rainfall from spatially separated cave records. *Earth and Planetary Science Letters*, **266**(3-4): 221-232.

Hu J., Peng P. a., Jia G., Mai B. and Zhang G. (2006). Distribution and sources of organic carbon, nitrogen and their isotopes in sediments of the subtropical Pearl River estuary and adjacent shelf, Southern China. *Marine Chemistry*, **98**: 274-285.

Hu J., Zhang G., Li K., Peng P. a. and Chivas A. R. (2008). Increased eutrophication offshore Hong Kong, China during the past 75 years: Evidence from high-resolution sedimentary records. *Marine Chemistry*, **110**(1-2): 7-17.

Huang J., Wang S., Wen X. and Yang B. (2008). Progress in studies of the climate of humid period and the impacts of changing precession in early-mid Holocene. *Progress in Natural Science*, **18**: 1459-1464.

Huang L., Jian W., Song X., Huang X., Liu S., Qian P., Yin K. and Wu M. (2004). Species diversity and distribution for phytoplankton of the Pearl River estuary during rainy and dry seasons. *Marine Pollution Bulletin*, **49**: 588-596.

Huang X. P., Huang L. M. and Yue W. Z. (2003). The characteristics and sources of eutrophication in Pearl River estuary, South China. *Marine Pollution Bulletin*, **47**: 30-36.

Huang Z., Li P., Zhang Z., Li K. and Qiao P. (1982). *Zhujiang (Pearl) Delta*. General Scientific Press, Guangzhou (in Chinese).

Huang Z., Li P., Zhang Z., Li K. and Zong Y. (1983). Implication of trace elements of Quaternary sediment from Peral River delta. *Tropic Geography*, **1**: 41-49.

Hunt J. M. (1970). The significance of carbon isotope variations in marine sediments. Advances in Organic Geochemistry, In 'Proceedings of the Third International Congress, London, 1966. International Series of Monographs in Earth Science, 32', by Hobson G. D. and Speers G. C. (Eds.). Pergamon Press, Oxford: 27-35.

Imbrie J., Berger A. and Shackleton N. J. (1993). Role of orbital forcing: a two-million-year perspective, In 'Global Changes in the Perspective of the Past', by Eddy J. A. and Oeschger H. (Eds.). Chichster & New York: 263-277.

Imbrie J., Boyle E. A., Clemens S. C., Duffy A., Howard W. R., Kukla G., Kutzbach J., Martinson D. G., McIntyre A., Mix A. C., Molfino B., Morley J. J., Peterson L. C., Pisias N. G., Prell W. L., Raymo M. E., Shackleton N. J. and Toggweiler J. R. (1992). On the structure and origin of major glaciation cycles 1. Linear responses to Milankovitch forcing. *Paleoceanography*, **7**: 701-738.

Imbrie J., Hays J. D., Martinson D. G., McIntyre A., Mix A. C., Morley J. J., Pisias N. G., Prell W. L. and Shackleton N. J. (1984). The orbital theory of Pleistocene climate: support from a revised chronology of the marine $\delta^{18}O$ record, In 'Milankovitch and Climate', by Berger A., Imbrie J., Hays J., Kukla G. and Saltzman B. (Eds.). Reidel, Dordrecht: 269-306.

Ishiwatari R. and Uzaki M. (1987). Diagenetic changes of lignin compounds in a

more than 0.6 million-year-old lacustrine sediment (Lake Biwa, Japan). *Geochimica et Cosmochimica Acta*, **51**: 321-328.

Jasper J. P. and Gagosian R. B., 1990. (1990). The sources and deposition of organic matter in the Late Quaternary Pygmy Basin, Gulf of Mexico. *Geochimica et Cosmochimica Acta*, **54**: 1117-1132.

Ji J., Balsam W., Shen J., Wang M., Wang H. and Chen J. (2009). Centennial blooming of anoxygenic phototrophic bacteria in Qinghai Lake linked to solar and monsoon activities during the last 18,000 years. *Quaternary Science Reviews*, **doi:10.1016/j.quascirev.2008.12.015**.

Jia G. and Peng P. (2003). Temporal and spatial variations in signatures of sedimented organic matter in Lingding Bay (Pearl estuary), southern China. *Marine Chemistry*, **82**: 47-54.

Jian Z., Wang P., Saito Y., Wang J., Pflaumann U., Oba T. and Cheng X. (2000). Holocene variability of the Kuroshio current Trough, northwestern Pacific ocean. *Earth and Planetary Science Letters*, **184**(1): 305-319.

Jiang W., Guo Z., Sun X., Wu H., Chu G., Yuan B., Hatté C. and Guiot J. (2006). Reconstruction of climate and vegetation changes of Lake Bayanchagan (Inner Mongolia): Holocene variability of the East Asian monsoon. *Quaternary Research*, **65**: 411-420.

Jin Z., Wang S., Shen J., zhang E., Li F., Ji J. and Lu X. (2001). Chemical weathering since the Little Ice Age recorded in lake sediments: a high-resolution proxy of past climate. *Earth Surface Processes and Landforms*, **26**: 775-782.

Kang Y., Mai B., Huang X., Zhang G., Sheng G. and Fu, J. (2000). Primary study on status of organic pollution in surface sediments of the Pearl River Delta. *Acta Science Circumstantiae*, **20**: 164-170 (in Chinese, with English abstract).

Keeley J. E. and Sandquist D. R. (1992). Carbon: freshwater plants. *Plant, Cell and Environment*, **15**: 1021– 1035.

Kerr R. A. (1996). Climate: Volcano-Ice Age discounted. *Science,* **272**: 817-0.

Kershaw A. P. (1994). Pleistocene vegetation of the humid tropics of northeastern Queensland, Australia. *Palaeogeography, Palaeoclimatology, Palaeoecology*, **109**: 399-412.

Kezhen Z. (1973). A preliminary study on the climatic fluctuation during the last 5000 years in China. *Scienctia Sinica (Series B)*, **16**: 226-256.

Kienast M., Steinke S., Stattegger K. and Calvert S. E. (2001). Synchronous tropical South China Sea SST change and Greenland warming during deglaciation. *Science*, **291**: 2132-2134.

Kim J.-M. and Kucera M. (2000). Benthic foraminifer record of environmental changes in the Yellow Sea (Hwanghae) during the last 15 000 years. *Quaternary Science Reviews*, **19**: 1067-1085.

Kortschak H. P., Hartt C. E. and Burr G. O. (1965). Carbon dioxide fixation in sugarcane leaves. *Plant Physiology*, **40**: 209-213.

Kot S. C. and Hu S. L. (1995). Water flows and sediment transport in Pearl River Estuary and waves in South China near Hong Kong, In 'Proceedings of a Symposium on the Hydraulics of Hong Kong Waters', by Civil Engineering Department H. K. U., Hong Kong: 13-24.

Kukla G. (1987). Loess stratigraphy in central China. *Quaternary Science Reviews*, **6**: 191-219.

Kukla G., An Z., Melice J. L., Gavin J. and Xiao J. L. (1990). Magnetic susceptibility record of Chinese loess. *Transitions of the Royal Society of Edinburgh: Earth Science*, **81**: 263-288.

Kuwae M., Yamaguchi H., Tsugeki N. K., Miyasaka H., Fukumori K., Ikehara M., Genkai-Kato M., Omori K., Sugimoto T., Ishida S. and Takeoka H. (2007). Spatial distribution of organic and sulfur geochemical parameters of oxic to anoxic surface sediments in Beppu Bay in southwest Japan. *Estuarine, Coastal and Shelf Science*, **72**(1-2): 348-358.

Lamb A. L., Wilson G. P. and Leng M. J. (2006). A review of coastal palaeoclimate

and relative sea-level reconstructions using d13C and C/N ratios in organic material. *Earth-Science Reviews*, **75**: 29-57.

Lamb H. H. (1965). The early Medieval Warm Epoch and its sequel. *Palaeogeography, Palaeoclimatology, Palaeoecology*, **1**: 13-37.

Landergren S. (1945). Contribution to the geochemistry of boron II. The distribution of boron in some Swedish sediments, rocks and iron ores. The boron cycle in the upper lithosphere. *Arkiv Kemi Mineral Geology*, **19A**(26).

Lau K. M., Yang G. J., Sheu S. H. (1988). Seasonal and intraseasonal climatology of monsoon rainfall over East Asia. *Monthly Weather Review*, **116:** 18-37.

Lea D. W., Pak D. K. and Spero H. J. (2000). Climate impact of late Quaternary equatorial Pacific sea surface temperature variations. *Science*, **289**: 1719-1724.

Leavitt S. W., Follett R. F., Kimble J. M. and Pruessner E. G. (2007). Radiocarbon and δ^{13}C depth profiles of soil organic carbon in the U.S. Great Plains: A possible spatial record of paleoenvironment and paleovegetation. *Quaternary International*, **162-163**: 21-34.

Levinson A. A. and Ludwick J. C. (1966). Speculation on the incorporation of boron into argillaceous sediments. *Geochimica Cosmochimica Acta*, **30**(9): 855-861.

Li B., Li Y., Liu Q., Melieres F., Van Campo E., Wang F. and Zhang Q. (1991). A 13,000-year climate record from western Tibet. *Nature*, **353**: 742-745.

Li P., Qiao P., Zheng H., Fang G. and Huang G. (1990). *The environmental evolution of the Pearl River Delta in the last 10,000 years*. China Ocean Press, Beijing (in Chinese).

Li Z. H. and Liang S. H. (1995). Modern sedimentary environment and heavy metal content distribution in bottom load in Pearl River estuary. *Marine Science Bulletin*, **14**: 43-49 (in Chinese).

Liew P. M., Lee C. Y. and Kuo C. M. (2006). Holocene thermal optimal and climate variability of East Asian monsoon inferred from forest reconstruction of a subalpine

pollen sequence, Taiwan. *Earth and Planetary Science Letters*, **250**: 596-605.

Lim D. I., Jung H. S., Choi J. Y., Yang S. and Ahn K. S. (2006). Geochemical compositions of river and shelf sediments in the Yellow Sea: Grain-size normalization and sediment provenance. *Continental Shelf Research*, **26**: 15-24.

Liu K.-K., Kao S.-J., Hu H.-C., Chou W.-C., Hung G.-W. and Tseng C.-M. (2007). Carbon isotopic composition of suspended and sinking particulate organic matter in the northern South China Sea--From production to deposition. *Deep Sea Research Part II: Topical Studies in Oceanography*, **54**(14-15): 1504-1527.

Liu K.-K., Kao S.-J., Hu H.-C., Chou W.-C., Hung G.-W. and Tseng C.-M. (2007). Carbon isotopic composition of suspended and sinking particulate organic matter in the northern South China Sea--From production to deposition. *Deep Sea Research Part II: Topical Studies in Oceanography*, **54**(14-15): 1504-1527.

Liu T. S. (1985). *Loess and the Environment* China Ocean Press, Beijing, 171-174 (in Chinese).

Liu W., An Z., Zhou W., Head M. J. and Cai D. (2003). Carbon isotope and C/N ratios of suspended matter in rivers: an indicator of seasonal change in C4/C3 vegetation. *Applied Geochemistry*, **18**: 1241-1249.

Lowe J. J. and Walker M. J. C. (1997). *Reconstructing Quaternary Environments*. Addison Wesley Longman Limited, Halow, 446.

Lu H., Liu J., Chu G. and Gu Z. (2003). A study of pollen and environment in the Huguangyan Marr Lake since the last glaciation. *Acta Palaeontologica Sinica*, **42**(2): 284-291 (in Chinese with English abstract).

Lutaenko K. A. (1993). Climatic optimum during the Holocene and the distribution of warm-water mollusks in the Sea of Japan. *Palaeogeography, Palaeoclimatology, Palaeoecology*, **102**: 273-281.

Mackie E. A. V., Leng M. J., Lloyd J. M. and Arrowsmith C. (2005). Bulk organic d13C and C/N ratios as palaeosalinity indicators within a Scottish isolation basin. *Journal of Quaternary Science*, **20**: 301-408.

Mackie E. A. V., Lloyd J. M., Leng M. J., Bentley C. J. and Arrowsmith C. (2007). Assessment of $\delta^{13}C$ and C/N ratios in bulk organic matter as palaeosalinity indicators in Holocene and Lateglacial insolation basin sediments, northwest Scotland. *Journal of Quaternary Science*, **22**(6): 579-591.

Mann M., Bradley R. and Hughes M. (1999). Northern Hemisphere temperatures during the past millennium: inferences, uncertainties, and limitations. *Geophysical Research Letters*, **26**(6): 759-762.

Martin J. M. and Whitfield M. (1983). The significance of the river input of chemical elements to the ocean, In 'Treace metals in sea water', by Wong C. S., Boyle E., Bruland K. W., Burton J. D. and Goldberg E. D. (Eds.). Plenum, New York: 265-296.

Masarik J. and Beer J. (1999). Simulation of particle fluxes and cosmogenic nuclide production in the Earth's atmosphere. *Journal of Geophysical Research* **104**: 12099–12111.

Melillo J. M., Aber J. D., Linkins A. E., Ricca A., Fry B. and Nadelhoffer K. J. (1989). Carbon and nitrogen dynamics along the decay continuum: plant litter to soil organic matter. *Plant Physiology*, **115**: 189-198.

Meyers P. A. (1994). Preservation of elemental and isotopic source identification of sedimentary organic matter. *Chemical Geology*, **114**: 289-302.

Meyers P. A. (1997). Organic geochemical proxies of paleoceanographic, paleolimnologic, and paleoclimatic processes. *Organic Geochemistry*, **27**: 213– 250.

Meyers P. A. and Arnaboldi M. (2008). Paleoceanographic implications of nitrogen and organic carbon isotopic excursions in mid-Pleistocene sapropels from the Tyrrhenian and Levantine Basins, Mediterranean Sea. *Palaeogeography, Palaeoclimatology, Palaeoecology*, **266**: 112-118.

Middelburg J. J. and Herman P. M. J. (2007). Organic matter processing in tidal estuaries. *Marine Chemistry*, **106**(1-2): 127-147.

Middelburg J. J. and Nieuwenhuize J. (1998). Carbon and nitrogen stable isotopes in suspended matter and sediments from the Schelde Estuary. *Marine Chemistry*, **60**: 217-

225.

Middelburg J. J., Nieuwenhuize J., Lubberts R. K. and van de Plassche O. (1997). Organic carbon isotope systematics of coastal marshes. *Estuarine, Coastal and Shelf Science*, **45**: 681-687.

Moberg A., Sonechkin D. M., Holmgren K., Datsenko N. M. and Karlé W. (2005). Highly variable Northern Hemisphere temperatures reconstructed from low- and high-resolution proxy data. *Nature*, **433**: 613-617.

Müller A. and Mathesius U. (1999). The palaeoenvironments of coastal lagoons in the southern Baltic Sea, I. The application of sedimentary C_{org}/N ratios as source indicators of organic matter. *Palaeogeography, Palaeoclimatology, Palaeoecology*, **145**: 1-16.

Müller A. and Voss M. (1999). The palaeoenvironments of coastal lagoons in the southern Baltic Sea, II. $\delta^{13}C$ and $\delta^{15}N$ ratios of organic matter - sources and sediments. *Palaeogeography, Palaeoclimatology, Palaeoecology*, **145**: 17-32.

Murphey B. F. and Nier A. O. (1941). Variations in the relative abundance of the carbon isotopes. *Physical Review*, **59**(9): 771-772.

Muscheler R., Beer J. and Vonmoos M. (2004). Causes and timing of the 8200 yr BP event inferred from the comparison of the GRIP ^{10}Be and the tree ring $\delta^{14}C$ record. *Quaternary Science Reviews*, **23**: 2101-2111.

Muschelera R., Joos F., Beerc J., Müller S. A., Vonmoos M. and Snowball I. (2007). Solar activity during the last 1000 yr inferred from radionuclide records. *Quaternary science Reviews*, **26**: 82-97.

Nesbitt H. W. (1979). Mobility and fractionation of rare earth elements during weathering of a granodiorite. *Nature*, **279**: 206-210.

Nesbitt H. W., Markovics G. and Price R. C. (1980). Chemical processes affecting alkalis and alkaline earths during continental weathering. *Geochimica et Cosmochimica Acta*, **44**: 1659-1666.

Nesbitt H. W. and Young G. M. (1982). Early Proterozoic climates and plate motions

inferred from major element chemistry of lutites. *Nature*, **299**: 715-717.

Nier A. O. and Gulbransen E. A. (1939). Variations in the relative abundance of the carbon isotopes. *Journal of the American Chemical Society*, **61**: 697-698.

Nordt L. C., Boutton T. W., Hallmark C. T. and Waters M. R. (1994). Late Quaternary vegetation and climate change in Central Texas based on the isotopic composition of organic carbon. *Quaternary Research*, **41**: 109–120.

O'Leary M. H. (1985). Carbon isotope fractionation in plants. *Phytochemistry*, **20**: 553-567.

O'Brien S. R., Mayewski P. A., Meeker L. D., Meese D. A., Twickler M. S. and Whitlow S. I. (1995). Complexity of Holocene climate as reconstructed from a Greenland ice core. *Science*, **270**: 1962-1964.

O'Hare G., Sweeney G. and Wilby R. (2005). *Weather, Climate and Climate Change - Human Perspectives*. Pearson Education Limited, England, 403.

O'Leary M. H. (1981). Carbon isotope fractionation in plants. *Phytochemistry*, **20**: 553-567.

O'Leary M. H. (1988). Carbon isotopes in photosynthesis. *Bioscience*, **38**: 328-336.

Osmond C. B., Valaane N., Haslam S. M., Uotila P., Roksandic Z. and 1981. (1981). Comparisons of $\delta^{13}C$ values in leaves of aquatic macrophytes from different habitats in Britain and Finland; some implications for photosynthetic processes in aquatic plants. *Oecologia*, **50**: 117-124.

Owen R. B. (2005). Modern fine-grained sedimentation – spatial variability and environmental controls on an inner pericontinental shelf, Hong Kong. *Marine Geology*, **214**: 1-26.

Owen R. B. and Lee R. (2004). Human impacts on organic matter sedimentation in a proximal shelf setting, Hong Kong. *Continental Shelf Research*, **24**: 583-602.

Park R. and Epstein S. (1960). Carbon isotope fractionation during photosynthesis.

Geochimica et Cosmochimica Acta, **21**(1-2): 110-126.

Park R. and Epstein S. (1961). Metabolic fractionation of C^{13} and C^{12} in plants. *Plant Physiology*, **36**: 133-138.

Peel D. A. (1994). The Greenland Ice-Core Project (GRIP): reducing uncertainties in climatic changes? *NERC News*, **April** (26-30).

Peters K. E., Sweeney R. E. and Kaplan I. R. (1978). Correlation of carbon and nitrogen stable isotopes in sedimentary organic matter. *Limnology and Oceanography* **23**: 598– 604.

Poore R. Z., Dowsett H. J., Verardo S. and Quinn T. M. (2003). Millennial- to centuryscale variability in Gulf of Mexico Holocene climate records. *Paleoceanography*, **18**(2): 26–11.

Porter S. C. and An Z. (1995). Correlation between climatic events of the last glaciation in the North Atlantic and China. *Nature*, **375**: 305-308.

Prahl F. G., Bennett J. T. and Carpenter R. (1980). The early diagenesis of aliphatic hydrocarbons and organic matter in sedimentary particulates from Dabob Bay, Washington. *Geochimica et Cosmochimica Acta*, **44**: 1967-1976.

Premuzic E. T., Benkovitz C. M., Gaffney J. S. and Walsh J. J. (1982). The nature and distribution of organic matter in the surface sediments of world oceans and seas. *Organic Geochemistry*, **4**: 63-77.

Qu T., Song Y. T. and Yamagata T. (2009). An introduction to the South China Sea throughflow: Its dynamics, variability, and application for climate. *Dynamics of Atmospheres and Oceans*, **47**(1-3): 3-14.

Qu T. and Yamagata T. (2009). The South China Sea and its impact on climate. *Dynamics of Atmospheres and Oceans*, **47**(1-3): 1-2.

Raisbeck G. M., Yiou F., Jouzel J. and Petit J. R. (1990). ^{10}Be and ∂^2H in polar ice cores as a probe of the solar variability's influence on climate. *Philosophical Transactions of the Royal Society of London Series A*, **330**: 65-72.

Ramaswamy V., Gaye B., Shirodkar P. V., Rao P. S., Chivas A. R., Wheeler D. and Thwin S. (2008). Distribution and sources of organic carbon, nitrogen and their isotopic signatures in sediments from the Ayeyarwady (Irrawaddy) continental shelf, northern Andaman Sea. *Marine Chemistry*, **111**: 137-150.

Rampino M. R. and Self S. (1992). Bolcanic winter and accelerated glaciation following the Toba super-eruption. *Nature*, **359** 50-52.

Rampino M. R., Self S. and Fairbbridge R. W. (1979). Can rapid climatic change cause volcanic eruptions? *Nature*, **206**: 826-828.

Rankama K. (1948). A note on the original isotopic composition of terrestrial carbon. *Journal of Geology*, **56**: 199.

Rankama K. and Sahama T. G. (1950). *Geochemistry*. The University of Chicago Press, Chicago, 911.

Rea D. K. (1994). The palaeoclimatic record provided by eolian deposition in the deep sea: the geologic history of the wind. *Review of Geophysics*, **32**: 159-195.

Rea D. K. and Hovan S. A. (1995). Grain-size distribution and depositional processes of the Mineral component of abyssal sediments: lessons from the North Pacific. *Paleoceanography*, **12**: 251–258.

Rice D. L. and Tenore K. R. (1981). Dynamics of carbon and nitrogen during the decomposition of detritus derived from estuarine macrophytes. *Estuarine, Coastal and Shelf Science*, **13**: 681– 690.

Rind D. and Overpeck J. (1993). Hypothesied causes of decade-to-century-scale climate variability: climate model results. *Quaternary Science Reviews*, **12**: 357-374.

Rodbell D. T., Seltzer G. O., Anderson D. M., Abbott M. B., Enfield D. B. and Newman J. H. (1999). An ~15,000-year record of El Nino-driven alluviation in Southwestern Ecuador. *Science*, **283**: 516-520.

Rollinson H. R. (1993). *Using Geochemical Data: Evaluation, Presentation, and Interpretation*. Longman Scientific and Technical.

Ruddiman W. f. and Kutzbach J. E. (1990). Late Cenozoic plateau uplift and climate change. *Transactions of the Royoal Society of Edingburgh: Earth Science*, **81**: 301-314.

Sackett W. M., Eckelmann W. R., Bender M. L. and Bé A. W. H. (1965). Temperature dependence of carbon isotope composition in marine plankton and sediments. *Science*, **148**: 235-237.

Saia S. E. M. G., Pessenda L. C. R., Gouveia S. E. M., Aravena R. and Bendassolli J. A. (2008). Last glacial maximum (LGM) vegetation changes in the Atlantic Forest, southeastern Brazil. *Quaternary International*, **184**(1): 195-201.

Saito Y., Yang Z. and Hori K. (2001). The Huanghe (Yellow River) and Changjiang (Yangtze River) deltas: a review on their characteristics, evolution and sediment discharge during the Holocene. *Geomorphology*, **41**: 219-231.

Salomons W. and Mook W. G. (1981). Field observations of the isotopic composition of particulate organic carbon in the southern North Sea and adjacent estuaries. *Marine Geology*, **41**: M11–M20.

Sandweiss D. H., James B. Richardson I., Reitz E. J., Rollins H. B. and Maasch K. A. (1996). Geoarchaeological evidence from Peru for a 5000 years B.P. onset of El Niño. *Science*, **273**: 1531-1533.

Schidlowski M., Hayes J. M. and Kaplan I. R. (1983). Isotopic inferences of ancient biochemistries: carbon, sulphur, hydrogen and nitrogen, In 'Earth's Earliest Biosphere, Its Origin and Evolution', by Scholf J. W. (Eds.). Princeton University Press, Princeton: 149–186.

Schleser G. H. (1995). Parameters determining carbon isotope ratios in plants, In 'Problems of Stable Isotopes in Tree-Rings, Lake Sediments and Peat Bogs as Climate Evidence for the Holocene', by Frenzel B., Stauffer B. and Weib M. (Eds.). Fischer Verlag, Stuttgart: 71– 96.

Sewell R. J. (1999). *Geochemical atlas of Hong Kong*. Publications Office, Civil Engineering Department, Hong Kong SAR., Hong Kong.

Shi Y., Kong Z., Wang S., Tang L., Wang F., Yao T., Zhao X., Zhang P. and Shi S.

(1994). Climates and environments of the Holocene Megathermal Maximum in China. *science in China (Series B)*, **37**(4): 481-493.

Shindell D. T., Schmidt G. A., Mann M. E., Rind D. and Waple A. (2001). Solar forcing of regional climate change during the Maunder Minimum *Science*, **294**: 2149-2152.

Shultz D. J. and Calder J. A. (1976). Organic carbon 13C/12C variations in estuarine sediments. *Geochimica et Cosmochimica Acta*, **40**(4): 381-385.

Siegel F. R., Gupta N., Shergill B., Stanley D. J. and Gerber C. (1995). Geochemistry of Holocene sediments from the Nile Delta. *Journal of Coastal Research*, **11**(2): 415-431.

Smith B. N. and Epstein S. (1970). Biogeochemistry of the stable isotopes of hydrogen and carbon in salt marsh biota. *Plant Physiology*, **46**: 738-742.

Smittenberg R. H., Pancost R. D., Hopmans E. C., Paetzel M. and Damste J. S. S. (2004). A 400-year record of environmental change in an euxinic fjord as revealed by the sedimentary biomarker record. *Palaeogeography, Palaeoclimatology, Palaeoecology*, **202**: 331-351.

Southon J., Kashgarian M., Fontugne M., Metivier B. and Yim W. W.-S. (2002). Marine reservoir corrections for the Indian Ocean and southeast Asia. *Radiocarbon*, **44**(1): 167-180.

Spiker E. C. and Hatcher P. G. (1987). The effects of early diagenesis on the chemical and stable carbon isotopic composition of wood. *Geochimica et Cosmochimica Acta*, **51**: 1385-1391.

Sternberg L., DenNiro M. J. and Keeley J. E. (1984). Hydorgen, oxygen and carbon isotope ratios of cellulose from submerged aquatic crassulacean acid metabolism and non-crassulacean acid metabolism plants. *Plant Physiology*, **76**: 69-70.

St-Onge G. and Hillaire-Marcel C. (2001). Isotopic constraints of sedimentary inputs and organic carbon burial rates in the Saguenay Fjord, Quebec. *Marine Geology*, **176**: 1-22.

Stuiver M., Reimer P. J. and Braziunas T. F. (1998). High-precision radiocarbon age calibration for terrestrial and marine samples. *Radiocarbon*, **40**: 1127-1151.

Sun D. H., Liu T. S., Cheng M. Y., An Z. S. and Shaw J. (1997). Magnetostratigraphy and paleoclimate of Red Clay sequences from the Chinese Loess Plateau. *Science in China (Series D)*, **40**: 337-343.

Sun D. H., Shaw J., An Z. S., Cheng M. Y. and Yue L. P. (1998). Magnetostratigraphy and paleoclimatic interpretation of a continuous 7.2 Ma Late Cenozoic eolian sediments from the Chinese Loess Plateau. *Geophysical Research Letters*, **25**(1): 85-88.

Swarzenski P. W., Campbell P. L., Osterman L. E. and Poore R. Z. (2008). A 1000-year sediment record of recurring hypoxia off the Mississippi River: The potential role of terrestrially-derived organic matter inputs. *Marine Chemistry*, **109**: 130-142.

Talley L. D. (1996). North Pacific intermediate water formation and the role of the Okhotsk Sea, In 'Proceedings, Workshop on the Okhotsk Sea and Adjacent Areas, PECES Scientific Report (6)', 150-157.

Tam J., Taylor M. H., Blaskovic V., Espinoza P., Ballón R. M., Díaz E., Wosnitza-Mendo C., Argüelles J., Purca S., Ayón P., Quipuzcoa L., Gutiérrez D., Goya E., Ochoa N. and Wolff M. (2008). Trophic modeling of the Northern Humboldt Current Ecosystem, Part I: Comparing trophic linkages under La Niña and El Niño conditions. *Progress in Oceanography*, **79**: 352-365.

Tan Y., Huang L., Chen Q. and Huang X. (2004). Seasonal variation in zooplankton composition and grazing impact on phytoplankton standingstock in the Pearl River Estuary, China. *Continental Shelf Research*, **24**: 1949-1968.

Taylor M. H., Tam J., Blaskovic V., Espinoza P., Ballón R. M., Wosnitza-Mendo C., Argüelles J., Díaz E., Purca S., Ochoa N., Ayón P., Goya E., Gutiérrez D., Quipuzcoa L. and Wolff M. (2008). Trophic modeling of the Northern Humboldt Current Ecosystem, Part II: Elucidating ecosystem dynamics from 1995 to 2004 with a focus on the impact of ENSO. *Progress in Oceanography*, **79**: 366-378.

Teeri J. A. and Stowe L. G. (1976). Climatic patterns and the distribution of C4 grasses in North America. *Oecologia (Berl.)* **23**: 1-12.

Tesi T., Miserocchi S., Goñi M. A. and Langone L. (2007a). Source, transport and fate of terrestrial organic carbon on the western Mediterranean Sea, Gulf of Lions, France. *Marine Chemistry*, **105**(1-2): 101-117.

Tesi T., Miserocchi S., Goñi M. A., Langone L., Boldrin A. and Turchetto M. (2007b). Organic matter origin and distribution in suspended particulate materials and surficial sediments from the western Adriatic Sea (Italy). *Estuarine, Coastal and Shelf Science*, **73**(3-4): 431-446.

Thompson L. G., Moseley-Thompson E., Davis M. E., Lin P. N., Yao T., Dyurgerov M., Dai J., Faure H., Faure-Denard L. and Liu T. (1993). Recent warming: ice core evidence from tropical ice cores with emphasis on central Asia. *Global and Planetary Change*, **7**(1-3): 145-156.

Thompson L. G., Mosley-Thompson E., Davis M. E., Henderson K. A., Brecher H. H., Zagorodnov V. S., Mashiotta T. A., Lin P.-N., Mikhalenko V. N., Hardy D. R. and Beer J. (2002). Kilimanjaro ice core records: evidence of Holocene climate change in tropical Africa. *Science*, **298**(589): 589-593.

Thompson L. G., Mosley-Thompson E., Davis M. E., Lin P.-N., Henderson K. and Mashiotta T. A. (2003). Tropical glacier and ice core evidence of climate change on annual to millennial time scales *Climatic Change*, **59**: 137-155.

Thompson L. G., Thompson M. E., Davis M. E., Bolzan J. F., Dai J., Yao T., Gundestrup N., Wu X., Klein L. and Xie Z. (1989). Holocene-late Pleistocene climatic ice core records from the Qinghai-Tibetan Plateau. *Science*, **246**: 474-477.

Tsukada M. (1967). Vegetation in subtropical Formosa during the Pleistocene and the Holocene *Paleogeography, Paleoclimatology, Paleoecology*, **3**: 49–64.

Tudhope A. W., Chilcott C. P., McCulloch M. T., Cook E. R., Chappell J, Ellam R. M., Lea D. W., Lough J. M. and Shimmield G. B. (2001). Variability in the El Nino Southern Oscillation Through a Glacial-Interglacial Cycle. *Science*, **291**: 1511-

1517.

Tyson R. V. (1995). *Sedimentary Organic Matter: Organic Facies and Palynofacies.* Chapman and Hall, London.

Valiela I. (1995). *Marine Ecological Processes* Springer-Verlag, New York.

Valiela I., Teal J. M. and Allen S. D. (1985). Decomposition in salt marsh ecosystems: the phases and major factors affecting disappearance of above-ground organic matter. *Journal of Experimental Marine Biology and Ecology*, **89**: 29-54.

Van der Hammen T. and Absy M. L. (1994). Amazonia during the last glacial. *Palaeogeography, Palaeoclimatology, Palaeoecology*, **109**: 247-261.

Vecoli M., Riboulleau A. and Versteegh G. (2009). Palynology, organic geochemistry and carbon isotope analysis of a latest Ordovician through Silurian clastic succession from borehole Tt1, Ghadamis Basin, southern Tunisia, North Africa: Palaeoenvironmental interpretation. *Palaeogeography, Palaeoclimatology, Palaeoecology*, **273**(3-4): 378-394.

Vigdorchik M. E. (1980). *Submarine Permafrost on the Alaska Continental Shelf.* Westview Press, Boulder, CO, 118.

Wada E., Minagawa M., Mizutani H., Tsuji T., Imaizumi R. and Karasawa K. (1987). Biogeochemical studies on the transport of organic matter along the Otsuchi River watershed, Japan. *Estuarine, Coastal and Shelf Science*, **25**: 321-336.

Wang P. and Chappell J. (2001). Foraminifera as Holocene environmental indicators in the South Alligator River, Northern Australia. *Quaternary International*, **83-85**: 47-62.

Wang P. X. (2005). Cenozoic deformation and the history of Sea-land interactions in Asia. *Earth Science - Journal of China University of Geoscience*, **30**(1): 1-18.

Wang X.-C., Chen R. F. and Berry A. (2003). Sources and preservation of organic matter in Plum Island salt marsh sediments (MA, USA): long-chain n-alkanes and stable carbon isotope compositions. *Estuarine, Coastal and Shelf Science*, **58**: 917– 928.

Wang Y., Cheng H., Edwards R. L., He Y., Kong X., An Z., Wu J., Kelly M. J., Dykoski C. A. and Li X. (2005). The Holocene Asian Monsoon: Links to Solar Changes and North Atlantic Climate. *Science*, **308**: 854-857.

Wang Y. J., Cheng H., Edwards R. L., An Z. S., Wu J. Y., Shen C.-C. and Dorale J. A. (2001). A high-resolution absolute-dated late Pleistocene monsoon record from Hulu Cave, China. *Science*, **294**: 2345-2348.

Webb III T., Ruddiman W. R., Street-Perrott F. A., Markgraf V., Kulzbach J. E., Bartlein P. J. and H.E. Wright J. (1993). Climatic changes during the past 18,000 years: regional syntheses, mechanisms and causes, In 'Global Climates since the Last Glacial Maximum', by Wright H. E., Kutzbach J. E., Webb III T., Ruddiman W. E., Street-Perrott F. A. and Bartlein P. J. (Eds.). University of Minnesota Press, Minneapolis, MN: 514-535.

Webster P. J., Magaña V. O., Palmer T. N., Shukla J. and Tomas R. A. (1998). Monsoons: Processes, predictability, and the prospects for prediction. *Journal of Geophysical Research*, **103**(C7): 14451-14510.

Wen W. Y. and He Y. Q. (1987). An analysis of sediment pollution status quo in Pearl River estuary, In 'Investigation Report of Coastal Environment Quality in Guangdong Province'. China Ocean Press, Beijing: 112–122 (in Chinese).

Westman P. and Hedenström A. (2002). Environmental changes during isolation processes from the Litorina Sea as reflected by diatoms

and geochemical parameters—a case study. *The Holocene*, **12**: 531–540.

White D. S. and Howes B. L. (1994). Nitrogen incorporation into decomposing litter of Spartina alterniflora. . *Limnology and Oceanography*, **39**: 133-140.

Wickman F. E. (1952). Variations in the relative abundance of the carbon isotopes in plants. *Geochimica et Cosmochimica Acta*, **2**(4): 243-254.

Widmann M. and Tett S. F. B. (2003). Simulating the climate of the last millennium. *Pages News*, **11**: 21-23.

Williams D. F., Peck J., Karabanov E. B., Prokopenko A. A., Kravchinsky V., King J. and Kuzmin M. L. (1997). Lake Baikal record of continental climate response to orbital insolation during the past 5 million years. *Science*, **278**: 1114-1117.

Wilson G. P., Lamb A. L., Leng M. J., Gonzalez S. and Huddart D. (2004). The potential of carbon isotope ratios as indicators of coastal palaeoenvironmental change: preliminary results from the Mersey Estuary, North West England, In 'The Quaternary of the Isle of Man and North West England: Field Guide', by Chiverrell R. C., Plater A. J. and Thomas G. S. P. (Eds.). Quaternary Research Association, London: 217– 225.

Wilson G. P., Lamb A. L., Leng M. J., Gonzalez S. and Huddart D. (2005a). Variability of organic δ^{13}C and C/N in the Mersey Estuary, U.K. and its implications for sea-level reconstruction studies. *Estuarine, Coastal and Shelf Science*, **64**: 685-698.

Wilson G. P., Lamb A. L., Leng M. J., Gonzalez S. and Huddart D. (2005b). δ^{13}C and C/N as potentialcoastalpal aeoenvironmental indicators in the Mersey Estuary, UK. *Quaternary Science Reviews*, **24**: 2015-2029.

Winkler M. G. and Wang P. K. (1993). The late Quaternary vegetation and climate of China, In 'Global Climates Since The Last Glacial Maximum', by Wright W. H. E., Jr., Kutzbach J. E., Webb III T., Ruddiman W. F., Street-Perrott F. A. and Bartlein P. J. (Eds.). University of Minnesoda Press, Minneapolis, MN: 221–264.

Woodroffe C. D., Beech M. R. and Gagan M. K. (2003). Mid-late Holocene El Nino variability in the equatorial Pacific from coral microatolls. *Geophysical Research Letters*, **30**(7): 1358, doi:10.1029/2002GL015868.

Woods A. (2009). *Tracing the distribution of heavy metals in the sediments of the Pearl River estuary: the true anthropogenic signature and environmental forcing*, **MSc thesis, University of Durham.**

Wright H. E., Kutzbach J. E., Webb III T., Ruddiman W. E., Street-Perrott F. A. and Bartlein P. J. (1993). *Global Climates Since the Last Glacial Maximum.* University of Minnesota Press, Minneapolis, MN, 547.

Wu X. D. (1992). Dendroclimatic study in China, In 'Climatic Since AD 1500', by

Bradley R. and Jones P. (Eds.). Routledge, London: 432-445.

Wu X. D., Lin Z. Y. and Sun L. (1988). A preliminary study on the climatic change of Hengduan Moutains area since AD 1600. *Advances in Atmospheric Sciences*, **5**: 437-443.

Wu Y., Dittmar T., Ludwichowski K.-U., Kattner G., Zhang J., Zhu Z. Y. and Koch B. P. (2007). Tracing suspended organic nitrogen from the Yangtze River catchment into the East China Sea. *Marine Chemistry*, **107**(3): 367-377.

Xiao J., Nakamura T., Lu H. and Zhang G. (2002). Holocene climate changes over the desert/loess transition of north-central China. *Earth and Planetary Science Letters*, **197**: 11-18.

Xiao J., Wang J., An Z., wu X. and Zhou W. (1998). Evidence for the Younger Dryas event in the eastern part of Nanling region. *Acta Botanica Sinica*, **40**(11): 1079-1082.

Xiao S., Li A., Liu J. P., Chen M., Xie Q., Jiang F., Li T., Xiang R. and Chen Z. (2006). Coherence between solar activity and the East Asian winter monsoon variability in the past 8000 years from Yangtze River-derived mud in the East China Sea. *Palaeogeography, Palaeoclimatology, Palaeoecology*, **237**(2-4): 293-304.

Xu J., Li Y., Cai F. and Chen Q. (1985). *The morphology of the Pearl River estuary*. China Ocean Press, Beijing.

Xu X. J. and Zhang X. G. (1983). The distribution and trend of droughts and floods in east China during the last 500 years. In *'Paper Collections of Meteorology Sciences (4)'*, Meteorology Press, Beijing.

Yamaguchi H., Montani S., Tsutsumi H., Hamada K. and Ueda N. (2003). Estimation of particulate organic carbon flux in relation to photosynthetic production in a shallow coastal area in the Seto Inland Sea. *Marine Pollution Bulletin,* **47**: 18-24.

Yamamuro M. (2000). Chemical tracers of sediment organic matter origins in two coastal lagoons. *Journal of Marine Systems*, **26**: 127–134.

Yang G., Chen Z., Yu F., Wang Z., Zhao Y. and Wang Z. (2007). Sediment rating

curve parameters and their implications: Yangtze River, China. *Geomorphology*, **85**: 166-175.

Yang S., Wang W., Zhang W. and Zhang Y. (2004). Study on ecosystemeffect and the remediation methods of arsenic pollution in water and soil system. *Journal of Ear th Sciences and Environment*, **2**(3): 69-73 (in Chinese, with English abstract).

Yang S., Yim W. W.-S. and Huang G. (2008). Geochemical composition of inner shelf Quaternary sediments in the northern South China Sea with implications for provenance discrimination and paleoenvironmental reconstruction. *Global and Planetary Change*, **60**: 207-221.

Yim W. W.-S. (1994). Offshore Quaternary sediments and their engineering significance in Hong Kong. *Engineering Geology*, **37**: 31-50.

Yim W. W.-S., Huang G., Fontugne M. R., Hale R. E., Paterne M., Pirazzoli P. A. and Ridley Thomas W. N. (2006). Postglacial sealevel changes in the northern South China Sea continental shelf: evidence for a post-8200 calendar year meltwater pulse. *Quaternary International*, (145/146): 55–67.

Yin K., Qian, P.-Y., Chen, J.C., Hsieh, D.P.H., Harrison, P.J., (2000). Dynamics of nutrients and phytoplankton biomass in the Pearl River estuary and adjacent waters of Hong Kong during summer: preliminary evidence for phosphorus and silicon limitation. *Marine Ecology Progress Series*, **194**: 295–305.

Yin K., Zhang J., Qian P.-Y., Jian W., Huang L., Chen J. and Wu M. C. S. (2004). Effect of wind events on phytoplankton blooms in the Pearl River estuary during summer. *Continental Shelf Research*, **24**: 1909-1923.

Yiou F., Raisbeck G. M., Baumgartner S., Beer J., Hammer C., Johnsen S., Jouzel J., Kubik P. W., Lestringuez J., Stiévenard M., Suter M. and Yiou P. (1997). Beryllium-10 in the Greenland Ice Core Project ice core at Summit, Greenland. *Journal of Geophysical Research*, **102**: 26783–26794.

Yu F. (2006). Suspended sediment rating curve of the Yangtze (Changjiang) River, eastern China: characteristics, interpretations and practices. *MSc thesis*. East China

Normal University, Shanghai, China (in Chinese with English abstract).

Yu G., Ke X. and Scott A. E. (2007). Lake level studies | Asia, In 'Encyclopedia of Quaternary Science'. Elsevier, Oxford: 1343-1359.

Yu K.-F., Zhao J.-X., Wei G.-J., Cheng X.-R. and Wang P.-X. (2005). Mid–late Holocene monsoon climate retrieved from seasonal Sr/Ca and d18O records of Porites lutea corals at Leizhou Peninsula, northern coast of South China Sea. *Global and Planetary Change*, **47**: 301-316.

Yu Z. and Ito E. (1999). Possible solar forcing of century-scale drought frequency in the northern Great Plains. *Geology* **27**: 263–266.

Yuan D., Cheng H., Edwards R. L., Dykoski C. A., Kelly M. J., zhang M., Qing J., Lin Y., Wang Y., Wu J., Dorale J. A., An Z. and Cai Y. (2004). Timing, duration, and transitions of the last interglaical Asian monsoon. *Science*, **304**: 575-578.

Zechun L. (1991). *Quaternary sediment and environmental changes*. Southeast Culture Printing House, Nanjing, 182-199.

Zhang D. E. (1995). High resolution records available from Chinese historical documents. *Quanternary Science*, **1**: 76-81.

Zhang J. (1995). Geochemistry of trace metals from Chinese river/estuary systems: an overview. *Estuarine, Coastal and Shelf Science*, **41**: 631-658.

Zhang J. (1995). Geochemistry of trace metals from Chinese river/estuary systems: an overview. *Estuarine and Coastal Marine Science*, **41**: 631-658.

Zhang J., Wu Y., Jennerjahn T. C., Ittekkot V. and He Q. (2007). Distribution of organic matter in the Changjiang (Yangtze River) Estuary and their stable carbon and nitrogen isotopic ratios: Implications for source discrimination and sedimentary dynamics. *Marine Chemistry*, **106**(1-2): 111-126.

Zhang J., Yu Z. G., Liu S. M., Xu H., Wen Q. B., Shao B. and Chen J. F. (1997). Dominance of terrigenous particulate organic carbon in the high-turbidity Shuangtaizihe estuary. *Chemical Geology*, **138**: 211-219.

Zhang J., Zhang Z. F., Liu S. M., Wu Y., Xiong H. and Chen H. T. (1999). Human impacts on the large world rivers: would the Changjiang (Yangtze River) be an illustration? *Global Biogeochemistry Cycles*, **13**: 1099-1105.

Zhang J. C. (1983). The droughts and floods in China during the last 500 years, In 'Paper Collections of Meteorology Sciences (4)'. Meteorology Press, Beijing:

Zhang P. Y., Wang Z., Liu X. L. and Zhang S. H. (1994). The stages of climate evolution in China during the last 2000 years. *Science in China (Series B)*, **24**: 998-1008.

Zhang S. R., Lu X. X., Higgitt D. L., Chen C. T. A., Han J, T. and Sun H. G. (2007a). Recent changes of water discharge and sediment load in the Zhujiang (Pearl River) Basin, China, *Global and Planetary Change*, in press: doi:10.1016/j.gloplacha.2007.04.003.

Zhang S., Lu X. X., Higgitt D. L., Chen C.-T. A., Han J. and Sun H. (2008). Recent changes of water discharge and sediment load in the Zhujiang (Pearl River) Basin, China. *Global and Planetary Change*, **60**: 365-380.

Zhang S. R., Lu X. X., Higgitt D. L., Chen C. T. A., Sun H. G. and Han J. T. (2007b). Water chemistry of the Zhujiang (Pearl River): Natural processes and anthropogenic influences, *Journal of Geophysical Research*, **112**: doi:10.1029/2006JF000493.

Zheng Z. and Lei Z.-Q. (1999). A 400,000 year record of vegetational and climatic changes from a volcanic basin, Leizhou Peninsula, southern China. *Palaeogeography, Paleoclimatology, Palaeoecology*, **145**: 339-362.

Zhou H., Peng X. and Pan J. (2004). Distribution, source and enrichment of some chemical elements in sediments of the Pearl River Estuary, China. *Continental Shelf Research*, **24**: 1857-1875.

Zhou K. (1991). *Researches of Environment Archaeology (I)*. Science Press, Beijing, 236.

Zhou W. J., An Z. S., Porter S. C., Donahue D. J. and Jull A. J. T. (1997).

Correlation of climatic events between East Asia and Norwegian Sea during the last deglaciation. *Science in China (Series D)*, **40**: 496-501.

Zhou W. J., Donahue D. J., Porter S. C., Jull A. J. T., Li X. Q., Stuiver M., An Z. S., Matsumoto E. and Dong G. R. (1996). Variability of monsoon climate in East Asia at the end of the Last Glaciation. *Quaternary Research*, **46**: 219-229.

Zhou W. J., Jull A. J. T., Donahue D. J. and Head M. J. (1998). Reappraisal of Chinese Loess Plateau stratigraphy sequence over the last 30,000 yr: precursors of an important Holocene monsoon climatic event. *Radiocarbon*, **40**(2): 905-913.

Zielinski G. A., Mayewski D. A., Meeker L. D., Whitlow S. and Twickler M. S. (1996). Potential atmospheric impact of the Toba mega – eruption ~71 000 years ago. . *Geophysical Research Letter*, **23**: 837-840.

Zong Y. (1989). On depositional cycles and geomorphological development of the Han River Delta of South China. *Zeitschrift fur Geomophologie Neues Funde*, **73**: 33-48.

Zong Y. (2004). Mid-Holocene sea-level highstand along the Southeast Coast of China. *Quaternary International*, **117**: 55-67.

Zong Y., Huang G., Switzer A. D., Yu F. and Yim W. W.-S. (2009a). An evolutionary model for the Holocene formation of the Pearl River delta, China. *The Holocene*, **19**: 129-142.

Zong Y., Lloyd J. M., Leng M. J., Yim W. W.-S. and Huang G. (2006). Reconstruction of Holocene monsoon history from the Pearl River Estuary, southern China, using diatoms and carbon isotope ratios. *The Holocene*, **16**(2): 251-263.

Zong Y., Yim W. W.-S., Yu F. and Huang G. (2009b). Late Quaternary environmental changes in the Pearl River mouth region, China. *Quaternary International*, doi:10.1016/j.quaint.2008.10.012.

Appendices

Appendix 1 Organic carbon results of the plants samples and their sampling sites.

			$\delta^{13}C$ (‰)	TOC (%)	TN (%)	C/N	Type	Label	Site
C$_3$ plants	General terrestrial C$_3$ plants		-28.5	41.6	3.1	13.4	C$_3$ Plant	B1	N1
			-29.9	46.7	3.7	12.5	C$_3$ Plant	B2	N2
			-29.3	42.0	2.3	18.1	C$_3$ Plant	B3	N2
			-28.1	43.3	5.9	7.4	C$_3$ Plant	B4	N2
			-30.3	45.3	3.9	11.5	C$_3$ Plant	B5	N3
			-28.1	40.1	1.9	21.4	C$_3$ Plant	B6	N3
			-31.0	45.3	1.8	25.4	C$_3$ Plant	B7	N3
			-29.9	40.9	2.9	14.0	C$_3$ Plant	B8	N3
			-28.3	41.1	4.2	9.8	C$_3$ Plant	B9	N4
			-29.6	42.3	2.0	21.0	C$_3$ Plant	B10	N4
			-29.6	38.6	2.0	19.1	C$_3$ Plant	B11	N4
			-31.4	45.1	1.4	31.2	C$_3$ Plant	B12	N4
			-30.2	44.3	2.1	20.8	C$_3$ Plant	B13	N4
			-30.7	36.6	1.9	19.2	C$_3$ Plant	B14	N5
			-28.9	37.0	3.5	10.7	C$_3$ Plant	B15	N5
			-29.5	39.2	2.4	16.3	C$_3$ Plant	B16	N5
			-28.7	39.6	3.8	10.4	C$_3$ Plant	B17	N5
			-28.7	48.1	0.8	61.8	C$_3$ Plant	B18	N6
			-28.3	44.9	1.4	31.1	C$_3$ Plant	B19	N6
			-30.6	42.2	1.9	22.2	C$_3$ Plant	B20	N6
			-30.9	44.4	2.1	20.9	C$_3$ Plant	B21	N6
			-30.2	47.2	1.6	30.3	C$_3$ Plant	B22	N6
			-29.9	38.0	1.9	20.1	C$_3$ Plant	B23	N6
			-32.6	43.2	2.1	20.5	C$_3$ Plant	B24	N6
			-31.7	39.2	1.7	23.5	C$_3$ Plant	B25	N6
			-30.4	40.8	1.9	21.7	C$_3$ Plant	B26	N6
			-31.6	42.3	3.1	13.5	C$_3$ Plant	B27	N6
			-30.0	41.1	1.2	33.3	C$_3$ Plant	B28	N6
			-31.8	40.3	0.9	43.1	C$_3$ Plant	B29	N6
			-28.0	45.6	2.1	21.6	C$_3$ Plant	B31	E1
			-28.3	48.1	1.6	30.2	C$_3$ Plant	B32	E1
			-28.4	35.2	2.4	14.6	C$_3$ Plant	B35	E1
			-32.1	48.0	2.0	24.2	C$_3$ Plant	B47	E1
		Ave.	*-29.9 ±1.3*	*42.3 ±3.5*	*2.4 ±1.1*	*21.7 ±10.7*			
	Agricultural C$_3$ plants		-28.2	42.0	2.8	15.1	Reeds	F3	E5
			-30.2	35.7	2.3	15.3	Reeds	F5	E5
			-28.7	38.0	3.4	11.1	Rice	F10	E5
			-28.6	40.0	3.3	12.2	Rice	F11	E5
			-28.9	39.4	3.5	11.1	Rice	F13	E5
			-27.3	43.2	2.4	18.3	Banana	F12	E5
			-25.8	44.1	3.5	12.6	Lotus	F14	E5
		Ave.	*-28.2 ±1.4*	*40.3 ±3.0*	*3.0 ±0.5*	*13.7 ±2.7*			
	Mangroves		-28.9	45.3	2.0	22.5	Avicennia	B30	E2
			-27.9	46.6	1.4	32.8	Kandelia obovata, Rhizophoraceae	B36	E3
			-28.1	49.1	0.9	53.2	Kandelia obovata, Rhizophoraceae	B45	E4
			-28.5	45.8	1.3	34.5	Kandelia obovato, Rhizophoraceae	B42	E4
			-25.0	43.6	0.9	46.3	Bruguiera gymhorrhiza, Rhizophoraceae	B44	E4
			-25.0	42.2	2.2	19.1	Acanthus ilicifolius, flowers	B37	E3
			-24.0	40.7	3.0	13.4	Aegiceras corniculatum, Myrsinaceae	B38	E3
			-28.4	46.7	1.3	36.6	Acanthus ilicifolius, Acanthaceae	B40	E3
			-25.6	41.1	1.8	22.4	Acanthus ilicifolius, Acanthaceae	B41	E3
			-28.3	45.4	1.7	27.2	Avicennia marina, Avicenniaceae	B43	E4
			-28.1	44.2	1.0	45.2	Ficus microcarpa, Moraceae	B39	E3
			-27.4	45.1	2.3	19.4	Ficus microcarpa, Moraceae	B46	E4
		Ave.	*-27.1 ±1.7*	*44.6 ±2.4*	*1.7 ±0.6*	*31.0 ±12.5*			
		Ave.	-29.0 ±1.8	42.6 ±3.4	2.3 ±1.0	22.7 ±11.6			
C$_4$ plants	General C$_4$ plants		-13.1	35.5	4.3	8.2	C$_4$ grass	F6	E5
			-13.2	39.8	1.2	33.1	C$_4$ grass	F1	E5
			-13.7	40.0	1.7	23.9	C$_4$ grass	F2	E5
			-13.7	41.2	1.7	23.8	C$_4$ grass	B33	E1
			-13.3	38.8	1.5	26.1	C$_4$ grass	B34	E1
			-12.3	39.7	2.8	14.2	C$_4$ grass	F4	E5
		Ave.	*-13.2 ±0.5*	*39.2 ±1.9*	*2.2 ±1.2*	*21.5 ±8.9*			
	Agricultural C$_4$ plants		-12.9	41.6	1.0	40.3	sugarcane	F7	E5
			-12.8	42.4	1.6	25.9	sugarcane	F8	E5
			-12.5	41.4	1.6	25.6	sugarcane	F9	E5
		Ave.	*-12.7 ±0.2*	*41.8 ±0.5*	*1.4 ±0.3*	*30.6 ±8.4*			
		Ave.	-13.1 ±0.5	40 ±2.0	1.9 ±1.0	24.6 ±9.4			

Appendix 2 Organic carbon results of the soil samples and their sampling sites.

	δ¹³C (‰)	TOC (%)	TN (%)	C/N	Label	Site
Forest soil	-28.9	2.7	0.2	15.4	A5	N4
	-27.7	3.9	0.2	20.4	A9	N6
Ave.	*-28.3 ±0.8*	*3.3 ±0.9*	*0.2 ±0.0*	*17.9 ±3.6*		
Riverbank soil	-23.2	1.9	0.2	12.1	A1	N1
	-22.9	1.2	0.1	9.8	A2	N2
	-24.9	2.0	0.2	12.7	A3	N3
	-23.6	1.4	0.1	11.1	A4	N4
	-25.0	2.6	0.1	17.3	A6	N4
	-23.6	0.9	0.1	10.7	A7	N5
	-24.0	3.1	0.2	13.4	A8	N5
	-25.6	3.4	0.3	12.7	G1	E5
Ave.	*-24.1 ±1.0*	*2.1 ±1.0*	*0.2 ±0.1*	*12.5 ±2.3*		
Mangrove soil	-25.6	2.7	0.3	9.7	A10	E3
	-23.8	1.1	0.1	8.6	A11	E3
	-24.7	1.8	0.2	9.3	A12	E3
	-24.2	2.4	0.2	11.4	A13	E3
	-26.1	1.8	0.1	12.9	A14	E3
	-25.4	1.1	0.1	11.0	A15	E3
	-19.3	4.4	0.3	15.7	A16	E3
	-22.5	0.9	0.0	19.3	A17	E3
	-25.8	2.4	0.1	18.8	A18	E4
	-23.0	2.5	0.2	10.4	A19	E4
	-23.8	0.7	0.1	10.7	A20	E4
	-24.0	1.5	0.1	10.8	PE76	E1
Ave.	*-24.0 ±1.9*	*1.9 ±1.0*	*0.2 ±0.1*	*12.4 ±3.6*		
Agricultural soil	-21.2	1.6	0.2	9.9	G2	E5
	-22.5	1.7	0.2	9.1	G3	E5
	-21.5	2.3	0.3	7.7	G4	E5
Ave.	*-21.7 ±0.7*	*1.9 ±0.4*	*0.2 ±0.1*	*8.9 ±1.1*		

Appendix 3 Results of the POC samples and environmental parameters of the sampling sites (to be continued).

Gr.		δ^{13}C-W (‰)	C/N-W	δ^{13}C-S (‰)	C/N-S	Sal-W (‰)	Sal-S (‰)	PH-W	PH-S	TDS-W (g/l)	TDS-S (g/l)	DO-W (%)	DO-S (%)	Temp-W (°C)	Temp-S (°C)
	PE 41	-27.3	6.4	-25.0	8.3	0.9	0.1	7.7	7.5	1.2	0.1	98.5	79.3	17.4	28.2
	PE 42		6.6	-25.4	9.0	0.2	0.1	7.5	7.4	0.2	0.1	94.0	79.6	16.9	29.2
	PE43	-27.8	6.9	-25.2	8.6	0.1	0.1	7.5	7.4	0.2	0.1	93.0	94.0	17.2	28.9
G2	PE 44	-28.5	6.9	-25.2	8.5	0.1	0.1	7.6	7.4	0.2	0.1	93.3	88.6	17.1	28.8
	PE 45	-28.3	6.5	-25.4	8.1	0.1	0.1	7.5	7.4	0.2	0.1	94.0	88.7	16.7	28.9
	PE 46	-27.5	8.1	-24.8	9.0	0.1	0.1	7.5	7.4	0.2	0.1	96.5	87.8	16.6	28.8
	PE 47	-26.2	6.5	-23.3	9.6	0.1	0.1	7.6	7.5	0.2	0.2	85.5	81.0	17.7	27.9
Ave.		*-27.6±0.8*	*6.8±0.6*	*-24.9±0.7*	*8.7±0.5*	*0.2±0.3*	*0.1±0.0*	*7.5±0.1*	*7.4±0.0*	*0.3±0.4*	*0.1±0.0*	*93.5±4.1*	*85.6±5.6*	*17.1±0.4*	*28.7±0.4*
	PE 48			-23.0	10.0	0.8	0.1	7.6	7.6		0.2		92.1		27.8
	PE 49	-24.7	7.5	-22.9	9.9	0.5	0.1	7.6	7.5	0.6	0.2	87.5	84.8	17.5	28.0
	PE 50	-26.0	7.6	-23.4	7.6	1.8	0.1	7.6	7.5	2.2	0.2	89.5	75.1	17.6	27.8
	PE 51	-25.2	7.5	-24.3	11.3	1.5	0.1	7.6	7.6	1.8	0.2	89.0	76.3	17.7	27.8
G4	PE 52	-26.0	7.5	-23.6	10.2	1.5	0.1	7.6	7.7	1.9	0.2	90.2	76.3	17.6	27.9
	PE 53	-26.0	7.3	-24.1	10.1	4.3	0.1	7.7	7.6	5.0	0.2	101.9	72.5	17.2	28.1
	PE 56	-24.7	7.2	-24.8	9.2	12.5	0.1	7.8	7.8	13.5	0.2	115.0	83.8	16.6	27.8
	PE 54	-27.7	6.4	-25.6	6.9	2.3	0.1	7.7	7.6	2.8	0.2	96.6	73.8	17.6	27.7
Ave.		*-25.8±1.0*	*7.3±0.4*	*-24.0±0.9*	*9.4±1.5*	*3.1±4.0*	*0.1±0.0*	*7.7±0.1*	*7.6±0.1*	*4.0±4.4*	*0.2±0.0*	*95.7±9.9*	*79.3±6.8*	*17.4±0.4*	*27.8±0.1*
	PE 76					4.8	0.1								
	PE 55	-26.4	6.8	-24.9	8.8	6.3	0.1	7.8	7.7	7.2	0.2	106.6	84.5	17.1	27.6
G3	PE 59	-23.7	6.5	-25.9	8.1	23.1	2.9	8.0	7.9	23.6	3.8	112.0	86.5	18.3	28.5
	PE 60	-24.0	7.7	-26.1	8.8	26.9	5.9	8.0	7.8	27.1	6.9	109.9	79.7	18.5	28.3
	PE 61	-23.9	7.7	-24.7	9.8	22.1	4.0	7.9	7.7	22.8	4.6	108.7	77.2	18.6	28.4
Ave.		*-24.5±1.3*	*7.2±0.6*	*-25.4±0.7*	*8.9±0.7*	*16.6±10.3*	*2.6±2.5*	*7.9±0.1*	*7.7±0.1*	*20.2±8.9*	*3.9±2.8*	*109.3±2.3*	*82.0±4.3*	*18.1±0.7*	*28.2±0.4*

S: summer; W: winter; 'Gr.' shows different clustering groups of the POC samples.

Gr.		δ¹³C-W (‰)	C/N-W	δ¹³C-S (‰)	C/N-S	Sal-W (‰)	Sal-S (‰)	PH-W	PH-S	TDS-W (g/l)	TDS-S (g/l)	DO-W (%)	DO-S (%)	Temp-W (ºC)	Temp-S (ºC)
	PE 69	-22.3	7.5	-24.4	8.8	31.5	3.4	8.1	8.2	31.3	4.7	113.2	80.4	18.1	28.1
	PE 70	-21.6	8.3	-25.7	10.6	33.6	6.6	8.15	8.1	33.2	7.6	111.6	79.6	18.6	28.2
	PE 71	-22.5	6.8	-26.1		33.9	5.8	8.1	8.1	33.5	6.7	110.7	81.2	18.5	28.2
	PE 72	-21.8	8.6	-25.6		32.8	3.6	8.1	8.3	32.5	4.3	116.8	86.4	18.1	28.2
	PE 73	-21.7	8.7	-25.7		32.3	5.7	8.2	8.2	32.0	7.7	113.1	93.7	18.1	28.2
	PE 64	-23.9	8.4	-23.3	10.1	18.6	0.2	8.0	8.0	19.5	0.2	113.6	97.0	17.0	28.8
	PE 57	-24.0	9.9	-23.0	9.8	11.8	0.1	7.9	7.9	12.8	0.2	116.0	92.3	16.5	27.9
	PE 58	-24.8	6.1	-23.1	11.4	13.1	1.0	7.9	7.9	14.1	1.4	115.7	89.2	17.1	28.1
G5	PE 62	-25.2	7.3	-23.0	9.9	11.6	0.2	7.9	8.1	12.6	0.2	104.0	86.1	17.4	27.9
	PE 63	-23.8	8.9	-23.3	8.0	13.4	0.1	7.9	8.0	14.0	0.2	114.3	100.1	16.6	28.6
	PE 75	-25.0	8.9	-22.9	11.3	14.1	0.1	7.9	8.0	14.8	0.2	113.0	102.8	17.5	28.2
	PE 77					14.8	7.0								
	PE 65	-23.6	7.3	-24.1	8.7	22.2	0.8	8.1	8.0	22.8	1.1	113.0	92.7	17.1	29.1
	PE 66	-24.5	8.2	-24.6	8.1	23.9	5.5	8.0	7.9	24.4	6.5	115.0	90.2	16.9	29.5
	PE 67	-24.9	6.5	-24.7	9.6	22.3	2.7	8.0	8.3	22.9	3.3	117.0	88.1	16.9	29.1
	PE 68	-25.1	6.8	-24.6	9.4	25.7	4.9	8.1	8.2	26.7	5.7	117.2	85.1	17.6	28.2
	PE 74	-23.9	6.8	-25.1	8.2	24.3	2.0	8.1	8.0	24.8	2.3	115.4	88.7	17.6	28.3
	PE 78	-23.4	7.1			25.4	13.5	7.9		25.8		91.6		17.6	
	PE 79	-23.2	6.4			25.5	15.2	8.0		25.9		95.8		17.9	
	PE 80	-22.9	6.9			16.9	18.2	7.9		27.2		93.6		18.2	
	PE 81	-24.3	7.1			18.1	15.8	7.8		28.7		94.7		18.0	
Ave.		*-23.6±1.2*	*7.6±1.0*	*-24.3±1.1*	*9.5±1.2*	*22.2±7.6*	*5.4±5.7*	*8.0±0.1*	*8.1±0.1*	*24.0±7.2*	*3.3±2.9*	*109.8±8.6*	*89.6±6.7*	*17.6±0.6*	*28.4±0.5*
	PE 82	-23.0	7.2			32.9	18.6	7.9		32.5		96.4		18.8	
	PE 83	-22.6	6.9			31.9	22.0	8.1		31.7		96.0		19.0	
	PE 84	-23.3	5.9			30.9	20.3	8.1		30.6		99.0		19.2	
	PE 85	-21.9	5.7			35.0	24.0	7.9		34.4		101.0		19.8	
	PE 86	-22.6	6.4			31.3	25.4	8.1		31.1		98.5		18.8	
G6	PE 87	-21.7	6.2			34.7	27.5	8.2		34.1		97.0		19.4	
	PE 88	-22.5	6.1			30.8	20.0	8.1		30.7		94.1		19.0	
	PE 89	-22.6	6.9			32.5	25.0	8.0		32.2		94.8		18.9	
	PE 90	-22.2	5.9			34.3	26.2	8.2		33.8		96.3		19.3	
	PE 91	-21.8	6.1			35.1	28.2	8.2		34.5		97.4		19.7	
	PE 92	-22.3	6.3			34.8	28.4	8.0		34.2		93.5		19.4	
Ave.		*-22.4±0.5*	*6.3±0.5*			*33.1±1.7*	*24.1±3.5*	*8.1±0.1*		*32.7±1.6*		*96.7±2.2*		*19.2±0.3*	

S: summer; W: winter; 'Gr.' shows different clustering groups of the POC samples.

Appendix 4 Results of the POC samples on the70 µm net and on the filter paper

Summer POC (70 µm net)	$\delta^{13}C$	C/N	Summer POC (filter paper)	$\delta^{13}C$	C/N	Winter POC (filter paper)	$\delta^{13}C$	C/N
PN50	-25.9	18.4	PS50	-23.4	7.6	PW50	-26.0	7.6
PN51	-25.8	14.6	PS51	-24.3	11.3	PW51	-25.2	7.5
PN52	-24.8	12.1	PS52	-23.6	10.2	PW52	-26.0	7.5
PN53	-24.4	12.5	PS53	-24.1	10.1	PW53	-26.0	7.3
PN56	-25.4	9.7	PS56	-24.8	9.2	PW56	-24.7	7.2
PN57	-25.1	12.7	PS57	-23.0	9.8	PW57	-24.0	9.9
PN63	-25.1	13.6	PS63	-23.3	8.0	PW63	-23.8	8.9
PN64	-25.1	13.8	PS64	-23.3	10.1	PW64	-23.9	8.4
PN72	-24.2	15.3	PS72	-25.6		PW72	-21.8	8.6
PN65	-27.2	5.7	PS65	-24.1	8.7	PW65	-23.6	7.3
PN67	-26.2	4.6	PS67	-24.7	9.6	PW67	-24.9	6.5
PN68	-27.0	6.5	PS68	-24.6	9.4	PW68	-25.1	6.8
PN71	-27.2	5.0	PS71	-26.1		PW71	-22.5	6.8
PN73		5.5	PS73	-25.7		PW73	-21.7	8.7
Ave.	*-25.6*	*+10.7*		*-24.3*	*+9.5*		*-24.2*	*+7.8*
SD	*+1.0*	*+4.5*		*+1.0*	*+1.1*		*+1.5*	*+1.0*

PS: summer plankton samples on filter paper; PW: winter plankton samples on filter paper; PN: summer plankton samples on a 70µm net; S.D.: standard deviation.

Appendix 5 Organic carbon results of the surface sediment (to be continued)

Gr.(n)	Sample ID	Long (ºE)	Lat(ºN)	δ^{13}C (‰)	C/N	TOC (%)	TN(%)	Mean Sal. (‰)	Sand (%)	Clay (%)	Silt (%)	WD (m)
	PE 17	113.57	22.95	-26.6	20.1	3.79	0.11	5.1	42.8	15.0	42.2	2.1
	PE 18	113.55	23.00	-23.3	12.6	0.91	0.07	3.2	34.9	20.7	44.4	2.4
G1(4)	PE 19	113.52	23.05	-25.1	13.8	1.88	0.14	2.6	29.3	22.5	48.2	2.3
	PE 20	113.48	23.10	-25.0	14.4	2.13	0.15	1.4	23.7	24.2	52.1	2.1
Ave.				*-25.0±1.3*	*15.2±3.3*	*2.2±1.2*	*0.1±0.0*	*3.1±1.6*	*32.7±8.2*	*20.6±4.0*	*46.7±4.4*	*2.2±0.1*
	PE 16	113.58	22.88	-23.7	13.4	1.02	0.08	6.4	33.3	19.5	47.2	2.5
	PE 15	113.62	22.82	-25.4	14.6	1.28	0.09	8.2	22.6	24.0	53.5	10.5
	PE 14	113.65	22.77	-22.7	11.4	0.74	0.07	12.2	8.4	32.4	59.2	3.8
	PE 10	113.64	22.68	-22.8	11.4	1.14	0.10	9.8	12.5	30.5	57.0	5.0
	PE 09	113.67	22.63	-23.6	13.0	0.99	0.08	11.6	24.0	22.0	53.9	2.1
	PE 11	113.58	22.76	-23.4	13.4	1.50	0.11	3.3	12.1	21.3	66.6	2.2
G2(14)	PE 12	113.54	22.78	-22.7	13.9	1.11	0.08	1.6	44.0	13.2	42.8	4.0
	PE 13	113.49	22.80	-24.5	16.3	1.30	0.08	0.8	34.2	11.8	54.0	3.2
	PE 41	113.53	22.77	-24.8	15.9	1.39	0.09	1.6	20.6	12.7	66.7	5.0
	PE 42	113.44	22.80	-23.4	11.7	0.79	0.07	1.6	53.6	8.2	38.2	2.2
	PE 44	113.37	22.88		10.5	0.28	0.03	0.4	67.4	10.3	22.3	2.2
	PE 45	113.33	22.88		10.2	0.22	0.02	-0.2	65.6	7.3	27.1	1.8
	PE 46	113.47	22.86	-23.0	12.8	1.37	0.11	-0.1	19.4	23.7	56.9	3.5
	PE 47	113.36	22.78	-26.8	12.9	0.45	0.04	-0.1	53.1	11.9	35.0	3.8
Ave.				*-23.9±1.2*	*13.0±1.8*	*1.0±0.4*	*0.1±0.0*	*4.1±4.6*	*33.6±20.0*	*17.8±8.1*	*48.6±13.8*	*3.7±2.2*
	PE 48	113.39	22.75	-22.0	10.7	0.98	0.09	0.4	24.8	20.7	54.5	2.3
	PE 49	113.46	22.72	-21.9	9.2	1.03	0.11	0.4	11.7	23.3	65.0	2.9
	PE 50	113.52	22.68	-26.7	11.4	1.41	0.12	1.0	8.3	30.7	61.0	3.2
	PE 51	113.54	22.66	-22.6	10.9	0.75	0.07	1.0	27.2	19.6	53.2	5.2
G3(8)	PE 52	113.57	22.64	-23.8	13.4	0.52	0.04	2.0	20.5	12.9	66.6	4.1
	PE 53	113.59	22.61	-22.0	10.7	1.14	0.11	3.0	1.7	25.7	72.7	7.1
	PE 56	113.65	22.47	-22.2	10.0	0.77	0.08	6.5	20.6	27.2	52.2	3.5
	PE 54	113.62	22.57	-22.9	12.3	1.54	0.13	3.9	6.6	22.6	70.8	6.0
Ave.				*-23.0±1.6*	*11.1±1.3*	*1.0±0.3*	*0.1±0.0*	*2.3±2.1*	*15.2±9.3*	*22.8±5.4*	*62.0±8.0*	*4.3±1.7*
	PE 76	113.68	22.44	-24.0	10.8	1.49	0.14	2.5	14.9	23.9	61.2	7.1
	PE 01	113.64	22.58	-24.2	17.5	1.02	0.06	6.0	32.9	12.8	54.3	4.4
	PE 55	113.63	22.53	-23.9	17.1	1.40	0.08	7.0	55.8	7.3	37.0	8.0
	PE 08	113.72	22.61	-24.1	12.7	1.51	0.12	14.5	19.9	25.4	54.7	2.8
	PE 03	113.74	22.45	-23.1	11.5	1.17	0.10	19.9	22.3	26.1	51.6	5.0
G4(11)	PE 05	113.83	22.54	-23.3	12.3	1.32	0.11	23.4	18.9	29.1	52.0	4.0
	PE 06	113.80	22.52	-23.5	14.6	1.27	0.09	20.3	16.8	28.2	55.0	5.8
	PE 07	113.76	22.56	-23.5	17.7	1.13	0.06	17.2	30.8	17.8	51.4	4.8
	PE 59	113.72	22.47	-23.4	10.5	1.34	0.13	16.0	12.7	23.9	63.4	15.0
	PE 60	113.75	22.50	-24.2	14.9	0.66	0.04	19.3	63.2	8.6	28.2	18.0
	PE 61	113.72	22.55	-27.0	15.1	0.38	0.03	14.0	42.5	17.9	39.5	16.0
Ave.				*-24.0±1.1*	*14.1±2.7*	*1.2±0.4*	*0.1±0.0*	*14.5±6.7*	*30.1±17.1*	*20.1±7.7*	*49.8±10.7*	*8.3±5.4*

'Gr.(n)' shows the number (n) of samples in each clustering groups (Gr.).

Gr.(n)	Sample ID	Long (°E)	Lat(°N)	δ¹³C (‰)	C/N	TOC (%)	TN(%)	Mean Sal. (‰)	Sand (%)	Clay (%)	Silt (%)	WD (m)
	PE 69	113.72	22.34	-23.1	9.9	1.23	0.12	20.8	12.5	33.3	54.1	13.5
	PE 70	113.77	22.37	-23.6	12.0	1.38	0.12	24.1	15.7	31.3	53.0	*20.0*
	PE 71	113.78	22.38	-23.8	11.6	0.95	0.08	24.0	15.8	28.4	55.8	13.0
	PE 72	113.75	22.39	-22.0	9.9	0.96	0.10	17.9	16.8	30.5	52.8	15.0
	PE 73	113.75	22.35	-22.9	10.3	1.13	0.11	20.3	18.4	28.9	52.7	15.0
	PE 02	113.69	22.50	-23.7	11.7	1.69	0.14	11.9	24.6	28.6	46.8	6.9
	PE 64	113.65	22.38	-23.2	9.9	1.27	0.13	13.5	36.0	11.1	53.0	7.0
	PE 57	113.65	22.45	-22.7	10.7	1.35	0.13	10.7	13.3	29.8	57.0	7.0
	PE 58	113.68	22.46	-23.2	11.4	1.26	0.11	12.0	12.5	29.2	58.3	10.0
G5(22)	PE 62	113.68	22.58		8.5	0.25	0.03	11.0	37.8	11.2	51.0	8.0
	PE 63	113.66	22.45	-23.5	11.2	1.21	0.11	13.1	9.3	27.0	63.7	5.5
	PE 75	113.68	22.49	-23.1	11.8	1.11	0.09	11.0	26.9	20.8	52.3	7.0
	PE 77	113.65	22.49	-22.3	11.7	1.11	0.10	10.9	23.5	17.8	58.7	5.4
	PE 65	113.62	22.33	-23.5	11.3	0.71	0.06	14.1	12.8	34.5	52.7	5.0
	PE 66	113.60	22.29	-22.9	8.9	0.94	0.11	13.8	22.0	31.1	46.9	3.5
	PE 67	113.64	22.31	-22.6	8.9	1.07	0.12	15.5	7.1	38.3	54.6	13.0
	PE 68	113.68	22.32	-23.4	12.2	1.13	0.09	18.5	19.9	18.4	61.6	12.0
	PE 74	113.70	22.36	-22.9	11.1	1.38	0.12	17.0	16.2	33.0	50.8	9.0
	PE 78	113.60	22.25	-23.1	8.4	1.24	0.15	17.6	20.3	33.2	46.5	6.2
	PE 79	113.65	22.25	-23.1	9.1	1.25	0.14	19.9	9.0	32.5	58.6	5.3
	PE 80	113.70	22.25	-23.4	9.7	1.26	0.13	22.1	13.7	35.2	51.1	5.8
	PE 81	113.60	22.19	-23.1	8.8	1.24	0.14	20.3	16.1	31.3	52.6	5.3
Ave.				*-23.1±0.4*	*10.4±1.3*	*1.1±0.3*	*0.1±0.0*	*16.4±4.4*	*18.2±7.9*	*28.0±7.4*	*53.8±4.5*	*9.0±.4.3*
	PE 82	113.65	22.19	-22.9	9.4	1.13	0.12	23.0	16.9	28.2	54.9	7.0
	PE 83	113.70	22.19	-23.2	9.6	1.16	0.12	25.9	14.7	29.7	55.6	6.0
	PE 84	113.62	22.13	-23.3	9.4	1.23	0.13	24.3	15.4	29.5	55.1	6.8
	PE 85	113.67	22.13	-22.9	9.7	0.90	0.09	27.4	19.6	25.2	55.2	8.5
	PE 86	113.60	22.08	-23.4	10.3	1.50	0.15	28.8	17.1	28.7	54.2	6.0
G6 (11)	PE 87	113.65	22.08	-23.0	10.3	0.93	0.09	30.0	20.9	20.2	58.9	8.5
	PE 88	113.77	22.25	-23.2	9.4	1.09	0.12	25.4	16.0	30.2	53.8	6.3
	PE 89	113.76	22.19	-23.2	9.7	1.10	0.11	28.5	14.8	25.6	59.6	8.5
	PE 90	113.75	22.13	-22.9	9.9	1.09	0.11	29.4	18.6	24.3	57.1	8.5
	PE 91	113.73	22.08	-23.1	10.6	0.91	0.09	30.7	16.9	19.8	63.3	11.5
	PE 92	113.80	22.10	-22.5	8.8	0.98	0.11	30.9	15.9	21.5	62.6	14.0
Ave.				*-23.1±0.2*	*9.7±0.5*	*1.1±0.2*	*0.1±0.0*	*27.7±2.7*	*17.0±2.0*	*25.7±3.9*	*57.3±3.3*	*8.3±2.5*
	PE 29	114.08	22.23	-22.3	8.8	1.02	0.12	31.3	15.8	24.8	59.4	8.0
	PE 30	114.12	22.25	-23.2	9.0	0.83	0.09	32.1	2.6	31.0	66.5	35.0
	PE 31	114.02	22.26	-21.8	7.8	1.13	0.14	30.4	6.8	32.8	60.4	8.0
	PE 32	113.96	22.22	-21.9	8.0	0.62	0.08	31.4	8.3	15.8	75.9	6.0
	PE 33	114.10	22.32	-24.1	10.3	0.59	0.06	31.5	29.0	21.7	49.2	20.0
	PE 34	113.98	22.35	-24.1	10.1	0.78	0.08	30.3	18.9	24.9	56.2	11.0
G7(13)	PE 39	113.93	22.46	-23.8	9.3	1.05	0.11	24.9	4.0	32.3	63.8	4.0
	PE 40	113.96	22.48	-23.9	9.0	1.23	0.14	20.3	13.8	23.3	62.9	3.0
	PE 35	113.95	22.36	-22.2	10.6	1.45	0.07	30.5	13.9	29.3	56.8	14.0
	PE 36	113.90	22.32	-22.8	9.0	0.39	0.04	30.2	24.9	22.4	52.6	5.0
	PE 37	113.90	22.38	-23.2	10.4	0.56	0.05	29.8	47.8	15.2	37.0	20.0
	PE 04	113.83	22.46	-23.9	11.1	0.90	0.08	26.0	35.7	21.5	42.8	4.8
	PE 38	113.89	22.43	-22.8	12.3	0.75	0.06	29.8	11.9	28.2	59.9	8.0
Ave.				*-23.1±0.9*	*10.4±3.0*	*0.9±0.3*	*0.1±0.0*	*29.1±3.4*	*18.0±13.2*	*24.9±5.7*	*57.2±10.1*	*11.3±9.1*
	PE 25	114.27	22.24	-21.5	8.0	0.57	0.07	33.5	21.3	17.6	61.1	21.0
	PE 26	114.23	22.21	-21.0	7.1	0.68	0.09	32.4	16.5	17.4	66.1	14.0
G8(4)	PE 27	114.18	22.22	-21.8	7.7	0.92	0.12	32.4	9.9	26.0	64.1	14.0
	PE 28	114.08	22.19	-22.5	10.0	1.60	0.09	31.1	23.5	18.1	58.4	14.0
Ave.				*-21.7±0.6*	*8.2±1.2*	*0.9±0.5*	*0.1±0.0*	*32.4±1.0*	*17.8±6.0*	*19.8±4.1*	*62.4±3.4*	*15.8±3.5*
	PE 21	114.45	22.37	-21.0	6.8	0.68	0.10	33.3	17.3	18.8	63.9	24.0
	PE 22	114.45	22.29	-20.8	6.8	0.75	0.11	33.4	14.4	21.6	63.9	25.0
G9(4)	PE 23	114.45	22.22	-21.2	6.5	0.63	0.10	33.5	19.8	24.6	55.6	28.0
	PE 24	114.32	22.20	-21.1	7.1	0.92	0.13	33.5	3.4	27.8	68.7	31.0
Ave.				*-21.0±0.2*	*6.8±0.2*	*0.7±0.1*	*0.1±0.0*	*33.4±0.1*	*13,7±7.2*	*23.2±3.9*	*63.0±5.5*	*27.0±3.2*

Appendix 6 Concentration of key metals in soil samples

	Fe	Mn	Co	As	Li	Ba	Al	K	Rb	Sr	Na	Mg	Ca	B/Be	Label	Site
Forest soil	21309	173	4	60	34	123	22345	14541	23	11	628	189	8560	23	S5	N4
	17969	140	2	26	22	89	27881	3997	18	14	6759	1187	52362	41	S9	N6
Ave.	*19639 ±2362*	*156 ±24*	*3 ±1*	*43 ±24*	*28 ±8*	*106 ±24*	*25113 ±3914*	*9269 ±7455*	*20 ±4*	*12 ±2*	*3694 ±4335*	*688 ±705*	*30461 ±30972*	*32 ±12*		
Riverbank soil	24787	806	9	124	64	225	31519	17207	53	29	3660	312	9544	9	A1	N1
	32906	522	8	136	48	245	35035	22987	56	9	2368	289	16672	27	A2	N2
	42956	1315	13	244	72	183	28963	18490	33	14	5570	594	30181	10	A3	N3
	43242	686	12	113	73	137	30999	20944	30	5	5383	664	51984	11	A4	N4
	14274	235	4	17	27	187	8844	24341	146	77	5811	3049	62164	15	A6	N4
	28862	764	9	77	50	208	29817	20802	53	17	3795	281	17566	11	A7	N5
	15536	125	2	26	34	97	26181	2311	24	17	2266	129	9346	26	A8	N5
	41036	814	18	19	38	213	28884	12382	12	51	3482	383	9127	23	G1	E5
Ave.	*30450 ±11691*	*658 ±373*	*9 ±5*	*95 ±78*	*51 ±17*	*187 ±49*	*27530 ±7967*	*17433 ±7147*	*51 ±42*	*27 ±25*	*4042 ±1401*	*713 ±960*	*25823 ±20672*	*17 ±8*		
Mangrove soil	50161	799	14	21	124	228	27386	17773	15	26	7828	964	8836	18	A10	E3
	31321	448	8	12	79	163	42692	15079	21	39	6256	1207	11180	20	A11	E3
	39429	1455	11	16	88	164	24212	21792	109	231	13580	3788	28809	23	A12	E3
	14776	134	3	14	52	181	27370	12967	40	31	10571	1067	8605	32	A13	E3
	28405	343	8	12	73	240	28214	18011	31	71	9731	727	11523	27	A14	E3
	30718	380	8	10	70	225	27119	19117	22	76	9846	824	23472	25	A15	E3
	8930	115	2	18	88	94	30261	15769	46	23	9086	676	17141	19	A16	E3
	4826	70	0	7	45	54	24697	11410	53	13	4066	933	20816	14	A17	E3
	16467	374	3	16	40	85	23522	13458	26	29	6242	704	36485	16	A18	E4
	32780	1115	9	22	84	180	28318	15798	18	40	9550	2335	38538	24	A19	E4
	13186	217	2	12	38	87	24038	12410	33	53	5157	837	28714	17	A20	E4
Ave.	*24636 ±14024*	*495 ±445*	*6 ±4*	*14 ±5*	*71 ±26*	*155 ±65*	*27984 ±5326*	*15780 ±3170*	*38 ±26*	*58 ±61*	*8356 ±2758*	*1278 ±953*	*21284 ±10844*	*21 ±5*		
Agricultural soil	52902	905	20	28	57	213	29853	13292	12	30	6906	752	4921	24	G2	E5
	49374	983	19	23	52	220	35348	15172	19	40	4219	626	4697	17	G3	E5
	46441	1339	18	23	50	212	30964	15073	13	46	5648	419	8607	18	G4	E5
Ave.	*49572 ±3235*	*1076 ±232*	*19 ±1*	*24 ±3*	*53 ±3*	*215 ±5*	*32055 ±2905*	*14512 ±1058*	*15 ±4*	*39 ±8*	*5591 ±1345*	*599 ±168*	*6075 ±2195*	*20 ±3*		

Appendix 7 Concentration of key metals in the estuarine surface sediment (to be continued)

Gr.	Sample ID	Fe	Mn	Co	As	*Li*	*Ba*	*Al*	*K*	*Rb*	Sr	Na	Mg	Ca	B/Be
	PE 17	29184	341.6	9.25	19.9	59.2	177.3	18492	13961	20	25.7	3438	818.3	13382.6	24.3
	PE 18	43047	945.2	18.67	32.5	117.9	182.1	25640	18564	16.7	14.2	3461	1214	18426.8	15.2
	PE 19	36500	504.8	11.8	30	51.5	234.4	24372	16817	17.7	23.7	7579	1355	48249.9	18.7
G1	PE 20	47591	866.1	21.03	58.5	116.5	418.3	22324	16756	13.7	24.3	3677	403.8	8202.1	17.5
	PE 16	32257	627.2	12.34	17.5	50.7	186.3	22991	16645	21.5	29.2	3270	546.5	9062.1	18.3
	PE 15	39199	776.8	16.71	28.5	82.8	168.1	20584	18850	23.4	13.6	5194	971.3	10188.5	20.2
	PE 14	47340	831.9	16.16	25.9	87	226.4	23082	16078	15	45.6	3431	880.1	9716.5	20.5
	PE 10	42924	801.1	17.18	22.8	50.7	222.1	28691	15129	13	46.5	7542	1979	39674.7	22.3
	PE 09	49500	1165.9	21.37	34.6	86.6	220.5	25714	14320	8.3	41.6	5540	1020	8449.7	24.1
	PE 11	54484	1722.5	24.68	44.9	85.7	261.4	29897	13867	7.3	38.3	3376	871.4	5391.7	21.9
	PE 12	46172	1007.1	20.64	21	56.6	189.8	25175	12447	7.7	41.4	3756	728.3	10581.2	23.2
	PE 13	35288	855.3	14.68	42	54	216.7	27864	14565	17.6	31.9	3530	549.5	8150.4	17.9
	PE 41	37196	775.2	13.9	28.6	55.9	204.2	23242	21302	25.9	26.9	3863	839.9	11552.8	24.2
	PE 42	28715	554.8	12.14	12.7	36.6	181.1	21415	18811	15.8	30.9	4200	1086	16437.5	19.8
	PE 44	32913	298.1	14.91	12.6	37.3	207.9	23168	14067	19.1	21.1	1828	1020	10365.4	11.2
	PE 45	23954	417.8	8.6	14.1	28.9	195.3	22614	17343	21.6	25.9	5369	1509	63895.9	22.3
	PE 46	48121	1032.1	20.36	21.1	54.7	192	30160	15982	12.9	39.4	6768	1739	43425.7	24.4
G2	PE 47	17323	317.2	7.59	7.3	43.1	134.1	18296	6807	5.7	52.1	2300	1122	21129.7	27.1
	Ave.	*38428 ±9876*	*768 ±352*	*15±5*	*26 ±12*	*64 ±26*	*212 ±59*	*24096 ±3479*	*15688 ±3140*	*15 ±6*	*32 ±11*	*4340 ±1654*	*1036 ±410*	*19794 ±17014*	*21 ±4*
	PE 48	40227	563.0	16.09	20.4	55.9	188.2	23362	15907	5.5	33.7	7297	1934	98056.1	25.4
	PE 49	55399	1265.2	20.1	20.6	54.8	184.9	27257	11174	10.1	40.3	3895	1547	28362.1	24.4
	PE 50	41318	614.8	16.05	12.5	84.1	203	18888	12783	6.3	40.2	4387	895.2	9760.8	24.7
	PE 51	52235	1640.8	16.16	19.2	44	192.3	26544	11120	7.2	31.2	2409	406.6	9072	20.8
	PE 52	31030	661.8	12.81	15.9	33.4	199.4	20103	8132	6.7	40.3	6097	942.6	25698.8	31.6
	PE 53	48473	931.8	20.44	17.7	52.1	224.9	30456	12412	23.7	33.3	4684	2017	20869.4	23.2
	PE 56	38400	665.0	15.72	15.9	61.1	183	24555	14974	6.9	38.7	7189	2588	74557.5	29.9
G3	PE 54	53479	974.7	24.12	20.9	56.4	191.4	20671	11293	3.6	47.7	5356	1116	43750.1	29.1
	PE 76	51625	1221.0	19.39	32.1	65.1	280	27438	13446	10.3	36.7	3329	419.9	10463.6	23.5
	PE 01	36112	802.9	14.52	21.8	31.6	200.4	20095	10235	5.8	34.7	4712	1242	20298.4	28.1
	PE 55	38937	720.9	17.18	22.9	46.4	191.7	21236	12802	7.7	39.6	5451	866.3	34539.8	25.3
	PE 08	52436	1046.7	21.54	37.2	94.2	242	30591	16244	13.2	40.5	5821	727.1	4417.3	25.4
	PE 03	48384	959.1	21.64	36.4	96.2	185.3	26544	17445	23	23.2	5683	991.7	5944.1	23.9
	PE 05	46693	650.5	19.77	34.7	119.5	197.8	28852	16438	17.8	22.9	7770	473.4	9761.5	21.6
	PE 06	49730	656.8	20.2	33.7	105.2	212.6	41676	17598	17.4	25.6	6586	925.3	4198.6	22.6
	PE 07	41792	615.6	16.62	20.6	66.5	185.6	27245	14833	13.7	50.7	4591	568.7	5122.1	22.9
	PE 59	49464	1142.4	20.28	43.7	74.9	265.3	24332	16169	9.6	35.1	9648	1309	26923.8	26.2
	PE 60	27240	531.9	11.74	12.2	43	160.2	21999	14188	21.8	45.7	5670	1434	36376.3	25.7
G4	PE 61	14178	297.9	5.72	5.6	33	176.3	14784	16898	85.5	87.6	4511	1646	33202.6	23.2
	Ave.	*43008 ±10518*	*840 ±321*	*17 ±4*	*23 ±10*	*64 ±26*	*203 ±30*	*25086 ±5820*	*13899 ±2708*	*16 ±18*	*39 ±14*	*5531 ±1689*	*1160 ±590*	*26388 ±24715*	*25 ±3*

Gr.	Sample ID	Fe	Mn	Co	As	Li	Ba	Al	K	Rb	Sr	Na	Mg	Ca	B/Be
	PE 69	50110	786.4	18.19	31.1	85.8	211.2	32292	15376	13.8	28.9	8676	1178	9644.3	25.6
	PE 70	45751	626.1	18.01	19.7	79.2	163.7	26890	14329	6.7	28.9	9934	1780	55513.8	26.2
	PE 71	38146	543.2	14.75	22.2	81.5	190.7	26711	13140	10.7	31.2	7207	539.9	6191.1	23.5
	PE 72	45956	568.8	17.81	20.7	79.7	212.2	28737	13542	9.6	28.7	6542	782.9	17946.5	30.6
	PE 73	50964	636.8	18.31	23.1	89.5	172.8	28658	14209	7.8	27.9	8655	1489	23204.9	28.1
	PE 02	54091	1024.8	21.87	37.5	89.1	172.5	23017	16172	12.3	19.7	4841	575.7	8345.3	24
	PE 64	34994	632.0	16.06	14.6	49.1	175	20718	10460	4.3	92.2	5310	822.4	15150.6	26.3
	PE 57	55476	1063.1	23.28	24.4	74.3	167.3	21946	11174	5.3	36.7	5891	1562	20191	25.4
	PE 58	49841	970.8	19.27	28.7	62.9	142.5	23319	16097	9.2	36.6	6668	1068	29635.7	29.8
	PE 62	30382	620.2	13.7	16.3	35.3	169.3	22126	11371	10.8	37.4	4530	656	26237.5	27.9
G5	PE 63	49376	1104.0	19.07	29.5	76.9	196.9	21595	12734	6.3	34.8	6497	1074	25655	26.5
	PE 75	74074	1213.8	28.11	35.5	106.1	315.9	24199	23883	10.6	66.3	8152	747.7	63983.2	25.6
	PE 77	40859	695.3	16.7	17.2	49.8	196.7	36712	10466	9	38.6	4292	1276	37943.7	24.3
	PE 65	48490	1082.7	20.14	27.8	75.5	168.5	25476	11327	5.5	37.5	6839	916.6	7795.3	24.7
	PE 66	45413	1068.8	20.61	29.9	100	233.6	27873	12742	5.5	68.9	7255	966.8	22455	23.5
	PE 67	56243	1117.2	22.21	24.2	92.2	158.4	25464	11895	4.9	35.3	5596	766.2	8612	25.2
	PE 68	42957	849.3	16.99	33	62.6	209.7	23156	12053	5.7	43.7	7321	702.3	32226	30.5
	PE 74	52167	863.9	20.46	31.4	74.3	194.5	23174	13326	7	47.7	8311	1132	29401.4	29
	PE 78	52267	1390.2	24.57	38.6	130.3	278.5	26796	16112	17.1	33.4	10043	542.2	3280.5	22.3
	PE 79	48842	1237.5	16.78	32.8	86.4	226.1	30941	15774	15.6	28.6	11372	758	9269.6	27
	PE 80	51328	981.8	16.17	32.1	83.2	220.3	35090	19412	18.4	23.8	12028	632.8	9212.6	24.9
	PE 81	50329	1143.6	17.54	34.7	91.7	212.6	31066	17342	17	28.9	10897	473.4	4605.1	26.3
	PE 82	46276	798.8	16.99	28.4	83.4	231.1	27842	16362	13.1	75.2	10331	772.4	8352.8	29
	PE 83	45904	746.5	15.91	29.3	85.4	233.9	29959	16937	19.6	30.5	11939	391.2	8424.6	27
	PE 84	47911	937.6	17.31	28.1	91.3	242.4	34416	17524	20.3	30.8	10210	568.1	9245.6	29.4
	PE 85	42514	727.6	15.41	22.9	75.1	248.2	30980	17471	21	49.9	9376	658.4	5088.9	27.9
	PE 86	47514	1187.2	17.11	32.6	91.5	300.2	39666	16812	36.1	42.9	11543	2306	6624.3	31.3
G6	PE 87	41472	743.3	15.04	22	73.3	241.6	30712	15024	23.7	105.7	10341	1930	12900.7	30.7
	PE 88	51916	747.5	17.79	29.4	112.8	275.8	38268	20469	41.9	32.5	15431	2039	10223.6	23.1
	PE 89	53737	870.0	19.51	34.2	99.8	257.3	33294	20361	27.3	26.5	14188	672.3	8206.8	27.1
	PE 90	44925	777.0	15.76	25.1	88.2	284.3	49253	19182	46.9	48.2	12990	3484	16255	31
	PE 91	39363	672.5	14.32	21.3	70.5	244	30144	17545	25.3	64.1	9150	1330	18389.8	34.5
	PE 92	41543	744.5	14.19	18.8	83.2	272.8	44819	19893	40.8	52.9	11313	2567	15117.2	30.2
	PE 29	40346	309.1	11.52	14.8	132.7	275.1	40297	20982	34.4	36.7	5538	1858	4415.4	27
	PE 30	33780	255.8	9.95	19.2	105.3	240.9	22396	18550	20.2	21.6	4087	424	4123.2	27.3
	PE 31	33692	205.3	8.51	10.7	91.7	196	28212	15740	23.8	18.4	4554	763.7	7519.6	32.5
	PE 32	26727	239.0	7.42	11.2	91	250.4	31874	17410	21.6	35.6	4036	506.2	10674.1	29.3
	PE 33	19687	142.3	5.88	10.2	78.7	216.3	31061	20036	45.4	19.9	2823	433.4	4690.5	19
	PE 34	31824	208.8	8.88	14.3	107.7	211.8	30590	19949	25.3	16.7	3085	432.9	5137.8	25.5
	PE 39	36875	229.4	9.43	20.8	106.5	183.9	39985	16767	27.8	12.2	3276	1189	4659.7	26.9
	PE 40	38392	264.1	10.18	22.3	112.1	192.3	29985	18770	31.9	12.4	2989	985.9	4077.8	25.8
	PE 35	33608	262.9	12.59	16.4	116.9	293.7	24229	15829	19.6	137.6	2918	402.9	4118.4	16.3
	PE 36	18682	171.7	5.96	12.8	69.9	172.9	22234	13786	32.5	16.7	2702	431.9	7080	27.5
	PE 37	34701	284.3	7.55	13.5	57.1	184.9	19843	16761	9.9	26.1	4219	722.6	27940.7	23.2
	PE 04	34736	446.8	12.73	23.2	56.4	215.7	26781	20719	28.1	22.3	7643	477.2	8360.4	19.4
G7	PE 38	54363	304.1	12.91	27.2	134.1	237.1	34192	20771	23.9	26.7	3104	499.7	5288.3	26.5
	Ave.	43664 ±10141	706 ±344	16 ±5	24 ±8	86 ±21	219 ±42	29500 ±6558	16230 ±3267	19 ±12	40 ±24	7492 ±3372	1006 ±655	14857 ±13195	27 ±3

Gr.	Sample ID	Fe	Mn	Co	As	*Li*	*Ba*	*Al*	*K*	*Rb*	Sr	Na	Mg	Ca	B/Be
	PE 25	25021	243.7	7.2	8.2	74.7	263.1	38567	18133	26.5	53.8	6586	773.1	8393.3	27.3
	PE 26	32076	268.5	8.32	11.1	91.4	294.5	34681	19314	26.2	50	7362	1643	4208.5	27.5
	PE 27	36896	262.9	9.79	16.5	113.8	258.1	34566	20547	18.1	26.1	5693	1794	5282.4	27.3
G8	PE 28	37185	357.9	10.52	9.3	96.8	294	30483	18269	17.2	73.7	5359	1008	4826.1	23.8
	PE 21	32365	267.0	8.54	10.1	96.8	286	40370	19617	22.4	51.6	4215	853.9	8234.5	28.5
	PE 22	35119	240.0	8.01	10.4	78.7	276.8	49024	18890	22.9	43.8	9531	917.1	15132.3	30.1
	PE 23	35699	252.4	9.05	11.4	104.5	232.3	45227	18022	24.6	31.5	5663	602.1	11712.1	29.3
G9	PE 24	36384	279.3	9.85	12.5	115.5	251.9	43290	17635	22.2	34.3	6148	748.3	8951.1	27.5
	Ave.	*33843 ±4055*	*271 ±37*	*9 ±1*	*11 ±3*	*97 ±15*	*270 ±22*	*39526 ±6192*	*18803 ±977*	*23 ±3*	*46 ±15*	*6320 ±1589*	*1042 ±436*	*8343 ±3716*	*27 ±2*

Appendix 8 Concentration of F1 metals from UV1 (10.07-1.31m) (to be continued)

Depth (m)	**Fe**	*Fe*	**Mn**	*Mn*	**Co**	*Co*	**As**	*As*	**Cu**	*Cu*
1.31	30837	34728.4	511	517.5	11	12.6	11.4	11.4	18.8	27.6
1.33	30283	34339.3	475	516.8	10.4	12.4	7.9	11.4	14.3	26.7
1.35	28918	33933.6	469	512.6	10.3	12.2	8.7	11.0	16.3	25.5
1.37	29557	33432.1	491	508.3	11.1	12.0	7.8	10.8	15.2	24.6
1.39	29971	33044.6	493	506.5	10.8	11.9	7.7	10.5	16.1	23.6
1.41	30237	32737.2	492	505.2	10.95	11.8	7.8	10.2	16.2	22.9
1.43	30502	32487.1	489	503.9	10.8	11.7	7.4	10.0	16.3	22.2
1.45	33216	32288.6	526	502.4	11.7	11.6	9.4	9.7	26.1	21.6
1.47	29981	32381.4	487	504.7	10.6	11.6	7.0	9.7	16.2	22.1
1.49	31158	32141.3	497	503.0	11.3	11.5	9.5	9.4	18.5	21.5
1.51	29556	32043.0	496	502.4	10.7	11.5	7.5	9.4	14	21.2
1.53	30357	31794.3	497.5	501.7	10.95	11.4	7.9	9.2	14.71	20.5
1.54	34420	31650.6	510	501.3	11.19	11.4	8.3	9.1	15.41	19.9
1.55	29511	31927.5	498	502.2	10.7	11.4	7.5	9.0	13.3	19.4
1.57	31541	31685.9	507	501.8	11.2	11.3	6.8	8.9	17.2	18.8
1.59	29649	31671.4	513	502.3	11.2	11.3	8.1	8.7	18.2	18.7
1.61	31003	31469.1	515	503.4	11.4	11.3	9.0	8.6	16	18.6
1.63	30106	31422.5	528	504.5	11.7	11.3	8.3	8.6	22.6	18.4
1.65	31028	31290.9	530	506.9	11.55	11.3	8.5	8.6	16.8	18.8
1.67	31052	31264.5	532	509.2	11.2	11.4	7.7	8.6	17.1	18.6
1.69	31674	31243.3	543	511.5	12.2	11.3	8.7	8.5	16.5	18.4
1.71	31128	31286.4	541	514.6	11.7	11.4	8.4	8.5	16.6	18.2
1.73	32088	31270.5	515	517.3	11.5	11.5	7.9	8.5	19.4	18.1
1.75	30916	31352.3	541	517.0	11.9	11.5	8.1	8.5	16.7	18.2
1.77	30784	31308.6	528	519.4	11.7	11.5	7.7	8.4	18.05	18.1
1.79	30651	31256.1	556	520.3	12.7	11.5	7.5	8.3	15	18.1
1.81	30356	31195.6	508	523.9	11.3	11.6	7.1	8.3	23.3	17.8
1.83	30938	31111.7	528	522.3	11.4	11.6	8.0	8.1	14.6	18.3
1.85	31372	31094.3	521	522.8	11.5	11.6	8.3	8.1	12.7	17.9
1.87	31024	31122.1	558	522.7	11.5	11.6	8.2	8.1	17.8	17.4
1.89	30951	31112.3	550	526.2	11.6	11.6	8.2	8.2	16.75	17.5
1.91	29825	31096.1	560	528.6	11.7	11.6	8.0	8.2	15.7	17.4
1.93	30877	30969.0	542	531.7	11.8	11.6	8.1	8.1	20.9	17.2
1.95	32790	30959.8	521	532.7	11.4	11.6	8.7	8.1	51	17.6
1.97	31837	31142.8	507	531.6	11.2	11.6	8.7	8.2	18.4	20.9
1.99	33160	31212.2	500	529.1	11.1	11.5	8.0	8.2	18	20.7
2.01	31603	31407.0	496	526.2	10.8	11.5	8.1	8.2	21.2	20.4
2.03	31707	31426.6	487	523.2	10.7	11.4	8.1	8.2	19.25	20.5
2.05	30567	31454.6	463	519.6	10	11.4	8.0	8.2	17.2	20.4
2.07	31811	31365.9	478	513.9	10.6	11.2	8.4	8.2	20.5	20.0
2.09	31050	31410.4	487	510.3	10.6	11.2	7.5	8.2	18.9	20.1
2.11	29739	31374.3	425	508.0	9.6	11.1	8.0	8.1	19.5	20.0
2.13	31006	31210.8	466	499.7	16.3	11.0	7.1	8.1	17.2	19.9
2.15	30890	31190.3	467.5	496.3	10.25	11.5	7.8	8.0	18.5	19.7
2.17	31000	31160.3	469	493.4	10.4	11.4	7.9	8.0	19.6	19.5
2.19	30780	31144.3	471	491.0	10.1	11.3	7.7	8.0	17.5	19.5
2.21	31862	31107.8	437	489.0	10	11.2	7.7	8.0	17.2	19.3
2.23	31975	31183.3	471	483.8	10.7	11.0	8.9	7.9	21.8	19.1
2.25	31275	31262.4	472	482.5	10.6	11.0	8.6	8.0	20.1	19.4
2.27	32022	31263.7	471.5	481.5	10.65	11.0	8.5	8.1	20.15	19.5
2.29	32186	31339.5	485	480.5	10.8	10.9	8.3	8.1	20.2	19.5

Bold-raw data, *Italic*- exponentially smoothened data

223

Depth (m)	Fe	Fe	Mn	Mn	Co	Co	As	As	Cu	Cu
2.31	32068	31424.1	454	480.9	10.3	10.9	8.2	8.1	19.9	19.6
2.33	31867	31488.5	481	478.2	10.5	10.9	7.3	8.1	19.3	19.6
2.35	31247	31526.4	455	478.5	10.4	10.8	7.7	8.1	20.4	19.6
2.37	32526	31498.4	482	476.2	10.6	10.8	8.6	8.0	18.4	19.7
2.39	31887	31601.2	457.5	476.7	10.5	10.8	7.9	8.1	18.9	19.5
2.41	32715	31629.7	460	474.8	10.6	10.7	8.1	8.1	19.4	19.5
2.43	30970	31738.2	441	473.3	9.6	10.7	7.4	8.1	16.6	19.5
2.45	31993	31661.4	474	470.1	10.5	10.6	7.6	8.0	19.8	19.2
2.47	33142	31694.6	464	470.5	10.6	10.6	7.9	8.0	17.7	19.2
2.49	34419	31839.3	483	469.8	11.1	10.6	8.0	8.0	21.5	19.1
2.51	33725	32097.3	483	471.2	11.3	10.6	8.3	8.0	19.2	19.3
2.53	33089	32260.1	475	472.3	11.1	10.7	8.3	8.0	21.15	19.3
2.55	32041	32343.0	467	472.6	10.5	10.8	8.5	8.0	21.3	19.5
2.57	32884	32312.8	475	472.0	11.2	10.7	8.4	8.1	20.3	19.7
2.59	32884	32369.8	475	472.3	11.2	10.8	8.4	8.1	20.3	19.7
2.61	32453	32421.2	462	472.6	11.1	10.8	8.2	8.1	21	19.8
2.63	33314	32424.4	527	471.5	12.1	10.8	9.1	8.1	19.6	19.9
2.65	32536	32513.3	525	477.1	11.65	11.0	8.7	8.2	18.95	19.9
2.67	32618	32515.6	529	481.9	11.7	11.0	9.1	8.3	18.3	19.8
2.69	31703	32525.8	523	486.6	11.6	11.1	8.1	8.4	17.8	19.6
2.71	30157	32443.5	481	490.2	10.9	11.2	7.6	8.3	22.9	19.5
2.73	32535	32214.9	518	489.3	15.6	11.1	7.7	8.3	21	19.8
2.75	32767	32246.9	527	492.2	11.7	11.6	7.9	8.2	19.9	19.9
2.77	32651	32298.9	512.5	495.7	11.6	11.6	7.8	8.2	19.45	19.9
2.79	33982	32334.1	507	497.3	11.5	11.6	7.7	8.1	17.3	19.9
2.81	30811	32498.9	496	498.3	11.4	11.6	8.0	8.1	19	19.6
2.85	30546	32330.1	435	498.1	10	11.6	6.8	8.1	17.5	19.6
2.87	32172	32151.7	515	491.8	11.7	11.4	8.1	8.0	29.2	19.3
2.89	31125	32153.7	505	494.1	11.65	11.4	7.3	8.0	20.65	20.3
2.91	31703	32050.8	532	495.2	12.2	11.5	7.8	7.9	22.2	20.4
2.93	30212	32016.0	495	498.9	11.6	11.5	6.6	7.9	19.1	20.5
2.95	32025	31835.6	528	498.5	12.2	11.5	7.7	7.8	19.6	20.4
2.97	31997	31854.6	526	501.4	19.7	11.6	7.3	7.8	20.8	20.3
2.99	32205	31868.8	518	503.9	12.5	12.4	7.7	7.7	22.4	20.4
3.01	32088	31902.4	520	505.3	12.5	12.4	7.7	7.7	23.7	20.6
3.03	31698	31921.0	519	506.8	12.35	12.4	7.7	7.7	23.25	20.9
3.07	31308	31898.7	536	508.0	12.2	12.4	7.7	7.7	51.7	21.1
3.09	31698	31839.6	528	510.8	12.35	12.4	7.7	7.7	23.25	24.2
3.11	30024	31825.5	512	512.5	11.9	12.4	8.6	7.7	22.8	24.1
3.13	33205	31645.3	538	512.5	14.3	12.3	7.7	7.8	20.4	24.0
3.15	31712	31801.3	525	515.0	12.15	12.5	8.2	7.8	19.85	23.6
3.17	31549	31792.3	536	516.0	12.4	12.5	7.7	7.8	19.3	23.2
3.19	31875	31768.0	514	518.0	11.7	12.5	8.6	7.8	18	22.8
3.21	32000	31778.7	506	517.6	13.2	12.4	9.5	7.9	19.8	22.4
3.23	32870	31800.8	514	516.5	12.1	12.5	10.2	8.1	22.8	22.1
3.25	33026	31907.8	536	516.2	12.4	12.5	8.7	8.3	19.4	22.2
3.27	32846	32019.6	517.5	518.2	12.1	12.4	9.2	8.3	21.75	21.9
3.29	32821	32102.2	521	518.1	12.1	12.4	9.6	8.4	28.7	21.9

Depth (m)	Fe	Fe	Mn	Mn	Co	Co	As	As	Cu	Cu
3.31	30302	32174.1	508	518.4	11.9	12.4	8.4	8.5	20.7	22.6
3.33	32981	31986.9	548	517.4	12.8	12.3	9.3	8.5	27.1	22.4
3.35	32749	32086.3	551	520.4	12.8	12.4	10.1	8.6	22.4	22.8
3.37	34130	32152.5	545	523.5	12.5	12.4	10.2	8.7	19.4	22.8
3.39	33777	32350.3	543.5	525.6	12.75	12.4	10.4	8.9	22.15	22.5
3.41	33423	32492.9	542	527.4	12.7	12.5	10.5	9.0	32.2	22.4
3.43	34604	32585.9	535	528.9	13.1	12.5	10.6	9.2	21.9	23.4
3.45	34433	32787.7	543	529.5	13	12.5	10.5	9.3	19.7	23.3
3.47	31409	32952.3	498	530.8	12.4	12.6	10.0	9.4	22.3	22.9
3.49	32441	32797.9	539	527.6	11.9	12.6	10.1	9.5	19.4	22.8
3.51	32417	32762.2	530	528.7	12	12.5	11.1	9.6	38.7	22.5
3.53	32429	32727.7	534.5	528.8	12.05	12.5	9.4	9.7	19.9	24.1
3.55	33222	32697.8	542	529.4	12.5	12.4	8.7	9.7	20.4	23.7
3.57	32394	32750.3	529.5	530.7	12.05	12.4	8.5	9.6	19.8	23.4
3.59	32029	32714.6	510	530.5	12.1	12.4	8.3	9.5	18.7	23.0
3.61	32371	32646.1	529	528.5	12	12.4	8.2	9.4	19.2	22.6
3.63	32931	32618.6	508	528.5	11.8	12.3	9.9	9.2	20.6	22.2
3.65	32397	32649.8	521.5	526.5	11.95	12.3	9.4	9.3	20.2	22.1
3.67	31513	32624.5	524	526.0	14.3	12.2	10.5	9.3	20	21.9
3.69	32422	32513.3	519	525.8	11.9	12.4	8.8	9.4	20.4	21.7
3.71	32221	32504.2	501	525.1	14.1	12.4	9.2	9.4	19.4	21.6
3.73	31107	32475.9	494	522.7	11.7	12.6	10.5	9.3	43.4	21.4
3.75	31414	32339.0	477	519.8	11.3	12.5	8.7	9.5	21	23.6
3.77	31475	32246.5	483	515.5	11.55	12.4	9.6	9.4	20.8	23.3
3.79	31536	32169.3	472	512.3	11.4	12.3	8.7	9.4	18.4	23.1
3.81	34314	32106.0	489	508.3	11.9	12.2	10.5	9.3	20.6	22.6
3.83	30727	32326.8	476	506.3	11	12.2	8.5	9.5	37.7	22.4
3.85	30598	32166.8	477	503.3	11.5	12.0	8.5	9.4	19.5	23.9
3.87	31726	32009.9	491	500.7	11.5	12.0	8.7	9.3	20.6	23.5
3.89	31902	31981.5	484.5	499.7	11.6	11.9	9.2	9.2	20.05	23.2
3.91	33150	31973.6	484	498.2	11.7	11.9	9.9	9.2	25.1	22.9
3.93	32078	32091.2	485	496.8	15.7	11.9	9.7	9.3	18.7	23.1
3.95	31217	32089.9	513	495.6	11.9	12.3	9.8	9.3	18.9	22.7
3.97	32788	32002.6	510	497.3	12.3	12.2	10.3	9.4	23.3	22.3
3.99	32449	32081.2	518	498.6	11.9	12.2	9.6	9.5	19.8	22.4
4.01	33363	32117.9	522	500.5	12	12.2	9.9	9.5	22.5	22.1
4.03	32139	32242.4	495	502.7	11.5	12.2	11.1	9.5	18.9	22.2
4.04	32301	32232.1	496.5	501.9	11.65	12.1	10.9	9.7	21	21.8
4.05	32462	32238.9	498	501.4	11.8	12.1	10.6	9.8	23.7	21.8
4.07	31788	32261.2	486	501.0	11.5	12.0	11.3	9.9	19.5	21.9
4.09	31960	32213.9	498	499.5	11.5	12.0	11.0	10.0	26.1	21.7
4.11	32371	32188.5	482	499.4	11.4	11.9	10.4	10.1	27.9	22.1
4.13	31124	32206.8	496	497.6	11.6	11.9	9.9	10.1	20.6	22.7
4.15	31845	32098.5	490	497.5	11.6	11.9	9.6	10.1	20.55	22.5
4.17	32045	32073.2	484	496.7	11.6	11.8	8.8	10.1	20.1	22.3
4.19	31645	32070.3	496	495.5	11.7	11.8	9.2	9.9	20.5	22.1
4.21	31294	32027.8	508	495.5	11.3	11.8	9.2	9.9	25.3	21.9

Depth (m)	Fe	Fe	Mn	Mn	Co	Co	As	As	Cu	Cu
4.23	32544	31954.4	500	496.8	11.7	11.7	9.7	9.8	21	22.3
4.25	33396	32013.4	533	497.1	12.4	11.7	11.4	9.8	20.3	22.1
4.27	32435	32151.6	535	500.7	12.35	11.8	10.7	9.9	20.65	22.0
4.29	32326	32180.0	537	504.1	12.3	11.9	11.2	10.0	20.3	21.8
4.31	31779	32194.6	575	507.4	12.4	11.9	10.1	10.1	24.1	21.7
4.33	30166	32153.0	507	514.2	11.8	12.0	9.7	10.1	19	21.9
4.35	31864	31954.3	531	513.4	12.6	11.9	10.8	10.1	21.7	21.6
4.37	31993	31945.3	530	515.2	12	12.0	9.7	10.2	20.8	21.6
4.39	32494	31950.1	529	516.7	12.4	12.0	11.0	10.1	21.25	21.5
4.41	32995	32004.5	528	517.9	12.2	12.0	11.2	10.2	19.7	21.5
4.43	33575	32103.5	525	518.9	12.8	12.1	11.4	10.3	31	21.3
4.45	33834	32250.7	522	519.5	13	12.1	13.0	10.4	24.2	22.3
4.47	33998	32409.0	521	519.8	12.7	12.2	10.8	10.7	22.1	22.5
4.49	32569	32567.9	505	519.9	12.8	12.3	10.7	10.7	20.2	22.5
4.51	33206	32568.0	519	518.4	12.5	12.3	9.9	10.7	20	22.2
4.53	33203	32631.8	525.5	518.5	12.6	12.3	10.6	10.6	20.35	22.0
4.55	33199	32688.9	534	519.2	12.7	12.4	10.5	10.6	21	21.8
4.57	34080	32739.9	526	520.7	12.6	12.4	10.7	10.6	20.75	21.8
4.59	35313	32873.8	532	521.2	12.3	12.4	10.8	10.6	20.5	21.7
4.61	34953	33117.8	520	522.3	12.7	12.4	11.2	10.6	22	21.5
4.63	35374	33301.3	558	522.0	12.7	12.4	10.4	10.7	22.1	21.6
4.65	34232	33508.6	539	525.6	12.7	12.5	10.5	10.7	22.05	21.6
4.67	33511	33580.9	566	527.0	13.2	12.5	10.6	10.6	22.8	21.7
4.69	30890	33573.9	504	530.9	12.1	12.6	9.7	10.6	22	21.8
4.71	33954	33305.5	549	528.2	12.8	12.5	10.4	10.5	22.3	21.8
4.73	34218	33370.4	521	530.3	12.7	12.5	11.5	10.5	21.5	21.9
4.75	34734	33455.1	559	529.3	12.7	12.6	12.9	10.6	21.3	21.8
4.77	33810	33583.0	553.5	532.3	12.8	12.6	11.4	10.9	21.2	21.8
4.79	33401	33605.7	548	534.4	12.9	12.6	10.9	10.9	21	21.7
4.81	33302	33585.2	592	535.8	12.9	12.6	11.3	10.9	21.1	21.6
4.83	34269	33556.9	548	541.4	12.5	12.7	11.9	10.9	20.3	21.6
4.85	33158	33628.1	548	542.1	12.4	12.6	11.0	11.0	19	21.5
4.87	32157	33581.1	555	542.7	12.4	12.6	12.4	11.0	28.5	21.2
4.89	33866	33438.7	558.5	543.9	12.7	12.6	12.1	11.2	22.75	21.9
4.91	34573	33481.4	596	545.4	13.5	12.6	12.2	11.3	24.6	22.0
4.93	36159	33590.5	562	550.4	13	12.7	11.9	11.4	20.9	22.3
4.95	35919	33847.4	556	551.6	13	12.7	12.5	11.4	20.9	22.1
4.97	35489	34054.5	560	552.0	14.4	12.8	12.4	11.5	21.6	22.0
4.99	35274	34198.0	541	552.8	13	12.9	12.5	11.6	24.7	22.0
5.01	35065	34305.6	545	551.6	13.3	12.9	11.4	11.7	21.9	22.2
5.03	35256	34381.5	543	551.0	13.2	13.0	11.9	11.7	23.3	22.2
5.05	36845	34469.0	567	550.2	13.1	13.0	12.3	11.7	26.2	22.3
5.07	35238	34706.6	536	551.9	19.2	13.0	11.4	11.7	21.4	22.7
5.09	35849	34759.7	515	550.3	12.6	13.6	12.2	11.7	20.7	22.6
5.11	35540	34868.6	520.5	546.7	12.6	13.5	12.3	11.8	22.2	22.4
5.13	35207	34935.8	523	544.1	12.6	13.4	12.3	11.8	58.4	22.4
5.15	35842	34962.9	518	542.0	12.3	13.3	14.1	11.9	23	26.0
5.17	35620	35050.8	520	539.6	13.3	13.2	13.1	12.1	26.5	25.7

Depth (m)	Fe	Fe	Mn	Mn	Co	Co	As	As	Cu	Cu
5.19	35879	35107.7	512	537.6	12.8	13.2	12.9	12.2	22.7	25.8
5.21	34171	35184.9	543	535.1	12.7	13.2	12.1	12.3	22.7	25.5
5.23	34780	35083.5	524	535.9	12.75	13.1	11.7	12.2	23.25	25.2
5.25	33877	35053.1	535	534.7	12.8	13.1	11.0	12.2	23.8	25.0
5.27	35388	34935.5	513	534.7	12.7	13.1	11.2	12.1	26	24.9
5.29	35432	34980.7	515	532.5	12.8	13.0	11.0	12.0	22.6	25.0
5.31	33751	35025.8	511	530.8	12.5	13.0	10.6	11.9	25.5	24.7
5.33	35077	34898.4	526	528.8	13.4	13.0	10.6	11.8	87.2	24.8
5.35	35257	34916.2	529.5	528.5	13.1	13.0	11.7	11.6	24.4	31.1
5.37	35437	34950.3	539	528.6	13.3	13.0	12.7	11.6	23.3	30.4
5.39	37965	34999.0	533	529.7	12.9	13.0	13.4	11.7	20.5	29.7
5.41	37065	35295.6	524	530.0	13.5	13.0	13.1	11.9	23.5	28.8
5.43	36537	35472.5	557	529.4	12.9	13.1	13.0	12.0	21.1	28.2
5.45	34143	35579.0	531	532.2	13.2	13.1	12.3	12.1	22.2	27.5
5.47	35814	35435.4	529.5	532.0	13.3	13.1	13.0	12.1	22.35	27.0
5.49	35090	35473.2	525	531.8	13.4	13.1	14.0	12.2	22.5	26.5
5.51	37482	35434.9	528	531.1	13.6	13.1	13.0	12.4	25.9	26.1
5.53	38007	35639.6	577	530.8	14	13.2	11.0	12.5	25.9	26.1
5.55	39110	35876.3	580	535.4	14.3	13.3	14.7	12.3	24.5	26.1
5.57	38000	36199.7	569	539.9	14.05	13.4	12.1	12.6	24	25.9
5.59	36808	36379.7	541	542.8	13.4	13.4	12.9	12.5	23.5	25.7
5.61	37692	36422.5	551.5	542.6	13.75	13.4	12.1	12.6	22.2	25.5
5.63	37993	36549.4	561	543.5	14.1	13.5	11.3	12.5	20.9	25.2
5.65	37390	36693.8	542	545.2	13.1	13.5	11.1	12.4	19.6	24.7
5.67	38019	36763.4	562	544.9	13	13.5	13.3	12.3	19.2	24.2
5.69	37647	36889.0	546	546.6	13.8	13.4	11.9	12.4	20.4	23.7
5.71	36755	36964.8	545	546.6	13.3	13.5	11.7	12.3	21.1	23.4
5.73	37201	36943.8	545.5	546.4	13.55	13.5	12.2	12.3	22.05	23.2
5.75	37704	36969.5	547	546.3	13.8	13.5	12.9	12.2	23.7	23.1
5.77	35150	37043.0	533	546.4	13.3	13.5	12.4	12.3	23	23.1
5.79	35699	36853.7	520	545.0	13.1	13.5	13.3	12.3	22.7	23.1
5.81	37342	36738.2	552	542.5	14	13.4	13.5	12.4	25.5	23.1
5.83	33866	36798.6	526	543.5	12.8	13.5	12.8	12.5	30.5	23.3
5.85	35737	36505.3	539	541.7	13.3	13.4	13.2	12.6	26.4	24.0
5.87	34132	36428.5	514	541.5	12.1	13.4	13.8	12.6	26	24.3
5.89	38472	36198.8	558	538.7	13.8	13.3	12.9	12.7	26.8	24.4
5.91	33894	36426.2	530	540.6	12.7	13.3	12.2	12.8	23.8	24.7
5.93	36748	36172.9	528	539.6	13.3	13.3	12.4	12.7	22.9	24.6
5.95	34269	36230.4	538	538.4	11.9	13.3	12.5	12.7	20.1	24.4
5.97	35945	36034.3	536.5	538.4	13.1	13.1	12.6	12.7	22.4	24.0
5.99	35421	36025.3	535	538.2	12.9	13.1	12.7	12.6	21.9	23.8
6.29	35472	35964.9	536.5	537.9	13.15	13.1	12.6	12.6	22.95	23.6
6.31	36468	35915.6	553	537.7	13.5	13.1	12.6	12.6	24	23.6
6.33	35523	35970.8	512	539.3	13.4	13.2	11.8	12.6	25.1	23.6
6.35	35736	35926.1	541	536.5	13.2	13.2	13.7	12.5	22.5	23.8

Depth (m)	Fe	Fe	Mn	Mn	Co	Co	As	As	Cu	Cu
6.37	35944	35907.1	524	537.0	13.6	13.2	15.2	12.7	25.2	23.6
6.39	32126	35910.7	496	535.7	13.8	13.2	12.6	12.9	24.4	23.8
6.41	35714	35532.3	524.5	531.7	13.6	13.3	14.1	12.9	24.8	23.9
6.43	36819	35550.4	547	531.0	13.1	13.3	13.4	13.0	22.2	23.9
6.45	35484	35677.3	525	532.6	13.6	13.3	14.7	13.0	26.6	23.8
6.47	36186	35658.0	521	531.8	13.1	13.3	15.0	13.2	24.8	24.1
6.49	34775	35710.8	527	530.8	12.6	13.3	12.5	13.4	24	24.1
6.51	36791	35617.2	563	530.4	13.4	13.2	13.3	13.3	24.6	24.1
6.53	36353	35734.6	545	533.6	13.35	13.2	12.4	13.3	23.8	24.2
6.55	35914	35796.4	524	534.8	13.3	13.3	12.3	13.2	23.4	24.1
6.57	36397	35808.1	543.5	533.7	13.6	13.3	12.5	13.1	23.75	24.1
6.59	37564	35867.0	575	534.7	13.8	13.3	12.0	13.1	23.6	24.0
6.61	36002	36036.7	518	538.7	17.1	13.3	12.7	13.0	23.9	24.0
6.63	36271	36033.2	579	536.6	13.9	13.7	16.2	12.9	37.3	24.0
6.65	36003	36057.0	579.5	540.9	15.65	13.7	13.3	13.3	31.35	25.3
6.67	36004	36051.6	580	544.7	14.2	13.9	13.8	13.3	37.7	25.9
6.69	34897	36046.8	583	548.3	17.4	14.0	11.6	13.3	25.4	27.1
6.71	37716	35931.8	560	551.7	13.9	14.3	13.7	13.1	25.5	26.9
6.73	36652	36110.3	562	552.6	14.1	14.3	15.5	13.2	38	26.8
6.75	35184	36164.4	572	553.5	14	14.2	14.4	13.4	23.7	27.9
6.77	36578	36066.4	567	555.4	14.05	14.2	14.0	13.5	30.85	27.5
6.79	36913	36117.5	553	556.5	13.4	14.2	12.1	13.6	23	27.8
6.81	36503	36197.1	588	556.2	14.2	14.1	13.6	13.4	52.1	27.3
6.83	37064	36227.6	599	559.4	13.8	14.1	16.9	13.4	35.7	29.8
6.85	35078	36311.3	558	563.3	13.9	14.1	14.0	13.8	24.8	30.4
6.87	35567	36188.0	566	562.8	13.7	14.1	15.7	13.8	27.3	29.8
6.89	35816	36125.9	562	563.1	13.9	14.0	15.1	14.0	26.65	29.6
6.91	37483	36094.8	585	563.0	15.6	14.0	16.4	14.1	31.6	29.3
6.93	36064	36233.6	543	565.2	13.9	14.2	14.4	14.3	26	29.5
6.95	37926	36216.7	571	563.0	14.3	14.2	15.8	14.3	25.8	29.2
6.97	36550	36387.6	563	563.8	13.9	14.2	13.9	14.5	27.6	28.8
6.99	37262	36403.8	564	563.7	14.2	14.1	16.6	14.4	25.9	28.7
7.01	36686	36489.7	557	563.7	13.8	14.1	13.2	14.6	25	28.4
7.03	36822	36509.3	544	563.1	13.7	14.1	12.4	14.5	23.5	28.1
7.05	34388	36540.6	551	561.2	13.1	14.1	11.9	14.3	24.1	27.6
7.07	37373	36325.3	539	560.1	13.6	14.0	12.4	14.0	34.8	27.3
7.09	34184	36430.1	568	558.0	13	13.9	12.2	13.9	25.4	28.0
7.11	36240	36205.5	564	559.0	13.8	13.8	13.4	13.7	26.2	27.8
7.13	36281	36208.9	552.5	559.5	13.45	13.8	12.8	13.7	25.75	27.6
7.15	36444	36216.1	521	558.8	13.1	13.8	12.0	13.6	25.3	27.4
7.17	36322	36238.9	541	555.0	13.9	13.7	16.2	13.4	26.1	27.2
7.19	36846	36247.2	548	553.6	14.3	13.7	14.9	13.7	31.2	27.1
7.21	36488	36307.1	528	553.1	14.2	13.8	12.7	13.8	24.6	27.5
7.23	37186	36325.2	551	550.6	13.3	13.8	14.4	13.7	26.7	27.2
7.25	36837	36411.3	550.5	550.6	14.55	13.8	13.6	13.8	26.25	27.2
7.27	37447	36453.8	572	550.6	14.9	13.9	15.9	13.8	28.3	27.1
7.29	36021	36553.2	550	552.7	15.8	14.0	10.3	14.0	25.8	27.2
7.31	36767	36499.9	564	552.5	14.4	14.2	12.5	13.6	36.5	27.1

Appendix 8 (continued)

Depth (m)	Fe	Fe	Mn	Mn	Co	Co	As	As	Cu	Cu
7.33	37096	36526.7	560	553.6	13.8	14.2	16.0	13.5	25.2	28.0
7.35	37046	36583.6	531	554.3	15.3	14.1	13.4	13.7	27.6	27.7
7.37	37071	36629.8	538.5	551.9	13.65	14.3	14.5	13.7	24.85	27.7
7.39	37441	36673.9	521	550.6	13.2	14.2	11.6	13.8	23.8	27.4
7.41	36198	36750.7	546	547.6	13.5	14.1	15.6	13.6	24.5	27.1
7.43	37097	36695.4	548	547.5	13	14.0	12.9	13.8	23.6	26.8
7.45	36658	36735.5	516	547.5	13.7	13.9	11.6	13.7	26.9	26.5
7.47	37371	36727.8	521	544.4	13.4	13.9	11.1	13.5	24.7	26.5
7.49	36772	36792.1	521	542.0	13.55	13.9	12.0	13.2	25.8	26.3
7.51	34575	36790.1	521	539.9	12.4	13.8	12.4	13.1	22.5	26.3
7.53	36885	36568.5	547	538.0	13.8	13.7	13.0	13.0	37.6	25.9
7.55	36901	36600.2	517	538.9	12.9	13.7	13.8	13.0	25.2	27.1
7.57	36889	36630.3	517.5	536.7	12.9	13.6	13.0	13.1	28.3	26.9
7.59	36784	36656.1	518	534.8	12.9	13.5	13.0	13.1	31.4	27.0
7.61	36893	36668.9	513	533.1	12.9	13.5	12.1	13.1	22	27.5
7.63	36912	36691.3	544	531.1	13	13.4	13.2	13.0	20.2	26.9
7.65	36765	36713.4	516.5	532.4	12.95	13.4	12.7	13.0	22.65	26.2
7.67	36636	36718.5	520	530.8	13.3	13.3	13.6	13.0	23.3	25.9
7.69	35895	36710.3	491	529.7	12.8	13.3	11.8	13.0	23.3	25.6
7.71	36210	36628.7	519	525.9	13.3	13.3	14.7	12.9	23	25.4
7.73	35719	36586.9	503	525.2	16.9	13.3	13.9	13.1	22.8	25.2
7.75	35711	36500.1	547	523.0	13.3	13.6	13.0	13.2	24.6	24.9
7.77	36371	36421.2	512.5	525.4	13.7	13.6	13.5	13.2	22.6	24.9
7.79	37244	36416.1	522	524.1	14.1	13.6	15.7	13.2	21.2	24.7
7.81	37022	36498.9	502	523.9	13.1	13.7	12.9	13.4	22.4	24.3
7.83	34872	36551.2	499	521.7	13.1	13.6	12.2	13.4	24.7	24.1
7.85	35884	36383.3	500	519.4	12.3	13.6	16.3	13.3	24.7	24.2
7.87	35749	36333.4	512	517.5	15.6	13.4	12.9	13.6	25.8	24.2
7.89	35817	36274.9	511	516.9	12.5	13.6	12.8	13.5	23.25	24.4
7.91	36638	36229.1	630	516.3	12.7	13.5	12.6	13.4	20.2	24.3
7.93	35342	36270.0	510	527.7	12.3	13.5	12.7	13.3	21.8	23.9
7.95	38239	36177.2	525	525.9	13.1	13.3	13.2	13.3	20.7	23.7
7.97	36599	36383.4	489	525.8	12.8	13.3	13.3	13.3	22.7	23.4
7.99	37899	36404.9	510	522.2	12.8	13.3	12.9	13.3	19.1	23.3
8.01	38244	36554.3	512.5	520.9	12.8	13.2	13.1	13.2	23.4	22.9
8.03	38817	36723.2	515	520.1	13	13.2	14.9	13.2	24.1	22.9
8.05	38588	36932.6	519	519.6	12.5	13.2	12.4	13.4	25.5	23.0
8.07	36739	37098.2	569	519.5	13	13.1	10.5	13.3	508.3	23.3
8.09	36669	37062.2	540	524.5	12.6	13.1	13.7	13.0	24.4	71.8
8.11	37278	37022.9	520	526.0	12.9	13.0	14.5	13.1	25.3	67.1
8.13	36625	37048.4	525.5	525.4	13.05	13.0	14.1	13.2	24.85	62.9
8.15	36581	37006.1	531	525.4	18.9	13.0	15.3	13.3	27.3	59.1
8.17	36408	36963.6	506	526.0	13.2	13.6	13.6	13.5	24.2	55.9
8.19	38299	36908.0	522	524.0	13.2	13.6	13.9	13.5	23.2	52.7
8.21	36091	37047.1	490	523.8	12.3	13.5	12.8	13.6	22.8	49.8
8.23	38886	36951.5	533	520.4	13.1	13.4	14.1	13.5	28.2	47.1
8.25	36254	37145.0	509.5	521.7	12.6	13.4	14.2	13.5	26.1	45.2
8.27	36386	37055.8	502	520.5	12.9	13.3	15.2	13.6	24	43.3

Appendix 8 (continued)

Depth (m)	Fe	*Fe*	Mn	*Mn*	Co	*Co*	As	*As*	Cu	*Cu*
8.29	36121	36988.8	517	518.6	12.2	13.3	14.2	13.8	34.5	41.4
8.31	38976	36902.0	515	518.4	12.9	13.2	14.4	13.8	20.5	40.7
8.33	35904	37109.4	495	518.1	12.5	13.1	12.5	13.9	24.7	38.7
8.35	36403	36988.9	506	515.8	12	13.1	14.3	13.7	21.4	37.3
8.37	36154	36930.3	506.5	514.8	12.15	13.0	14.2	13.8	21.45	35.7
8.39	35182	36852.6	507	514.0	11.9	12.9	14.2	13.8	19.8	34.2
8.41	36472	36685.6	507	513.3	12.3	12.8	14.2	13.9	21.5	32.8
8.43	37003	36664.2	496	512.7	12.9	12.7	15.2	13.9	24.2	31.7
8.45	35400	36698.1	486	511.0	12.4	12.7	11.2	14.0	23	30.9
8.47	36504	36568.3	486	508.5	12.5	12.7	12.6	13.7	22.3	30.1
8.49	36101	36561.9	488.5	506.2	12.45	12.7	12.7	13.6	22.65	29.3
8.51	37129	36515.7	570	504.5	13.1	12.7	13.3	13.5	20	28.7
8.53	36470	36577.0	495.5	511.0	12.4	12.7	13.1	13.5	22.9	27.8
8.55	35697	36566.3	491	509.5	12.2	12.7	12.8	13.5	23.5	27.3
8.57	36436	36479.4	500	507.6	12.3	12.6	15.7	13.4	25.8	26.9
8.59	34894	36475.1	492	506.9	12	12.6	13.5	13.6	22.1	26.8
8.61	36672	36317.0	478	505.4	12.9	12.5	13.6	13.6	28.6	26.4
8.63	37077	36352.5	472	502.6	12	12.6	14.6	13.6	22.7	26.6
8.65	36875	36424.9	475.5	499.6	12.45	12.5	13.8	13.7	25.65	26.2
8.67	37913	36469.9	533	497.2	13.2	12.5	13.3	13.7	1499	26.1
8.69	34615	36614.2	473	500.7	11.9	12.6	13.9	13.7	22.5	173.4
8.71	35853	36414.3	500	498.0	11.9	12.5	13.2	13.7	21.9	158.3
8.73	34432	36358.1	472	498.2	11.5	12.5	12.2	13.6	28.7	144.7
8.75	35315	36165.5	431	495.6	11.4	12.4	11.1	13.5	21	133.1
8.77	35124	36080.5	466	489.1	11.55	12.3	11.8	13.3	23.85	121.9
8.79	35578	35984.8	476	486.8	11.8	12.2	13.5	13.1	20.1	112.1
8.81	34932	35944.1	460	485.7	11.6	12.2	11.3	13.2	26.7	102.9
8.83	35695	35842.9	444	483.1	11.1	12.1	12.2	13.0	24.9	95.3
8.85	36698	35828.1	495	479.2	11.4	12.0	11.5	12.9	20.8	88.2
8.87	36432	35915.1	483	480.8	11.2	11.9	13.0	12.8	20.7	81.5
8.89	36467	35966.8	481	481.0	11.3	11.9	11.9	12.8	21.15	75.4
8.91	35643	36016.8	479	481.0	11.2	11.8	11.8	12.7	22.5	70.0
8.93	36501	35979.4	429	480.8	11.5	11.7	11.9	12.6	21.5	65.2
8.95	35353	36031.5	479	475.6	11.7	11.7	12.4	12.5	24.6	60.9
8.97	35116	35963.7	462	476.0	11.6	11.7	12.5	12.5	22.6	57.2
8.99	35244	35878.9	468	474.6	11.6	11.7	12.2	12.5	19	53.8
9.01	35180	35815.4	465	473.9	11.6	11.7	12.0	12.5	21.9	50.3
9.03	36615	35751.9	535	473.0	12.8	11.7	10.5	12.4	22	47.5
9.05	35049	35838.2	444	479.2	11.4	11.8	11.8	12.2	21.8	44.9
9.07	36747	35759.3	535	475.7	12.1	11.8	11.3	12.2	17.8	42.6
9.09	35898	35858.0	490.5	481.6	11.8	11.8	11.5	12.1	19.65	40.1
9.11	36923	35862.0	502	482.5	12.6	11.8	10.3	12.0	19.8	38.1
9.13	34246	35968.1	479	484.5	11.5	11.9	11.7	11.9	19.5	36.2
9.15	37105	35795.9	544	483.9	12.6	11.8	11.8	11.9	21.6	34.6
9.17	34573	35926.8	476	489.9	11.7	11.9	12.2	11.8	20.5	33.3
9.19	37320	35791.4	514	488.5	12.4	11.9	11.8	11.9	20.6	32.0
9.21	35760	35944.3	495	491.1	12.2	11.9	12.2	11.9	22.75	30.9
9.23	36630	35925.8	516	491.5	12.8	12.0	12.8	11.9	67.1	30.0
9.25	34889	35996.2	467	493.9	12	12.1	12.2	12.0	24.9	33.8

Appendix 8 (continued)

Depth (m)	Fe	Fe	Mn	Mn	Co	Co	As	As	Cu	Cu
9.27	37218	35885.5	529	491.2	12.7	12.0	10.9	12.0	23.3	32.9
9.29	34858	36018.8	452	495.0	11.9	12.1	12.8	11.9	22.1	31.9
9.31	39211	35902.7	516	490.7	12.8	12.1	11.2	12.0	20.9	30.9
9.33	38920	36233.5	518	493.2	12.75	12.2	12.5	11.9	21.05	29.9
9.35	38939	36502.2	535	495.7	12.7	12.2	12.3	12.0	19.3	29.0
9.37	38901	36745.9	520	499.6	12.9	12.3	12.6	12.0	21.2	28.1
9.39	35697	36961.4	471	501.7	12.1	12.3	13.2	12.1	21.5	27.4
9.41	35153	36834.9	468	498.6	11.8	12.3	11.9	12.2	20.6	26.8
9.43	39748	36666.7	493	495.5	12.8	12.3	13.1	12.1	20.9	26.2
9.45	37210	36974.9	480.5	495.3	12.3	12.3	12.8	12.2	20.75	25.6
9.47	38604	36998.4	531	493.8	12.8	12.3	12.9	12.3	19.7	25.2
9.49	35816	37158.9	455	497.5	11.7	12.4	12.7	12.4	57.8	24.6
9.51	39872	37024.6	508	493.3	12.9	12.3	12.1	12.4	22.1	27.9
9.53	39524	37309.4	521	494.8	13	12.4	13.9	12.4	23	27.3
9.55	39526	37530.8	519	497.4	13.2	12.4	12.7	12.5	21.7	26.9
9.57	38807	37730.4	513.5	499.5	13.1	12.5	12.6	12.5	22.35	26.4
9.59	38090	37838.0	508	500.9	13.2	12.6	12.3	12.5	21.1	26.0
9.61	35398	37863.2	485	501.6	11.9	12.6	12.5	12.5	26.4	25.5
9.63	39473	37616.7	508	500.0	13	12.5	12.4	12.5	21.4	25.6
9.65	35442	37802.3	459	500.8	11.5	12.6	11.5	12.5	20.1	25.2
9.67	39810	37566.3	537	496.6	13	12.5	12.0	12.4	19.3	24.7
9.69	37277	37790.7	494	500.6	12.35	12.5	11.7	12.4	20.15	24.1
9.71	38766	37739.3	513	500.0	12.7	12.5	11.8	12.3	20.3	23.7
9.73	35788	37842.0	475	501.3	12	12.5	11.5	12.2	20.2	23.4
9.75	39164	37636.6	518	498.7	12.7	12.5	13.0	12.2	19.2	23.1
9.77	35294	37789.3	512	500.6	13.1	12.5	13.3	12.3	20.8	22.7
9.79	38345	37539.8	508	501.7	12.5	12.6	12.4	12.4	17.9	22.5
9.81	37659	37620.3	510	502.4	12.95	12.6	13.4	12.4	20.6	22.0
9.83	39975	37624.2	499	503.1	12.8	12.6	13.5	12.5	20.4	21.9
9.85	36973	37859.3	541	502.7	13.1	12.6	14.7	12.6	26.9	21.7
9.87	39137	37770.6	525	506.5	13.2	12.7	11.2	12.8	19.7	22.3
9.89	37420	37907.3	512	508.4	12.8	12.7	14.7	12.6	23.2	22.0
9.91	39867	37858.5	504	508.7	13	12.7	12.1	12.8	19.5	22.1
9.93	39307	38059.4	494	508.3	12.9	12.8	13.4	12.8	20.4	21.9
9.95	38948	38184.1	470	506.8	12.4	12.8	11.7	12.8	18.6	21.7
9.97	39666	38260.5	484	503.2	13.6	12.7	15.1	12.7	21.3	21.4
9.99	42070	38401.1	510	501.2	13.1	12.8	13.3	12.9	20	21.4
10.1	40979	38768.0	492	502.1	13.7	12.8	16.0	13.0	22.9	21.3
10.03	45141	38989.1	512	501.1	14.5	12.9	19.6	13.3	20	21.4
10.05	45996	39604.3	542	502.2	14.75	13.1	19.0	13.9	22.65	21.3
10.07	47440	40243.4	575	506.2	15.3	13.3	21.2	14.4	22.4	21.4

231

Depth (m)	**Li**	*Li*	**Ba**	*Ba*	**Al**	*Al*	**K**	*K*	**Rb**	*Rb*
1.31	61.3	73.8	252.0	244.0	26499.0	32466.6	16813.0	17137.0	15.9	15.6
1.33	66	72.5	247.0	244.8	24465.0	31869.9	15143.0	17104.6	12.0	15.6
1.35	66.7	71.9	238.0	245.0	17856.0	31129.4	13427.0	16908.4	8.4	15.3
1.37	65.7	71.3	240.0	244.3	22299.0	29802.0	14128.0	16560.3	8.6	14.6
1.39	70.5	70.8	244.0	243.9	22764.0	29051.7	14653.0	16317.0	9.4	14.0
1.41	68.65	70.8	242.0	243.9	23277.0	28423.0	14168.0	16150.6	9.5	13.5
1.43	66.8	70.5	246.0	243.7	23798.0	27908.4	14208.0	15952.4	10.0	13.1
1.45	71.7	70.2	238.0	243.9	23790.0	27497.3	13880.0	15777.9	9.5	12.8
1.47	69.3	70.3	245.0	243.3	17906.0	27126.6	12529.0	15588.1	5.6	12.5
1.49	61.9	70.2	247.0	243.5	25221.0	26204.5	15519.0	15282.2	11.4	11.8
1.51	63.4	69.4	243.0	243.9	22176.0	26106.2	13758.0	15305.9	8.5	11.8
1.53	62.65	68.8	240.0	243.8	23005.0	25713.2	14638.5	15151.1	10.0	11.4
1.54	56.43	68.2	219.0	243.4	23834.0	25442.3	20577.0	15099.9	12.3	11.3
1.55	64	67.0	237.0	241.0	19828.0	25281.5	13525.0	15647.6	6.1	11.4
1.57	56.8	66.7	243.0	240.6	25090.0	24736.2	18911.0	15435.3	18.2	10.8
1.59	54.6	65.7	239.0	240.8	27293.0	24771.5	18933.0	15782.9	19.1	11.6
1.61	58.8	64.6	245.0	240.6	25799.0	25023.7	18913.0	16097.9	18.2	12.3
1.63	57.3	64.0	250.0	241.1	26195.0	25101.2	19486.0	16379.4	19.6	12.9
1.65	60.5	63.3	248.0	242.0	25997.0	25210.6	19485.0	16690.1	19.6	13.6
1.67	62.2	63.1	246.0	242.6	25683.0	25289.2	19489.0	16969.6	19.5	14.2
1.69	67.9	63.0	268.0	242.9	33750.0	25328.6	19484.0	17221.5	40.1	14.7
1.71	59.3	63.5	256.0	245.4	28532.0	26170.8	20006.0	17447.8	26.7	17.3
1.73	54.9	63.1	238.0	246.5	19918.0	26406.9	14535.0	17703.6	16.8	18.2
1.75	57.4	62.2	235.0	245.6	23465.0	25758.0	19482.0	17386.7	20.9	18.1
1.77	63.25	61.8	236.5	244.6	23464.5	25528.7	17424.5	17596.2	16.2	18.3
1.79	76.1	61.9	232.0	243.8	23464.0	25322.3	16831.0	17579.1	6.1	18.1
1.81	69.1	63.3	241.0	242.6	28209.0	25136.4	18018.0	17504.3	15.5	16.9
1.83	70.8	63.9	246.0	242.4	27186.0	25443.7	15960.0	17555.6	16.5	16.8
1.85	72.2	64.6	249.0	242.8	27191.0	25617.9	16222.0	17396.1	16.8	16.8
1.87	71.9	65.4	249.0	243.4	26202.0	25775.2	16202.0	17278.7	17.0	16.8
1.89	72.55	66.0	249.0	244.0	25975.5	25817.9	15712.5	17171.0	16.4	16.8
1.91	72.9	66.7	249.0	244.5	25749.0	25833.7	15223.0	17025.2	16.0	16.7
1.93	74.3	67.3	244.0	244.9	22858.0	25825.2	14290.0	16844.9	13.4	16.7
1.95	70.9	68.0	246.0	244.8	26069.0	25528.5	16405.0	16589.4	14.2	16.3
1.97	74.2	68.3	245.0	244.9	26323.0	25582.5	15994.0	16571.0	14.3	16.1
1.99	72.5	68.9	240.0	244.9	26534.0	25656.6	16526.0	16513.3	13.4	15.9
2.01	71.6	69.2	235.0	244.5	23278.0	25744.3	14218.0	16514.6	14.2	15.7
2.03	70.5	69.5	229.5	243.5	24504.0	25497.7	15282.5	16284.9	13.2	15.5
2.05	68.1	69.6	221.0	242.1	24416.0	25398.3	15349.0	16184.7	13.0	15.3
2.07	69.4	69.4	224.0	240.0	24592.0	25300.1	15216.0	16101.1	12.9	15.1
2.09	71	69.4	217.0	238.4	22329.0	25229.3	14379.0	16012.6	8.4	14.9
2.11	63.6	69.6	218.0	236.3	27530.0	24939.3	16144.0	15849.2	13.3	14.2
2.13	69	69.0	225.0	234.4	28402.0	25198.3	16245.0	15878.7	15.0	14.1
2.15	66	69.0	220.5	233.5	27966.0	25518.7	16406.0	15915.3	14.2	14.2
2.17	67.1	68.7	223.0	232.2	28575.0	25763.4	16567.0	15964.4	15.2	14.2
2.19	64.9	68.5	210.0	231.3	27125.0	26044.6	16682.0	16024.7	11.6	14.3
2.21	62.3	68.2	207.0	229.1	24666.0	26152.6	15336.0	16090.4	14.0	14.0
2.23	69.2	67.6	222.0	226.9	29086.0	26004.0	17069.0	16015.0	13.5	14.0
2.25	67.4	67.7	222.0	226.4	29336.0	26312.2	17413.0	16120.4	15.2	14.0
2.27	69.65	67.7	224.5	226.0	28574.0	26614.5	17168.0	16249.6	14.4	14.1
2.29	70.1	67.9	231.0	225.8	28062.0	26810.5	17267.0	16341.5	15.7	14.1

Bold-raw data, *Italic*- exponentially smoothened data

Depth (m)	Ba	*Ba*	K	*K*	Li	*Li*	Rb	*Rb*	Al	*Al*
2.31	227.0	226.4	14905.0	16434.0	71.8	68.1	11.0	14.3	23358.0	26935.6
2.33	227.0	226.4	18278.0	16281.1	68.3	68.5	19.1	14.0	33400.0	26577.9
2.35	225.0	226.5	17501.0	16480.8	66.9	68.5	18.1	14.5	31301.0	27260.1
2.37	220.0	226.3	16315.0	16582.8	69	68.3	16.7	14.8	28640.0	27664.2
2.39	222.5	225.7	16908.0	16556.0	67.65	68.4	17.4	15.0	29970.5	27761.8
2.41	231.0	225.4	18045.0	16591.2	68.4	68.3	19.4	15.3	34504.0	27982.6
2.43	216.0	225.9	14646.0	16736.6	65.6	68.3	7.4	15.7	21697.0	28634.8
2.45	251.0	224.9	16749.0	16527.6	72.2	68.0	19.0	14.8	34659.0	27941.0
2.47	220.0	227.6	17018.0	16549.7	67.3	68.5	14.2	15.3	29121.0	28612.8
2.49	227.0	226.8	18685.0	16596.5	70.8	68.3	19.6	15.2	35821.0	28663.6
2.51	231.0	226.8	18486.0	16805.4	72.4	68.6	17.2	15.6	32806.0	29379.4
2.53	222.0	227.2	17081.5	16973.4	69.55	69.0	13.5	15.8	28269.5	29722.0
2.55	217.0	226.7	15677.0	16984.2	67.8	69.0	9.7	15.5	23733.0	29576.8
2.57	224.0	225.7	16382.5	16853.5	69.85	68.9	11.2	14.9	26850.0	28992.4
2.59	224.0	225.6	16382.5	16806.4	69.85	69.0	11.2	14.6	26850.0	28778.2
2.61	205.0	225.4	14892.0	16764.0	68.3	69.1	7.9	14.2	22432.0	28585.3
2.63	231.0	223.4	17088.0	16576.8	71.4	69.0	12.6	13.6	29967.0	27970.0
2.65	223.0	224.1	16579.0	16627.9	72.4	69.2	10.2	13.5	26201.5	28169.7
2.67	224.0	224.0	16812.0	16623.0	73.4	69.6	9.8	13.2	26213.0	27972.9
2.69	222.0	224.0	16346.0	16641.9	73.8	69.9	10.6	12.8	26190.0	27796.9
2.71	208.0	223.8	15113.0	16612.3	71.7	70.3	8.9	12.6	23537.0	27636.2
2.73	226.0	222.2	17370.0	16462.4	75.5	70.5	11.6	12.2	28437.0	27226.3
2.75	228.0	222.6	18140.0	16553.2	72.8	71.0	12.0	12.2	28537.0	27347.4
2.77	227.0	223.1	17939.5	16711.9	72.25	71.2	11.9	12.2	28487.0	27466.3
2.79	231.0	223.5	20637.0	16834.6	71.7	71.3	12.7	12.1	32523.0	27568.4
2.81	215.0	224.3	17739.0	17214.9	68.2	71.3	11.8	12.2	27156.0	28063.8
2.85	192.0	223.4	19020.0	17267.3	58.7	71.0	10.9	12.1	27800.0	27973.1
2.87	218.0	220.2	16695.0	17442.5	77.9	69.8	8.0	12.0	20240.0	27955.8
2.89	210.0	220.0	16367.0	17367.8	77.45	70.6	8.2	11.6	20898.5	27184.2
2.91	208.0	219.0	14868.0	17267.7	80.9	71.3	6.7	11.3	20025.0	26555.6
2.93	212.0	217.9	16039.0	17027.7	77	72.2	8.3	10.8	21557.0	25902.6
2.95	217.0	217.3	15717.0	16928.9	83.9	72.7	7.2	10.6	20948.0	25468.0
2.97	217.0	217.3	16416.0	16807.7	84	73.8	8.7	10.2	23027.0	25016.0
2.99	221.0	217.2	16360.0	16768.5	86.4	74.8	9.4	10.1	25087.0	24817.1
3.01	245.0	217.6	17383.0	16727.7	86.2	76.0	11.4	10.0	26710.0	24844.1
3.03	221.5	220.4	16669.0	16793.2	83.6	77.0	9.5	10.1	24058.0	25030.7
3.07	222.0	220.5	16978.0	16780.8	81	77.7	9.6	10.1	23029.0	24933.4
3.09	217.0	220.6	16587.0	16800.5	83.6	78.0	9.3	10.0	23309.5	24743.0
3.11	210.0	220.3	14597.0	16779.1	79.9	78.6	9.0	10.0	14891.0	24599.6
3.13	212.0	219.2	16196.0	16560.9	87.2	78.7	9.0	9.9	23590.0	23628.8
3.15	212.0	218.5	15396.5	16524.4	81.95	79.6	9.0	9.8	21975.0	23624.9
3.17	221.0	217.9	16474.0	16411.6	83	79.8	9.1	9.7	22691.0	23459.9
3.19	212.0	218.2	14160.0	16417.9	80.9	80.1	7.8	9.6	21259.0	23383.0
3.21	248.0	217.6	19609.0	16192.1	81.1	80.2	24.9	9.5	29405.0	23170.6
3.23	237.0	220.6	19011.0	16533.8	82	80.3	20.6	11.0	31183.0	23794.0
3.25	243.0	222.2	19658.0	16781.5	82.8	80.5	25.7	12.0	32625.0	24532.9
3.27	240.0	224.3	19334.5	17069.2	82.4	80.7	23.8	13.3	31305.5	25342.1
3.29	245.0	225.9	19856.0	17295.7	82.8	80.9	24.6	14.4	31428.0	25938.5

Depth (m)	**Ba**	*Ba*	**K**	*K*	**Li**	*Li*	**Rb**	*Rb*	**Al**	*Al*
3.31	234.0	227.8	18622.0	17551.7	80	81.1	23.0	15.4	29596.0	26487.4
3.33	242.0	228.4	21792.0	17658.7	83.8	80.9	25.0	16.2	32003.0	26798.3
3.35	245.0	229.8	17998.0	18072.1	86.5	81.2	23.2	17.0	29227.0	27318.8
3.37	237.0	231.3	17993.0	18064.7	85.6	81.8	24.0	17.7	27461.0	27509.6
3.39	242.0	231.9	17869.0	18057.5	86.05	82.1	23.6	18.3	28678.5	27504.7
3.41	239.0	232.9	17585.0	18038.6	84.6	82.5	25.3	18.8	28130.0	27622.1
3.43	252.0	233.5	17745.0	17993.3	93.4	82.7	20.9	19.5	30571.0	27672.9
3.45	254.0	235.3	17782.0	17968.5	92.1	83.8	24.0	19.6	30968.0	27962.7
3.47	241.0	237.2	16438.0	17949.8	90.7	84.6	19.1	20.1	33082.0	28263.2
3.49	263.0	237.6	18270.0	17798.6	67.8	85.2	22.0	20.0	34608.0	28745.1
3.51	275.0	240.1	17768.0	17845.8	71	83.5	24.2	20.2	34528.0	29331.4
3.53	266.5	243.6	18032.0	17838.0	69.2	82.2	23.8	20.6	34429.0	29851.1
3.55	267.0	245.9	17794.0	17857.4	69.3	80.9	23.7	20.9	34330.0	30308.9
3.57	266.5	248.0	17781.0	17851.1	69.2	79.8	24.0	21.2	34176.5	30711.0
3.59	266.0	249.9	18432.0	17844.0	69.1	78.7	23.8	21.4	31235.0	31057.5
3.61	264.0	251.5	17669.0	17902.8	64.2	77.8	24.1	21.7	34023.0	31075.3
3.63	265.0	252.7	17159.0	17879.5	71.8	76.4	24.7	21.9	34130.0	31370.0
3.65	264.5	254.0	17414.0	17807.4	72.05	75.9	24.4	22.2	35163.0	31646.0
3.67	269.0	255.0	16461.0	17768.1	72.3	75.6	25.0	22.4	36196.0	31997.7
3.69	261.0	256.4	17836.0	17637.4	72.6	75.2	21.3	22.7	37161.0	32417.6
3.71	266.0	256.9	17882.0	17657.2	72.7	75.0	21.4	22.5	34893.0	32891.9
3.73	263.0	257.8	16170.0	17679.7	72.5	74.7	22.0	22.4	32342.0	33092.0
3.75	211.0	258.3	11937.0	17528.7	75.3	74.5	6.3	22.4	21129.0	33017.0
3.77	222.0	253.6	13622.5	16969.6	73.9	74.6	9.8	20.8	27241.5	31828.2
3.79	218.0	250.4	13738.0	16634.9	70.8	74.5	10.8	19.7	26884.0	31369.5
3.81	226.0	247.2	13507.0	16345.2	75.9	74.2	8.7	18.8	27599.0	30921.0
3.83	222.0	245.1	12360.0	16061.4	72.2	74.3	9.3	17.8	26358.0	30588.8
3.85	222.0	242.8	12408.0	15691.2	74.6	74.1	8.2	16.9	23251.0	30165.7
3.87	228.0	240.7	13661.0	15362.9	72.4	74.2	11.4	16.1	28912.0	29474.2
3.89	225.0	239.4	13416.0	15192.7	73.55	74.0	10.7	15.6	27919.5	29418.0
3.91	237.0	238.0	14583.0	15015.0	73.9	73.9	12.4	15.1	30525.0	29268.2
3.93	218.0	237.9	13171.0	14971.8	73.2	73.9	10.0	14.8	26927.0	29393.8
3.95	222.0	235.9	12377.0	14791.7	73.6	73.9	9.9	14.3	25499.0	29147.2
3.97	222.0	234.5	13667.0	14550.3	76.2	73.8	10.0	13.9	27232.0	28782.3
3.99	211.0	233.2	11775.0	14461.9	76.3	74.1	7.0	13.5	21934.0	28627.3
4.01	256.0	231.0	16958.0	14193.3	76.8	74.3	17.1	12.9	29067.0	27958.0
4.03	254.0	233.5	17698.0	14469.7	69.5	74.5	19.2	13.3	30781.0	28068.9
4.04	255.0	235.6	17853.5	14792.6	74.4	74.0	18.8	13.9	30721.5	28340.1
4.05	256.0	237.5	18332.0	15098.6	74.9	74.1	18.9	14.4	30662.0	28578.2
4.07	253.0	239.4	18009.0	15422.0	73.9	74.2	18.6	14.8	31711.0	28786.6
4.09	255.0	240.7	18149.0	15680.7	74.5	74.1	18.5	15.2	31658.0	29079.0
4.11	257.0	242.2	19859.0	15927.5	72.4	74.2	24.9	15.5	35035.0	29336.9
4.13	263.0	243.6	18454.0	16320.7	76.5	74.0	20.0	16.5	32494.0	29906.8
4.15	256.5	245.6	18558.0	16534.0	75.4	74.2	19.8	16.8	34339.0	30165.5
4.17	256.0	246.7	17526.0	16736.4	74.9	74.4	18.4	17.1	33745.0	30582.8
4.19	256.0	247.6	18662.0	16815.4	75.9	74.4	19.5	17.2	34933.0	30899.0
4.21	260.0	248.4	17799.0	17000.0	74.6	74.6	20.8	17.5	33638.0	31302.4

Depth (m)	**Ba**	*Ba*	**K**	*K*	**Li**	*Li*	**Rb**	*Rb*	**Al**	*Al*
4.23	251.0	249.6	17749.0	17079.9	75.4	74.6	19.4	17.8	29853.0	31536.0
4.25	260.0	249.7	18810.0	17146.8	70.6	74.6	17.6	18.0	34452.0	31367.7
4.27	262.0	250.8	18657.5	17313.1	68.7	74.2	20.1	17.9	35211.0	31676.1
4.29	264.0	251.9	19382.0	17447.6	65.9	73.7	21.6	18.1	37235.0	32029.6
4.31	267.0	253.1	18505.0	17641.0	66.8	72.9	20.7	18.5	35970.0	32550.2
4.33	258.0	254.5	18025.0	17727.4	65	72.3	18.7	18.7	33310.0	32892.1
4.35	267.0	254.8	19127.0	17757.2	69.4	71.6	19.2	18.7	34329.0	32933.9
4.37	241.0	256.1	18743.0	17894.2	60.2	71.4	19.7	18.8	36723.0	33073.4
4.39	260.0	254.5	18824.5	17979.0	65.1	70.2	19.5	18.8	35017.0	33438.4
4.41	253.0	255.1	16943.0	18063.6	63.1	69.7	17.2	18.9	29979.0	33596.2
4.43	274.0	254.9	18906.0	17951.5	67.1	69.1	21.8	18.7	35705.0	33234.5
4.45	276.0	256.8	18308.0	18047.0	74	68.9	17.8	19.0	38222.0	33481.6
4.47	271.0	258.7	18719.0	18073.1	68	69.4	20.6	18.9	37539.0	33955.6
4.49	276.0	259.9	17771.0	18137.7	70.9	69.2	19.5	19.1	33822.0	34314.0
4.51	213.0	261.6	13699.0	18101.0	67.4	69.4	9.4	19.1	22831.0	34264.8
4.53	252.5	256.7	16414.5	17660.8	69.65	69.2	16.5	18.2	29911.0	33121.4
4.55	232.0	256.3	15342.0	17536.2	70	69.3	14.6	18.0	28868.0	32800.3
4.57	252.5	253.8	16414.5	17316.8	69.65	69.3	16.5	17.7	29911.0	32407.1
4.59	273.0	253.7	17487.0	17226.5	69.3	69.4	18.4	17.5	30954.0	32157.5
4.61	278.0	255.6	17877.0	17252.6	70.9	69.4	21.0	17.6	33721.0	32037.1
4.63	276.0	257.9	18238.0	17315.0	69.3	69.5	24.6	18.0	36112.0	32205.5
4.65	277.0	259.7	17968.0	17407.3	70.1	69.5	24.3	18.6	34071.0	32596.2
4.67	281.0	261.4	18059.0	17463.4	72.4	69.5	24.9	19.2	34421.0	32743.7
4.69	258.0	263.4	16776.0	17522.9	64.8	69.8	24.0	19.8	31760.0	32911.4
4.71	276.0	262.8	18044.0	17448.3	70.1	69.3	24.0	20.2	36449.0	32796.3
4.73	281.0	264.2	18385.0	17507.8	70.9	69.4	22.6	20.6	37972.0	33161.5
4.75	284.0	265.8	18502.0	17595.5	69	69.6	25.9	20.8	39180.0	33642.6
4.77	280.0	267.7	18126.5	17686.2	69.95	69.5	24.3	21.3	36865.0	34196.3
4.79	279.0	268.9	17682.0	17730.2	71.3	69.5	22.7	21.6	34818.0	34463.2
4.81	276.0	269.9	17868.0	17725.4	68	69.7	25.9	21.7	35758.0	34498.7
4.83	272.0	270.5	17407.0	17739.7	68.5	69.5	21.1	22.1	35110.0	34624.6
4.85	236.0	270.7	15227.0	17706.4	60.3	69.4	17.7	22.0	22045.0	34673.1
4.87	260.0	267.2	17310.0	17458.5	61.4	68.5	25.7	21.6	30753.0	33410.3
4.89	267.5	266.5	17563.0	17443.6	64.05	67.8	20.6	22.0	34070.5	33144.6
4.91	275.0	266.6	17816.0	17455.5	70.1	67.4	18.9	21.9	37388.0	33237.2
4.93	278.0	267.4	20513.0	17491.6	66.7	67.7	22.2	21.6	37882.0	33652.3
4.95	278.0	268.5	19014.0	17793.7	68	67.6	22.1	21.6	39209.0	34075.2
4.97	266.0	269.4	18367.0	17915.8	64.4	67.6	23.4	21.7	41057.0	34588.6
4.99	280.0	269.1	18489.0	17960.9	64.6	67.3	20.5	21.8	39598.0	35235.5
5.01	274.0	270.2	18239.0	18013.7	65.3	67.0	22.8	21.7	36263.0	35671.7
5.03	277.5	270.6	18508.0	18036.2	65.4	66.9	22.2	21.8	36805.0	35730.8
5.05	278.0	271.3	20701.0	18083.4	67.3	66.7	25.1	21.8	37347.0	35838.3
5.07	277.0	271.9	18527.0	18345.2	65.5	66.8	21.5	22.2	35439.0	35989.1
5.09	276.0	272.4	18134.0	18363.3	62.5	66.7	20.7	22.1	34841.0	35934.1
5.11	266.5	272.8	17793.0	18340.4	63.05	66.2	21.1	22.0	31535.5	35824.8
5.13	237.0	272.2	15809.0	18285.7	61.7	65.9	12.1	21.9	22922.0	35395.9
5.15	257.0	268.6	17452.0	18038.0	63.6	65.5	22.2	20.9	28230.0	34148.5
5.17	254.0	267.5	16741.0	17979.4	61.6	65.3	16.5	21.0	26938.0	33556.6

Depth (m)	**Ba**	*Ba*	**K**	*K*	**Li**	*Li*	**Rb**	*Rb*	**Al**	*Al*
5.19	258.0	266.1	16703.0	17855.6	64.4	64.9	16.6	20.6	27057.0	32894.8
5.21	249.0	265.3	16632.0	17740.3	62.2	64.9	17.4	20.2	26544.0	32311.0
5.23	250.0	263.7	16747.5	17629.5	63.3	64.6	17.0	19.9	26800.5	31734.3
5.25	241.0	262.3	16792.0	17541.3	61.8	64.5	21.2	19.6	28280.0	31240.9
5.27	251.0	260.2	17176.0	17466.4	64.6	64.2	15.2	19.8	25984.0	30944.8
5.29	253.0	259.3	16968.0	17437.3	61.9	64.3	19.0	19.3	27614.0	30448.7
5.31	246.0	258.6	16219.0	17390.4	61.6	64.0	17.3	19.3	24620.0	30165.3
5.33	250.0	257.4	16369.0	17273.2	64.2	63.8	15.4	19.1	25650.0	29610.7
5.35	245.0	256.6	15845.5	17182.8	64.5	63.8	15.4	18.7	24712.5	29214.7
5.37	244.0	255.5	15472.0	17049.1	64.8	63.9	15.4	18.4	23175.0	28764.5
5.39	235.0	254.3	12926.0	16891.4	77.3	64.0	9.2	18.1	24805.0	28205.5
5.41	249.0	252.4	17950.0	16494.8	59.9	65.3	23.3	17.2	30776.0	27865.5
5.43	247.0	252.1	15766.0	16640.4	75.8	64.8	14.3	17.8	32652.0	28156.5
5.45	243.0	251.6	17368.0	16552.9	62.2	65.9	20.1	17.5	33629.0	28606.1
5.47	249.0	250.7	17212.0	16634.4	69	65.5	18.1	17.7	33845.0	29108.4
5.49	251.0	250.5	17625.0	16692.2	61.8	65.9	21.5	17.8	34061.0	29582.0
5.51	251.0	250.6	17056.0	16785.5	77.2	65.4	16.0	18.1	36567.0	30029.9
5.53	254.0	250.6	16035.0	16812.5	78.4	66.6	14.6	17.9	35483.0	30683.6
5.55	259.0	251.0	16236.0	16734.8	78.2	67.8	16.1	17.6	32799.0	31163.6
5.57	259.5	251.8	16320.0	16684.9	76.85	68.8	17.0	17.4	32331.5	31327.1
5.59	261.0	252.5	16404.0	16648.4	75.2	69.6	18.2	17.4	30331.0	31427.5
5.61	260.5	253.4	16494.5	16624.0	75.5	70.2	18.1	17.5	31683.5	31317.9
5.63	260.0	254.1	16585.0	16611.0	75.5	70.7	17.9	17.5	31864.0	31354.5
5.65	268.0	254.7	17287.0	16608.4	75.5	71.2	21.3	17.6	31503.0	31405.4
5.67	245.0	256.0	15520.0	16676.3	73.8	71.6	14.9	17.9	32005.0	31415.2
5.69	262.0	254.9	16833.0	16560.6	78.3	71.9	18.1	17.6	34151.0	31474.1
5.71	256.0	255.6	15523.0	16587.9	77.1	72.5	15.4	17.7	30211.0	31741.8
5.73	259.0	255.7	15874.0	16481.4	77.35	73.0	16.0	17.5	32282.0	31588.8
5.75	264.0	256.0	15824.0	16420.7	77.6	73.4	16.5	17.3	33724.0	31658.1
5.77	224.0	256.8	15924.0	16361.0	73.3	73.8	12.9	17.2	30840.0	31864.7
5.79	222.0	253.5	15169.0	16317.3	73.7	73.8	12.3	16.8	29732.0	31762.2
5.81	264.0	250.4	17351.0	16202.5	74.7	73.8	22.8	16.3	41802.0	31559.2
5.83	215.0	251.7	15072.0	16317.3	69.8	73.9	10.8	17.0	29976.0	32583.5
5.85	238.5	248.1	16025.5	16192.8	73.05	73.4	13.9	16.4	32857.5	32322.7
5.87	212.0	247.1	14508.0	16176.1	71.4	73.4	10.0	16.1	27470.0	32376.2
5.89	262.0	243.6	16979.0	16009.2	77.6	73.2	16.9	15.5	35739.0	31885.6
5.91	220.0	245.4	15573.0	16106.2	68	73.6	13.2	15.6	33873.0	32270.9
5.93	221.0	242.9	14889.0	16052.9	72.8	73.1	10.9	15.4	27174.0	32431.1
5.95	205.0	240.7	12836.0	15936.5	66.8	73.1	6.9	15.0	21895.0	31905.4
5.97	222.5	237.1	15286.0	15626.5	70.5	72.4	11.7	14.1	29095.5	30904.4
5.99	224.0	235.7	15683.0	15592.4	68.2	72.2	12.5	13.9	31017.0	30723.5
6.29	236.0	234.5	16056.0	15601.5	67.5	71.8	15.1	13.8	32437.0	30752.8
6.31	269.0	234.6	16429.0	15646.9	81.3	71.4	17.6	13.9	38430.0	30921.3
6.33	248.0	238.1	17296.0	15725.1	65.9	72.4	19.5	14.3	33857.0	31672.1
6.35	247.0	239.1	17934.0	15882.2	64	71.7	20.4	14.8	33654.0	31890.6

Depth (m)	**Ba**	*Ba*	**K**	*K*	**Li**	*Li*	**Rb**	*Rb*	**Al**	*Al*
6.37	244.0	239.9	18314.0	16087.4	64.4	71.0	20.3	15.3	37226.0	32067.0
6.39	234.0	240.3	16990.0	16310.1	57	70.3	20.3	15.8	33982.0	32582.9
6.41	247.5	239.7	17616.5	16378.1	63.45	69.0	20.3	16.3	35534.0	32722.8
6.43	258.0	240.4	16747.0	16501.9	74.3	68.4	16.3	16.7	37086.0	33003.9
6.45	251.0	242.2	18243.0	16526.4	62.5	69.0	20.9	16.6	32904.0	33412.1
6.47	242.0	243.1	18481.0	16698.1	61.5	68.4	21.3	17.1	38097.0	33361.3
6.49	250.0	243.0	17869.0	16876.4	60.6	67.7	21.9	17.5	31642.0	33834.9
6.51	254.0	243.7	16555.0	16975.6	71.5	67.0	17.2	17.9	37729.0	33615.6
6.53	252.0	244.7	17325.5	16933.6	68.25	67.4	18.2	17.9	35452.5	34026.9
6.55	247.0	245.4	17463.0	16972.8	65	67.5	18.9	17.9	33176.0	34169.5
6.57	252.5	245.6	17325.5	17021.8	68.25	67.3	17.3	18.0	35869.5	34070.1
6.59	263.0	246.3	17188.0	17052.2	76.1	67.4	17.4	17.9	38605.0	34250.1
6.61	251.0	248.0	17559.0	17065.7	64.5	68.2	15.7	17.9	34010.0	34685.6
6.63	269.0	248.3	17657.0	17115.1	80	67.9	16.1	17.7	36346.0	34618.0
6.65	268.5	250.3	17422.0	17169.3	82.4	69.1	15.1	17.5	34105.0	34790.8
6.67	274.0	252.1	17285.0	17194.5	84.8	70.4	14.4	17.3	33907.0	34722.2
6.69	268.0	254.3	17143.0	17203.6	84.9	71.8	14.4	17.0	34200.0	34640.7
6.71	267.0	255.7	17366.0	17197.5	75.1	73.1	17.8	16.7	40448.0	34596.6
6.73	268.0	256.8	17785.0	17214.4	83.2	73.3	16.4	16.8	33914.0	35181.8
6.75	264.0	257.9	17306.0	17271.4	81.1	74.3	15.7	16.8	34139.0	35055.0
6.77	266.0	258.6	17550.5	17274.9	81.75	75.0	16.6	16.7	35556.5	34963.4
6.79	257.0	259.3	17316.0	17302.4	75.1	75.7	17.0	16.7	38379.0	35022.7
6.81	273.0	259.1	18052.0	17303.8	82.4	75.6	16.7	16.7	36974.0	35358.3
6.83	264.0	260.5	17882.0	17378.6	78.7	76.3	19.0	16.7	32920.0	35519.9
6.85	265.0	260.8	17713.0	17429.0	81.2	76.5	15.8	16.9	35233.0	35259.9
6.87	261.0	261.2	17584.0	17457.4	82	77.0	16.7	16.8	33135.0	35257.2
6.89	264.5	261.2	18141.0	17470.0	81.5	77.5	16.6	16.8	36329.0	35045.0
6.91	266.0	261.5	18569.0	17537.1	81.8	77.9	19.7	16.8	37425.0	35173.4
6.93	264.0	262.0	19921.0	17640.3	79.6	78.3	16.4	17.1	39307.0	35398.6
6.95	265.0	262.2	18835.0	17868.4	81.5	78.4	14.7	17.0	40079.0	35789.4
6.97	260.0	262.5	18640.0	17965.0	78.8	78.7	17.5	16.8	39386.0	36218.4
6.99	263.0	262.2	18847.0	18032.5	82.7	78.7	15.5	16.8	37184.0	36535.1
7.01	260.0	262.3	18743.5	18114.0	76.95	79.1	16.9	16.7	38952.5	36600.0
7.03	257.0	262.1	16968.0	18176.9	75.1	78.9	16.2	16.7	38519.0	36835.3
7.05	260.0	261.6	19071.0	18056.0	71.3	78.5	27.4	16.7	40581.0	37003.6
7.07	256.0	261.4	16644.0	18157.5	75.7	77.8	15.9	17.7	33719.0	37361.4
7.09	248.0	260.9	17947.0	18006.2	65.2	77.6	19.7	17.6	37464.0	36997.1
7.11	268.0	259.6	18757.0	18000.3	76.2	76.4	16.1	17.8	41883.0	37043.8
7.13	252.5	260.4	18228.5	18075.9	75.55	76.3	15.6	17.6	38229.0	37527.7
7.15	244.0	259.6	14802.0	18091.2	74.9	76.3	13.8	17.4	28462.0	37597.9
7.17	257.0	258.1	18510.0	17762.3	80.7	76.1	15.1	17.0	38994.0	36684.3
7.19	260.0	258.0	18505.0	17837.0	79.8	76.6	16.5	16.9	35757.0	36915.3
7.21	258.0	258.2	18358.0	17903.8	82.7	76.9	15.9	16.8	40621.0	36799.4
7.23	240.0	258.1	15155.0	17949.3	78.3	77.5	11.3	16.7	28388.0	37181.6
7.25	252.0	256.3	17786.5	17669.8	83.05	77.6	14.9	16.2	32932.5	36302.2
7.27	246.0	255.9	17215.0	17681.5	83.4	78.1	13.8	16.0	30420.0	35965.3
7.29	260.0	254.9	18831.0	17634.9	83.6	78.6	18.1	15.8	35445.0	35410.7
7.31	241.0	255.4	17040.0	17754.5	84.9	79.1	12.8	16.1	34648.0	35414.2

Depth (m)	**Ba**	*Ba*	**K**	*K*	**Li**	*Li*	**Rb**	*Rb*	**Al**	*Al*
7.33	234.0	254.0	16971.0	17683.0	84.9	79.7	12.9	15.7	36549.0	35337.5
7.35	238.0	252.0	17381.0	17611.8	83.5	80.2	12.5	15.4	34338.0	35458.7
7.37	236.0	250.6	16895.0	17588.7	83.1	80.6	12.7	15.1	35443.5	35346.6
7.39	249.0	249.1	16177.0	17519.4	78.9	80.8	13.2	14.9	33319.0	35356.3
7.41	228.0	249.1	16819.0	17385.1	82.7	80.6	12.5	14.7	37340.0	35152.6
7.43	237.0	247.0	15382.0	17328.5	74.8	80.8	11.5	14.5	29699.0	35371.3
7.45	241.0	246.0	17915.0	17133.9	82.9	80.2	12.2	14.2	36487.0	34804.1
7.47	249.0	245.5	15893.0	17212.0	76.9	80.5	14.5	14.0	33190.0	34972.4
7.49	245.0	245.8	16916.0	17080.1	80.25	80.1	13.4	14.1	34838.5	34794.1
7.51	241.0	245.8	15917.0	17063.7	78	80.1	10.9	14.0	31421.0	34798.6
7.53	256.0	245.3	18747.0	16949.0	82.5	79.9	16.2	13.7	36809.0	34460.8
7.55	222.0	246.4	16664.0	17128.8	80	80.2	13.5	13.9	32219.0	34695.6
7.57	235.5	243.9	17415.5	17082.3	80.3	80.2	13.7	13.9	34395.0	34448.0
7.59	249.0	243.1	18167.0	17115.6	80.2	80.2	13.8	13.9	36513.0	34442.7
7.61	220.0	243.7	16615.0	17220.8	80.4	80.2	10.3	13.9	32277.0	34649.7
7.63	252.0	241.3	15054.0	17160.2	83.5	80.2	11.4	13.5	29433.0	34412.4
7.65	239.5	242.4	18186.0	16949.6	81.95	80.5	11.9	13.3	34223.0	33914.5
7.67	240.0	242.1	22079.0	17073.2	86.1	80.7	12.3	13.1	36169.0	33945.3
7.69	239.0	241.9	19757.0	17573.8	78.7	81.2	15.1	13.1	41555.0	34167.7
7.71	249.0	241.6	18906.0	17792.1	76.1	81.0	13.2	13.3	36146.0	34906.4
7.73	250.0	242.3	18552.0	17903.5	76.2	80.5	12.3	13.3	35035.0	35030.4
7.75	255.0	243.1	19082.0	17968.4	78.9	80.1	13.2	13.2	38567.0	35030.9
7.77	254.5	244.3	19280.5	18079.7	76.1	79.9	13.5	13.2	39434.5	35384.5
7.79	254.0	245.3	19595.0	18199.8	74	79.6	14.8	13.2	44449.0	35789.5
7.81	261.0	246.2	19479.0	18339.3	76	79.0	13.7	13.4	40302.0	36655.4
7.83	246.0	247.7	18322.0	18453.3	78.4	78.7	13.1	13.4	36193.0	37020.1
7.85	248.0	247.5	19200.0	18440.2	70.8	78.7	15.2	13.4	44666.0	36937.4
7.87	255.0	247.5	20061.0	18516.1	70.3	77.9	19.0	13.5	38760.0	37710.2
7.89	245.0	248.3	19009.0	18670.6	71.3	77.1	14.6	14.1	37447.5	37815.2
7.91	231.0	248.0	12893.0	18704.5	80.4	76.5	7.1	14.1	21830.0	37778.4
7.93	242.0	246.3	18818.0	18123.3	71.8	76.9	14.0	13.4	36135.0	36183.6
7.95	258.0	245.8	15988.0	18192.8	81.9	76.4	12.6	13.5	31900.0	36178.7
7.97	224.0	247.1	18324.0	17972.3	75.5	77.0	12.1	13.4	40837.0	35750.9
7.99	258.0	244.7	17264.0	18007.5	84.2	76.8	19.1	13.3	33590.0	36259.5
8.01	232.0	246.1	19158.5	17933.1	76.95	77.6	15.7	13.9	45019.5	35992.5
8.03	236.0	244.7	19993.0	18055.7	78.3	77.5	15.2	14.0	49202.0	36895.2
8.05	228.0	243.8	20213.0	18249.4	75.6	77.6	16.2	14.2	49720.0	38125.9
8.07	250.0	242.2	15868.0	18445.8	83.7	77.4	16.0	14.4	30946.0	39285.3
8.09	229.0	243.0	19607.0	18188.0	75.4	78.0	23.1	14.5	47722.0	38451.4
8.11	229.0	241.6	19725.0	18329.9	77.2	77.7	13.3	15.4	47636.0	39378.4
8.13	229.0	240.3	19080.5	18469.4	76.3	77.7	13.2	15.2	46289.5	40204.2
8.15	211.0	239.2	18554.0	18530.5	74.1	77.6	13.0	15.0	44365.0	40812.7
8.17	230.0	236.4	18467.0	18532.9	79.7	77.2	12.9	14.8	44943.0	41168.0
8.19	250.0	235.7	16925.0	18526.3	87.2	77.5	11.8	14.6	30762.0	41545.5
8.21	216.0	237.2	19006.0	18366.1	76.9	78.4	13.7	14.3	48610.0	40467.1
8.23	255.0	235.1	17276.0	18430.1	85.3	78.3	13.7	14.2	34406.0	41281.4
8.25	225.0	237.0	19314.0	18314.7	76.5	79.0	13.7	14.2	48358.5	40593.9
8.27	222.0	235.8	19655.0	18414.6	76.1	78.7	13.1	14.1	49306.0	41370.3

Depth (m)	Ba	*Ba*	K	*K*	Li	*Li*	Rb	*Rb*	Al	*Al*
8.29	228.0	234.5	19622.0	18538.7	76	78.5	14.5	14.0	48107.0	42163.9
8.31	275.0	233.8	16632.0	18647.0	88.9	78.2	13.0	14.1	34224.0	42758.2
8.33	221.0	237.9	19330.0	18445.5	78.4	79.3	13.2	14.0	46173.0	41904.8
8.35	206.0	236.2	17334.0	18534.0	74	79.2	11.1	13.9	32835.0	42331.6
8.37	217.5	233.2	17987.5	18414.0	76.85	78.7	12.2	13.6	35852.0	41381.9
8.39	214.0	231.6	12798.0	18371.3	83.3	78.5	7.5	13.5	19031.0	40829.0
8.41	221.0	229.9	18641.0	17814.0	75.3	79.0	13.2	12.9	38869.0	38649.2
8.43	227.0	229.0	18462.0	17896.7	76.8	78.6	12.9	12.9	37818.0	38671.1
8.45	234.0	228.8	18979.0	17953.2	78.4	78.4	13.3	12.9	38571.0	38585.8
8.47	232.0	229.3	18923.0	18055.8	80	78.4	16.8	12.9	39406.0	38584.3
8.49	233.0	229.6	18951.0	18142.5	79.2	78.6	13.4	13.3	38988.5	38666.5
8.51	247.0	229.9	16097.0	18223.4	87.7	78.6	12.1	13.3	30871.0	38698.7
8.53	229.5	231.6	18886.0	18010.7	79.1	79.6	14.0	13.2	40289.0	37915.9
8.55	227.0	231.4	19217.0	18098.3	78.2	79.5	13.5	13.3	42686.0	38153.2
8.57	226.0	231.0	18849.0	18210.1	76.6	79.4	14.4	13.3	41172.0	38606.5
8.59	219.0	230.5	18421.0	18274.0	71.1	79.1	13.2	13.4	38179.0	38863.1
8.61	226.0	229.3	19435.0	18288.7	71.2	78.3	19.3	13.4	41124.0	38794.7
8.63	221.0	229.0	18261.0	18403.3	70.4	77.6	15.0	14.0	36515.0	39027.6
8.65	223.5	228.2	18121.5	18389.1	71.25	76.9	14.7	14.1	37830.0	38776.3
8.67	263.0	227.7	17982.0	18362.3	87.3	76.3	14.4	14.1	39145.0	38681.7
8.69	213.0	231.3	17388.0	18324.3	71.3	77.4	12.3	14.2	35438.0	38728.0
8.71	219.0	229.4	16359.0	18230.7	72.1	76.8	9.6	14.0	29430.0	38399.0
8.73	230.0	228.4	17703.0	18043.5	69.3	76.3	12.6	13.5	36303.0	37502.1
8.75	226.0	228.5	17291.0	18009.5	73.1	75.6	10.8	13.5	33213.0	37382.2
8.77	226.5	228.3	17594.5	17937.6	70.4	75.4	11.7	13.2	35264.0	36965.3
8.79	221.0	228.1	17774.0	17903.3	67	74.9	12.8	13.0	35719.0	36795.2
8.81	227.0	227.4	17486.0	17890.4	71.5	74.1	10.6	13.0	34809.0	36687.5
8.83	226.0	227.4	17606.0	17849.9	67	73.8	11.5	12.8	34765.0	36499.7
8.85	226.0	227.2	19277.0	17825.5	66.5	73.1	12.7	12.6	42312.0	36326.2
8.87	212.0	227.1	16607.0	17970.7	65.9	72.5	10.2	12.7	31825.0	36924.8
8.89	219.5	225.6	17819.5	17834.3	66.2	71.8	12.2	12.4	35642.5	36414.8
8.91	213.0	225.0	17420.0	17832.8	64.7	71.3	12.8	12.4	33570.0	36337.6
8.93	229.0	223.8	18219.0	17791.6	69.7	70.6	11.7	12.4	37715.0	36060.8
8.95	244.0	224.3	20296.0	17834.3	67.5	70.5	21.0	12.4	33529.0	36226.2
8.97	246.0	226.3	18445.0	18080.5	72	70.2	13.6	13.2	38976.0	35956.5
8.99	237.0	228.2	18075.0	18116.9	71.1	70.4	13.6	13.3	33472.0	36258.5
9.01	245.5	229.1	18260.0	18112.7	71.55	70.5	13.9	13.3	37564.5	35979.8
9.03	253.0	230.8	17860.0	18127.5	86.8	70.6	14.1	13.3	36974.0	36138.3
9.05	245.0	233.0	18992.0	18100.7	67	72.2	15.7	13.4	38155.0	36221.9
9.07	236.0	234.2	16114.0	18189.8	78.9	71.7	12.0	13.7	31444.0	36415.2
9.09	239.5	234.4	17553.0	17982.3	72.95	72.4	14.6	13.5	33717.5	35918.1
9.11	243.0	234.9	16114.0	17939.3	84	72.5	13.4	13.6	35991.0	35698.0
9.13	230.0	235.7	19185.0	17756.8	58.7	73.6	21.5	13.6	30694.0	35727.3
9.15	238.0	235.1	16104.0	17899.6	84.8	72.1	12.0	14.4	35435.0	35224.0
9.17	247.0	235.4	19426.0	17720.1	67.9	73.4	16.2	14.1	42048.0	35245.1
9.19	237.0	236.6	16402.0	17890.7	84.6	72.8	11.8	14.3	32188.0	35925.4
9.21	248.0	236.6	17522.0	17741.8	77.45	74.0	12.6	14.1	36050.5	35551.6
9.23	252.0	237.8	13822.0	17719.8	88.8	74.4	9.1	13.9	28663.0	35601.5
9.25	249.0	239.2	18642.0	17330.0	70.3	75.8	13.4	13.5	39913.0	34907.7

Depth (m)	**Ba**	*Ba*	**K**	*K*	**Li**	*Li*	**Rb**	*Rb*	**Al**	*Al*
9.27	263.0	240.2	15125.0	17461.2	88.9	75.3	11.5	13.4	34103.0	35408.2
9.29	243.0	242.4	18683.0	17227.6	69.8	76.6	13.4	13.3	36380.0	35277.7
9.31	265.0	242.5	16988.0	17373.1	87	75.9	12.4	13.3	36920.0	35387.9
9.33	264.5	244.7	16348.5	17334.6	87.2	77.0	12.6	13.2	36606.0	35541.1
9.35	268.0	246.7	15432.0	17236.0	87.4	78.1	11.5	13.1	34862.0	35647.6
9.37	264.0	248.9	15709.0	17055.6	90.9	79.0	12.8	13.0	36832.0	35569.0
9.39	252.0	250.4	19625.0	16921.0	68.9	80.2	15.6	12.9	41293.0	35695.3
9.41	245.0	250.5	19048.0	17191.4	68.7	79.1	15.0	13.2	37682.0	36255.1
9.43	259.0	250.0	15123.0	17377.0	84.7	78.0	15.4	13.4	33626.0	36397.8
9.45	252.0	250.9	16899.0	17151.6	76.85	78.7	15.2	13.6	34834.0	36120.6
9.47	259.0	251.0	14607.0	17126.4	86.8	78.5	11.9	13.8	34702.0	35992.0
9.49	243.0	251.8	18675.0	16874.4	69	79.3	15.5	13.6	34966.0	35863.0
9.51	266.0	250.9	16331.0	17054.5	88.7	78.3	18.8	13.8	41602.0	35773.3
9.53	267.0	252.4	15998.0	16982.1	89.1	79.3	19.2	14.3	38111.0	36356.1
9.55	268.0	253.9	15769.0	16883.7	88.4	80.3	20.5	14.8	38957.0	36531.6
9.57	265.5	255.3	15819.0	16772.2	88.75	81.1	16.1	15.3	36000.5	36774.2
9.59	264.0	256.3	14736.0	16676.9	89.9	81.9	12.9	15.4	33890.0	36696.8
9.61	235.0	257.1	15869.0	16482.8	72.6	82.7	10.2	15.2	28378.0	36416.1
9.63	255.0	254.9	15189.0	16421.4	92.4	81.7	10.9	14.7	33450.0	35612.3
9.65	244.0	254.9	17290.0	16298.2	71.1	82.8	13.1	14.3	34252.0	35396.1
9.67	260.0	253.8	16679.0	16397.4	87.2	81.6	13.0	14.2	39509.0	35281.7
9.69	245.0	254.4	16984.5	16425.5	76.9	82.1	14.3	14.0	35139.5	35704.4
9.71	246.0	253.5	16079.0	16481.4	82.7	81.6	15.4	14.1	33071.0	35647.9
9.73	239.0	252.7	18556.0	16441.2	61.4	81.7	20.7	14.2	36027.0	35390.2
9.75	252.0	251.4	15413.0	16652.7	87	79.7	12.3	14.9	34863.0	35453.9
9.77	254.0	251.4	17977.0	16528.7	79.6	80.4	17.8	14.6	37784.0	35394.8
9.79	216.0	251.7	11270.0	16673.5	84.9	80.3	6.3	14.9	20782.0	35633.7
9.81	251.0	248.1	17565.5	16133.2	84.8	80.8	13.4	14.1	37944.5	34148.6
9.83	259.0	248.4	17423.0	16276.4	88	81.2	12.7	14.0	41656.0	34528.1
9.85	248.0	249.5	17708.0	16391.1	84.7	81.9	14.1	13.9	38105.0	35240.9
9.87	270.0	249.3	17205.0	16522.8	78.3	82.2	16.6	13.9	39913.0	35527.3
9.89	253.0	251.4	18480.0	16591.0	82.5	81.8	15.4	14.2	35221.0	35965.9
9.91	258.0	251.5	17065.0	16779.9	81.7	81.8	14.6	14.3	36437.0	35891.4
9.93	254.5	252.2	17143.5	16808.4	81.4	81.8	15.0	14.3	35829.0	35946.0
9.95	256.0	252.4	17222.0	16841.9	81.1	81.8	13.7	14.4	41877.0	35934.3
9.97	222.0	252.8	16725.0	16879.9	74	81.7	16.1	14.3	30138.0	36528.5
9.99	254.0	249.7	16509.0	16864.4	80.4	80.9	15.9	14.5	35004.0	35889.5
10.1	237.0	250.1	16964.0	16828.9	78.5	80.9	11.9	14.6	35914.0	35800.9
10.03	212.0	248.8	15392.0	16842.4	71.9	80.7	10.1	14.4	26600.0	35812.3
10.05	206.0	245.1	14762.0	16697.4	71.2	79.8	10.1	13.9	26243.0	34891.0
10.07	194.0	241.2	14070.0	16503.8	68.3	78.9	8.4	13.5	25886.0	34026.2

Depth (m)	**Sr**	*Sr*	**Na**	*Na*	**Mg**	*Mg*	**Ca**	*Ca*	B/Be	*B/Be*
1.31	122.9	82.3	10080.0	8310.0	1287.0	751.0	13161.0	8869.5	22.5	22.3
1.33	88.2	86.4	10021.0	8487.0	1069.0	804.6	10925.0	9298.6	26.3	22.3
1.35	181.6	86.6	11490.0	8640.4	1745.0	831.0	16296.0	9461.3	25.9	22.7
1.37	109.9	96.1	10549.0	8925.3	1286.0	922.4	11993.0	10144.7	24.0	23.0
1.39	94.8	97.5	11305.0	9087.7	1458.0	958.8	14534.0	10329.6	25.5	23.1
1.41	98.7	97.2	10896.0	9309.4	1404.0	1008.7	12518.0	10750.0	25.3	23.4
1.43	91.8	97.3	10668.0	9468.1	1350.0	1048.2	11898.0	10926.8	25.0	23.5
1.45	102.6	96.8	11124.0	9588.1	1474.0	1078.4	13043.0	11023.9	24.3	23.7
1.47	123.4	97.4	12504.0	9741.7	1577.0	1118.0	16479.0	11225.8	24.1	23.7
1.49	97.0	100.0	10738.0	10017.9	1142.0	1163.9	11708.0	11751.1	26.0	23.8
1.51	95.2	99.7	10536.0	10089.9	1333.0	1161.7	11391.0	11746.8	25.7	24.0
1.53	96.1	99.2	10700.0	10134.5	1417.0	1178.8	13147.5	11711.2	25.8	24.2
1.54	65.5	98.9	10662.0	10191.1	1501.0	1202.6	49375.0	11854.9	25.8	24.3
1.55	116.0	95.6	12443.0	10238.2	1764.0	1232.5	14587.0	15606.9	25.9	24.5
1.57	80.0	97.6	9364.0	10458.6	932.0	1285.6	11708.0	15504.9	25.8	24.6
1.59	70.6	95.9	7915.0	10349.2	430.0	1250.3	5777.0	15125.2	25.6	24.7
1.61	77.3	93.3	8724.0	10105.8	498.0	1168.2	7732.0	14190.4	25.2	24.8
1.63	76.4	91.7	8262.0	9967.6	504.0	1101.2	6001.0	13544.5	23.8	24.9
1.65	76.9	90.2	8789.0	9797.0	641.0	1041.5	7751.0	12790.2	24.8	24.8
1.67	73.4	88.9	8854.0	9696.2	778.0	1001.4	7770.0	12286.3	25.8	24.8
1.69	89.4	87.3	9395.0	9612.0	3230.0	979.1	8175.0	11834.6	23.6	24.9
1.71	81.0	87.5	9153.0	9590.3	1629.0	1204.2	8659.0	11468.7	26.9	24.7
1.73	75.1	86.9	12577.0	9546.6	1590.0	1246.7	11811.0	11187.7	24.3	25.0
1.75	77.2	85.7	9556.0	9849.6	702.0	1281.0	8761.0	11250.0	24.2	24.9
1.77	80.7	84.8	9409.5	9820.3	928.5	1223.1	7508.5	11001.1	25.1	24.8
1.79	102.8	84.4	9263.0	9779.2	630.0	1193.6	5776.0	10651.9	27.3	24.9
1.81	84.1	86.3	8266.0	9727.6	1155.0	1137.3	6256.0	10164.3	25.0	25.1
1.83	86.6	86.0	10123.0	9581.4	933.0	1139.0	13024.0	9773.5	25.2	25.1
1.85	84.5	86.1	9470.0	9635.6	999.0	1118.4	11156.0	10098.5	28.5	25.1
1.87	92.5	85.9	10335.0	9619.0	939.0	1106.5	9208.0	10204.3	25.0	25.4
1.89	89.7	86.6	10125.5	9690.6	969.0	1089.7	10221.5	10104.6	25.6	25.4
1.91	88.9	86.9	9916.0	9734.1	933.0	1077.7	9287.0	10116.3	25.4	25.4
1.93	90.4	87.1	11212.0	9752.3	1528.0	1063.2	11691.0	10033.4	26.4	25.4
1.95	98.2	87.4	11526.0	9898.3	1173.0	1109.7	13583.0	10199.2	27.3	25.5
1.97	99.0	88.5	9979.0	10061.0	960.0	1116.0	10081.0	10537.5	24.8	25.7
1.99	102.7	89.6	12129.0	10052.8	1344.0	1100.4	11502.0	10491.9	27.0	25.6
2.01	111.4	90.9	11743.0	10260.4	1949.0	1124.8	11192.0	10592.9	26.7	25.7
2.03	107.1	92.9	11366.0	10408.7	1336.5	1207.2	10844.5	10652.8	26.8	25.8
2.05	93.7	94.3	9691.0	10504.4	757.0	1220.1	8981.0	10672.0	29.0	25.9
2.07	120.5	94.3	10989.0	10423.1	1329.0	1173.8	10497.0	10502.9	25.5	26.2
2.09	107.5	96.9	11046.0	10479.7	1046.0	1189.3	11042.0	10502.3	26.3	26.2
2.11	91.1	98.0	9503.0	10536.3	722.0	1175.0	9806.0	10556.3	26.7	26.2
2.13	92.8	97.3	9930.0	10433.0	729.0	1129.7	10290.0	10481.2	26.1	26.2
2.15	92.5	96.8	9706.0	10382.7	735.5	1089.6	9629.5	10462.1	26.9	26.2
2.17	92.2	96.4	9737.0	10315.0	976.0	1054.2	9453.0	10378.8	28.0	26.3
2.19	94.9	96.0	9675.0	10257.2	742.0	1046.4	9254.0	10286.3	25.9	26.5
2.21	90.6	95.9	10463.0	10199.0	1227.0	1016.0	10151.0	10183.0	23.6	26.4
2.23	97.4	95.3	9704.0	10225.4	775.0	1037.1	10625.0	10179.8	24.7	26.1
2.25	93.8	95.5	9628.0	10173.3	749.0	1010.9	9299.0	10224.4	25.8	26.0
2.27	95.6	95.4	9932.5	10118.7	762.0	984.7	9979.0	10131.8	27.9	26.0
2.29	89.7	95.4	10161.0	10100.1	653.0	962.4	9333.0	10116.5	28.6	26.2

Bold-raw data, *Italic*- exponentially smoothened data

Depth (m)	**Sr**	*Sr*	**Na**	*Na*	**Mg**	*Mg*	**Ca**	*Ca*	B/Be	*B/Be*
2.31	102.8	94.8	11442.0	10106.2	1701.0	931.5	11594.0	10038.2	32.6	26.4
2.33	94.2	95.6	9244.0	10239.8	796.0	1008.4	9174.0	10193.8	25.3	27.0
2.35	93.2	95.5	9476.0	10140.2	811.0	987.2	10395.0	10091.8	26.2	26.8
2.37	103.0	95.3	10585.0	10073.8	957.0	969.6	12238.0	10122.1	23.8	26.8
2.39	101.9	96.0	10272.5	10124.9	926.5	968.3	11411.5	10333.7	24.7	26.5
2.41	100.8	96.6	9960.0	10139.7	896.0	964.1	10585.0	10441.5	24.8	26.3
2.43	137.5	97.0	12950.0	10121.7	1742.0	957.3	18893.0	10455.8	22.5	26.1
2.45	151.7	101.1	14142.0	10404.5	1954.0	1035.8	17974.0	11299.5	23.2	25.8
2.47	111.2	106.1	11909.0	10778.3	1722.0	1127.6	13053.0	11967.0	24.2	25.5
2.49	98.6	106.6	10448.0	10891.3	841.0	1187.0	10923.0	12075.6	23.4	25.4
2.51	103.8	105.8	11451.0	10847.0	1024.0	1152.4	15245.0	11960.3	26.1	25.2
2.53	107.6	105.6	11810.5	10907.4	1244.0	1139.6	14013.5	12288.8	26.3	25.3
2.55	126.3	105.8	12170.0	10997.7	1464.0	1150.0	13963.0	12461.3	26.7	25.4
2.57	107.6	107.9	12169.5	11114.9	1244.0	1181.4	14013.5	12611.4	26.3	25.5
2.59	107.6	107.9	12169.5	11220.4	1244.0	1187.7	14013.5	12751.6	26.3	25.6
2.61	111.4	107.8	12905.0	11315.3	1476.0	1193.3	14064.0	12877.8	29.5	25.7
2.63	89.1	108.2	12169.0	11474.3	927.0	1221.6	10742.0	12996.5	24.8	26.1
2.65	95.9	106.3	12537.0	11543.8	1263.5	1192.1	12403.0	12771.0	27.7	25.9
2.67	96.8	105.2	13242.0	11643.1	1608.0	1199.3	16109.0	12734.2	27.6	26.1
2.69	94.9	104.4	11766.0	11803.0	1051.0	1240.1	10054.0	13071.7	28.8	26.3
2.71	88.7	103.4	12212.0	11799.3	1039.0	1221.2	10794.0	12769.9	25.4	26.5
2.73	96.5	102.0	12014.0	11840.5	1140.0	1203.0	10873.0	12572.3	22.3	26.4
2.75	92.4	101.4	11851.0	11857.9	880.0	1196.7	9884.0	12402.4	24.1	26.0
2.77	93.9	100.5	11932.5	11857.2	999.5	1165.0	10691.5	12150.6	24.5	25.8
2.79	91.3	99.9	12142.0	11864.7	1059.0	1148.5	13791.0	12004.6	26.8	25.7
2.81	95.3	99.0	11007.0	11892.5	940.0	1139.5	10510.0	12183.3	24.9	25.8
2.85	80.9	98.6	10689.0	11803.9	1063.0	1119.6	11444.0	12016.0	27.0	25.7
2.87	160.9	96.9	14010.0	11692.4	1532.0	1113.9	14943.0	11958.8	27.7	25.8
2.89	100.5	103.3	12337.0	11924.2	1107.5	1155.7	11416.0	12257.2	27.9	26.0
2.91	100.9	103.0	13078.0	11965.5	1152.0	1150.9	11388.0	12173.1	28.0	26.2
2.93	100.1	102.8	11596.0	12076.7	1044.0	1151.0	11081.0	12094.6	28.1	26.4
2.95	94.2	102.5	11779.0	12028.6	1114.0	1140.3	11395.0	11993.2	26.9	26.6
2.97	94.9	101.7	13327.0	12003.7	1128.0	1137.7	13142.0	11933.4	24.5	26.6
2.99	87.6	101.0	11159.0	12136.0	868.0	1136.7	9372.0	12054.2	27.2	26.4
3.01	89.3	99.7	10329.0	12038.3	708.0	1109.8	8841.0	11786.0	22.7	26.5
3.03	94.4	98.6	10987.5	11867.4	1007.0	1069.7	10320.5	11491.5	25.5	26.1
3.07	99.4	98.2	10816.0	11779.4	1146.0	1063.4	11269.0	11374.4	29.8	26.0
3.09	95.8	98.3	11030.0	11683.1	1029.5	1071.7	10382.0	11363.9	25.8	26.4
3.11	190.9	98.1	11616.0	11617.7	1404.0	1067.4	13950.0	11265.7	25.3	26.3
3.13	92.1	107.3	11244.0	11617.6	913.0	1101.1	9495.0	11534.1	25.4	26.2
3.15	104.5	105.8	11261.0	11580.2	1244.0	1082.3	12328.5	11330.2	25.9	26.2
3.17	103.4	105.7	10781.0	11548.3	1496.0	1098.5	12707.0	11430.0	23.5	26.1
3.19	105.5	105.5	11278.0	11471.6	1084.0	1138.2	11950.0	11557.7	27.3	25.9
3.21	99.9	105.5	9265.0	11452.2	767.0	1132.8	9556.0	11597.0	29.0	26.0
3.23	110.2	104.9	8811.0	11233.5	1033.0	1096.2	10318.0	11392.9	27.2	26.3
3.25	106.6	105.4	12665.0	10991.2	927.0	1089.9	10678.0	11285.4	25.7	26.4
3.27	106.5	105.5	9052.5	11158.6	934.5	1073.6	10498.0	11224.6	27.1	26.3
3.29	106.3	105.6	9047.0	10948.0	942.0	1059.7	11014.0	11152.0	26.9	26.4

Depth (m)	**Sr**	*Sr*	**Na**	*Na*	**Mg**	*Mg*	**Ca**	*Ca*	B/Be	*B/Be*
3.31	102.4	105.7	9058.0	10757.9	825.0	1047.9	9890.0	11138.2	25.5	26.5
3.33	112.4	105.4	9121.0	10587.9	787.0	1025.6	10257.0	11013.4	25.2	26.4
3.35	102.1	106.1	7353.0	10441.2	955.0	1001.8	8943.0	10937.7	27.6	26.2
3.37	109.7	105.7	8248.0	10132.4	750.0	997.1	9104.0	10738.3	26.7	26.4
3.39	102.0	106.1	7929.5	9944.0	774.5	972.4	8638.0	10574.8	27.2	26.4
3.41	101.8	105.7	7611.0	9742.5	763.0	952.6	8333.0	10381.1	27.5	26.5
3.43	89.8	105.3	8287.0	9529.4	786.0	933.6	7754.0	10176.3	25.2	26.6
3.45	99.1	103.7	7845.0	9405.1	718.0	918.9	7899.0	9934.1	26.8	26.5
3.47	87.4	103.3	7150.0	9249.1	569.0	898.8	6603.0	9730.6	27.0	26.5
3.49	88.2	101.7	7126.0	9039.2	591.0	865.8	7648.0	9417.8	26.7	26.5
3.51	88.8	100.3	7251.0	8847.9	566.0	838.3	7317.0	9240.8	24.8	26.6
3.53	88.9	99.2	7404.5	8688.2	598.5	811.1	7627.5	9048.5	26.1	26.4
3.55	98.7	98.1	7673.0	8559.8	723.0	789.8	9982.0	8906.4	25.8	26.3
3.57	93.2	98.2	7404.5	8471.1	602.5	783.1	7889.5	9013.9	26.0	26.3
3.59	88.9	97.7	7558.0	8364.5	606.0	765.1	7607.0	8901.5	26.9	26.3
3.61	97.5	96.8	6965.0	8283.8	599.0	749.2	8172.0	8772.0	26.8	26.3
3.63	89.0	96.9	8051.0	8151.9	642.0	734.2	7501.0	8712.0	23.7	26.4
3.65	87.5	96.1	7284.5	8141.9	584.5	724.9	7299.0	8590.9	24.0	26.1
3.67	86.0	95.2	7568.0	8056.1	551.0	710.9	6995.0	8461.7	24.4	25.9
3.69	85.0	94.3	7001.0	8007.3	570.0	694.9	7097.0	8315.1	24.4	25.7
3.71	84.8	93.4	7312.0	7906.7	599.0	682.4	6824.0	8193.3	25.5	25.6
3.73	84.2	92.5	7074.0	7847.2	641.0	674.1	7258.0	8056.3	29.3	25.6
3.75	100.2	91.7	10804.0	7769.9	1208.0	670.8	11076.0	7976.5	27.4	26.0
3.77	84.9	92.5	9585.5	8073.3	927.0	724.5	9010.5	8286.4	26.8	26.1
3.79	82.8	91.8	9183.0	8224.5	793.0	744.7	8852.0	8358.9	25.7	26.2
3.81	85.6	90.9	9988.0	8320.4	1061.0	749.6	9169.0	8408.2	26.1	26.1
3.83	84.6	90.4	9964.0	8487.1	893.0	780.7	8932.0	8484.3	27.1	26.1
3.85	84.9	89.8	9546.0	8634.8	925.0	791.9	9622.0	8529.0	26.1	26.2
3.87	85.9	89.3	8383.0	8725.9	821.0	805.2	8970.0	8638.3	24.0	26.2
3.89	85.2	89.0	9134.5	8691.6	898.5	806.8	9591.5	8671.5	22.5	26.0
3.91	85.4	88.6	8765.0	8735.9	872.0	816.0	9561.0	8763.5	21.3	25.6
3.93	83.6	88.3	9504.0	8738.8	1062.0	821.6	10682.0	8843.2	22.4	25.2
3.95	84.1	87.8	9288.0	8815.4	782.0	845.6	7561.0	9027.1	24.2	24.9
3.97	82.4	87.4	9275.0	8862.6	800.0	839.3	8391.0	8880.5	24.2	24.9
3.99	97.0	86.9	10615.0	8903.9	1084.0	835.3	9199.0	8831.6	24.2	24.8
4.01	81.3	87.9	7507.0	9075.0	623.0	860.2	6750.0	8868.3	29.9	24.7
4.03	89.2	87.3	7920.0	8918.2	656.0	836.5	8207.0	8656.5	28.0	25.2
4.04	81.3	87.5	7787.5	8818.4	604.0	818.4	6742.0	8611.5	26.5	25.5
4.05	81.1	86.8	7924.0	8715.3	585.0	797.0	6734.0	8424.6	26.6	25.6
4.07	81.2	86.3	7655.0	8636.1	508.0	775.8	6348.0	8255.5	24.4	25.7
4.09	82.8	85.8	7745.0	8538.0	552.0	749.0	6929.0	8064.8	25.2	25.6
4.11	85.1	85.5	8209.0	8458.7	1045.0	729.3	7277.0	7951.2	24.3	25.5
4.13	83.5	85.4	7859.0	8433.8	712.0	760.9	6905.0	7883.8	24.1	25.4
4.15	82.8	85.2	7806.5	8376.3	713.0	756.0	6999.0	7785.9	23.9	25.3
4.17	82.1	85.0	7638.0	8319.3	714.0	751.7	7093.0	7707.2	22.3	25.2
4.19	81.2	84.7	7754.0	8251.2	555.0	747.9	6453.0	7645.8	24.6	24.9
4.21	84.8	84.4	7771.0	8201.5	997.0	728.6	6870.0	7526.5	25.2	24.8

Depth (m)	**Sr**	*Sr*	**Na**	*Na*	**Mg**	*Mg*	**Ca**	*Ca*	B/Be	*B/Be*
4.23	88.6	84.4	8291.0	8158.4	816.0	755.5	7136.0	7460.9	24.3	24.9
4.25	82.7	84.8	7799.0	8171.7	732.0	761.5	7902.0	7428.4	26.8	24.8
4.27	84.3	84.6	7551.0	8134.4	703.0	758.6	7046.0	7475.7	23.9	25.0
4.29	85.1	84.6	7280.0	8076.1	440.0	753.0	6751.0	7432.8	21.1	24.9
4.31	83.5	84.6	7303.0	7996.5	674.0	721.7	6956.0	7364.6	23.0	24.5
4.33	78.3	84.5	6992.0	7927.1	537.0	716.9	5789.0	7323.7	19.3	24.4
4.35	81.0	83.9	7432.0	7833.6	582.0	698.9	6543.0	7170.3	20.9	23.9
4.37	89.2	83.6	6972.0	7793.4	619.0	687.3	6823.0	7107.5	20.2	23.6
4.39	88.4	84.2	7051.5	7711.3	574.5	680.4	6683.0	7079.1	22.7	23.2
4.41	106.4	84.6	7131.0	7645.3	515.0	669.8	6533.0	7039.5	23.3	23.2
4.43	87.6	86.8	6901.0	7593.9	567.0	654.4	7846.0	6988.8	24.1	23.2
4.45	73.6	86.9	6186.0	7524.6	483.0	645.6	4561.0	7074.5	20.7	23.3
4.47	79.8	85.5	6155.0	7390.7	490.0	629.4	5672.0	6823.2	21.0	23.0
4.49	80.9	85.0	6389.0	7267.2	429.0	615.4	5216.0	6708.1	21.4	22.8
4.51	80.7	84.5	9498.0	7179.3	610.0	596.8	6700.0	6558.9	28.9	22.7
4.53	80.8	84.2	7360.0	7411.2	610.5	598.1	6418.5	6573.0	24.0	23.3
4.55	75.6	83.8	7844.0	7406.1	611.0	599.3	6153.0	6557.5	23.3	23.4
4.57	81.6	83.0	7360.0	7449.9	610.5	600.5	6604.5	6517.1	25.5	23.4
4.59	83.9	82.9	6876.0	7440.9	708.0	601.5	6684.0	6525.8	23.1	23.6
4.61	82.4	83.0	6693.0	7384.4	586.0	612.2	6525.0	6541.6	26.0	23.5
4.63	85.4	82.9	6592.0	7315.3	475.0	609.5	6671.0	6540.0	21.0	23.8
4.65	82.6	83.2	6642.5	7242.9	530.5	596.1	7953.5	6553.1	21.9	23.5
4.67	82.7	83.1	7088.0	7182.9	859.0	589.5	10937.0	6693.1	23.7	23.3
4.69	76.8	83.1	6368.0	7173.4	432.0	616.5	9236.0	7117.5	17.8	23.4
4.71	79.8	82.4	6527.0	7092.9	376.0	598.0	7450.0	7329.4	20.6	22.8
4.73	80.6	82.2	6450.0	7036.3	627.0	575.8	8371.0	7341.4	18.1	22.6
4.75	85.7	82.0	6380.0	6977.6	654.0	580.9	8311.0	7444.4	17.1	22.2
4.77	83.2	82.4	6319.5	6917.9	537.5	588.2	8341.0	7531.0	18.0	21.7
4.79	79.3	82.5	6197.0	6858.0	332.0	583.2	7669.0	7612.0	20.3	21.3
4.81	87.8	82.1	6259.0	6791.9	448.0	558.1	8567.0	7617.7	17.8	21.2
4.83	84.0	82.7	6577.0	6738.6	520.0	547.0	9230.0	7712.7	21.9	20.8
4.85	139.2	82.8	7888.0	6722.5	712.0	544.3	10864.0	7864.4	17.9	20.9
4.87	92.6	88.5	6432.0	6839.0	532.0	561.1	5768.0	8164.4	21.8	20.6
4.89	87.1	88.9	7483.5	6798.3	536.0	558.2	6879.0	7924.7	17.8	20.8
4.91	80.6	88.7	7171.0	6866.8	540.0	556.0	6230.0	7820.1	18.2	20.5
4.93	81.5	87.9	7796.0	6897.3	511.0	554.4	7528.0	7661.1	16.2	20.2
4.95	81.1	87.3	7635.0	6987.1	491.0	550.0	7277.0	7647.8	19.4	19.8
4.97	78.6	86.6	7647.0	7051.9	513.0	544.1	8277.0	7610.7	19.2	19.8
4.99	81.2	85.8	8106.0	7111.4	650.0	541.0	8470.0	7677.4	19.6	19.7
5.01	92.5	85.4	7911.0	7210.9	872.0	551.9	8604.0	7756.6	21.7	19.7
5.03	87.8	86.1	7554.5	7280.9	681.0	583.9	8115.5	7841.4	20.2	19.9
5.05	90.9	86.2	7075.0	7308.3	645.0	593.6	7741.0	7868.8	19.7	19.9
5.07	84.6	86.7	7198.0	7284.9	712.0	598.8	7761.0	7856.0	20.8	19.9
5.09	89.4	86.5	6955.0	7276.2	518.0	610.1	8689.0	7846.5	21.2	20.0
5.11	89.1	86.8	7119.5	7244.1	787.0	600.9	8890.5	7930.7	20.4	20.1
5.13	98.2	87.0	8095.0	7231.7	862.0	619.5	10228.0	8026.7	19.7	20.2
5.15	88.7	88.1	7041.0	7318.0	1052.0	643.7	9092.0	8246.9	19.2	20.1
5.17	87.5	88.2	7003.0	7290.3	728.0	684.6	9471.0	8331.4	20.7	20.0

Depth (m)	**Sr**	*Sr*	**Na**	*Na*	**Mg**	*Mg*	**Ca**	*Ca*	B/Be	*B/Be*
5.19	87.6	88.1	6954.0	7261.6	637.0	688.9	9362.0	8445.3	19.7	20.1
5.21	85.2	88.1	6521.0	7230.8	650.0	683.7	8654.0	8537.0	19.9	20.0
5.23	86.6	87.8	6942.0	7159.8	643.5	680.4	9621.0	8548.7	20.0	20.0
5.25	88.4	87.7	7268.0	7138.0	984.0	676.7	9880.0	8655.9	18.7	20.0
5.27	85.5	87.7	6930.0	7151.0	573.0	707.4	9934.0	8778.3	20.0	19.9
5.29	88.5	87.5	6477.0	7128.9	716.0	694.0	10638.0	8893.9	20.3	19.9
5.31	95.1	87.6	6710.0	7063.7	669.0	696.2	11033.0	9068.3	20.0	19.9
5.33	88.0	88.4	6835.0	7028.4	615.0	693.4	11093.0	9264.8	20.3	19.9
5.35	91.6	88.3	7233.5	7009.0	685.5	685.6	11063.0	9447.6	20.6	20.0
5.37	97.7	88.6	7632.0	7031.5	702.0	685.6	11976.0	9609.1	18.1	20.0
5.39	76.5	89.6	9926.0	7091.5	1411.0	687.2	8861.0	9845.8	24.2	19.8
5.41	87.9	88.2	6765.0	7375.0	494.0	759.6	12103.0	9747.3	19.0	20.3
5.43	70.8	88.2	8572.0	7314.0	806.0	733.0	7318.0	9982.9	24.4	20.2
5.45	78.2	86.5	5886.0	7439.8	435.0	740.3	10864.0	9716.4	19.4	20.6
5.47	74.5	85.6	7167.0	7284.4	561.0	709.8	9091.0	9831.2	21.4	20.5
5.49	81.4	84.5	5980.0	7272.7	362.0	694.9	11081.0	9757.2	19.1	20.6
5.51	67.3	84.2	8354.0	7143.4	687.0	661.6	6877.0	9889.5	22.2	20.4
5.53	67.4	82.5	8642.0	7264.5	778.0	664.2	6675.0	9588.3	23.9	20.6
5.55	61.6	81.0	8412.0	7402.2	679.0	675.6	5083.0	9297.0	21.7	20.9
5.57	66.5	79.1	8182.5	7503.2	695.0	675.9	5277.5	8875.6	23.9	21.0
5.59	66.2	77.8	7953.0	7571.1	711.0	677.8	5472.0	8515.8	25.9	21.3
5.61	65.9	76.6	7898.5	7609.3	672.0	681.1	4959.5	8211.4	24.7	21.7
5.63	66.7	75.6	7667.0	7638.2	665.0	680.2	4836.0	7886.2	23.7	22.0
5.65	65.6	74.7	7844.0	7641.1	458.0	678.7	3883.0	7581.2	27.2	22.2
5.67	80.4	73.8	8868.0	7661.4	661.0	656.6	8030.0	7211.4	24.1	22.7
5.69	74.9	74.4	8929.0	7782.1	756.0	657.1	5718.0	7293.2	25.2	22.8
5.71	70.3	74.5	8417.0	7896.7	665.0	667.0	5625.0	7135.7	23.9	23.1
5.73	72.6	74.1	8673.0	7948.8	710.5	666.8	5671.5	6984.6	24.7	23.2
5.75	75.4	73.9	9559.0	8021.2	931.0	671.1	7419.0	6853.3	25.6	23.3
5.77	66.1	74.1	8401.0	8175.0	322.0	697.1	5412.0	6909.9	22.8	23.5
5.79	69.9	73.3	8498.0	8197.6	481.0	659.6	6183.0	6760.1	20.0	23.5
5.81	75.7	72.9	8114.0	8227.6	1023.0	641.7	6155.0	6702.4	23.1	23.1
5.83	72.7	73.2	7409.0	8216.3	356.0	679.9	4724.0	6647.6	17.4	23.1
5.85	74.1	73.2	8103.5	8135.5	606.0	647.5	5681.5	6455.3	21.4	22.5
5.87	73.4	73.3	8093.0	8132.3	434.0	643.3	5208.0	6377.9	20.4	22.4
5.89	74.8	73.3	8255.0	8128.4	778.0	622.4	6678.0	6260.9	25.3	22.2
5.91	66.6	73.4	7112.0	8141.1	334.0	638.0	4515.0	6302.6	20.4	22.5
5.93	67.4	72.7	8079.0	8038.2	430.0	607.6	6253.0	6123.9	24.2	22.3
5.95	93.3	72.2	9388.0	8042.2	589.0	589.8	7050.0	6136.8	23.1	22.5
5.97	82.6	74.3	8067.5	8176.8	497.0	589.7	6278.5	6228.1	22.1	22.6
5.99	71.9	75.1	8056.0	8165.9	316.0	580.5	6304.0	6233.1	21.1	22.5
6.29	85.3	74.8	7716.5	8154.9	493.0	554.0	6677.0	6240.2	22.1	22.4
6.31	107.3	75.9	7377.0	8111.1	564.0	547.9	5794.0	6283.9	22.8	22.4
6.33	77.2	79.0	5710.0	8037.6	422.0	549.5	10690.0	6234.9	18.6	22.4
6.35	77.5	78.8	6196.0	7804.9	346.0	536.8	12045.0	6680.4	18.3	22.0

Depth (m)	**Sr**	*Sr*	**Na**	*Na*	**Mg**	*Mg*	**Ca**	*Ca*	B/Be	*B/Be*
6.37	79.8	78.7	5824.0	7644.0	391.0	517.7	11975.0	7216.9	19.9	21.6
6.39	76.5	78.8	5260.0	7462.0	323.0	505.0	11669.0	7692.7	18.7	21.5
6.41	78.2	78.6	5911.5	7241.8	395.5	486.8	11822.0	8090.3	19.5	21.2
6.43	70.7	78.5	7666.0	7108.8	648.0	477.7	6332.0	8463.5	22.7	21.0
6.45	86.6	77.7	5999.0	7164.5	400.0	494.7	12231.0	8250.3	19.1	21.2
6.47	75.6	78.6	5780.0	7047.9	344.0	485.2	13368.0	8648.4	20.1	21.0
6.49	90.1	78.3	5656.0	6921.1	400.0	471.1	13208.0	9120.4	17.3	20.9
6.51	76.4	79.5	7613.0	6794.6	676.0	464.0	6935.0	9529.1	22.0	20.5
6.53	75.1	79.2	6908.5	6876.5	476.5	485.2	9691.5	9269.7	20.3	20.7
6.55	73.7	78.8	6204.0	6879.7	319.0	484.3	12448.0	9311.9	20.4	20.6
6.57	75.1	78.3	7668.5	6812.1	557.5	467.8	8205.0	9625.5	21.3	20.6
6.59	72.4	78.0	7724.0	6897.7	553.0	476.8	6024.0	9483.5	22.5	20.7
6.61	89.5	77.4	8218.0	6980.4	562.0	484.4	9475.0	9137.5	22.5	20.9
6.63	80.8	78.6	7828.0	7104.1	503.0	492.2	8216.0	9171.3	22.2	21.0
6.65	79.3	78.8	8070.0	7176.5	487.5	493.2	7805.5	9075.7	22.8	21.1
6.67	77.8	78.9	7922.0	7265.9	472.0	492.7	7256.0	8948.7	23.5	21.3
6.69	75.9	78.8	9244.0	7331.5	461.0	490.6	7395.0	8779.4	22.2	21.5
6.71	71.1	78.5	7582.0	7522.7	522.0	487.6	5261.0	8641.0	23.0	21.6
6.73	83.9	77.7	8656.0	7528.7	530.0	491.1	7887.0	8303.0	23.3	21.7
6.75	79.6	78.4	8066.0	7641.4	488.0	495.0	7510.0	8261.4	21.2	21.9
6.77	79.7	78.5	8163.0	7683.9	509.0	494.3	7261.5	8186.3	21.9	21.8
6.79	73.2	78.6	7276.0	7731.8	576.0	495.7	5713.0	8093.8	22.9	21.8
6.81	79.8	78.1	8260.0	7686.2	414.0	503.8	7013.0	7855.7	20.2	21.9
6.83	97.0	78.2	8083.0	7743.6	747.0	494.8	8062.0	7771.4	21.8	21.8
6.85	75.7	80.1	7945.0	7777.5	449.0	520.0	7263.0	7800.5	18.9	21.8
6.87	89.5	79.7	7874.0	7794.3	641.0	512.9	8662.0	7746.7	20.0	21.5
6.89	79.4	80.7	7874.0	7802.2	586.0	525.7	7941.0	7838.3	21.2	21.3
6.91	83.1	80.5	7667.0	7809.4	751.0	531.7	7857.0	7848.5	22.6	21.3
6.93	74.4	80.8	7874.0	7795.2	531.0	553.7	8025.0	7849.4	23.6	21.4
6.95	73.9	80.1	7339.0	7803.1	411.0	551.4	7419.0	7866.9	21.0	21.7
6.97	78.1	79.5	7316.0	7756.6	521.0	537.4	7178.0	7822.2	19.8	21.6
6.99	78.6	79.4	7209.0	7712.6	410.0	535.7	7470.0	7757.7	18.6	21.4
7.01	78.4	79.3	7262.5	7662.2	515.5	523.2	7324.0	7729.0	20.1	21.1
7.03	71.1	79.2	6820.0	7622.3	510.0	522.4	5092.0	7688.5	22.7	21.0
7.05	89.0	78.4	7749.0	7542.0	1193.0	521.2	8714.0	7428.8	18.5	21.2
7.07	74.6	79.5	7634.0	7562.7	616.0	588.3	5984.0	7557.3	22.9	20.9
7.09	96.6	79.0	7624.0	7569.9	599.0	591.1	8374.0	7400.0	18.2	21.1
7.11	76.2	80.7	6267.0	7575.3	382.0	591.9	6687.0	7497.4	19.1	20.8
7.13	74.9	80.3	7207.0	7444.4	503.0	570.9	6975.0	7416.4	19.8	20.7
7.15	69.8	79.7	8304.0	7420.7	1004.0	564.1	5678.0	7372.2	24.8	20.6
7.17	73.6	78.7	6790.0	7509.0	407.0	608.1	7263.0	7202.8	18.0	21.0
7.19	83.5	78.2	7156.0	7437.1	544.0	588.0	8134.0	7208.8	18.8	20.7
7.21	68.0	78.8	6831.0	7409.0	435.0	583.6	6490.0	7301.3	18.1	20.5
7.23	68.7	77.7	8399.0	7351.2	832.0	568.7	5397.0	7220.2	25.4	20.3
7.25	68.4	76.8	7811.5	7456.0	496.5	595.1	6860.0	7037.9	21.6	20.8
7.27	65.2	75.9	8129.0	7491.5	512.0	585.2	7230.0	7020.1	21.2	20.8
7.29	75.9	74.9	7494.0	7555.3	481.0	577.9	7695.0	7041.1	21.9	20.9
7.31	65.7	75.0	8446.0	7549.2	311.0	568.2	7446.0	7106.5	23.5	21.0

Depth (m)	Sr	*Sr*	Na	*Na*	Mg	*Mg*	Ca	*Ca*	B/Be	*B/Be*
7.33	72.3	74.0	8472.0	7638.8	459.0	542.5	6946.0	7140.4	20.4	21.2
7.35	69.5	73.9	8264.0	7722.2	263.0	534.1	7998.0	7121.0	20.9	21.2
7.37	70.0	73.4	8268.0	7776.3	453.5	507.0	7271.0	7208.7	21.4	21.1
7.39	69.6	73.1	8269.0	7825.5	768.0	501.7	6209.0	7214.9	24.6	21.2
7.41	70.4	72.7	8267.0	7869.9	448.0	528.3	7596.0	7114.3	20.9	21.5
7.43	75.8	72.5	8663.0	7909.6	979.0	520.3	8233.0	7162.5	25.0	21.4
7.45	69.1	72.8	7511.0	7984.9	375.0	566.1	8495.0	7269.5	23.5	21.8
7.47	70.0	72.5	8225.0	7937.5	1051.0	547.0	6350.0	7392.1	21.5	22.0
7.49	69.6	72.2	7868.0	7966.3	713.0	597.4	8056.0	7287.9	22.5	21.9
7.51	62.0	71.9	9836.0	7956.4	1224.0	609.0	9300.0	7364.7	25.0	22.0
7.53	71.2	71.0	6918.0	8144.4	306.0	670.5	7617.0	7558.2	18.7	22.3
7.55	64.1	71.0	8381.0	8021.8	507.0	634.0	7702.0	7564.1	17.6	21.9
7.57	64.6	70.3	7755.0	8057.7	377.5	621.3	7761.5	7577.9	19.0	21.5
7.59	65.1	69.7	7129.0	8027.4	380.0	596.9	7821.0	7596.3	20.5	21.2
7.61	63.2	69.3	8412.0	7937.6	375.0	575.3	8423.0	7618.7	21.8	21.2
7.63	73.5	68.7	8400.0	7985.0	1131.0	555.2	8604.0	7699.2	23.0	21.2
7.65	62.5	69.1	7971.5	8026.5	472.0	612.8	9132.0	7789.6	21.0	21.4
7.67	55.6	68.5	7543.0	8021.0	432.0	598.7	10925.0	7923.9	17.7	21.4
7.69	61.7	67.2	7121.0	7973.2	512.0	582.1	9660.0	8224.0	20.9	21.0
7.71	63.8	66.6	7706.0	7888.0	401.0	575.0	11010.0	8367.6	19.7	21.0
7.73	60.2	66.4	6334.0	7869.8	286.0	557.6	9906.0	8631.8	17.1	20.9
7.75	64.2	65.7	7013.0	7716.2	337.0	530.5	10169.0	8759.2	17.7	20.5
7.77	62.8	65.6	6436.5	7645.9	304.0	511.1	10017.5	8900.2	17.9	20.2
7.79	66.9	65.3	6239.0	7525.0	255.0	490.4	9756.0	9012.0	19.5	20.0
7.81	61.3	65.5	6539.0	7396.4	322.0	466.9	10129.0	9086.4	18.2	19.9
7.83	60.7	65.0	6936.0	7310.6	408.0	452.4	10245.0	9190.6	17.3	19.8
7.85	71.9	64.6	5792.0	7273.2	386.0	447.9	10439.0	9296.1	14.9	19.5
7.87	82.7	65.3	6692.0	7125.0	427.0	441.8	11077.0	9410.4	18.2	19.0
7.89	77.3	67.1	6796.5	7081.7	420.0	440.3	10999.5	9577.0	16.4	19.0
7.91	167.1	68.1	10969.0	7053.2	1521.0	438.3	12159.0	9719.3	20.0	18.7
7.93	69.8	78.0	6901.0	7444.8	413.0	546.5	10922.0	9963.2	17.5	18.8
7.95	78.5	77.2	8774.0	7390.4	1073.0	533.2	9092.0	10059.1	21.5	18.7
7.97	62.9	77.3	7455.0	7528.8	361.0	587.2	10473.0	9962.4	16.8	19.0
7.99	74.1	75.9	9374.0	7521.4	1579.0	564.5	8407.0	10013.5	22.0	18.8
8.01	64.0	75.7	7245.5	7706.7	344.0	666.0	9910.5	9852.8	18.0	19.1
8.03	59.5	74.5	7036.0	7660.5	262.0	633.8	9348.0	9858.6	21.0	19.0
8.05	65.0	73.0	6968.0	7598.1	327.0	596.6	11317.0	9807.5	17.6	19.2
8.07	74.8	72.2	9006.0	7535.1	1196.0	569.6	7797.0	9958.5	24.4	19.0
8.09	65.9	72.5	7285.0	7682.2	972.0	632.3	11451.0	9742.3	17.8	19.6
8.11	57.8	71.8	6263.0	7642.5	275.0	666.3	11623.0	9913.2	15.5	19.4
8.13	61.6	70.4	7293.0	7504.5	282.0	627.1	11537.0	10084.2	16.6	19.0
8.15	65.2	69.5	7301.0	7483.4	289.0	592.6	12158.0	10229.5	17.9	18.8
8.17	57.9	69.1	7399.0	7465.1	256.0	562.3	10818.0	10422.3	15.5	18.7
8.19	56.5	68.0	8139.0	7458.5	1008.0	531.6	8028.0	10461.9	22.5	18.4
8.21	54.9	66.8	6625.0	7526.6	277.0	579.3	10212.0	10218.5	17.2	18.8
8.23	60.1	65.6	7289.0	7436.4	772.0	549.0	5314.0	10217.8	23.1	18.6
8.25	57.2	65.1	6511.0	7421.7	296.0	571.3	8093.5	9727.5	16.4	19.1
8.27	55.9	64.3	6397.0	7330.6	315.0	543.8	8456.0	9564.1	15.6	18.8

Depth (m)	**Sr**	*Sr*	**Na**	*Na*	**Mg**	*Mg*	**Ca**	*Ca*	B/Be	*B/Be*
8.29	58.4	63.4	6312.0	7237.2	271.0	520.9	7731.0	9453.3	15.9	18.5
8.31	64.2	62.9	7532.0	7144.7	766.0	495.9	6152.0	9281.0	21.6	18.2
8.33	56.6	63.1	6756.0	7183.4	264.0	522.9	8102.0	8968.1	14.9	18.6
8.35	59.6	62.4	8234.0	7140.7	317.0	497.0	8977.0	8881.5	15.2	18.2
8.37	58.1	62.1	7759.5	7250.0	292.5	479.0	8539.5	8891.1	16.2	17.9
8.39	160.9	61.7	11122.0	7301.0	1450.0	460.4	13273.0	8855.9	21.3	17.7
8.41	55.4	71.7	7285.0	7683.1	268.0	559.3	7723.0	9297.6	16.5	18.1
8.43	56.3	70.0	6392.0	7643.3	237.0	530.2	11213.0	9140.2	17.4	17.9
8.45	57.1	68.7	6377.0	7518.1	221.0	500.9	11441.0	9347.4	18.4	17.9
8.47	57.7	67.5	6818.0	7404.0	572.0	472.9	10040.0	9556.8	16.7	17.9
8.49	57.4	66.5	6597.5	7345.4	396.5	482.8	9457.5	9605.1	18.2	17.8
8.51	66.6	65.6	8653.0	7270.6	934.0	474.2	7628.0	9590.4	21.7	17.8
8.53	56.8	65.7	6535.5	7408.9	410.0	520.2	9457.5	9394.1	17.3	18.2
8.55	50.0	64.8	6253.0	7321.5	185.0	509.1	8875.0	9400.5	20.2	18.1
8.57	55.9	63.3	6234.0	7214.7	248.0	476.7	10293.0	9347.9	16.0	18.3
8.59	58.2	62.6	6690.0	7116.6	204.0	453.9	10075.0	9442.4	15.8	18.1
8.61	63.6	62.2	6378.0	7074.0	495.0	428.9	10052.0	9505.7	18.1	17.9
8.63	69.6	62.3	7207.0	7004.4	269.0	435.5	10408.0	9560.3	17.6	17.9
8.65	62.4	63.0	7332.0	7024.6	382.0	418.8	10230.0	9645.1	17.9	17.9
8.67	61.2	63.0	7559.0	7055.4	638.0	415.2	5018.0	9703.6	23.8	17.9
8.69	58.1	62.8	7457.0	7105.7	255.0	437.4	10485.0	9235.0	18.9	18.5
8.71	61.9	62.3	7970.0	7140.8	454.0	419.2	11621.0	9360.0	19.8	18.5
8.73	61.4	62.3	6863.0	7223.8	313.0	422.7	9600.0	9586.1	17.1	18.6
8.75	64.8	62.2	8362.0	7187.7	418.0	411.7	11309.0	9587.5	19.7	18.5
8.77	63.8	62.5	7595.0	7305.1	375.5	412.3	10870.5	9759.7	19.9	18.6
8.79	73.1	62.6	7555.0	7334.1	392.0	408.7	11449.0	9870.7	19.9	18.7
8.81	62.8	63.6	7635.0	7356.2	359.0	407.0	10432.0	10028.6	20.0	18.9
8.83	64.5	63.6	7415.0	7384.1	326.0	402.2	10005.0	10068.9	18.0	19.0
8.85	63.9	63.6	6846.0	7387.2	515.0	394.6	10449.0	10062.5	16.5	18.9
8.87	69.6	63.7	8391.0	7333.1	413.0	406.6	11645.0	10101.2	18.6	18.6
8.89	66.8	64.3	7647.5	7438.8	417.0	407.3	11047.0	10255.5	18.7	18.6
8.91	77.0	64.5	7938.0	7459.7	421.0	408.2	12386.0	10334.7	18.9	18.6
8.93	59.3	65.8	7357.0	7507.5	319.0	409.5	9381.0	10539.8	20.8	18.7
8.95	82.9	65.1	6844.0	7492.5	403.0	400.5	9172.0	10423.9	17.6	18.9
8.97	61.1	66.9	6552.0	7427.6	502.0	400.7	8724.0	10298.7	17.9	18.7
8.99	60.1	66.3	6721.0	7340.1	555.0	410.8	8092.0	10141.3	18.2	18.7
9.01	61.6	65.7	6636.5	7278.2	528.5	425.3	7868.0	9936.3	17.8	18.6
9.03	62.8	65.3	8079.0	7214.0	610.0	435.6	5367.0	9729.5	21.8	18.5
9.05	62.1	65.0	6437.0	7300.5	471.0	453.0	7644.0	9293.3	16.6	18.9
9.07	75.9	64.7	10329.0	7214.2	993.0	454.8	9887.0	9128.3	22.4	18.6
9.09	69.0	65.9	6984.5	7525.6	675.0	508.6	8765.5	9204.2	19.7	19.0
9.11	59.1	66.2	7271.0	7471.5	658.0	525.3	5313.0	9160.3	22.1	19.1
9.13	94.1	65.5	6698.0	7451.5	692.0	538.5	11827.0	8775.6	17.2	19.4
9.15	56.1	68.3	7328.0	7376.1	663.0	553.9	4710.0	9080.7	21.3	19.2
9.17	61.8	67.1	5901.0	7371.3	432.0	564.8	6401.0	8643.7	18.0	19.4
9.19	62.6	66.6	8386.0	7224.3	905.0	551.5	6772.0	8419.4	23.5	19.2
9.21	62.2	66.2	7143.5	7340.5	770.0	586.9	6209.0	8254.7	20.9	19.7
9.23	64.9	65.8	8709.0	7320.8	1346.0	605.2	6017.0	8050.1	21.4	19.8
9.25	60.7	65.7	5671.0	7459.6	635.0	679.3	3325.0	7846.8	17.7	20.0

Depth (m)	**Sr**	*Sr*	**Na**	*Na*	**Mg**	*Mg*	**Ca**	*Ca*	B/Be	*B/Be*
9.27	68.9	65.2	8194.0	7280.7	1146.0	674.8	5068.0	7394.6	22.6	19.7
9.29	56.6	65.6	6105.0	7372.1	546.0	722.0	6309.0	7161.9	17.2	20.0
9.31	69.1	64.7	9678.0	7245.3	1211.0	704.4	7321.0	7076.6	21.7	19.7
9.33	67.8	65.1	8589.5	7488.6	1207.5	755.0	6661.0	7101.1	22.1	19.9
9.35	71.4	65.4	8526.0	7598.7	1249.0	800.3	7013.0	7057.1	22.5	20.2
9.37	66.5	66.0	8653.0	7691.4	1204.0	845.1	5738.0	7052.7	21.7	20.4
9.39	65.8	66.0	6442.0	7787.6	605.0	881.0	6557.0	6921.2	17.3	20.5
9.41	65.7	66.0	6074.0	7653.0	518.0	853.4	6118.0	6884.8	17.2	20.2
9.43	83.7	66.0	8040.0	7495.1	1248.0	819.9	7482.0	6808.1	22.8	19.9
9.45	67.8	67.8	7206.5	7549.6	796.0	862.7	6078.0	6875.5	20.3	20.2
9.47	68.2	67.8	8051.0	7515.3	1002.0	856.0	4847.0	6795.7	22.9	20.2
9.49	67.3	67.8	6373.0	7568.9	590.0	870.6	6038.0	6600.9	18.0	20.5
9.51	67.4	67.7	10223.0	7449.3	1777.0	842.6	6569.0	6544.6	26.2	20.2
9.53	70.4	67.7	9178.0	7726.7	1513.0	936.0	5364.0	6547.0	21.9	20.8
9.55	69.7	68.0	9038.0	7871.8	1927.0	993.7	7508.0	6428.7	24.2	20.9
9.57	68.3	68.2	8831.0	7988.4	1377.0	1087.0	6507.5	6536.6	22.4	21.3
9.59	66.8	68.2	8624.0	8072.7	1241.0	1116.0	5507.0	6533.7	21.7	21.4
9.61	61.7	68.0	7655.0	8127.8	678.0	1128.5	7512.0	6431.1	18.0	21.4
9.63	63.1	67.4	8239.0	8080.5	834.0	1083.5	4847.0	6539.2	22.2	21.1
9.65	62.1	67.0	6677.0	8096.4	580.0	1058.5	3359.0	6369.9	18.7	21.2
9.67	67.2	66.5	7248.0	7954.4	638.0	1010.7	4929.0	6068.8	22.7	20.9
9.69	73.4	66.5	6962.5	7883.8	649.5	973.4	5747.5	5954.9	21.0	21.1
9.71	79.6	67.2	7717.0	7791.7	917.0	941.0	6566.0	5934.1	22.4	21.1
9.73	90.4	68.5	6160.0	7784.2	661.0	938.6	8265.0	5997.3	19.5	21.2
9.75	65.4	70.7	7815.0	7621.8	756.0	910.9	4287.0	6224.1	22.0	21.1
9.77	87.0	70.1	6147.0	7641.1	680.0	895.4	9810.0	6030.4	16.0	21.1
9.79	147.5	71.8	10445.0	7491.7	1146.0	873.8	10756.0	6408.3	22.2	20.6
9.81	73.2	79.4	6853.5	7787.0	703.5	901.0	8643.5	6843.1	19.5	20.8
9.83	59.1	78.8	7240.0	7693.7	727.0	881.3	6881.0	7023.1	21.6	20.7
9.85	59.3	76.8	6467.0	7648.3	630.0	865.9	7477.0	7008.9	17.1	20.8
9.87	71.1	75.1	7612.0	7530.2	921.0	842.3	5575.0	7055.7	26.3	20.4
9.89	61.2	74.7	6294.0	7538.4	611.0	850.1	6193.0	6907.7	16.5	21.0
9.91	74.7	73.3	6754.0	7413.9	698.0	826.2	5070.0	6836.2	23.0	20.5
9.93	69.1	73.4	6758.5	7347.9	774.5	813.4	5601.0	6659.6	19.3	20.8
9.95	63.5	73.0	7255.0	7289.0	851.0	809.5	4948.0	6553.7	21.2	20.6
9.97	108.5	72.1	6763.0	7285.6	905.0	813.7	6132.0	6393.1	17.5	20.7
9.99	92.1	75.7	7071.0	7233.3	824.0	822.8	5458.0	6367.0	23.2	20.4
10.1	70.6	77.3	4824.0	7217.1	759.0	822.9	4455.0	6276.1	16.1	20.7
10.03	149.8	76.7	6543.0	6977.8	959.0	816.5	7119.0	6094.0	14.8	20.2
10.05	116.5	84.0	5395.0	6934.3	965.5	830.8	6709.0	6196.5	14.3	19.7
10.07	133.3	87.2	5966.0	6780.4	972.0	844.2	6917.0	6247.8	12.3	19.1

Appendix 11 Results of organic carbon analysis from UV1 (to be continued)

Depth (m)	δ¹³C	δ¹³C	C/N	C/N	TOC	TOC
1.31	-24.5	-25.17	10.3	10.46	0.8	1.01
1.33	-24.7	-25.10	10.2	10.45	0.8	0.99
1.35	-24.6	-25.06	10.3	10.42	0.7	0.97
1.37	-24.6	-25.02	10	10.41	0.8	0.95
1.39	-24.4	-24.97	9.9	10.37	0.8	0.93
1.41	-24.5	-24.92	9.8	10.32	0.8	0.92
1.43	-24.9	-24.88	10	10.27	0.8	0.91
1.45	-25.2	-24.88	12.1	10.24	1.2	0.90
1.47	-24.6	-24.91	9.9	10.43	0.8	0.93
1.49	-24.7	-24.88	10.1	10.38	0.8	0.91
1.51	-24.6	-24.86	10.1	10.35	0.8	0.90
1.53	-24.6	-24.84	10.1	10.32	0.8	0.89
1.54	-24.4	-24.81	10.2	10.30	0.8	0.88
1.55	-25.1	-24.77	10.5	10.29	0.9	0.87
1.57	-24.9	-24.80	10.6	10.31	0.8	0.88
1.59	-24.9	-24.81	10.2	10.34	0.9	0.87
1.61	-24.7	-24.82	10	10.33	0.8	0.87
1.63	-24.8	-24.81	10	10.29	0.8	0.87
1.65	-24.6	-24.81	10	10.26	0.9	0.86
1.67	-24.9	-24.79	10	10.24	0.9	0.86
1.69	-24.7	-24.80	10.1	10.21	0.9	0.87
1.71	-24.9	-24.79	10	10.20	0.9	0.87
1.73	-24.9	-24.80	10	10.18	0.8	0.87
1.75	-24.7	-24.81	10.5	10.16	0.9	0.87
1.77	-24.8	-24.80	10.2	10.20	0.9	0.87
1.79	-25.2	-24.80	11.1	10.20	1.0	0.87
1.81	-25.1	-24.84	10.3	10.29	0.9	0.88
1.83	-25.2	-24.87	10.5	10.29	0.9	0.89
1.85	-24.9	-24.90	10.6	10.31	0.9	0.89
1.87	-24.8	-24.90	10.1	10.34	0.9	0.89
1.89	-24.8	-24.89	10	10.32	0.8	0.89
1.91	-24.9	-24.88	10.4	10.28	0.9	0.88
1.93	-25.0	-24.88	10.8	10.30	0.9	0.88
1.95	-25.1	-24.89	10.7	10.35	0.9	0.88
1.97	-24.9	-24.91	10.7	10.38	0.9	0.89
1.99	-25.1	-24.91	10.5	10.41	0.9	0.89
2.01	-25.0	-24.93	10.6	10.42	0.9	0.89
2.03	-24.7	-24.94	10.2	10.44	0.8	0.89
2.05	-25.1	-24.91	11.6	10.42	0.9	0.88
2.07	-24.9	-24.93	17.5	10.53	0.9	0.88
2.09	-24.8	-24.93	15.9	11.23	0.8	0.88
2.11	-25.2	-24.92	11.9	11.70	1.0	0.88
2.13	-25.1	-24.95	18.1	11.72	1.0	0.89
2.15	-24.7	-24.96	9.9	12.36	0.9	0.90
2.17	-24.9	-24.93		12.11	0.9	0.90
2.19	-25.0	-24.93	9.8	11.10	0.9	0.90
2.21	-25.0	-24.94	10	10.97	0.9	0.90
2.23	-25.2	-24.94	10.1	10.87	1.0	0.90
2.25	-25.4	-24.97	11.4	10.80	1.1	0.91
2.27	-24.8	-25.01	10.5	10.86	0.8	0.93
2.29	-24.8	-24.99	9.9	10.82	0.9	0.92

Bold-raw data; Italic-exponentially smoothened data

Depth (m)	$\delta^{13}C$	$\delta^{13}C$	C/N	C/N	TOC	TOC
2.31	-24.9	-24.97	9.7	10.73	0.9	0.91
2.33	-25.1	-24.97	10.3	10.63	0.9	0.91
2.35	-25.0	-24.98	9.7	10.59	0.9	0.91
2.37	-24.8	-24.98	9.9	10.50	0.9	0.91
2.39	-25.0	-24.96	10.3	10.44	0.9	0.91
2.41	-24.9	-24.97	9.8	10.43	0.9	0.91
2.43	-24.7	-24.96	9.4	10.37	0.8	0.91
2.45	-25.0	-24.93	10.2	10.27	0.9	0.90
2.47	-24.8	-24.94	9.8	10.26	0.9	0.90
2.49	-25.0	-24.93	10	10.22	1.0	0.90
2.51	-24.7	-24.93	9.4	10.19	0.9	0.91
2.53	-24.8	-24.91	10.5	10.12	0.9	0.91
2.55	-24.9	-24.90	10	10.15	0.9	0.91
2.57	-24.4	-24.90	9.7	10.14	0.8	0.91
2.59	-24.9	-24.85	10.3	10.09	0.9	0.90
2.61	-24.4	-24.85	9.6	10.11	0.8	0.90
2.63	-24.8	-24.81	9.9	10.06	0.9	0.89
2.65	-24.6	-24.81	10.1	10.05	0.8	0.89
2.67	-24.8	-24.79	10.5	10.05	0.9	0.88
2.69	-24.8	-24.79	10	10.10	0.9	0.88
2.71	-24.9	-24.79	10.4	10.09	0.9	0.88
2.73	-24.7	-24.80	9.8	10.12	0.9	0.88
2.75	-24.5	-24.79	9.7	10.09	0.9	0.89
2.77	-24.5	-24.76	9.5	10.05	0.8	0.89
2.79	-24.6	-24.74	9.6	9.99	0.9	0.88
2.81	-24.6	-24.72	9.6	9.95	0.8	0.88
2.83	-24.6	-24.71	9.6	9.92	0.8	0.87
2.85	-24.6	-24.70	9.6	9.89	0.8	0.87
2.87	-24.5	-24.69	9.6	9.86	0.9	0.86
2.89	-24.6	-24.67	9.8	9.83	0.8	0.86
2.91	-24.6	-24.66	9.9	9.83	0.9	0.86
2.93	-25.9	-24.66	11.2	9.84	0.9	0.86
2.95	-25.1	-24.78	10.6	9.97	0.9	0.86
2.97	-24.9	-24.81	9.9	10.04	1.0	0.87
2.99	-24.7	-24.82	9.8	10.02	0.9	0.88
3.01	-25.2	-24.81	10.3	10.00	1.0	0.88
3.03	-24.6	-24.85	10.5	10.03	0.8	0.90
3.05	-25.0	-24.82	10.3	10.08	0.9	0.89
3.07	-24.7	-24.84	9.3	10.10	0.8	0.89
3.09	-25.0	-24.83	10.3	10.02	0.9	0.88
3.11	-25.2	-24.84	10.2	10.05	0.9	0.88
3.13	-25.2	-24.88	9.7	10.06	1.0	0.88
3.15	-24.8	-24.91	10.5	10.03	0.9	0.89
3.17	-25.3	-24.90	10.2	10.07	0.9	0.89
3.19	-25.7	-24.94	10	10.09	0.9	0.90
3.21	-24.9	-25.02	10	10.08	0.9	0.90
3.23	-25.0	-25.00	10.2	10.07	1.0	0.90
3.25	-24.8	-25.00	9.7	10.08	0.9	0.91

Depth (m)	$\delta^{13}C$	$\delta^{13}C$	C/N	C/N	TOC	TOC
3.27	-24.8	-24.98	10.3	10.04	0.9	0.91
3.29	-25.0	-24.97	10.6	10.07	0.9	0.91
3.31	-25.0	-24.97	10.1	10.12	1.0	0.90
3.33	-25.4	-24.97	10.8	10.12	1.0	0.91
3.35	-25.4	-25.01	10.5	10.19	1.0	0.92
3.37	-25.0	-25.05	9.9	10.22	0.9	0.93
3.39	-24.9	-25.05	10.4	10.19	0.9	0.93
3.41	-25.2	-25.03	10.7	10.21	0.9	0.92
3.43	-25.0	-25.05	10.4	10.26	1.0	0.92
3.45	-25.0	-25.04	10.3	10.27	1.0	0.93
3.47	-25.0	-25.04	10.2	10.28	1.0	0.94
3.49	-25.1	-25.04	10.6	10.27	0.9	0.94
3.51	-24.8	-25.04	9.9	10.30	1.0	0.94
3.53	-24.7	-25.02	10.1	10.26	0.9	0.95
3.55	-25.0	-24.99	10.6	10.24	1.0	0.94
3.57	-24.8	-24.99	10.1	10.28	0.9	0.95
3.59	-25.0	-24.97	10.4	10.26	0.9	0.94
3.61	-24.7	-24.97	9.3	10.28	0.9	0.94
3.63	-25.1	-24.95	10.8	10.18	1.0	0.93
3.65	-24.9	-24.96	11	10.24	0.9	0.94
3.67	-25.2	-24.95	10.4	10.32	1.0	0.94
3.69	-25.1	-24.98	10.2	10.32	1.0	0.94
3.71	-25.1	-24.99	10.8	10.31	1.0	0.95
3.73	-25.7	-25.00	9.8	10.36	1.0	0.95
3.75	-25.6	-25.07	9.9	10.31	0.9	0.96
3.77	-25.0	-25.12	11.3	10.26	0.9	0.95
3.79	-25.8	-25.11	10.3	10.37	1.0	0.95
3.81	-26.0	-25.18	10.2	10.36	1.0	0.95
3.83	-25.1	-25.26	10.5	10.35	1.0	0.96
3.85	-25.1	-25.25	10.4	10.36	1.0	0.96
3.87	-25.1	-25.23	10.6	10.36	1.0	0.97
3.89	-24.9	-25.22	10.9	10.39	0.9	0.97
3.91	-25.2	-25.19	10.1	10.44	1.0	0.96
3.93	-25.4	-25.19	10.2	10.41	1.0	0.97
3.95	-25.1	-25.21	10	10.38	1.0	0.97
3.97	-25.4	-25.20	10.3	10.35	1.1	0.97
3.99	-25.1	-25.22	10	10.34	1.0	0.99
4.01	-25.0	-25.21	10.2	10.31	1.0	0.99
4.03	-25.4	-25.19	11.2	10.30	1.0	0.99
4.04	-25.2	-25.21	10.6	10.39	1.0	0.99
4.05	-25.2	-25.21	10.5	10.41	1.0	0.99
4.07	-25.2	-25.21	10.5	10.42	1.0	0.99
4.09	-25.1	-25.21	10.2	10.43	1.0	0.99
4.11	-25.3	-25.19	11	10.40	1.0	0.99
4.13	-25.2	-25.21	10	10.46	1.0	0.99
4.15	-24.9	-25.20	10.8	10.42	1.0	0.99
4.17	-25.4	-25.17	10.9	10.45	1.0	0.99

Depth (m)	δ¹³C	δ¹³C	C/N	C/N	TOC	TOC
4.19	-25.0	-25.20	10.2	10.50	1.0	1.00
4.21	-25.0	-25.18	10	10.47	1.0	1.00
4.23	-25.3	-25.16	10.7	10.42	1.0	1.00
4.25	-25.1	-25.17	10.2	10.45	1.0	1.00
4.27	-25.1	-25.17	11	10.43	0.9	1.00
4.29	-24.9	-25.16	9.8	10.48	0.9	0.99
4.31	-25.0	-25.13	10.3	10.41	1.0	0.98
4.33	-25.1	-25.12	10.6	10.40	0.9	0.98
4.35	-25.0	-25.12	10.2	10.42	1.0	0.97
4.37	-25.5	-25.11	10.6	10.40	1.0	0.98
4.39	-24.9	-25.15	10.9	10.42	0.9	0.98
4.41	-25.4	-25.12	10.5	10.47	1.0	0.97
4.43	-25.1	-25.15	10.4	10.47	1.0	0.97
4.45	-25.4	-25.14	10.3	10.46	1.1	0.98
4.47	-25.3	-25.17	10.4	10.45	1.1	0.99
4.49	-25.5	-25.18	10.9	10.44	1.1	1.00
4.51	-25.2	-25.21	10.4	10.49	1.0	1.01
4.53	-25.2	-25.21	11.3	10.48	1.0	1.01
4.55	-25.8	-25.21	11	10.56	1.1	1.01
4.57	-25.0	-25.27	10.8	10.61	0.9	1.02
4.59	-25.5	-25.24	11	10.63	1.1	1.01
4.61	-25.2	-25.27	10.4	10.66	0.9	1.01
4.63	-25.1	-25.26	10.1	10.64	0.9	1.00
4.65	-25.2	-25.25	10.4	10.58	0.9	0.99
4.67	-25.3	-25.24	10.6	10.56	0.9	0.98
4.69	-25.3	-25.25	10.5	10.57	1.0	0.98
4.71	-25.4	-25.25	10.5	10.56	0.9	0.98
4.73	-25.3	-25.27	10.5	10.56	0.9	0.97
4.75	-25.4	-25.27	10.4	10.55	1.0	0.96
4.77	-25.2	-25.28	10.4	10.53	1.0	0.97
4.79	-25.4	-25.28	10.8	10.52	1.0	0.97
4.81	-25.3	-25.29	10.5	10.55	1.0	0.97
4.83	-25.2	-25.29	10.3	10.54	1.0	0.98
4.85	-25.5	-25.28	10.7	10.52	1.0	0.98
4.87	-25.1	-25.30	10.1	10.54	1.0	0.98
4.89	-25.3	-25.28	10.6	10.49	1.0	0.98
4.91	-25.4	-25.28	10.6	10.50	1.0	0.98
4.93	-25.5	-25.30	10.6	10.51	1.0	0.99
4.95	-25.5	-25.32	10.4	10.52	1.0	0.99
4.97	-25.5	-25.33	10.8	10.51	1.1	0.99
4.99	-25.5	-25.35	11.1	10.54	1.0	1.00
5.01	-25.2	-25.37	10.2	10.60	1.0	1.00
5.03	-25.4	-25.35	10.4	10.56	1.0	1.00
5.05	-25.5	-25.35	10.7	10.54	1.1	1.00
5.07	-25.5	-25.37	11.2	10.56	1.0	1.01
5.09	-25.5	-25.38	10.9	10.62	1.1	1.01
5.11	-25.4	-25.39	10.5	10.65	1.0	1.02
5.13	-25.5	-25.39	10.9	10.63	1.0	1.02

Appendix 11 (continued)

Depth (m)	δ¹³C	δ¹³C	C/N	C/N	TOC	TOC
5.15	-25.4	-25.40	10.6	10.66	1.0	1.01
5.17	-25.5	-25.40	10.6	10.65	1.0	1.01
5.19	-25.7	-25.41	11.8	10.65	1.1	1.01
5.21	-25.5	-25.44	10.7	10.76	1.0	1.02
5.23	-25.4	-25.45	10.8	10.76	1.1	1.02
5.25	-25.5	-25.44	10.6	10.76	1.0	1.03
5.27	-25.6	-25.45	11.3	10.75	1.1	1.02
5.29	-25.5	-25.46	10.8	10.80	1.1	1.03
5.31	-25.6	-25.47	11.2	10.80	1.0	1.04
5.33	-25.4	-25.48	10.4	10.84	1.0	1.03
5.35	-25.1	-25.47	10.7	10.80	1.1	1.03
5.37	-25.5	-25.44	10.8	10.79	1.0	1.04
5.39	-25.3	-25.44	10.6	10.79	1.0	1.03
5.41	-25.7	-25.43	11.7	10.77	1.2	1.03
5.43	-25.3	-25.46	10.9	10.86	1.0	1.05
5.45	-25.6	-25.44	10.5	10.87	1.1	1.04
5.47	-25.1	-25.46	10.3	10.83	1.0	1.05
5.49	-25.3	-25.42	10.4	10.78	1.0	1.04
5.51	-25.3	-25.41	10.5	10.74	1.0	1.04
5.53	-25.7	-25.40	10.9	10.72	1.2	1.04
5.55	-25.3	-25.43	10.7	10.73	1.1	1.05
5.57	-25.3	-25.41	10.3	10.73	1.0	1.06
5.59	-25.3	-25.40	10.4	10.69	1.1	1.05
5.61	-25.3	-25.39	10.4	10.66	1.0	1.06
5.63	-25.2	-25.38	10.4	10.63	1.0	1.05
5.65	-25.3	-25.37	10.5	10.61	1.0	1.05
5.67	-25.2	-25.36	10.1	10.60	1.0	1.04
5.69	-25.1	-25.34	10.5	10.55	1.0	1.04
5.71	-25.6	-25.32	11.2	10.54	1.1	1.03
5.73	-25.2	-25.35	10.6	10.61	1.0	1.04
5.75	-25.3	-25.33	10.5	10.61	1.0	1.04
5.77	-25.3	-25.33	10.5	10.60	1.0	1.03
5.79	-25.4	-25.33	10.8	10.59	1.1	1.03
5.81	-25.3	-25.33	10.9	10.61	1.1	1.04
5.83	-25.2	-25.33	10.5	10.64	1.0	1.04
5.85	-25.3	-25.32	10.7	10.62	1.0	1.04
5.87	-25.3	-25.32	10.8	10.63	1.0	1.03
5.89	-25.5	-25.31	10.8	10.65	1.1	1.03
5.91	-25.2	-25.33	10.6	10.66	1.0	1.04
5.93	-25.7	-25.32	11.4	10.66	1.1	1.03
5.95	-25.6	-25.36	10.6	10.73	1.1	1.04
5.97	-25.6	-25.38	11.3	10.72	1.1	1.05
5.99	-26.1	-25.40	10.6	10.78	1.1	1.05
6.01	-25.2	-25.47	10.6	10.76	1.0	1.06
6.03	-25.2	-25.45	10.6	10.74	1.0	1.05

Depth (m)	$\delta^{13}C$	$\delta^{13}C$	C/N	C/N	TOC	TOC
6.05	-25.2	-25.42	10.6	10.73	1.0	1.05
6.07	-25.2	-25.40	10.6	10.72	1.0	1.04
6.09	-25.2	-25.38	10.6	10.70	1.0	1.04
6.11	-25.2	-25.36	10.6	10.69	1.0	1.03
6.13	-25.2	-25.35	10.6	10.68	1.0	1.03
6.15	-25.2	-25.33	10.6	10.68	1.0	1.03
6.17	-25.2	-25.32	10.6	10.67	1.0	1.02
6.19	-25.2	-25.31	10.6	10.66	1.0	1.02
6.21	-25.2	-25.30	10.6	10.66	1.0	1.02
6.23	-25.2	-25.29	10.6	10.65	1.0	1.02
6.25	-25.2	-25.28	10.6	10.64	1.0	1.02
6.27	-25.2	-25.27	10.6	10.64	1.0	1.01
6.29	-24.9	-25.26	10.5	10.64	1.0	1.01
6.31	-25.2	-25.23	10.6	10.62	1.0	1.01
6.33	-25.0	-25.22	10.6	10.62	1.1	1.01
6.35	-25.0	-25.20	10.6	10.62	1.0	1.02
6.37	-25.0	-25.18	10.6	10.62	1.1	1.02
6.39	-25.1	-25.16	10.7	10.61	1.0	1.03
6.41	-25.1	-25.16	10.7	10.62	1.1	1.02
6.43	-25.3	-25.15	11.1	10.63	1.0	1.03
6.45	-25.1	-25.17	11.5	10.68	1.1	1.03
6.47	-25.4	-25.16	11.5	10.76	1.1	1.04
6.49	-25.2	-25.18	11.3	10.83	1.0	1.04
6.51	-25.2	-25.19	11.7	10.88	1.1	1.04
6.53	-24.9	-25.19	10.5	10.96	0.9	1.04
6.55	-25.4	-25.16	10.7	10.92	1.1	1.03
6.57	-25.2	-25.18	10.3	10.89	1.1	1.04
6.59	-25.5	-25.18	10.6	10.84	1.0	1.04
6.61	-25.0	-25.22	10.6	10.81	1.0	1.04
6.63	-25.3	-25.19	10.7	10.79	1.0	1.03
6.65	-25.0	-25.20	10.5	10.78	1.0	1.03
6.67	-25.0	-25.18	10.7	10.75	1.0	1.03
6.69	-25.2	-25.17	11.1	10.75	1.1	1.03
6.71	-25.0	-25.17	10.6	10.78	1.0	1.03
6.73	-25.5	-25.15	11.4	10.76	1.1	1.03
6.75	-25.0	-25.19	11.1	10.83	1.0	1.04
6.77	-25.1	-25.17	10.4	10.86	1.1	1.03
6.79	-25.2	-25.16	11.2	10.81	1.0	1.04
6.81	-25.4	-25.17	11.4	10.85	1.1	1.04
6.83	-25.1	-25.19	11.2	10.90	1.1	1.04
6.85	-25.4	-25.18	11.2	10.93	1.1	1.05
6.87	-25.3	-25.20	11.6	10.96	1.1	1.05
6.89	-25.4	-25.21	11	11.02	1.1	1.06
6.91	-25.3	-25.23	12	11.02	1.2	1.06
6.93	-25.3	-25.24	11.8	11.12	1.1	1.08
6.95	-25.2	-25.24	11.6	11.19	1.1	1.08
6.97	-25.3	-25.24	11.5	11.23	1.1	1.08
6.99	-25.0	-25.25	11.3	11.26	1.1	1.08

Depth (m)	δ¹³C	δ¹³C	C/N	C/N	TOC	TOC
7.01	-25.2	-25.22	10.4	11.26	1.0	1.08
7.03	-24.9	-25.22	11.1	11.17	1.1	1.08
7.05	-24.9	-25.19	11.2	11.17	1.0	1.08
7.07	-24.9	-25.16	11.2	11.17	1.1	1.07
7.09	-24.1	-25.13	11	11.17	1.0	1.07
7.11	-25.1	-25.03	11.3	11.16	1.0	1.07
7.13	-24.9	-25.04	10.5	11.17	1.1	1.06
7.15	-24.8	-25.02	11.1	11.10	1.0	1.06
7.17	-24.8	-25.00	11.1	11.10	1.1	1.06
7.19	-24.9	-24.98	10.6	11.10	1.0	1.06
7.21	-24.9	-24.97	10.6	11.05	1.1	1.06
7.23	-25.2	-24.97	11	11.01	1.1	1.06
7.25	-25.0	-24.99	10.4	11.01	1.0	1.06
7.27	-25.2	-24.99	10.6	10.95	1.0	1.06
7.29	-24.9	-25.01	10.7	10.91	1.1	1.05
7.31	-24.8	-25.00	10.1	10.89	1.0	1.06
7.33	-24.7	-24.98	10.1	10.81	1.0	1.05
7.35	-25.0	-24.95	10.7	10.74	1.0	1.05
7.37	-25.0	-24.96	10.4	10.74	1.0	1.04
7.39	-25.1	-24.96	10.5	10.70	1.0	1.04
7.41	-24.7	-24.97	10.4	10.68	1.0	1.03
7.43	-25.0	-24.95	10.7	10.65	1.0	1.03
7.45	-24.9	-24.95	10.4	10.66	1.0	1.03
7.47	-25.0	-24.95	10.4	10.63	1.0	1.02
7.49	-24.9	-24.95	10.3	10.61	1.0	1.02
7.51	-24.7	-24.95	10.1	10.58	1.0	1.02
7.53	-24.8	-24.92	10.2	10.53	1.0	1.02
7.55	-24.8	-24.91	9.8	10.50	0.9	1.02
7.57	-24.7	-24.90	10	10.43	1.0	1.00
7.59	-25.1	-24.88	10.6	10.39	1.0	1.00
7.61	-24.8	-24.90	10.4	10.41	1.0	1.00
7.63	-24.9	-24.89	10.3	10.41	1.0	1.00
7.65	-24.7	-24.89	10.2	10.40	1.0	1.00
7.67	-24.9	-24.87	10	10.38	1.0	1.00
7.69	-24.9	-24.88	10.4	10.34	1.0	1.00
7.71	-24.9	-24.88	10.3	10.34	1.0	1.00
7.73	-24.8	-24.88	10.4	10.34	1.0	1.00
7.75	-24.9	-24.87	10	10.35	1.0	1.00
7.77	-24.8	-24.88	9.8	10.31	1.0	1.00
7.79	-25.0	-24.87	10.4	10.26	1.0	1.00
7.81	-25.1	-24.88	10.5	10.27	1.0	1.00
7.83	-24.9	-24.90	10.3	10.30	1.0	1.00
7.85	-25.0	-24.90	10.7	10.30	1.0	1.00
7.87	-25.1	-24.91	10.3	10.34	0.9	1.00
7.89	-24.9	-24.93	10	10.33	1.0	0.99
7.91	-25.2	-24.93	10.4	10.30	1.0	0.99
7.93	-25.0	-24.96	10.5	10.31	1.0	0.99
7.95	-25.2	-24.96	10.5	10.33	1.0	0.99

Depth (m)	δ¹³C	δ¹³C	C/N	C/N	TOC	TOC
7.97	-25.3	-24.98	10.9	10.35	1.0	0.99
7.99	-25.1	-25.02	10.6	10.40	1.0	0.99
8.01	-25.1	-25.02	11.2	10.42	1.1	1.00
8.03	-24.9	-25.03	10.6	10.50	1.0	1.01
8.05	-25.0	-25.02	10.6	10.51	1.1	1.01
8.07	-25.0	-25.02	10.2	10.52	1.0	1.01
8.09	-25.1	-25.01	10.5	10.49	1.1	1.01
8.11	-25.3	-25.02	10.6	10.49	1.1	1.02
8.13	-25.0	-25.05	11.2	10.50	1.1	1.03
8.15	-25.0	-25.05	10.5	10.57	1.0	1.04
8.17	-25.2	-25.04	10.8	10.56	1.0	1.03
8.19	-25.2	-25.06	10.6	10.59	1.1	1.03
8.21	-25.1	-25.07	10.5	10.59	1.1	1.04
8.23	-25.2	-25.07	10.6	10.58	1.1	1.04
8.25	-25.2	-25.09	11.1	10.58	1.1	1.05
8.27	-25.1	-25.10	10.4	10.63	1.0	1.05
8.29	-25.1	-25.10	10.7	10.61	1.1	1.05
8.31	-25.2	-25.10	10.7	10.62	1.1	1.05
8.33	-25.1	-25.11	10.5	10.63	1.1	1.06
8.35	-25.4	-25.11	11.3	10.61	1.1	1.06
8.37	-25.1	-25.14	11	10.68	1.0	1.07
8.39	-25.3	-25.13	11	10.71	1.1	1.06
8.41	-24.9	-25.15	10.4	10.74	1.0	1.06
8.43	-25.2	-25.12	10.7	10.71	1.1	1.06
8.45	-25.2	-25.13	10.8	10.71	1.1	1.06
8.47	-25.3	-25.14	10.8	10.72	1.1	1.07
8.49	-25.3	-25.16	11.4	10.73	1.1	1.07
8.51	-25.3	-25.17	10.8	10.79	1.1	1.07
8.53	-25.3	-25.18	11.3	10.79	1.1	1.07
8.55	-25.3	-25.19	10.5	10.84	1.1	1.08
8.57	-25.5	-25.21	11	10.81	1.1	1.08
8.59	-25.4	-25.23	10.7	10.83	1.1	1.08
8.61	-25.7	-25.25	11.6	10.82	1.2	1.08
8.63	-25.5	-25.30	10.7	10.89	1.1	1.10
8.65	-25.4	-25.32	11.6	10.87	1.1	1.10
8.67	-25.4	-25.32	10.8	10.95	1.1	1.10
8.69	-25.4	-25.33	10.9	10.93	1.1	1.10
8.71	-25.4	-25.34	11	10.93	1.1	1.10
8.73	-25.3	-25.35	10.9	10.94	1.1	1.10
8.75	-25.4	-25.34	10.8	10.93	1.1	1.10
8.77	-25.4	-25.35	11.4	10.92	1.1	1.10
8.79	-25.4	-25.35	10.7	10.97	1.1	1.10
8.81	-25.4	-25.36	10.8	10.94	1.2	1.10
8.83	-25.4	-25.36	11.2	10.93	1.1	1.11
8.85	-25.4	-25.36	11.1	10.95	1.1	1.11
8.87	-25.7	-25.37	11.6	10.97	1.2	1.11
8.89	-26.1	-25.40	13.6	11.03	1.4	1.12
8.91	-25.7	-25.47	11.6	11.29	1.2	1.14
8.93	-25.4	-25.49	11	11.32	1.1	1.15

Depth (m)	$\delta^{13}C$	$\delta^{13}C$	C/N	C/N	TOC	TOC
8.95	-25.5	-25.48	10.8	11.29	1.1	1.15
8.97	-25.5	-25.49	11.1	11.24	1.1	1.14
8.99	-25.5	-25.49	10.6	11.23	1.1	1.14
9.01	-25.4	-25.49	11.4	11.16	1.1	1.13
9.03	-25.5	-25.48	10.9	11.19	1.1	1.13
9.05	-25.4	-25.48	10.7	11.16	1.1	1.13
9.07	-25.7	-25.47	11	11.11	1.1	1.12
9.09	-25.4	-25.50	11.7	11.10	1.08	1.12
9.11	-25.4	-25.49	10.2	11.16	1.15	1.12
9.13	-25.4	-25.48	10.3	11.06	1.11	1.12
9.15	-25.6	-25.47	10.7	10.99	1.21	1.12
9.17	-25.5	-25.48	10.7	10.96	1.15	1.13
9.19	-25.4	-25.48	10.5	10.93	1.15	1.13
9.21	-25.4	-25.48	11.4	10.89	1.10	1.13
9.23	-25.5	-25.47	10.8	10.94	1.19	1.13
9.25	-25.4	-25.47	10.8	10.93	1.18	1.14
9.27	-25.3	-25.46	10.7	10.91	1.16	1.14
9.29	-25.6	-25.45	11.3	10.89	1.15	1.14
9.31	-25.3	-25.46	10.6	10.93	1.16	1.14
9.33	-25.1	-25.45	11.3	10.90	1.08	1.14
9.35	-25.2	-25.41	10.8	10.94	1.18	1.14
9.37	-25.5	-25.39	10.8	10.93	1.25	1.14
9.39	-25.5	-25.40	10.6	10.91	1.20	1.15
9.41	-25.4	-25.41	10.9	10.88	1.19	1.16
9.43	-25.5	-25.41	10.4	10.88	1.12	1.16
9.45	-25.5	-25.42	11.4	10.84	1.12	1.16
9.47	-25.6	-25.43	10.4	10.89	1.20	1.15
9.49	-25.7	-25.44	11	10.84	1.24	1.16
9.51	-25.6	-25.47	10.4	10.86	1.24	1.17
9.53	-25.7	-25.48	11.5	10.81	1.18	1.17
9.55	-25.6	-25.51	10.4	10.88	1.18	1.17
9.57	-25.5	-25.51	11.5	10.83	1.14	1.17
9.59	-26.0	-25.51	11.3	10.90	1.4	1.17
9.61	-25.7	-25.56	10.8	10.94	1.3	1.19
9.63	-25.6	-25.58	9.6	10.93	1.2	1.20
9.65	-25.6	-25.58	8.9	10.79	1.3	1.20
9.67	-25.7	-25.58	9.7	10.60	1.3	1.21
9.69	-25.6	-25.59	11.9	10.51	1.2	1.22
9.71	-25.9	-25.59	10.5	10.65	1.2	1.22
9.73	-25.6	-25.62	7.7	10.64	1.3	1.22
9.75	-25.9	-25.62	9.4	10.34	1.3	1.23
9.77	-25.5	-25.65	11.8	10.25	1.1	1.23
9.79	-25.7	-25.63	5.2	10.40	1.2	1.22
9.81	-25.5	-25.64	11.6	9.88	1.1	1.22
9.83	-25.8	-25.63	5.6	10.06	1.4	1.21
9.85	-25.9	-25.64	5.3	9.61	1.4	1.23
9.87	-25.7	-25.67	4	9.18	1.3	1.24
9.89	-25.8	-25.67	5	8.66	1.3	1.25
9.91	-25.8	-25.69	6.6	8.29	1.3	1.25
9.93	-25.6	-25.70	11.6	8.13	1.2	1.26
9.95	-25.9	-25.69	6.9	8.47	1.2	1.25
9.97	-25.7	-25.71	5.3	8.32	1.4	1.25
9.99	-25.7	-25.71	6.4	8.01	1.4	1.26
10.1	-25.6	-25.71	3.6	7.85	1.2	1.28
10.03	-25.4	-25.70	8.9	7.43	0.6	1.27
10.05	-24.7	-25.67	11.3	7.57	1.0	1.20
10.07	-25.8	-25.57	8.4	7.95	0.5	1.18